International
Progress Report

IPR-99-22

Äspö Hard Rock Laboratory

Äspö Task Force on Modelling of Groundwater Flow and Transport of Solutes

Proceedings from the 12th task force meeting at Gimo, Sweden, April 20-22, 1999

Part 2 of 3: Task 4 contributions

Mansueto Morosini

Svensk Kärnbränslehantering AB

September 1999

Svensk Kärnbränslehantering AB
Swedish Nuclear Fuel
and Waste Management Co
Box 5864
SE-102 40 Stockholm Sweden
Tel 08-459 84 00
+46 8 459 84 00
Fax 08-661 57 19
+46 8 661 57 19

Äspö Hard Rock Laboratory

Äspö Hard Rock Laboratory

Äspö Task Force on Modelling of Groundwater Flow and Transport of Solutes

Proceedings from the 12th task force meeting at Gimo, Sweden, April 20–22, 1999

Part 2 of 3: Task 4 contributions

Mansueto Morosini

Svensk Kärnbränslehantering AB

September 1999

Keywords: Groundwater flow, solute transport, tracer test, fractured rock, underground laboratory, stochastic modelling, deterministic modelling.

B.3 Contributions of modelling results of Task 4E and 4F

- Modelling of sorption behaviour of radioactive tracer in Feature A using different conceptual models. Hua Shao (BMBF/BGR)
- Modelling of STT1 tracer test and Predictive computations of STT2. C Grenier (ANDRA/CEA)
- Evaluation of STT1 and Prediction of STT2. J-O Selroos (SKB/WRE)
- Analysis of STT1 and STT1b tests and Predictions of the breakthrough times in the STT2 test. A Poteri (POSIVA/VTT)
- STT2 predictions. W Dershowitz (JNC/Golder)
- Numerical analysis with FEGM/FERM for TRUE-1 sorbing tracer tests. Y Tanaka, T Igarashi, M Kawanishi (CRIEPI)
- Estimation of STT1b and STT1, and Blind prediction of the STT-1 tracer tests with multiple rates of mass transfer. S McKenna (DOE/Sandia)
- Blind predictions for the Task 4F (STT2) tracer migration experiment at the Äspö TRUE-1 site. A Jakob, W Heer (NAGRA/PSI)

Modelling the sorption of radioactive tracers in Feature A

H. Shao and L Liedtke (BMWi/BGR)

PREDICTIVE MODELLING REPORT OF STT-2

MODELLING THE SORPTION OF RADIOACTIVE TRACERS IN FEATURE A

ÄSPÖ HARD ROCK LABORATORY, SWEDEN

Shao, H. & Liedtke, L.

Federal Institute for Geosciences and Natural Resources (BGR)
Hanover, Germany

April 19 – 22, 1999
12th Task Force Meeting
Gimo Herrgård, Sweden

TABLE OF CONTENTS

TABLE OF FIGURES

EXECUTIVE SUMMARY

Fracture geometry, hydraulic boundary conditions and transport processes in TRUE-1 have been analysed quite well after a series of the modelling work (4C, 4D, and 4E). The predictive results for the conservative and weak sorbing tracers in the Sorbing Tracer Tests STT-1 and STT-1b using single fracture model were generally satisfying the measured concentrations (Fig. 1-8). Therefore there no significant changes with respect to model geometry and model parameter values were necessary for the model calibration. For example, the hydraulic conductivity of Feature A was estimated to be 1e-5 ~ 6e-4 m/s assuming a constant fracture aperture of 1.4 mm (locally variable between 0.3 - 1.0 mm). For a transport distance 5 m, as used in the previous tests in KXTT4R3 - KXTT3R2 or KXTT1R2 - KXTT3R2, the effective porosity amounted to 0.3 ~ 0.4, the longitudinal / transverse dispersivities were 0.4 ~ 0.8 /0.04 ~ 0.08 m respectively, and the diffusion coefficient could be ignored for the conservative tracer (< 1e-7 m^2/s).

The main emphasis was laid on the modelling of the moderate sorbing tracers using the coupled fracture matrix model and mass balance. The results indicated that the overall tracers with a K_d value > 1e-4 m^3/kg, e.g. rubidium, cobalt, and caesium should be modelled using the coupled fracture matrix model, because sorption and desorption processes are not only restricted to the fracture surface. The processes seem to affect the immediate vicinity of the fracture, which can be defined as a certain volume of matrix or gauge volume, although its amount may be small.

The updated fracture model which was discussed within the 4F was analysed using two fictional models. The results of the modelling shows that the dispersivity of the transport model should be reduced about 10% using the fracture network model under the same hydraulic conditions in comparison of the single fracture model.

All predictive modelling are performed using the measured input function in the injection bore hole. The pulse function can describe the impulse injection process in this case, but it cannot reflect the second alternative peak of the injection curve. It can be used if dilution and circulation of tracers in the injection hole are considered in the numerical model.

1 INTRODUCTION

The aim of the Tracer Retention Understanding Experiment (TRUE) focuses on the further development of the understanding and modelling of radionuclide migration and retention processes in fractured host rock. Within the first stage of TRUE (TRUE-1) a series of tracer tests using different tracers (conservative and radioactive tracers) was performed over a transport distance of about 5 m in a single water conducting feature (Feature A) at a depth of approximately 400 m.

In order to build the model confidence and to prove the knowledge about sorbing tracers properties gained from the modelling for Sorbing Tracer Tests (STT-1 and STT-1b), another series of tracer tests (STT-2) was designed to be carried out by SKB in Feature A. The experiment applied a radially converging flow geometry between boreholes KXTT4 - KXTT3 and the pumping rate used amounted to 200 ml/min in borehole KXTT3R2. Ten tracers as tracer cocktail, three conservative (Uranine, ^{82}Br, and tritiated water) and eight weak to moderate radioactive sorbing tracers (^{22}Na, ^{85}Sr, ^{42}K, ^{86}Rb, ^{134}Cs, ^{47}Ca, ^{131}Ba, and ^{133}Ba) were injected into borehole KXTT4R3 as a pulse with a finite duration of four hours. Tracer breakthrough in the pumping section was monitored for all tracers.

For the predictive modelling of STT-2, the fracture geometry and the hydraulic data at the test site are known through interpretation of previous tests. Additionally the injected concentration data and monitoring times were also available.

2 MODEL CALIBRATION

The finite element mesh and hydraulic and transport parameter values used for the calculation of the sorbing tracer test STT-2 were not changed (tab.1), because the model was calibrated according to the hydraulic data e.g. pumping rate and draw-down, tracer transport information, breakthrough time and maximal concentration and mass balance from previous tests within 4C/4D. However slight modification of the dispersivity has been done with respect to the modelling for PDT-2 (Fig. 9).

Table 1: Parameter values used in STT-1, STT-1b and STT-2

Hydraulic conductivity (m/s)	Locally variable 6.5e-5 ~ 4e-4
Fracture aperture (mm)	Locally variable 0.3 ~ 1.0
Effective porosity (-)	Variation 0.3 ~ 0.4
Dispersivity α_L / α_T (m)	Variation 0.4 ~ 0.5 / 0.04 ~ 0.05
Diffusion (m²/s)	1e-7

3 UPDATED FRACTURE MODEL FOR FEATURE A

Detail characterisation of the bore core shows that there is a fracture in the test interval of the bore hole KXTT4R3, which is sub-parallel to the Feature A. Although the exact location of the intersection between this fracture and Feature A is not clearly known up to now, there may be two flow paths for the transport of tracers from KXTT4R3 to KXTT3R2, at least in close vicinity to the bore hole KXTT4. Whether there are any significant difference between the model results from the fracture network model and from the compact single fracture model, was analysed using a simplified model configuration.

Figure 10 shows there is only a 10% reduction of the dispersivity under the same flow conditions, in the case of network model. Furthermore there are no any influence on the characterisation of the breakthrough curve. Since the single fracture model has been used and regarded as plausible model to evaluate the tracer migration and retention processes in the Feature A, it will be as basic model for evaluating STT-2.

4 PULSE AND MEASURED INPUT FUNCTION

Since the tracer was injected as a finite pulse function with a duration of four hours in the experiment, it is convenient using the impulse (Dirac) response function for the modelling. But the second hump in the injection function, which may result from dilution and circulation processes in the injection hole, cannot be reproduced using a simple pulse input function. Therefore an actual breakthrough curve with two peaks could not be modelled in this case. If one considers that the breakthrough curves were simulated properly for STT-2, which was proved in the modelling of previous tracer tests, a better description of the tracer transport process using measured input function would increase the agreement between measured and calculated mass balance (Fig. 11). If the dilution and circulation processes in the bore hole are also taken into account in the numerical model, modelling using pulse function should derive more information for a better understanding of the system.

5 MODELS USED IN FEATURE A

Based on the results from previous work, two models were used to perform the modelling of sorbing tracer tests. The fracture model enable to calculate transport times and mass balances for conservative tracers (Uranine, bromine, and tritiated water) and weak sorbing tracers (the distribution coefficient K_d < 1.e-4 m³/kg estimated in the laboratory), because the matrix has less influence on the transport processes. However for moderate sorbing tracer with a distribution coefficient K_d > 1.e-4 m³/kg, the coupled fracture matrix model (Fig. 12) should be used, because surface sorption processes

on the fracture surface alone are not able to describe the retardation processes of theses traces.

On the other hand a complete 3 dimensional modelling demands a considerable CPU time and computer capacity. Therefore an analogue model - here called the Brush model – may be convenient to estimate transport processes. Such a model combines 2-D finite elements for the fracture and 1-D finite elements instead of 3-D elements for the matrix (Fig. 12). The advantage of this concept is that the different transport mechanisms in the fracture and the rock matrix are solved at the same time reducing the amount of computer time required dramatically. The 1-D elements are orientated perpendicular to the fracture plane and coupled to the 2-D fracture elements through common nodes. Since a chain of 1-D elements is attached to every node of the 2-D mesh, the mass exchange between different chains of 1-D elements has thus to be deliberately ignored. The cross-sectional area of the 1-D elements is equivalent to the area surrounding the nodes of the corresponding 2-D mesh. Due to the symmetrical geometry of the problem, only one half of the fracture aperture has to be considered.

6 PREDICTIVE MODELLING OF SORBING TRACER TEST STT-2

In STT-2, ten tracers were injected as mixed solutions into borehole section KXTT4R2, with an interval volume of 2154 ml. The concentration in the injection hole was registered by on-line measurement and aslo by evaluating samples in the laboratory. The sampling rate of 2.6 ml/h has been considered for calculating the mass balance.

The transport of conservative tracers (^{82}Br, tritiated water, and Uranine) and weak sorbing tracers (^{22}Na, ^{85}Sr and ^{42}K as well as ^{47}Ca, ^{131}Ba and ^{133}Ba) was modelled using the single fracture model. The transport of moderate sorbing tracers (^{86}Rb and ^{134}Cs) was simulated using the coupled fracture matrix model so that the large adsorption and desorption processes in the matrix could be incorporated.

Table 2: Predicted drawdown in STT-2

	Natural head (masl)	Head in STT-2 (masl)	Drawdown (m)
KXTT1R2	-53.09	-53.83	0.74
KXTT2R2	-52.88	-54.26	1.38
KXTT3R2	-52.60	-58.02	5.42
KXTT4R3	-52.89	-53.09	0.20

The predicted draw-down of STT-2 for all sections can be calculated by subtracting the natural head from the head deduced from the pumping process in the pumping hole. The modelled results are listed in table 2.

Table 3 shows all predicted breakthrough times with the respect to the time at which modelling stopped.

Table 3: Modelled breakthrough time of all tracers in STT-2

Tracer	$t_{5\%}$ (hr)	$t_{50\%}$ (hr)	$T_{95\%}$ (hr)	$T_{100\%}$ (hr)
HTO	13	140	440	1848
Uranine	13.8	150	460	1848
^{82}Br	17	235	-	1848
^{22}Na	14	160	1590	3078
^{47}Ca	12.5	115	-	1848
^{85}Sr	16	240	-	3078
^{131}Ba	50	500	-	1848
^{133}Ba	50	530	1990	3078
^{86}Rb	243	590	-	1848
^{134}Cs	840	3450	-	6350

The tracer mass recovery was calculated for all ten tracers by integrating the breakthrough curves for the mass flux (mg/h for Uranine or Bq/h for the other tracers) against time (h). The injected mass was determined in the same way by integrating the measured concentration in the injection interval against time. For the calculation of the injected mass, it is important to determine the flow rate through the injection interval. A mean flow rate of 29.4 ml/h in the model was used. Table 4 lists all predicted mass recoveries taking into consideration when time recording stopped.

Figures 13 – 22 depict the predictive results for all ten tracers used in the sorbing tracer test STT-2.

Table 4: Predicted mass recovery in STT-2

Tracer	T_t (hr)	Injected Mass [Bq]	Recovered Mass [Bq]	Recovery F_c[%]
HTO	641	7.75e+7	7.66e+7	99
Uranine	886	27.54 [mg]	27.47 [mg]	100
^{82}Br	234	4.8e+6	2.22e+6	46
^{22}Na	3078	9.5e+5	9.5e+5	100
^{47}Ca	458	1.95e+5	9.7e+4	49.7
^{85}Sr	3078	2.7e+6	2.5e+6	93
^{131}Ba	1130	1.05e+6	8.8e+5	84
^{133}Ba	3078	1.58e+5	1.58e+5	100
^{86}Rb	1322	2.796e+6	4.26e+5	14.4
^{134}Cs	3078	5.8e+6	3.28e+5	5.6

Table 5: Distribution coefficient and half-life time

Tracer	K_d [m³/kg][1]	K_d [m³/kg][2]	$T_{1/2}$	K_d [m³/kg][3]	K_d [m³/kg][4]	$T_{1/2}$[3/4]	comment
Ur	-	-	-	-	-	-	conservative
HTO	-	-	12.3 y	-	-	**12.3 y**	radioactive
^{22}Na	< 2.8e-5	1.4e-6	2.6 y	**1.4e-6**		**2.6 y**	weak
^{47}Ca	< 4.4e-5	5.2e-6	4.5 d	**4.4e-5**		**4.5 d**	weak
^{86}Rb	1.4e-3 +/- 3.5e-4	4.0e-4	19 d	5.0e-5 ~ 2.0e-4	**4.0e-4**	**19 d**	weak
^{85}Sr	< 2.3e-4	4.7e-6	65 d	4.7e-6	**2.0e-4**	**65 d**	weak
^{133}Ba	1.2e-3 +/- 1.2e-4	2.0e-4	10.5 y	**6.0e-4**		**10.5 y**	weak
^{137}Cs	1.4e-2 +/- 1.2 e-3	6.0e-3	30.2 y	**1.0e-3 – 2.5e-3**		**30.2 y**	moderate
^{42}K	-	2.0e-4	12.4 h	4.0e-5	**4.0e-4**	**12.4 h**	weak
^{58}Co	-	2.4e-2/2.8e-3	70.8 d	2.8e-3 ~ 2.4e-2		**70.8 d**	moderate

1) from through-diffusion experiment carried out by SKB
2) estimated from laboratory experiment
3) used in the predictive modelling
4) used in the evaluation modelling

7 CONCLUSIONS

The Task Force 4: numerical modelling of groundwater flow and transport of solutes in the TRUE-1 is coming to an end, and the results obtained can be concluded as follows through the participating of the 4C-4F:

- For flow and transport processes within a quite good characterised system, in which single water conducting feature was identified like Feature A, plausible numerical result can be gained under deterministic consideration;
- In such a system it is necessary and very important to determine the fracture geometry and hydraulic patterns under the test conditions. The latter can be achieved through iterative modelling of flow and transport;
- Flow and transport parameter values can be determined using numerical modelling of hydraulic and transport tests;
- Sorbing and decay properties of radioactive tracers can be modelled numerically; and
- Groundwater flow and transport of solutes in the fractured rock can be simulated using 'German'-code *Rockflow*.

EVALUATION OF SORBING TRACER TEST STT-1B

Tracer: Uranine
in Sorbing Tracer Test 1b
(KXTT1-KXTT3)
Q_{ext} = 400 ml/min

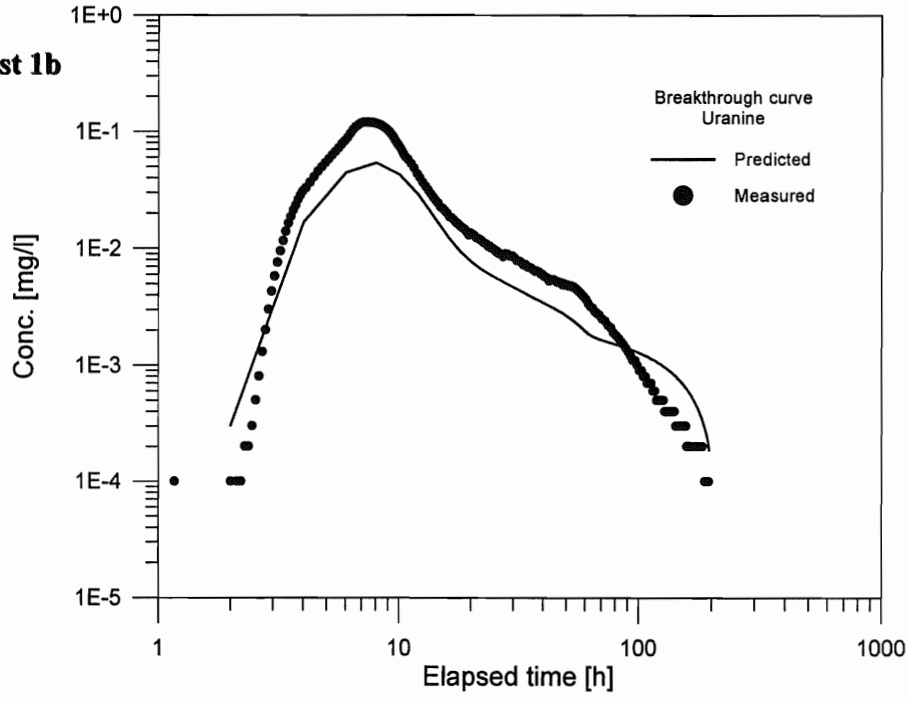

Fig. 1

EVALUATION OF SORBING TRACER TEST STT-1B

Tracer: HTO
in Sorbing Tracer Test 1b
(KXTT1-KXTT3)
Q_{ext} = 400 ml/min

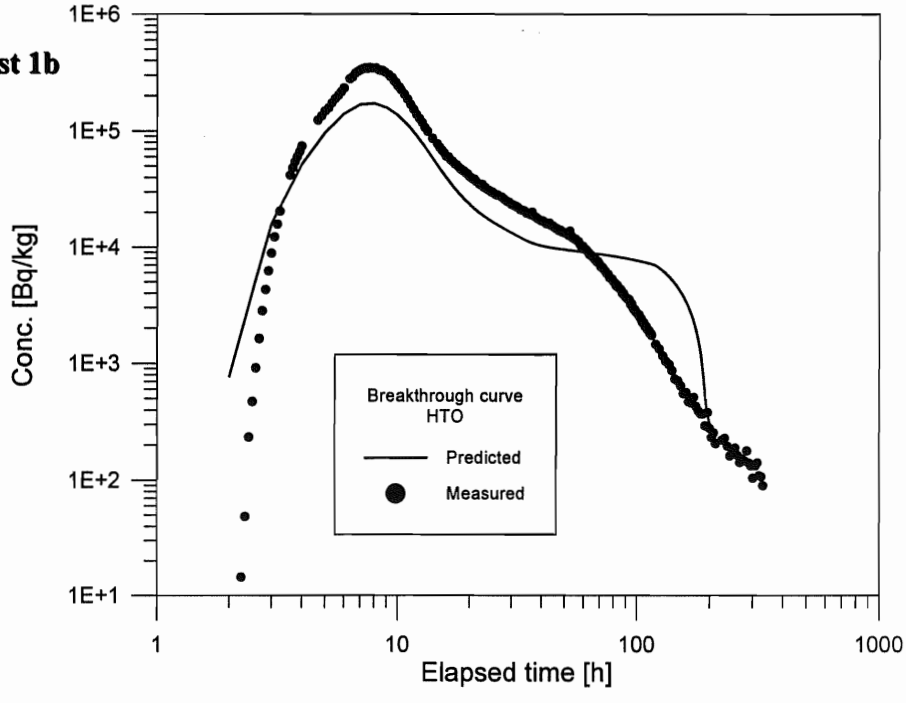

Fig. 2

EVALUATION OF SORBING TRACER TEST STT-1B

Tracer: ^{22}Na
in Sorbing Tracer Test 1b
(KXTT1-KXTT3)
Q_{ext} = 400 ml/min

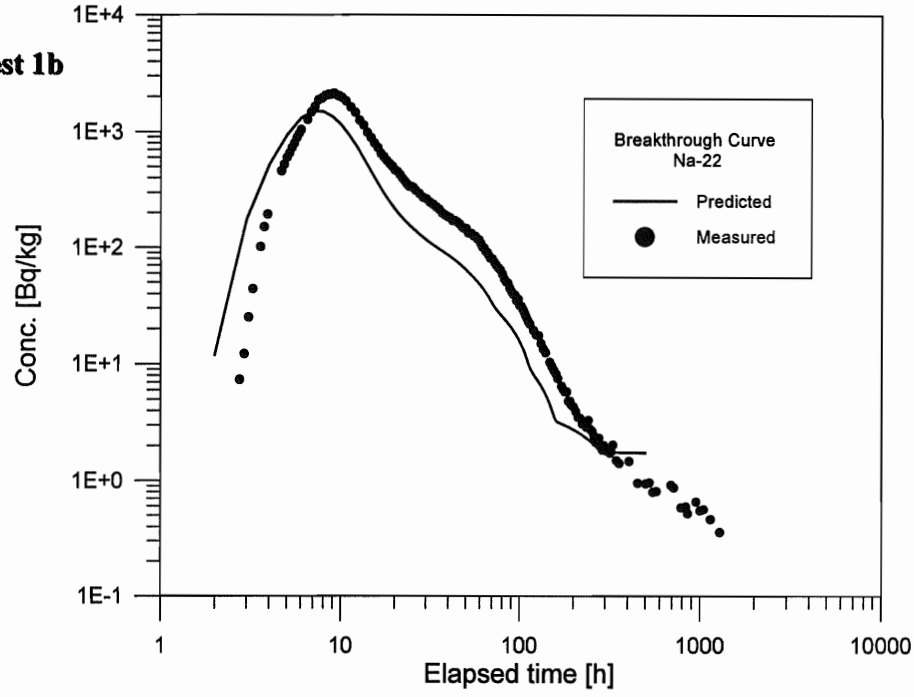

Fig. 3

EVALUATION OF SORBING TRACER TEST STT-1B

Tracer: ^{42}K
in Sorbing Tracer Test 1b
(KXTT1-KXTT3)
Q_{ext} = 400 ml/min

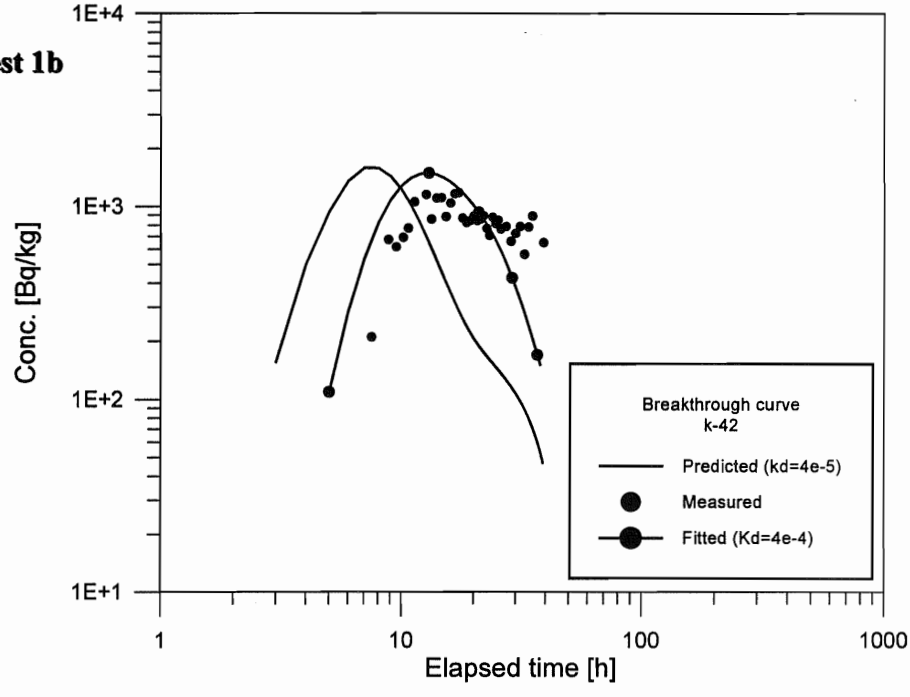

Fig. 4

EVALUATION OF SORBING TRACER TEST STT-1B

Tracer: ^{86}Rb
in Sorbing Tracer Test 1b
(KXTT1-KXTT3)
Q_{ext} = 400 ml/min

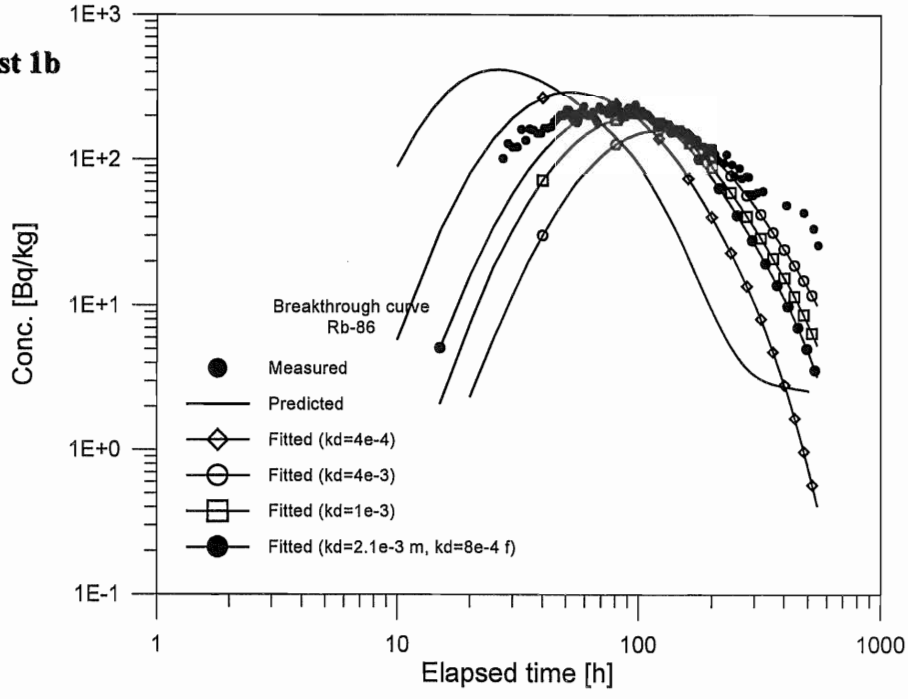

Fig. 5

EVALUATION OF SORBING TRACER TEST STT-1B

Tracer: ^{58}Co
in Sorbing Tracer Test 1b
(KXTT1-KXTT3)
Q_{ext} = 400 ml/min

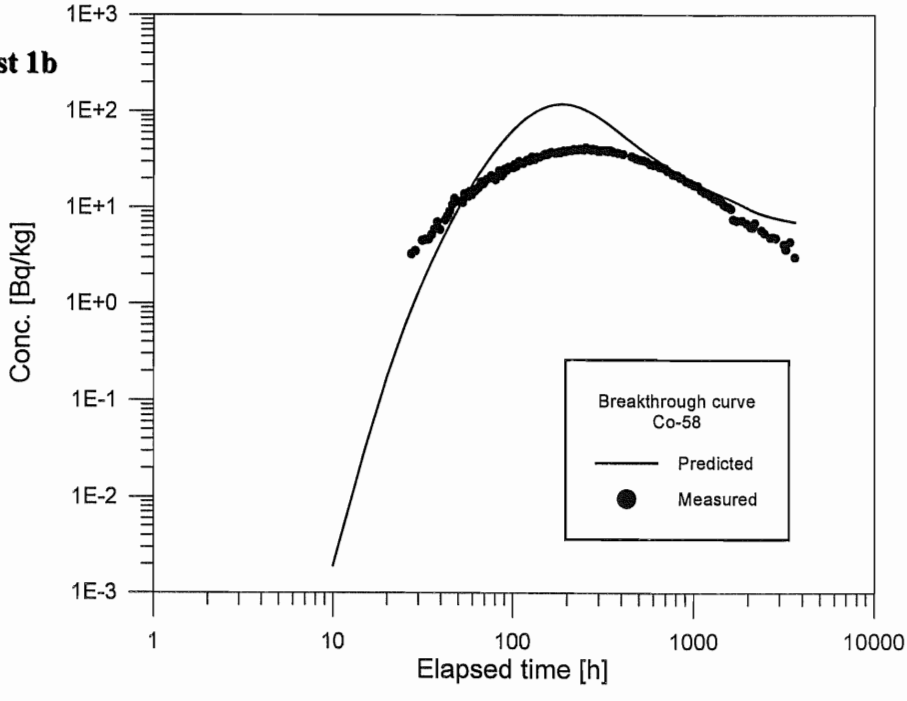

Fig. 6

EVALUATION OF SORBING TRACER TEST STT-1B

Tracer: ^{85}Sr
in Sorbing Tracer Test 1b
(KXTT1-KXTT3)
Q_{ext} = 400 ml/min

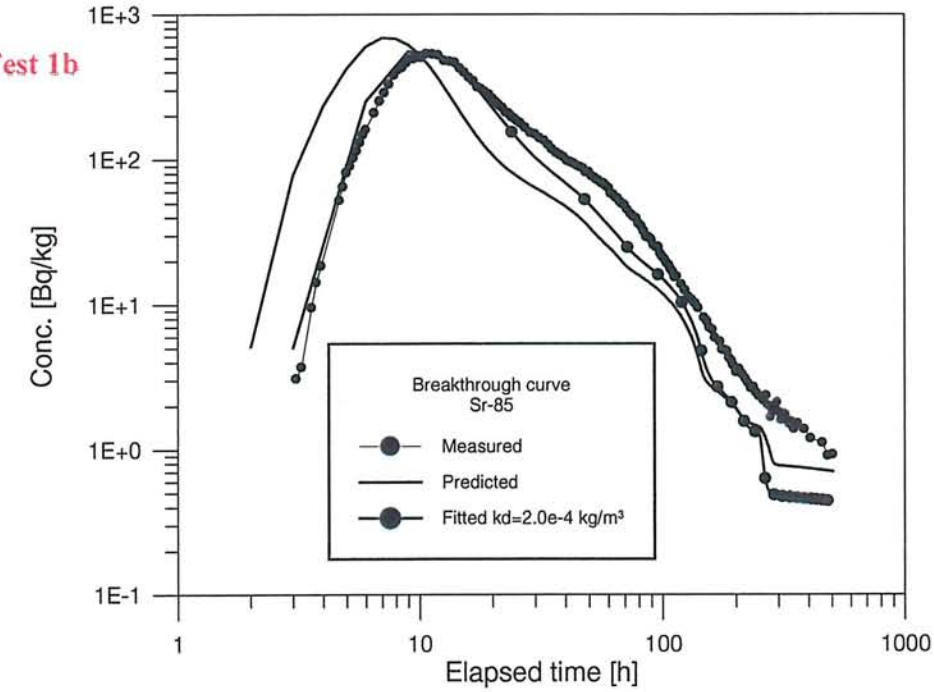

Fig. 7

MODELLING OF SORBING TRACER CS-137 IN STT-1

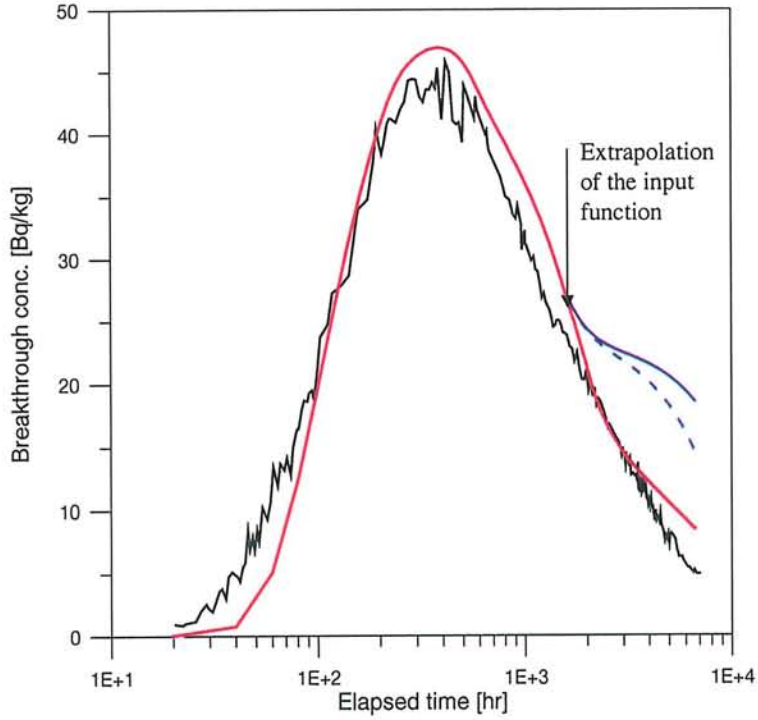

Coupled fracture / matrix model

Model parameter:

fracture:
- conductivity: partially variable
  1.0e-6 ~ 5.0e-4 m/s
- aperture: partially variable
  0.025 ~ 1.4 mm
- effective porosity: 0.3
- dispersivity: 0.5-0.9 m
- distribution coef.: 1.0e-3 m³/kg

matrix:
- perpendicular length: 0.5 m
- conductivity: 1.0e-9 m/s
- effective porosity: 0.01
- dispersivity: 0.01 m
- distribution coef.: 2.5e-3 m³/kg
- diffusion: 1.0e-7 m²/s

Fig. 8

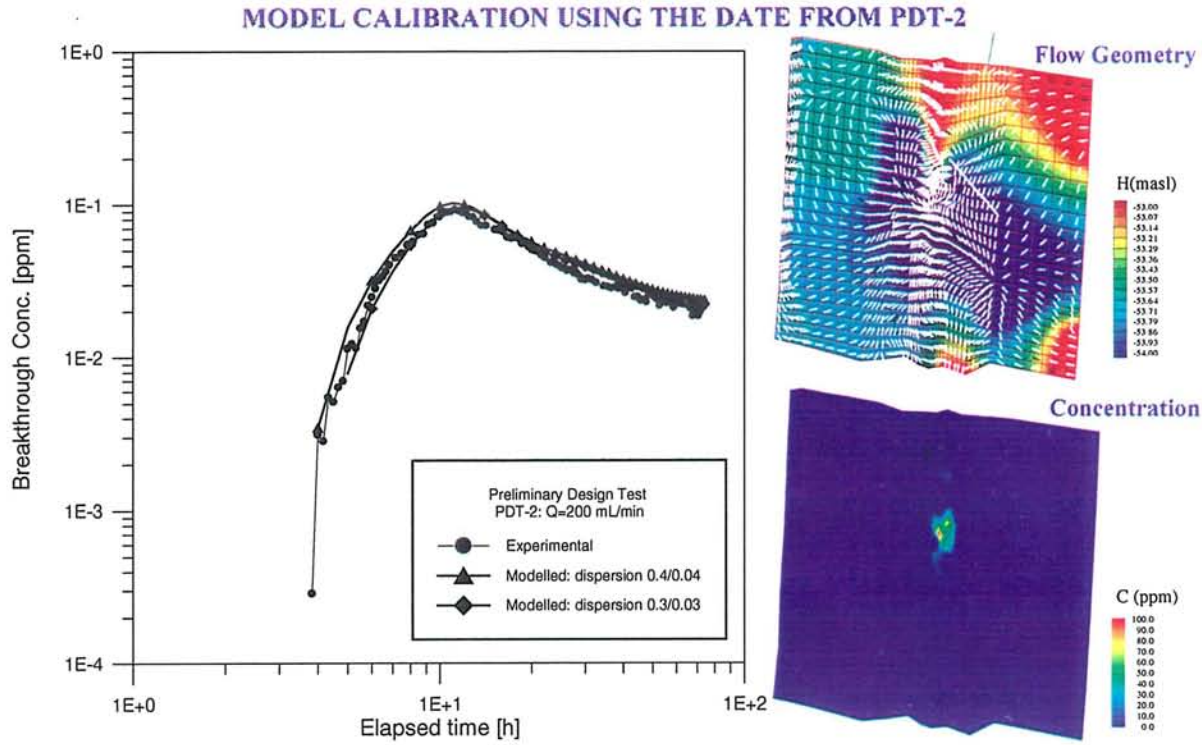
MODEL CALIBRATION USING THE DATE FROM PDT-2
Breakthrough Conc. [ppm]
1E+0
1E-1
1E-2
1E-3
1E-4
1E+0
1E+1
1E+2
Elapsed time [h]
Preliminary Design Test
PDT-2: Q=200 mL/min
Experimental
Modelled: dispersion 0.4/0.04
Modelled: dispersion 0.3/0.03
Flow Geometry
H(masl)
Concentration
C (ppm)

Fig. 9

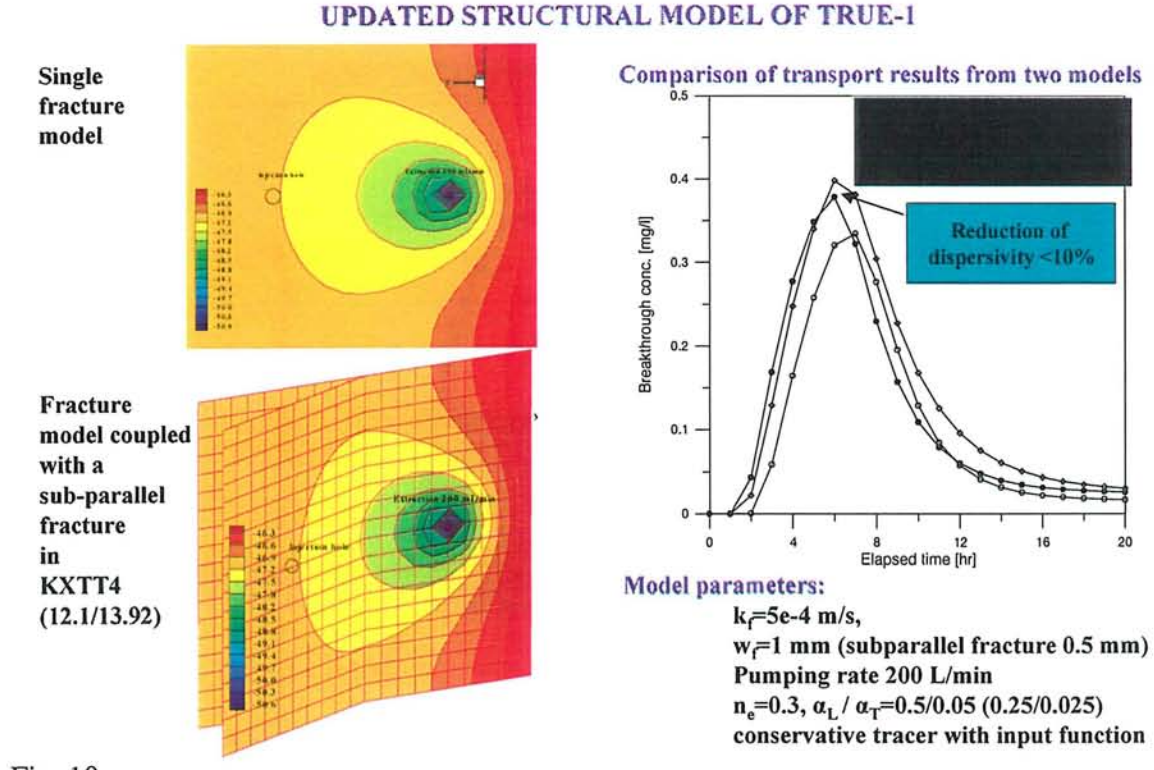
UPDATED STRUCTURAL MODEL OF TRUE-1
Single fracture model
Fracture model coupled with a sub-parallel fracture in KXTT4 (12.1/13.92)
Comparison of transport results from two models
Breakthrough conc. [mg/l]
Elapsed time [hr]
Reduction of dispersivity <10%
Model parameters:
k_f=5e-4 m/s,
w_f=1 mm (subparallel fracture 0.5 mm)
Pumping rate 200 L/min
n_e=0.3, α_L / α_T=0.5/0.05 (0.25/0.025)
conservative tracer with input function

Fig. 10

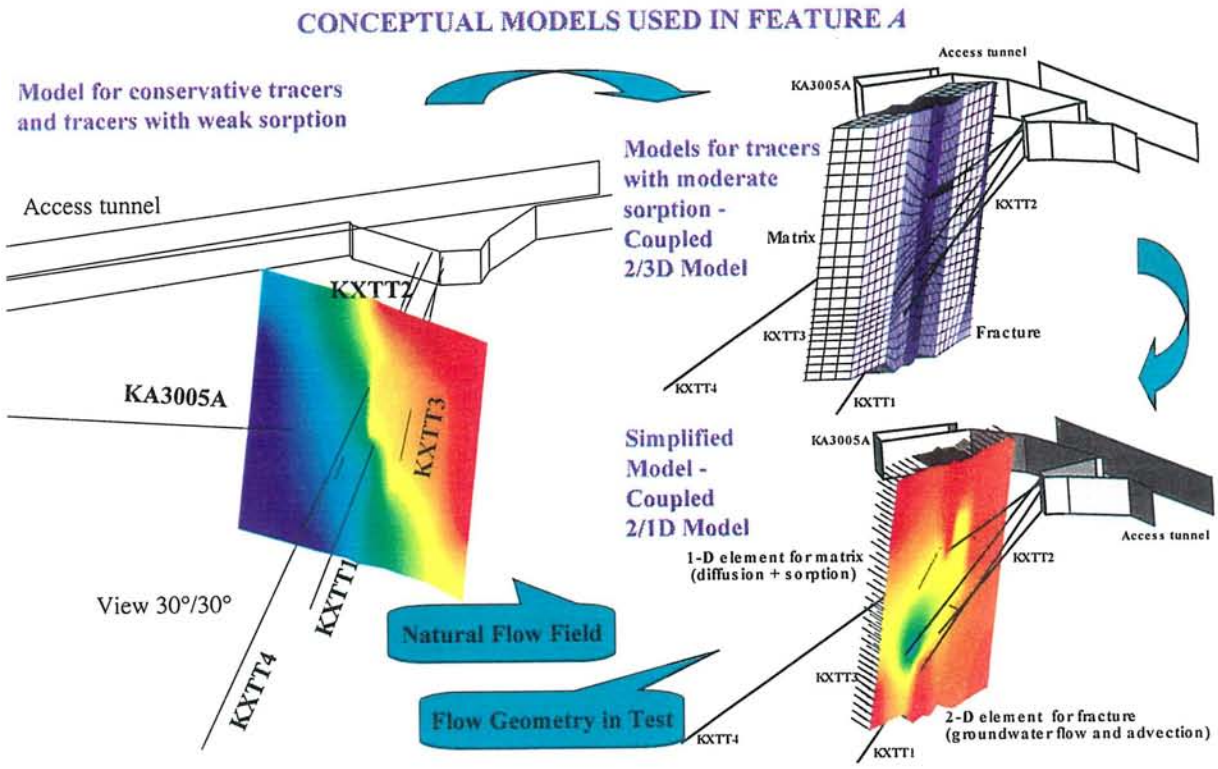
CONCEPTUAL MODELS USED IN FEATURE A
Model for conservative tracers and tracers with weak sorption
Access tunnel
KXTT2
KA3005A
KXTT3
KXTT1
KXTT4
View 30°/30°
Natural Flow Field
Flow Geometry in Test
Models for tracers with moderate sorption - Coupled 2/3D Model
Matrix
Fracture
Simplified Model - Coupled 2/1D Model
1-D element for matrix (diffusion + sorption)
2-D element for fracture (groundwater flow and advection)

Fig. 11

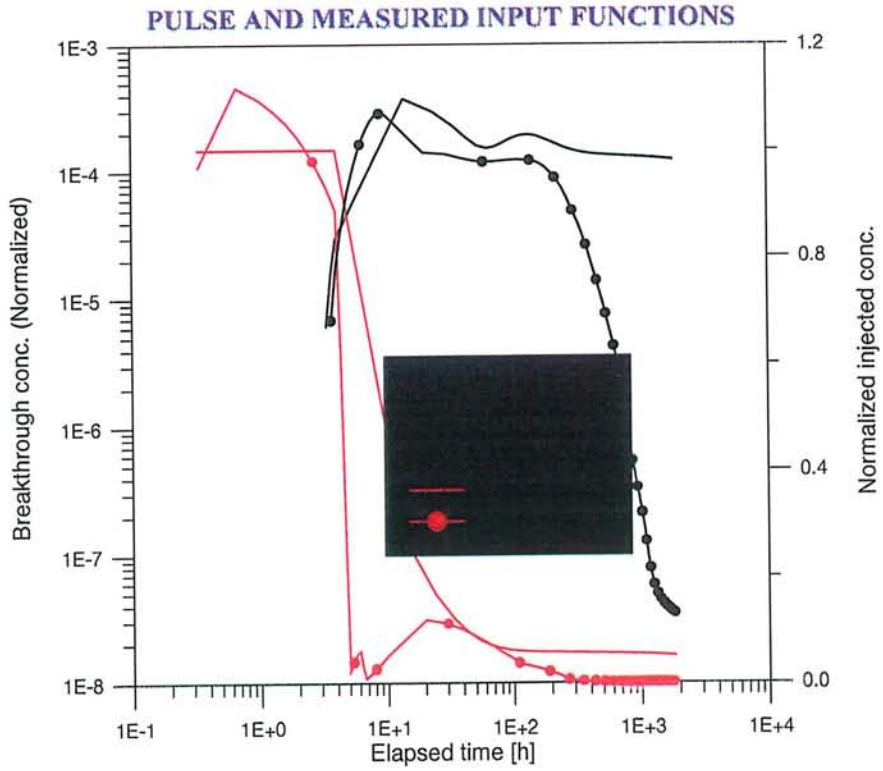
PULSE AND MEASURED INPUT FUNCTIONS
Breakthrough conc. (Normalized)
Normalized injected conc.
Elapsed time [h]
1E-3
1E-4
1E-5
1E-6
1E-7
1E-8
1.2
0.8
0.4
0.0
1E-1
1E+0
1E+1
1E+2
1E+3
1E+4

Fig. 12

BREAKTHROUGH CURVE AND NORMALIZED CUMULATIVE MASS

Tracer: HTO
in Sorbing Tracer Test 2
(STT-2)

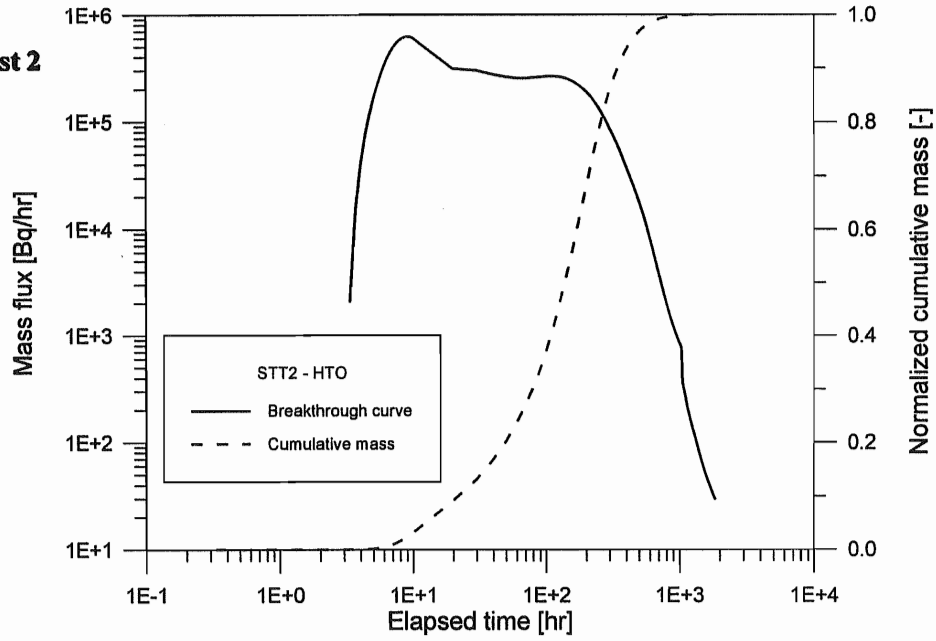

Task Force 4F

Fig. 13

BREAKTHROUGH CURVE AND NORMALIZED CUMULATIVE MASS

Tracer: Uranine
in Sorbing Tracer Test 2
(STT-2)

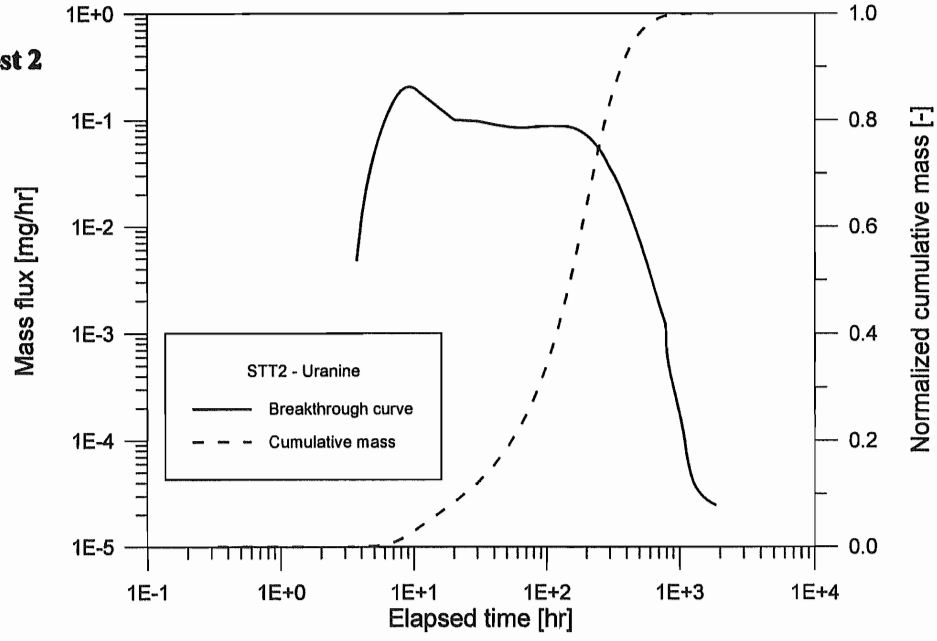

Task Force 4F

Fig. 14

BREAKTHROUGH CURVE AND NORMALIZED CUMULATIVE MASS

Tracer: ^{82}Br
in Sorbing Tracer Test 2
(STT-2)

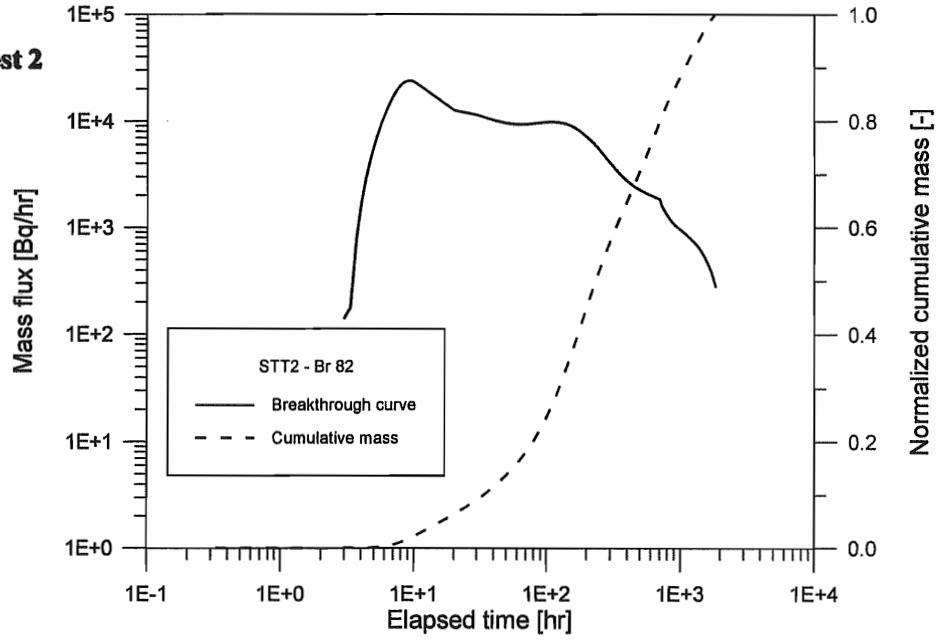

Task Force 4F

Fig. 15

BREAKTHROUGH CURVE AND NORMALIZED CUMULATIVE MASS

Tracer: ^{22}Na
in Sorbing Tracer Test 2
(STT-2)

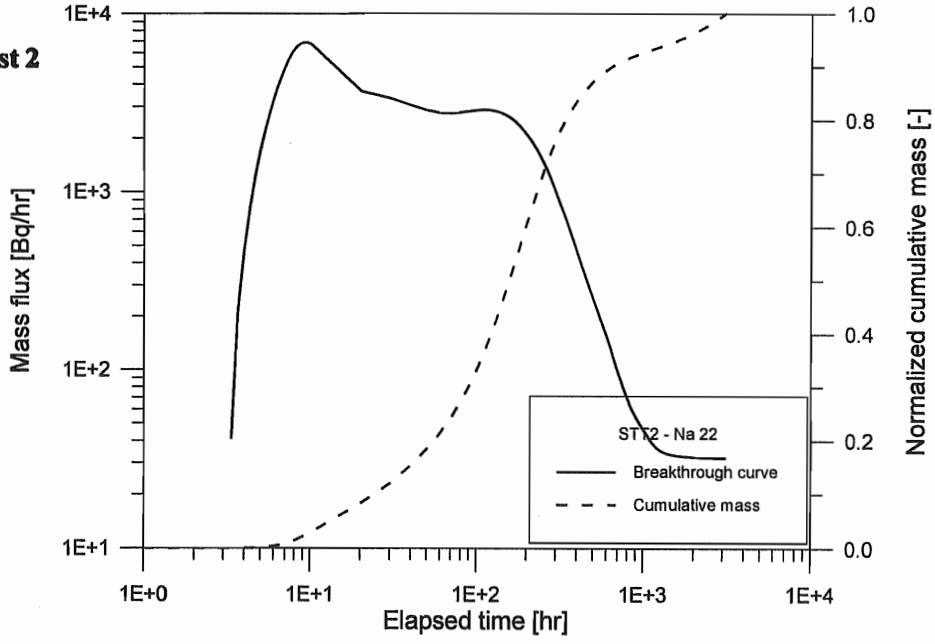

Task Force 4F

Fig. 16

BREAKTHROUGH CURVE AND NORMALIZED CUMULATIVE MASS

Tracer: ^{47}Ca
in Sorbing Tracer Test 2
(STT-2)

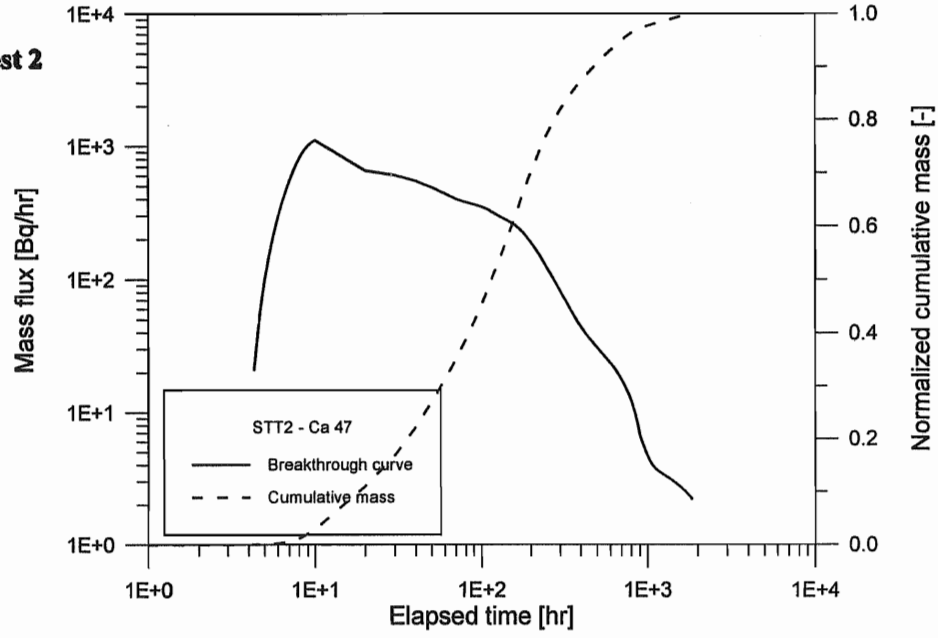

Task Force 4F

Fig. 17

BREAKTHROUGH CURVE AND NORMALIZED CUMULATIVE MASS

Tracer: ^{85}Sr
in Sorbing Tracer Test 2
(STT-2)

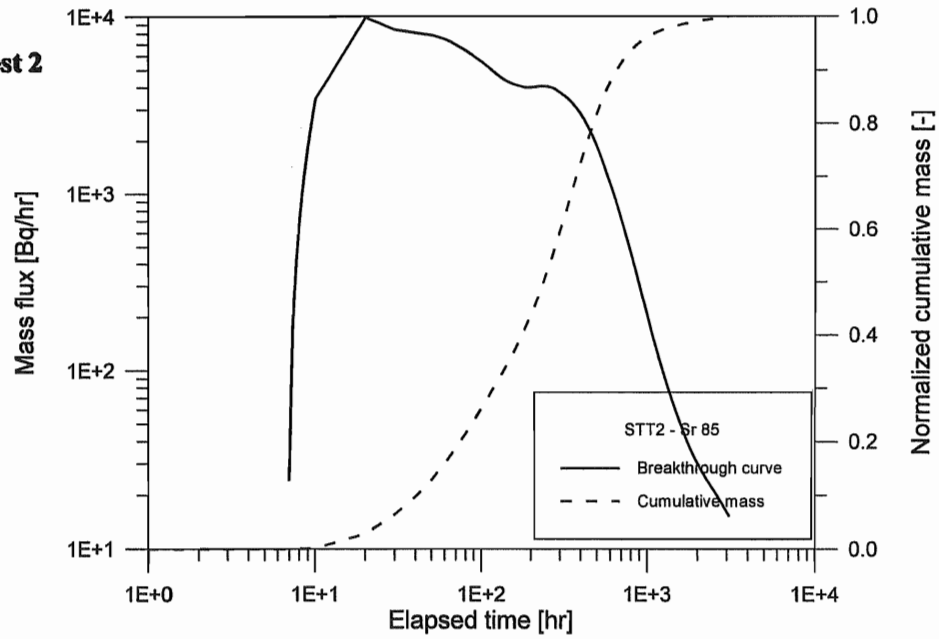

Task Force 4F

Fig. 18

BREAKTHROUGH CURVE AND NORMALIZED CUMULATIVE MASS

Tracer: ^{131}Ba in Sorbing Tracer Test 2 (STT-2)

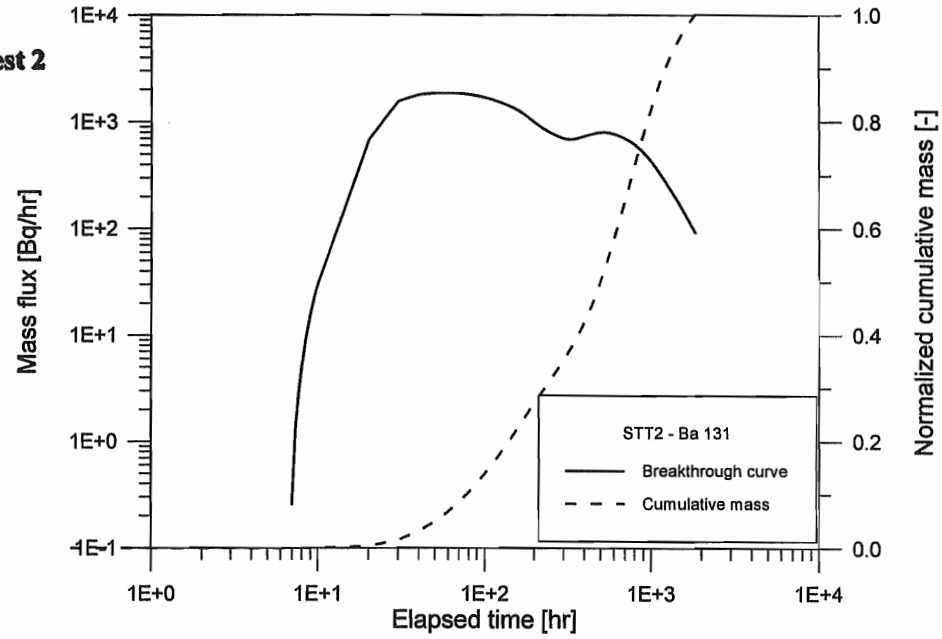

Task Force 4F

Fig. 19

BREAKTHROUGH CURVE AND NORMALIZED CUMULATIVE MASS

Tracer: ^{133}Ba in Sorbing Tracer Test 2 (STT-2)

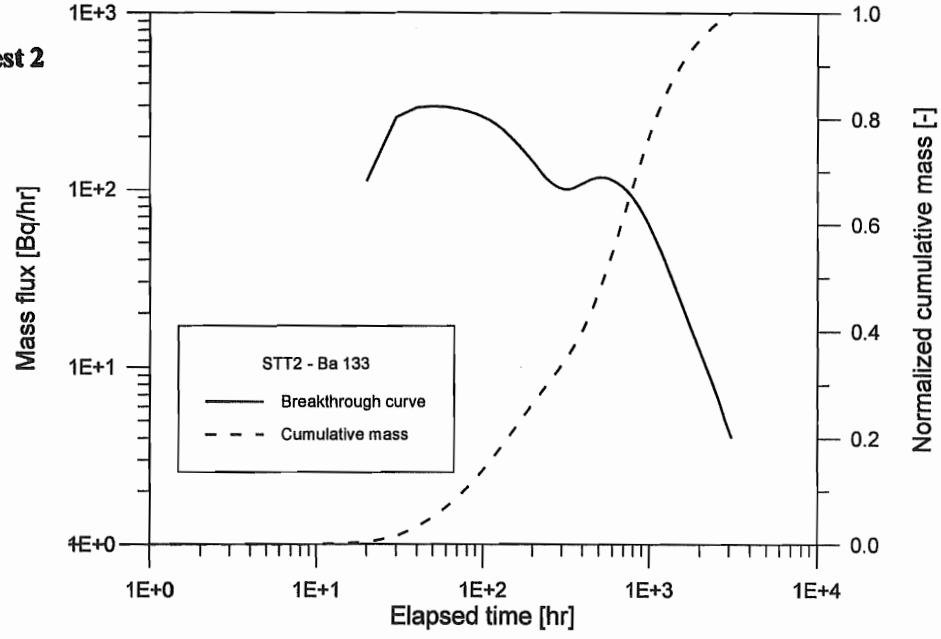

Task Force 4F

Fig. 20

BREAKTHROUGH CURVE AND NORMALIZED CUMULATIVE MASS

Tracer: ^{86}Rb
in Sorbing Tracer Test 2
(STT-2)

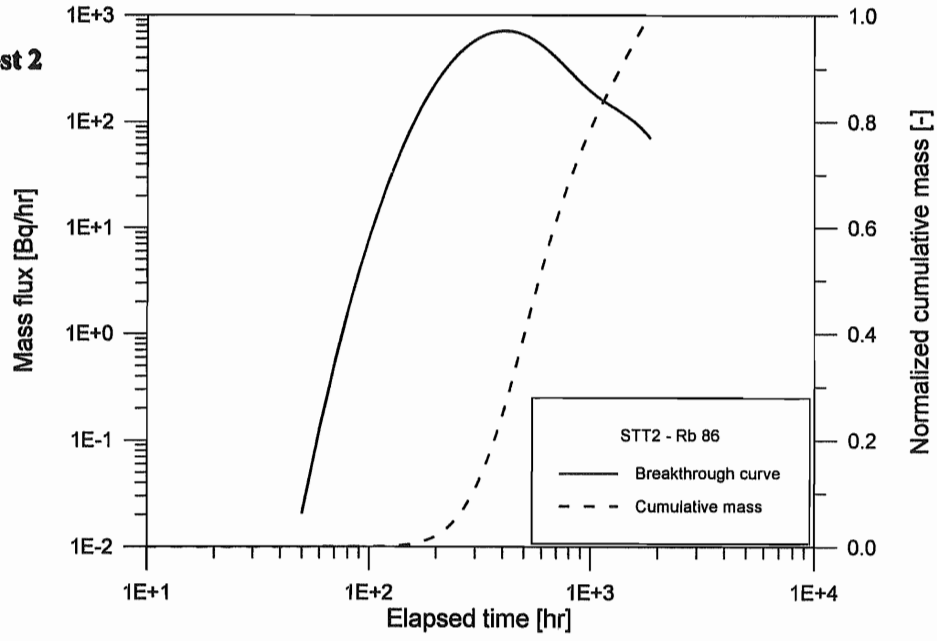

Task Force 4F

Fig. 21

BREAKTHROUGH CURVE AND NORMALIZED CUMULATIVE MASS

Tracer: ^{134}Cs
in Sorbing Tracer Test 2
(STT-2)

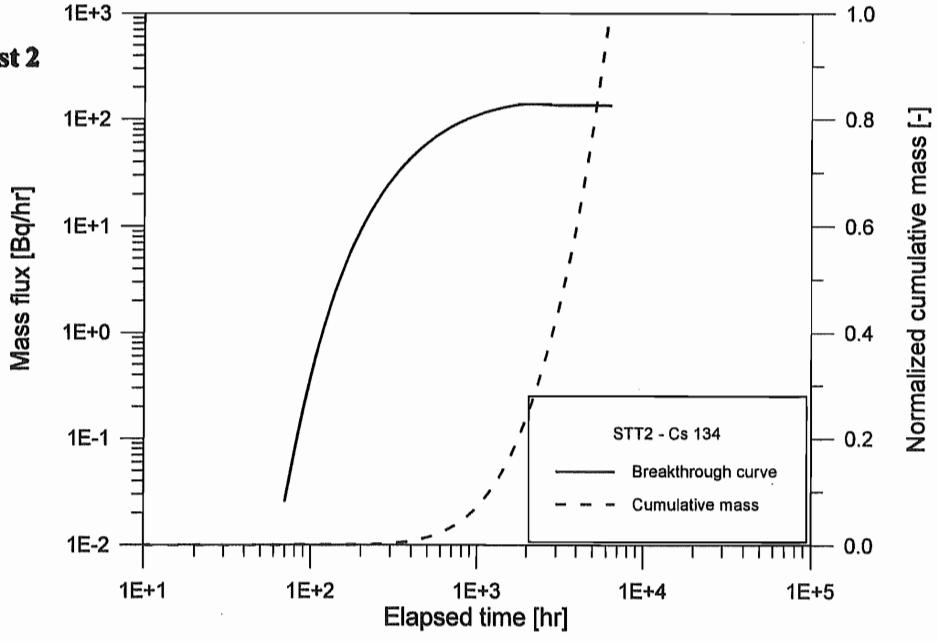

Task Force 4F

Fig. 22

Modelling of STT1 tracer test and Predictive computations of STT2

C Grenier (ANDRA/CEA)

TRUE Task 4F : Predictions for sorbing tracer tests STT2

C. Grenier and E. Mouche

1 Overview

Prediction for sorbing tracer tests requires modeling of the flow problem as well as transport processes. For STT2, radial convergent flow is monitored in Feature A between the wells KXTT4 R3 and KXTT3 R2. We first provide here with a brief overview of the work performed :

- For the flow problem, we first check that the natural flow is of secondary importance compared to the radial converging flow monitored in the experiment. The flow paths obtained for a mean constant transmissivity field showed very similar to the ones simulated in a purely radial converging flow. We secondly tried to address the problem of heterogeneity of the fracture transmissivity. This was done very roughly by simply simulating the flow paths for kriged maps of transmissivity. The kriging was done firstly based on transmissivity data alone and secondly on transmissivity and natural flow head data. The change in the flow paths showed to be of minor importance in the first case and important in the second case.

- The transport problem is then modeled for the flow obtained with the constant transmissivity field. Furthermore, transport is limited to a single flow path as opposed to the 2D fracture plane. It is indeed supposed that for radial converging flow, transverse dispersion (causing diffusion to side flow paths) is of secondary importance for the modeling of breakthrough curves at the outlet. We try here to address the issue of very large dispersivity observed by former tracer experiments between KXTT4 and KXTT3 ($\alpha = 1.6m$ was fitted to the curve for a inter well distance of $4.68m$). This is done following the line by PSI (see for instance [*Jakob and Heer 98*]), modeling diffusion mechanisms into different diffusive zones addressed below as matrix diffusion zones (gouge material, dead end pores, fine fracturation in granite close to the fracture ...). Doing so, the dispersion coefficient used for fracture transport remains compatible with the fracture heterogeneity. A preliminary study of the impact of matrix diffusion on breakthrough curves is provided for a simple analytic model. Calibration procedure is then fulfilled with PDT3 data leading to effective matrix diffusion coefficient and specific surface. The system geometry involved is limited to the size of the fracture opening ($1.7\ 10^{-3}m$) and includes an open fracture (advection and dispersion processes, retardation factor) as well as an equivalent "matrix"

(diffusion, adsorption) accounting for the above diffusion mechanisms. Predictive calculations are provided for non sorbing tracers (Uranin, HTO, Br82) as well as weakly sorbing tracers (Na22, Sr85, Ca47) based on the adsorption data provided. These calculations should although be considered as preliminary results for two reasons. First, a better characterization of the gouge is required as well as adsorption measurement of the gouge material. It is probably different from the Äspö diorite and Feature A material measurements provided. Second, due to a lack of time, we could not go through a thorough use of STT1 data that would improve the quality of the model.
Predictions for more sorbing tracers (Ba131, Ba133, Rb86, Cs134) are not provided here because the model leads to exessively large fracture retardation factors for these tracers.

We refer here to the Feature A data provided in [*Andersson et al. 97*] [*Winberg et al. 98*].

2 Flow problem

The purpose of this part of the work is to quantify the importance of natural flow compared to monitored radial converging flow (KXTT4 to KXTT3) as well as the impact of local potential heterogeneity on the flow paths. This is achieved by simulating the flow as well as flow paths within the CASTEM2000 code for the domain and discretization provided on figure 2(a). We first take the geometric mean of measured transmissivity into account as well as head boundary conditions corresponding to a constant head gradient inferred from natural flow head data superposed to the heads associated to flow converging to the well ($Q = 0.2\ l/min$). The flow paths obtained show that natural flow is of secondary importance (see figure 2(b)). The same was done for kriged maps of transmissivity conditional to transmissivity data measured at the boreholes. In a second step, kriged maps of transmissivity based on transmissivity data as well as natural flow heads are taken into account. The resulting flow paths are provided on figures 2(c) and 2(d) and show that little change is obtained in the first case whereas flow paths are strongly affected in the second case. The same conclusions can be drawn from the corresponding arrival times. It remains that these calculations involve a correlation length of $\lambda = 0.4m$ (according to the data provided in [*Winberg et al. 96*]) for a distance between KXTT4 and KXTT3 of $4.68m$. This means that the data density is quite scarce. It would be interesting to take all kind of additional data into account, like for instance head data obtained in different pumping conditions. This was not done here but partially in a former work presented at the Kamaishi meeting. The results were not very conclusive and one of the major conclusion was that the drawdown in KXTT3 could not be matched. Further work has been done on the subject since then [*Darcel et al. 99*] but was not applied to Feature A.
In the following, we consider the classical radial converging flow for a constant transmissivity field (geometric mean of measured transmissivities at the boreholes : $logT = -7.44m^2/s$).

3 Transport problem

We aim here at modeling the strong dispersivity observed for the KXTT4 to KXTT3 path. The value of dispersivity fitted to the breakthrough curve is not coherent with the fracture heterogeneity assumptions provided in [*Winberg et al. 96*]. The large dispersion observed should then be related to effects due to the presence of intersecting fractures [*Winberg et al. 98*] or to matrix diffusion effects. We proceed here in the line of PSI [*Jakob and Heer 98*], modeling the spreading of the breakthrough curve by "matrix diffusion". The diffusion zones should although include gouge filling zones, diffusion into altered cristaline blocks, dead pores ... In addition, as is further described below gouge filling provides different flow paths increasing the contact surface between the water flow and the "matrix" zones.

We firstly make a preliminary fit on PDT3 data by means of a simple model providing analytical solutions : convection in the fracture and orthogonal 1D diffusion in the matrix (see [*Moreno et al. 1985*] for instance). This model is of interest to us since we do not consider large dispersivity in the fracture and because the approximation to transport in radial converging flow is done here by replacing the actual velocity field by constant velocity at half wells distance ([*Mouche et al. 1985*] and [*Lenda and Zuber 1985*]). The analytical solution for a step at C_0 and of duration t_0 is given below :

$$C(x,t)/C_0 = [erfc(\frac{x}{\sqrt{D_f(t-t_w)}}) - erfc(\frac{x}{\sqrt{D_f(t-t_w-t_0)}})] \quad (1)$$

This system depends on two parameters : water arrival time $t_w = x/U$ and a diffusion coefficient having no physical meaning $D_f = (eU)^2/(\omega^2 D_p)$ (where U stands for water velocity, ω for matrix porosity, D_p for matrix pore diffusion coefficient). In the calibration situation provided, eU is imposed by the flux in the flow tube, the others result from calibration. Parameters t_w and D_f can be chosen independently. Solutions corresponding to different values of D_p are given on figure 3(a). Variations of t_w lead to simple translation of the curves on the time axis (delay). The duration t_0 of the signal is the same as the injection time for PDT3. PDT3 breakthrough curve is provided in full line. We conclude that diffusion into so called matrix zones can account for a large part of the tailing of this curve.

The actual system used in the rest of the study is given on figure 1 and the equation solved is given below for the fracture,

$$R_F \frac{\partial C}{\partial t} = \frac{\partial C}{\partial x}(-UC + \alpha U \frac{\partial C}{\partial x}) \quad (2)$$

and the matrix :

$$R_M \frac{\partial C}{\partial t} = D_p(\frac{\partial^2 C}{\partial x^2} + \frac{\partial^2 C}{\partial z^2}) \quad (3)$$

The model involves dispersivity α in the fracture and limited matrix diffusion ($Z = 1.\ 10^{-3} m$). U is the pore velocity at half distance between the wells. The flow direction is given by x and the z direction is orthogonal in the matrix. Retardation factors are computed as $R_F = 1 + \frac{2K_a}{e}$ and $R_M = 1 + \frac{(1-\omega)\rho_S K_d}{\omega}$. K_a is the surface sorption coefficient, K_d the bulk sorption coefficient in the matrix, e the fracture aperture, ρ_S the

granite mass density, ω the matrix porosity, D_p the matrix pore diffusion coefficient. The total depth of the system equals the fracture aperture provided ($e + Z = 1.7\ 10^{-3}m$). The calibration procedure is fulfilled on PDT3 data adjusting the dispersion coefficient, matrix porosity and matrix diffusion coefficient. The system showed weakly sensitive to the value of the dispersion coefficient. The final data set used is given below on table 1 and the comparison between PDT3 and the fit is provided on figure 3(b). Effective matrix diffusion coefficient is mainly increased through the value of matrix porosity. The value of matrix porosity chosen here is not a physical value but accounts for large contact surface area. Such a situation is found for a geometry of the gouge filling leading to multiple flow paths : we consider here a model of numerous parallel thin fractures within a matrix unit. This leads to increasing in the contact surface between the flow and the matrix. The sum of the small aperture sizes equals the final aperture size in the equivalent model. The values for the best fit are provided in table 1. Predictions for non sorbing tracers

Fracture aperture	$7.\ 10^{-4}m$
Matrix diffusion depth	$7.\ 10^{-4}m$
Fracture porosity	1
Matrix porosity	1
Velocity in fracture	$3.25\ 10^{-4}m/s$
Dispersion coefficient	$0.1m$
Matrix pore diffusion coefficient	$2.3\ 10^{-10}m^2/s$

Table 1: Fitted values according to PDT3

breakthrough curves is made with this data set and is provided on figure 4 : figure 4(a) gives the mass flux normalized to the injected mass and 4(b) the cumulative normalized mass. The restitution times corresponding to 5%, 50%, 95% are given below in table 4.

Predictions for sorbing tracers are provided on figures 4. The increase of contact surface for matrix diffusion considered in our model leads to an increase of surface for the adsorption phenomena on fracture walls. The resulting retardation coefficients are given below in table 2. Results given on figure 4(b) and in table 4 show different recoveries below 100%. They are due to the short half life of the tracers provided in table 3.

These results should anyway be considered preliminary for two reasons. First, the model explicitly deals with gouge filling material for which sorbing measurement results are not provided. Generally, a more thorough characterization of possible gouge filling material and geometry is required. In the predictions, we used the data provided for the Äspö diorite. Secondly, due to a lack of time, we could not work on the STT1 data set before predicting STT2. This would have been necessary because the retardation factors obtained for the moderate sorbing tracers (Ba131, Ba133, Rb86, Cs134) are large, leading to strong delay in the breakthrough curve. This is the reason why no predictions for these tracers are given in the present study.

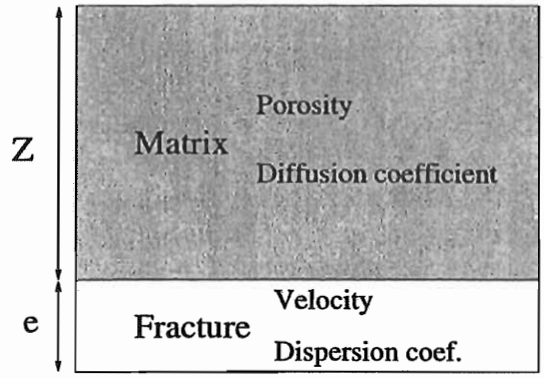

Figure 1: System geometry

Tracer	$R_{fracture}$	R_{matrix}
Na22	1.0	4.7
Sr85	1.2	13.5
Ca47	1.1	14.8

Table 2: Retardation factor introduced for sorption on fracture walls and into the bulk of the matrix

Tracer	HTO	Br82	Na22	Sr85	Ca47
Half life	12.3 y	35 h	2.6 y	65 d	4.5 d

Table 3: Half lives for the different isotopes involved

Tracer	$t_{5\%}$	$t_{50\%}$	$t_{95\%}$	Mass recovery
Uranin	11	54	227	100
HTO	10.5	49	211	100
Br82	10	61	-	79
Na22	25	78	263	100
Sr85	55	142	902	96
Ca47	60	223	-	56

Table 4: Restitution times (hours) for 5%, 50% and 95% of injected mass, mass recovery (percentages)

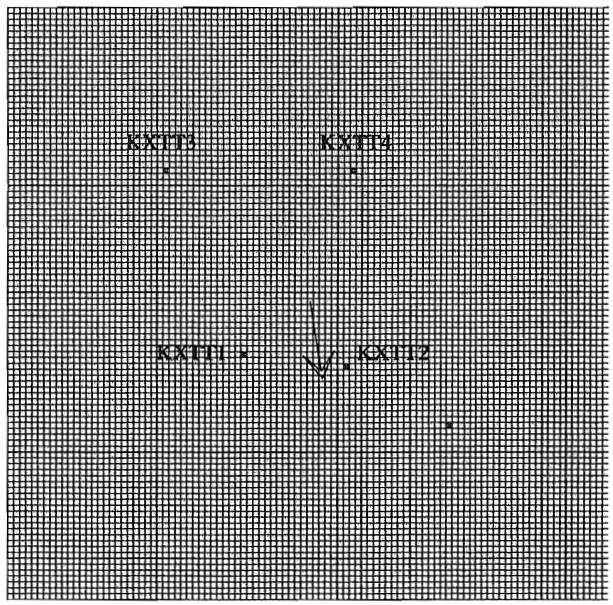

(a) Simulated fracture geometry and natural head gradient direction

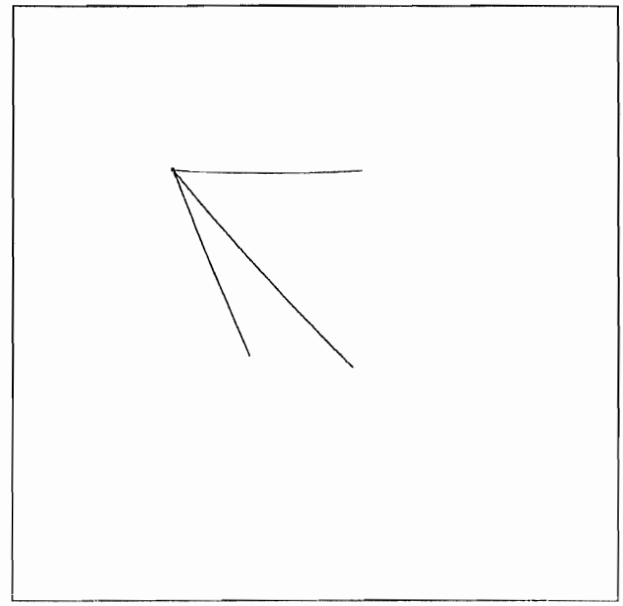

(b) Stream lines towards KXTT3 for $T = T_{geom}$

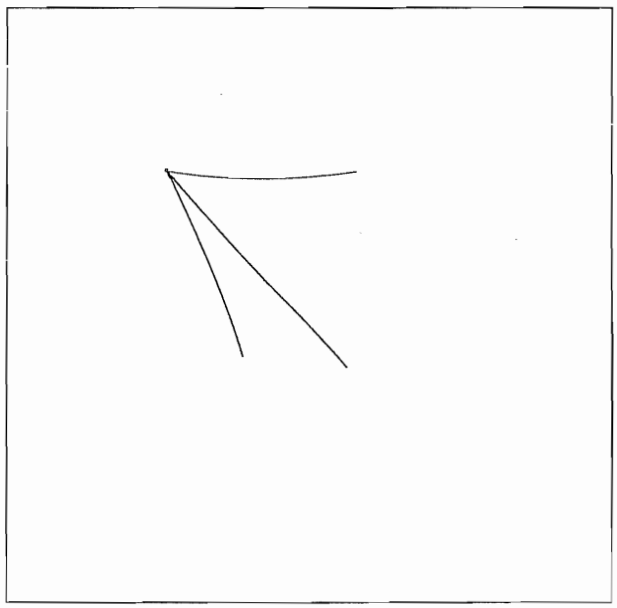

(c) Stream lines towards KXTT3 for $T = e^{(Y|Yi)}$

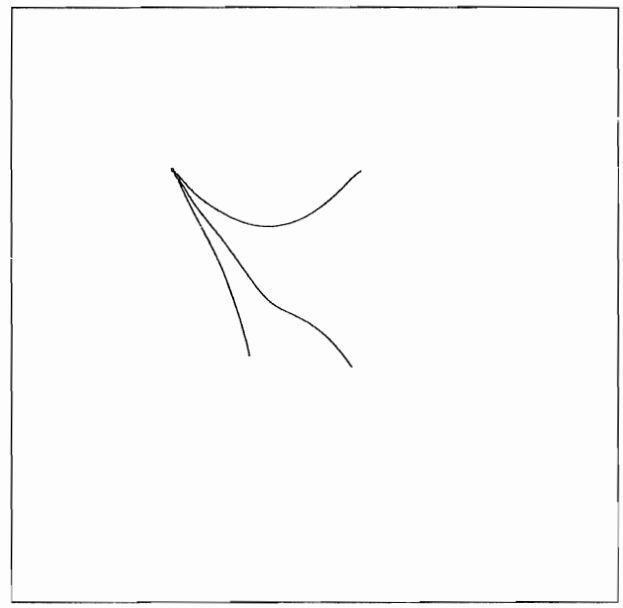

(d) Stream lines towards KXTT3 for $T = e^{(Y|Yi\&Hj)}$

Figure 2: Flow problem : fracture geometry, mean natural head gradient and stream lines obtained for different transmissivity fields

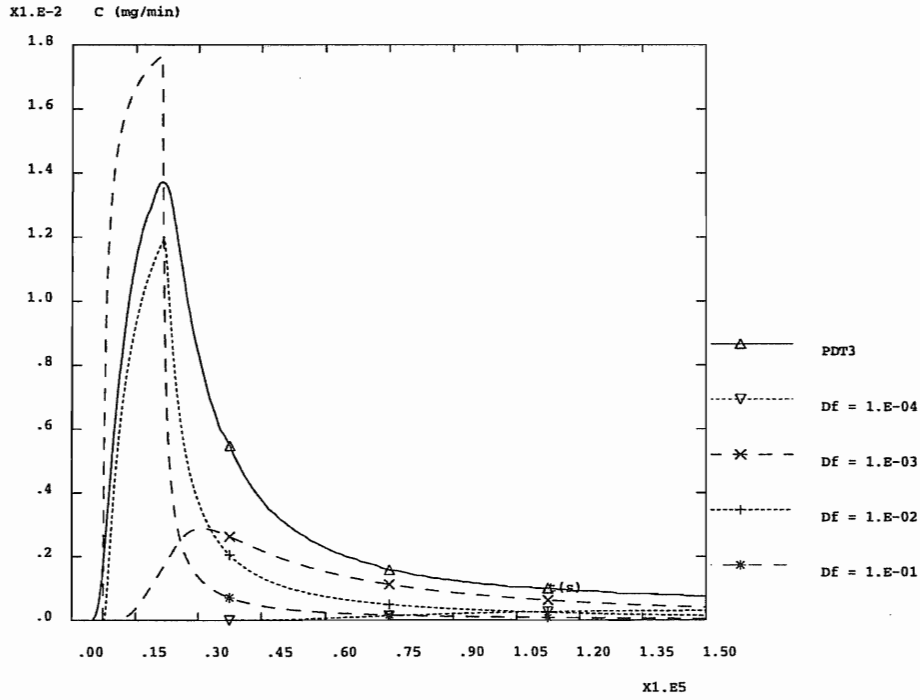

(a) Breakthrough curves for the simple analytical model (different values of Df) as well as for PDT3

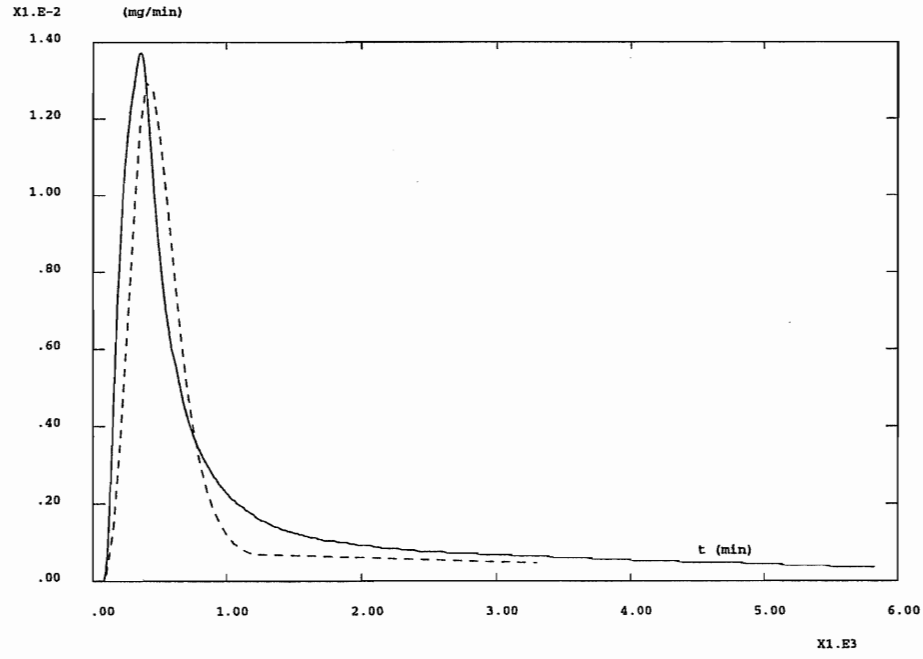

(b) Best fit for the model (dots) and PDT3 (full line)

Figure 3: Calibration with PDT3

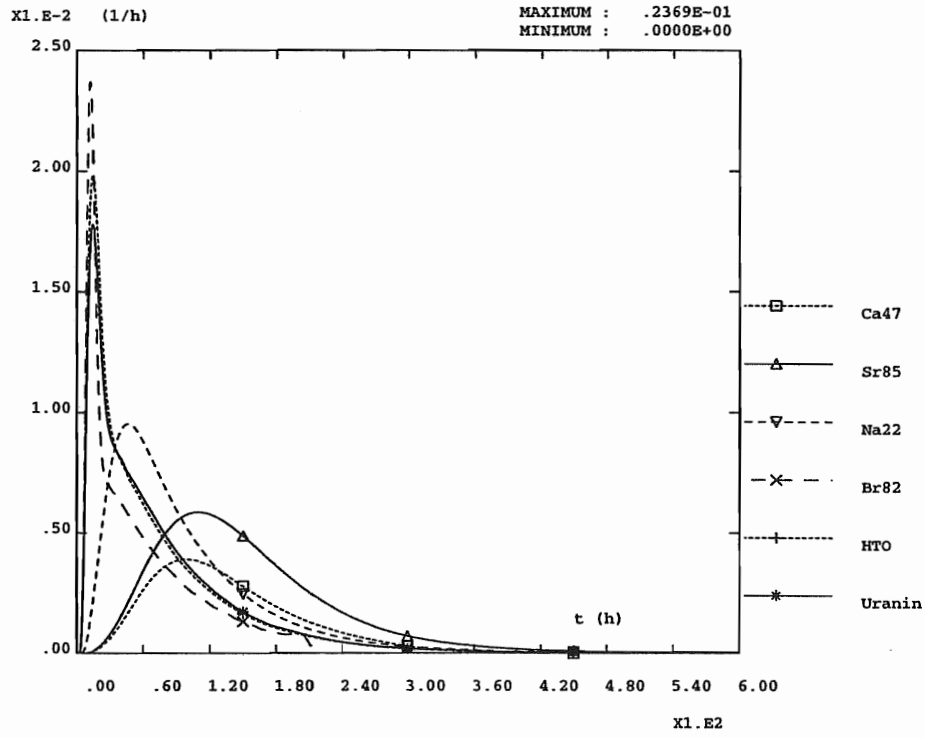

(a) Normalized mass flux for time span (0 - 600h)

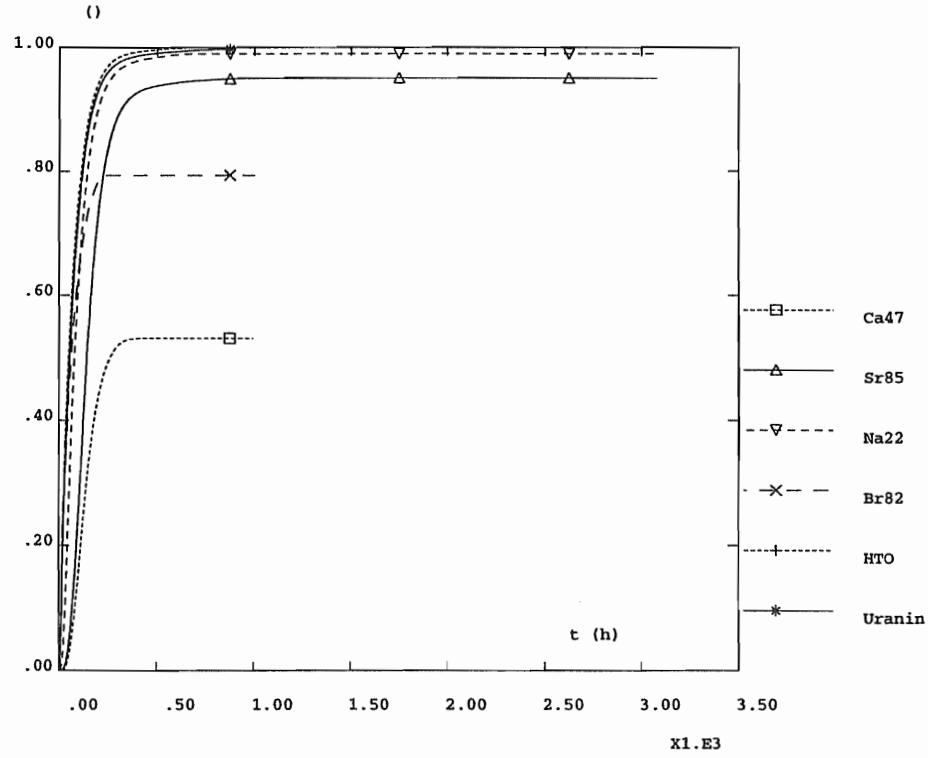

(b) Normalized cumulative flux

Figure 4: Predictions for STT2

References

[*Andersson et al. 97*] *TRUE first stage tracer test programme - Experimental plan for tests with sorbing tracers at the TRUE-1 site.* P.Andersson, J. Byegard, V. Cvetkovic, H. Johansson, R. Nordqvist, J.-O. Selroos, A. Winberg. HRL - 97 - 07.

[*Darcel et al. 99*] *Influence of pumping head data in the conditional estimation of a transmissivity field.* C. Darcel, E. Mouche, C. Grenier. In the proceedings of the ModelCARE'99 Conference in Zurich, 1999

[*Jakob and Heer 98*] *Predictions for the Task 4E tracer migration experiments at the TRUE-1 site.* In the proceedings of the 10th meeting in Kamaishi. HRL - 98 - 01.

[*Lenda and Zuber 1985*] *Tracer dispersion in groundwater experiments.* A. Lenda, A. Zuber. Isotope Hydrology, Vienna, Austria, 1970

[*Moreno et al. 1985*] *Analysis of some laboratory tracer runs in natural fissures.* L. Moreno, I. Neretnieks, T. Eriksen. WRR, Vol 21, No 7, PP 951-958, 1985

[*Mouche et al. 1985*] *Scoping calculations on sorbing tracer tests STT1.* In the proceedings of the 10th meeting in Kamaishi. HRL - 98 - 01.

[*Winberg et al. 96*] *Descriptive structural-hydraulic models on block and detailed scales.* A. Winberg editor. Final Draft 1996-02-10.

[*Winberg et al. 98*] *Updated structural model of the TRUE-1 block and detailed description of feature A.* A. Winberg, P. Andersson, J. Hermanson, J. Byegard. Final Draft 1998-12-23.

Contents

- Conditioning on data for flow model

- Reasons for high dispersivity by KXTT4-KXTT3 ?

→ Test the hypothesis of PSI with the Lenda Zuber transport model.

Flow model : stream tubes

Based on the following transmissivity fields

- T = Teq
- T = exp (<Yc|Yi>)
- T = exp (<Yc|Yi,Hj>)

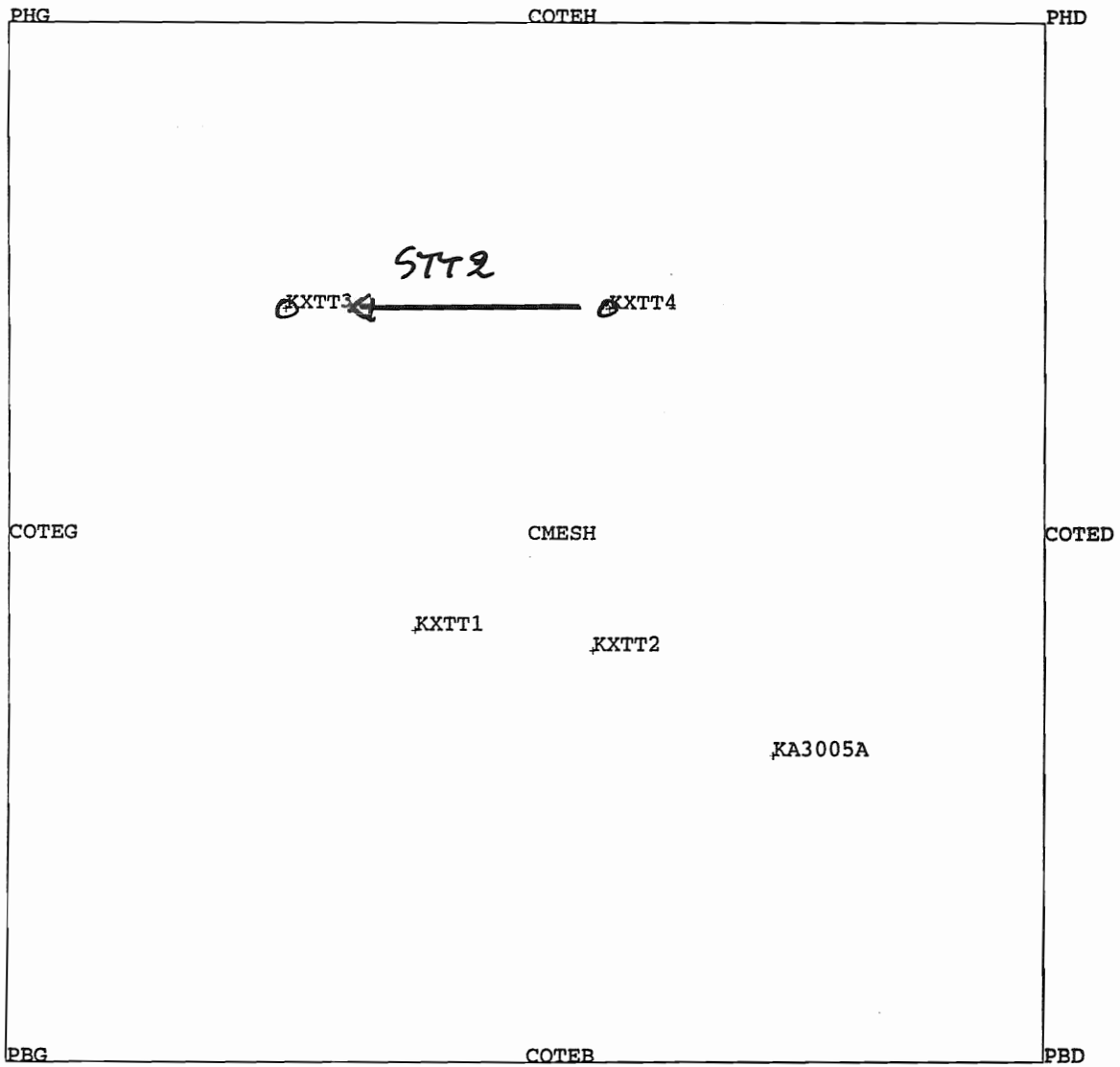

position des différents puits, dans le maillage

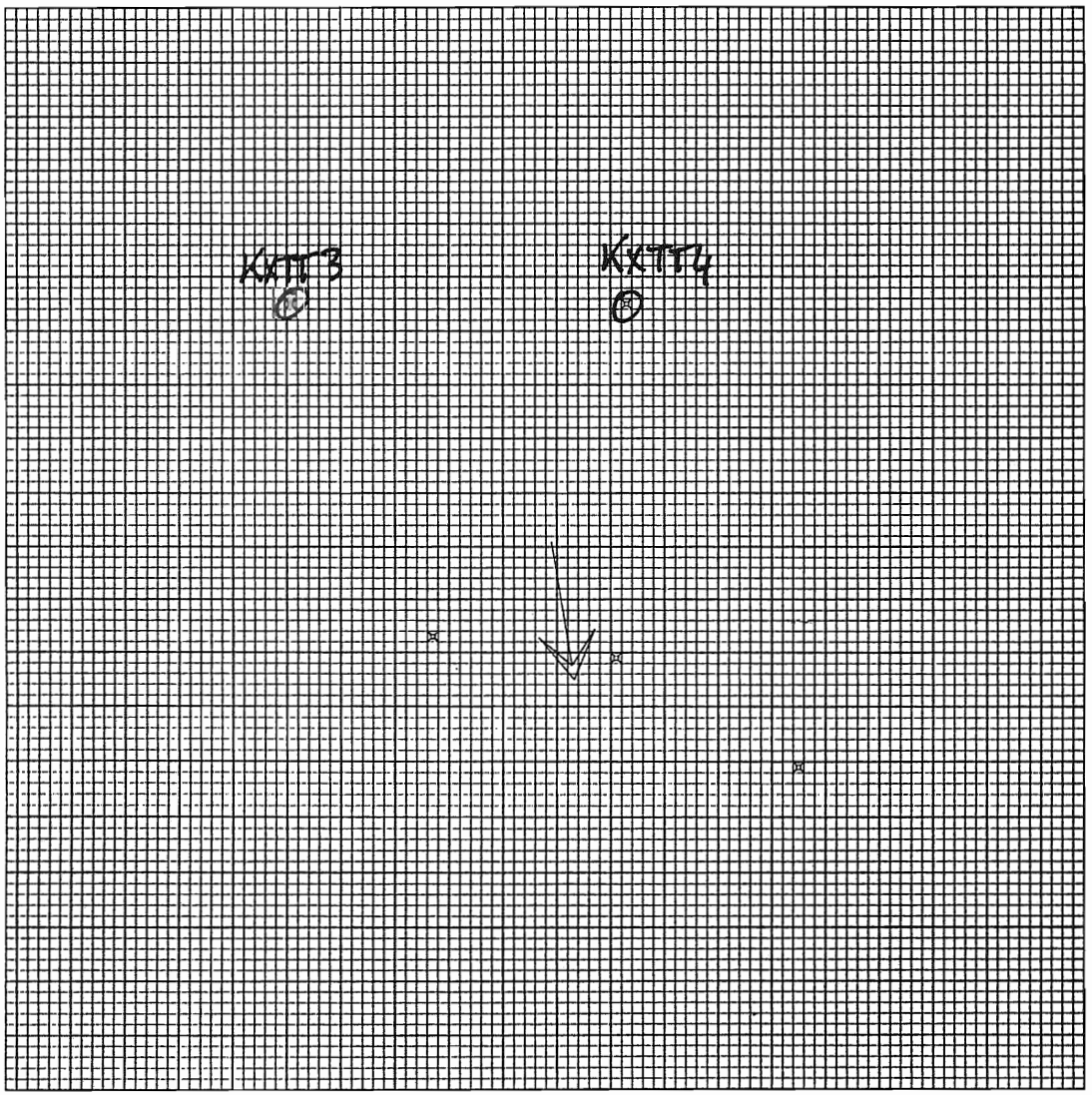

COMPOSANTES
VECTEURS

gdx gdy

-GradH

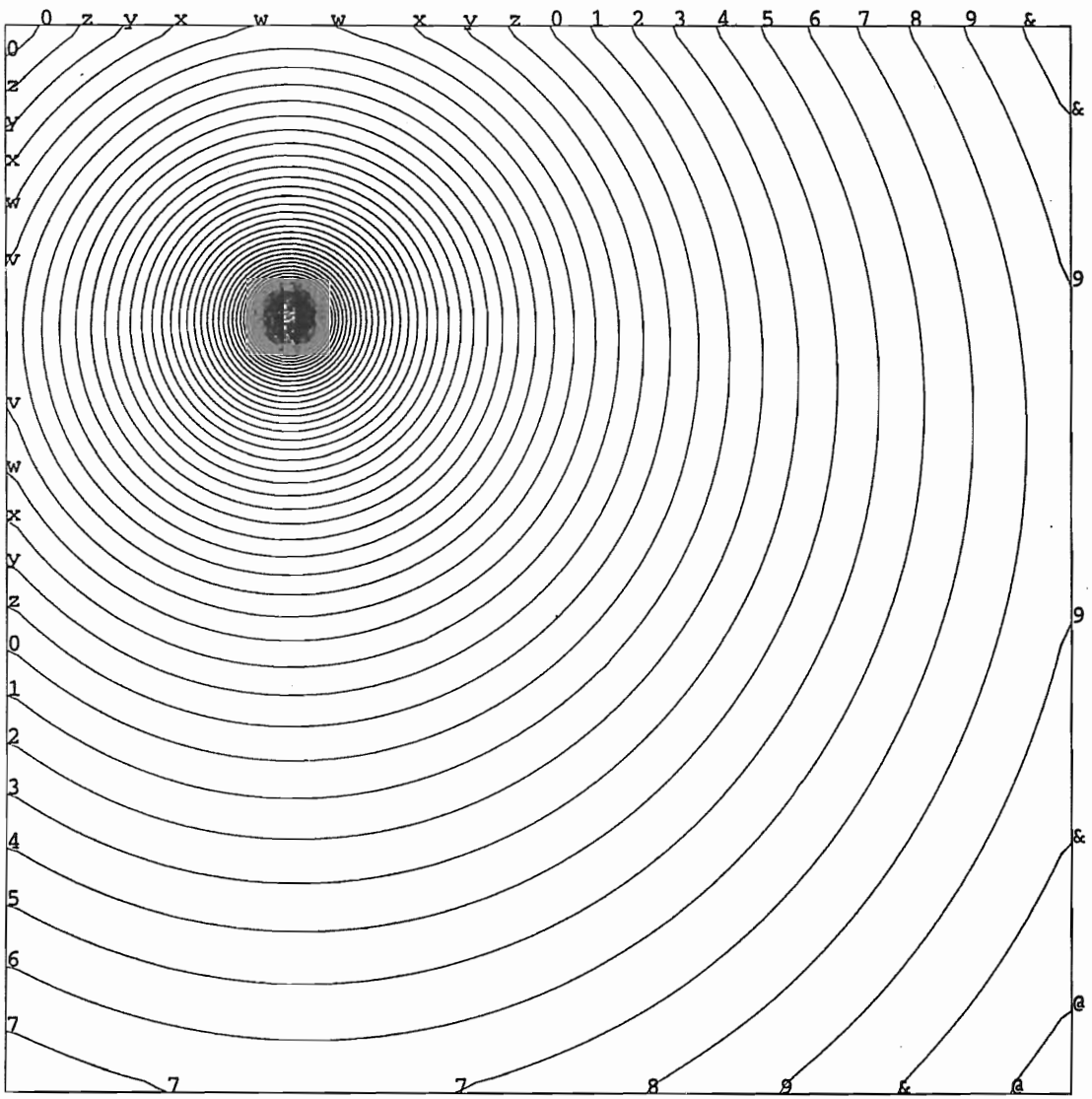

VAL - ISO

>-2.50E+01

< 3.39E+01

A -25.

D -22.

G -19.

J -16.

M -13.

P -11.

S -7.9

V -5.2

Y -2.4

b .34

e 3.1

h 5.9

k 8.6

n 11.

q 14.

t 17.

w 20.

z 22.

2 25.

5 28.

8 31.

@ 33.

Charges aux noeuds

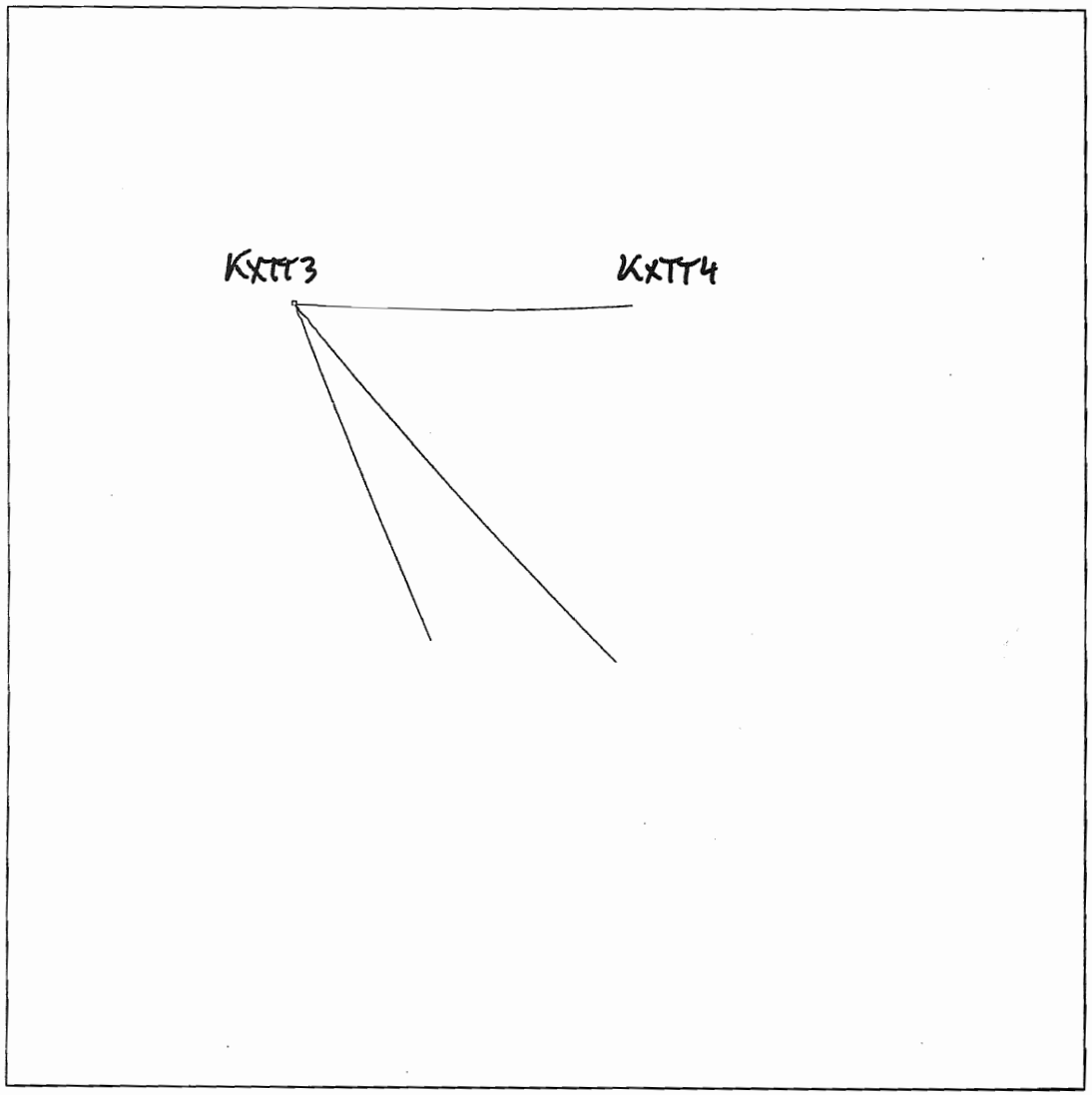

$T = T_{eq}$

Lignes de courant, Q = 0.2 1/min

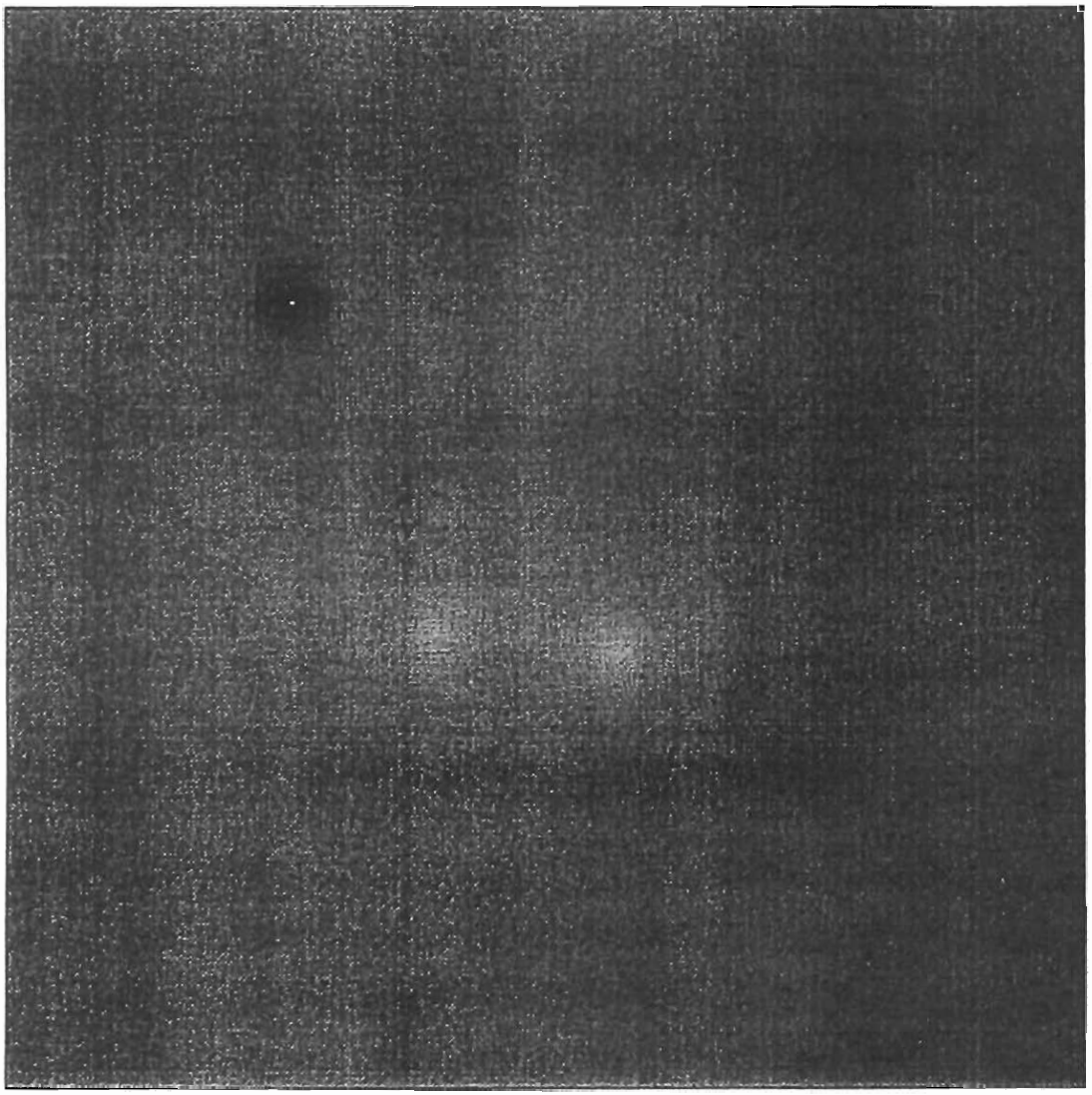

$\langle Y^c | Y_i \rangle$

Moyenne conditionnelle de Y sachant Yi

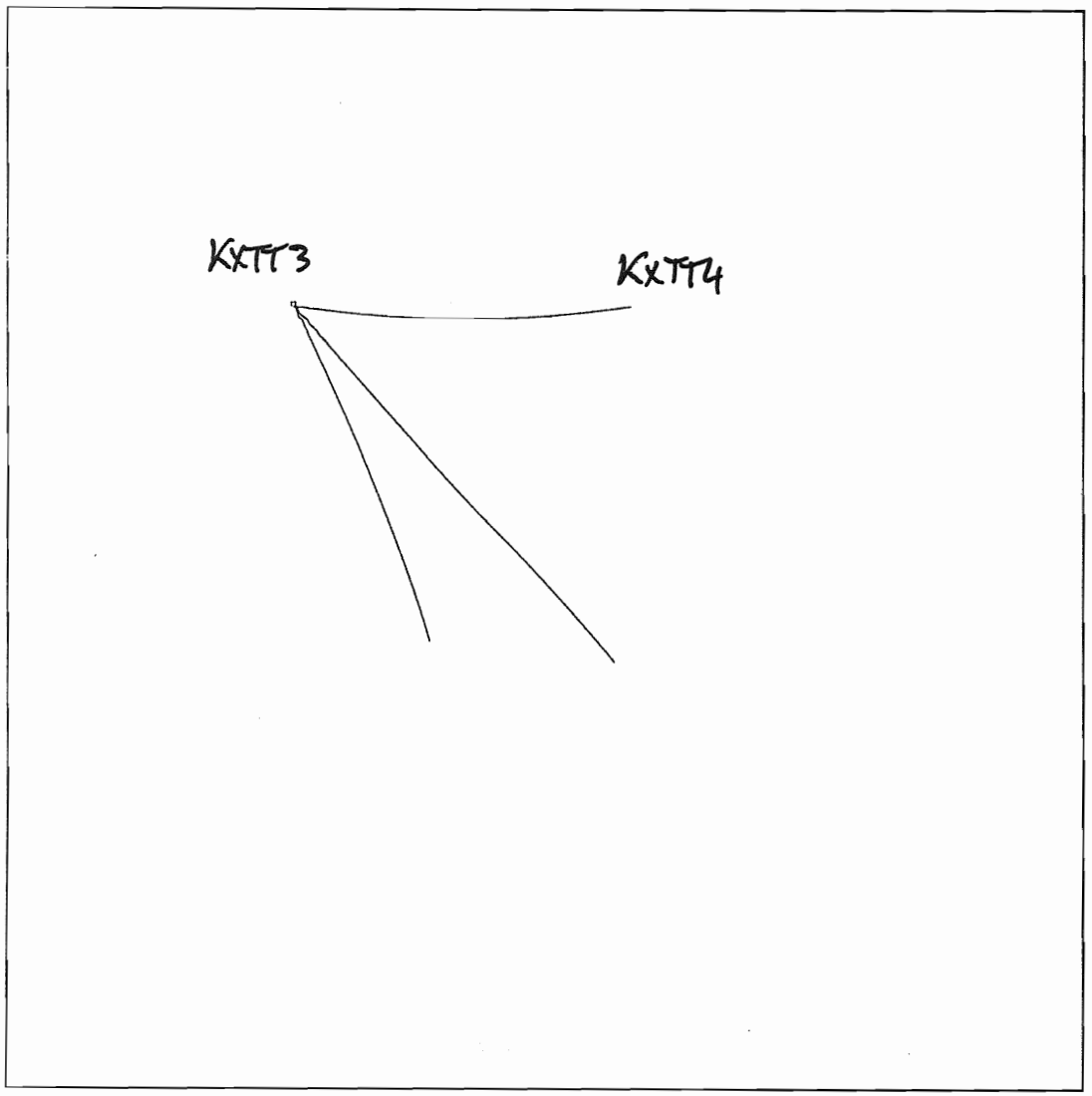

$$T = e^{\langle y^c | y_i \rangle}$$

Lignes de courant, Q = 0.2 l/min

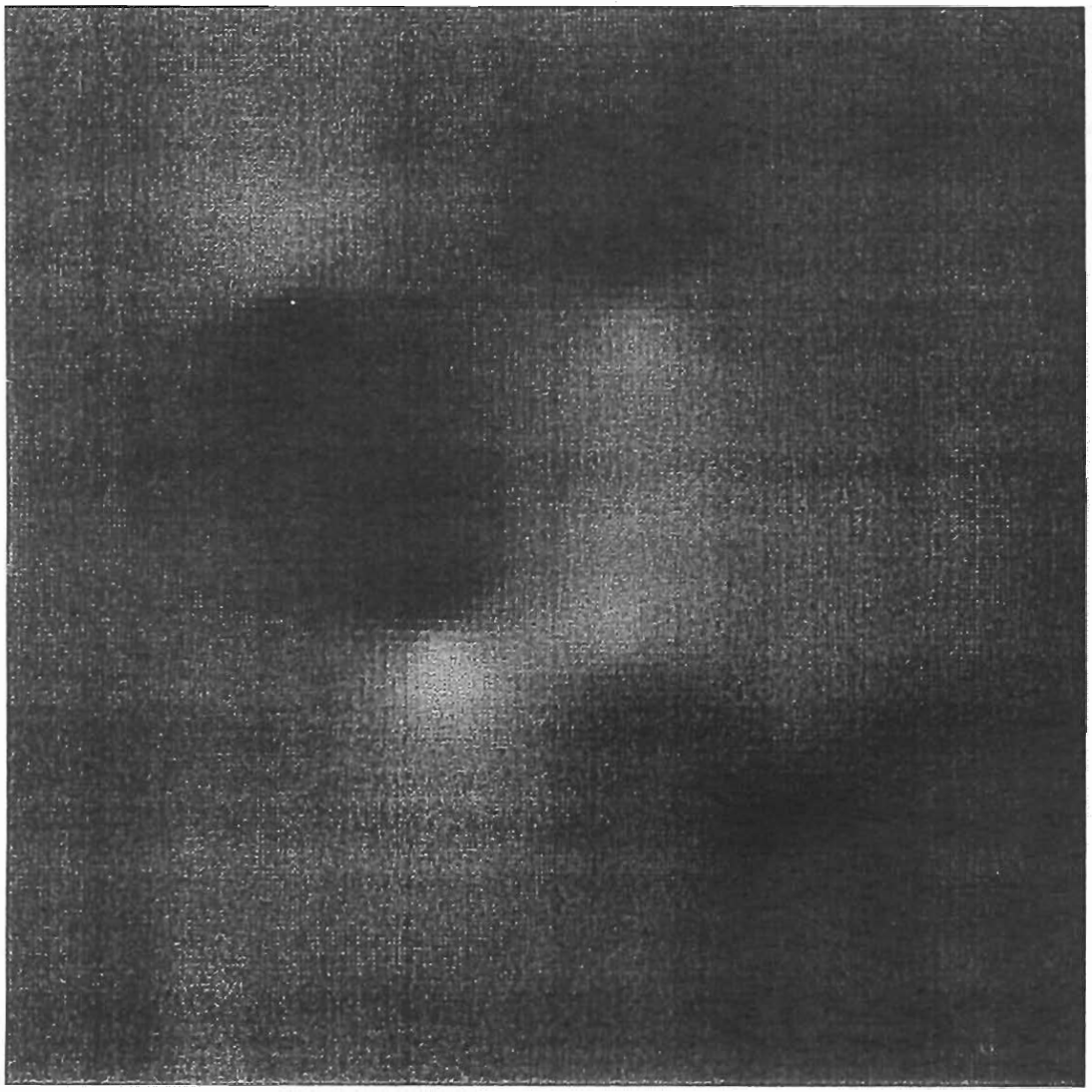

$\langle Y^c | Y_i \& H_j \rangle$

Moyenne conditionnelle de Y sachant Yi et Hj

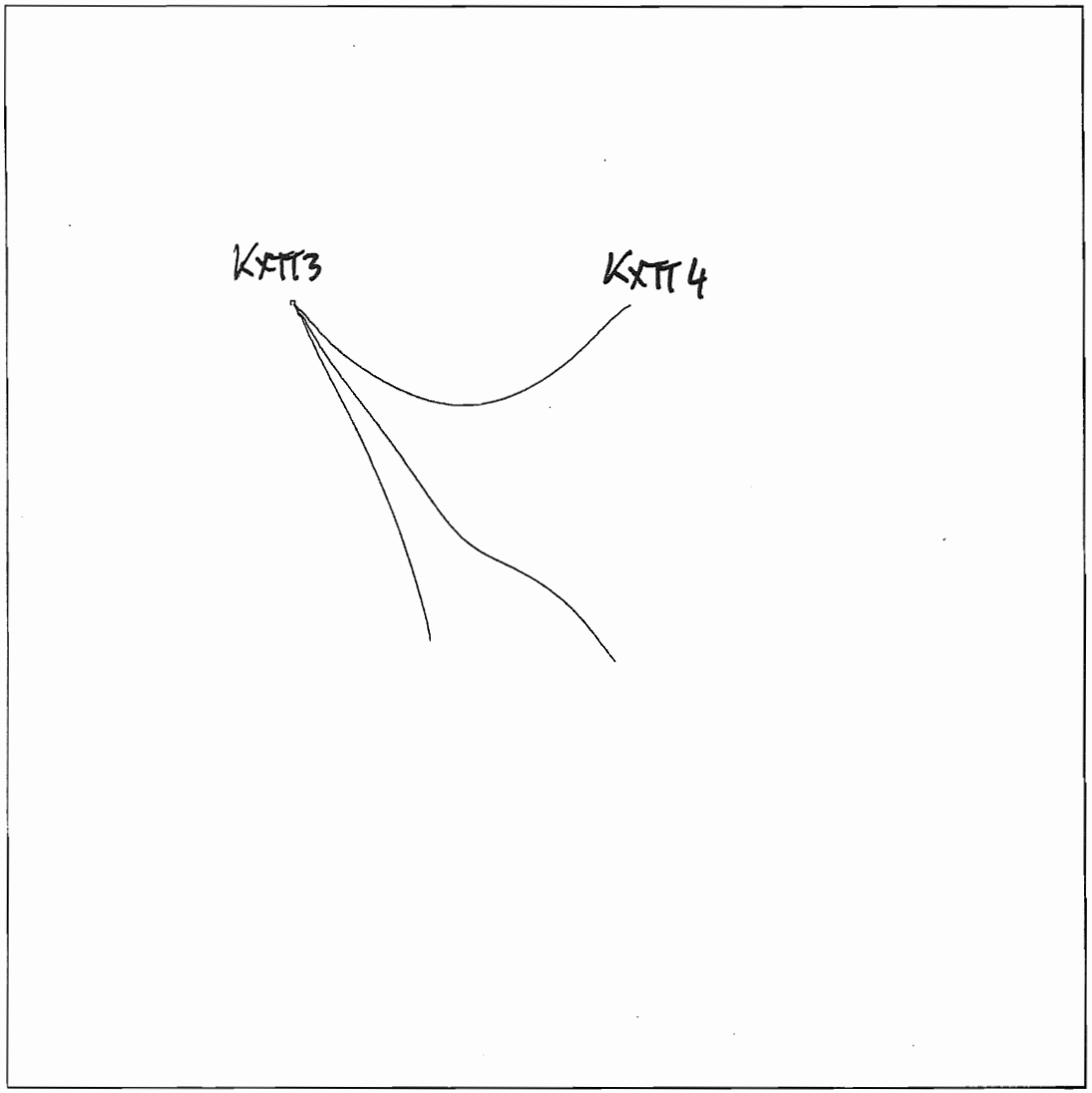

$$T = e^{\langle Y^c | Y_i \& H_j \rangle}$$

Lignes de courant, Q = 0.2 l/min

Transport model

- For constant transmissivity field Teq
- Lenda and zuber 1D approximation
- Matrix diffusion :

  → By KXTT4-KXTT3 take the large dispersion into account by a matrix diffusion process ?

Neretnieks model

$$Cf = Co\ [erfc(x/\sqrt{Df\ (t-Tw)}) - erfc(x/\sqrt{Df(t-Tw-T0)}]$$

→ Two parameters :

- $Tw = X/U^{1/2}$
- $Df = (eU^{1/2})^2 / (\omega^2\ Dp)$

→ Provides e and (ω, Dp)

Calibration procedure

- First, use the simple Neretnieks model : convective transport in fracture and 1D diffusion in matrix
- Second, test the set of values obtained on the Lenda and Zuber model with matrix diffusion

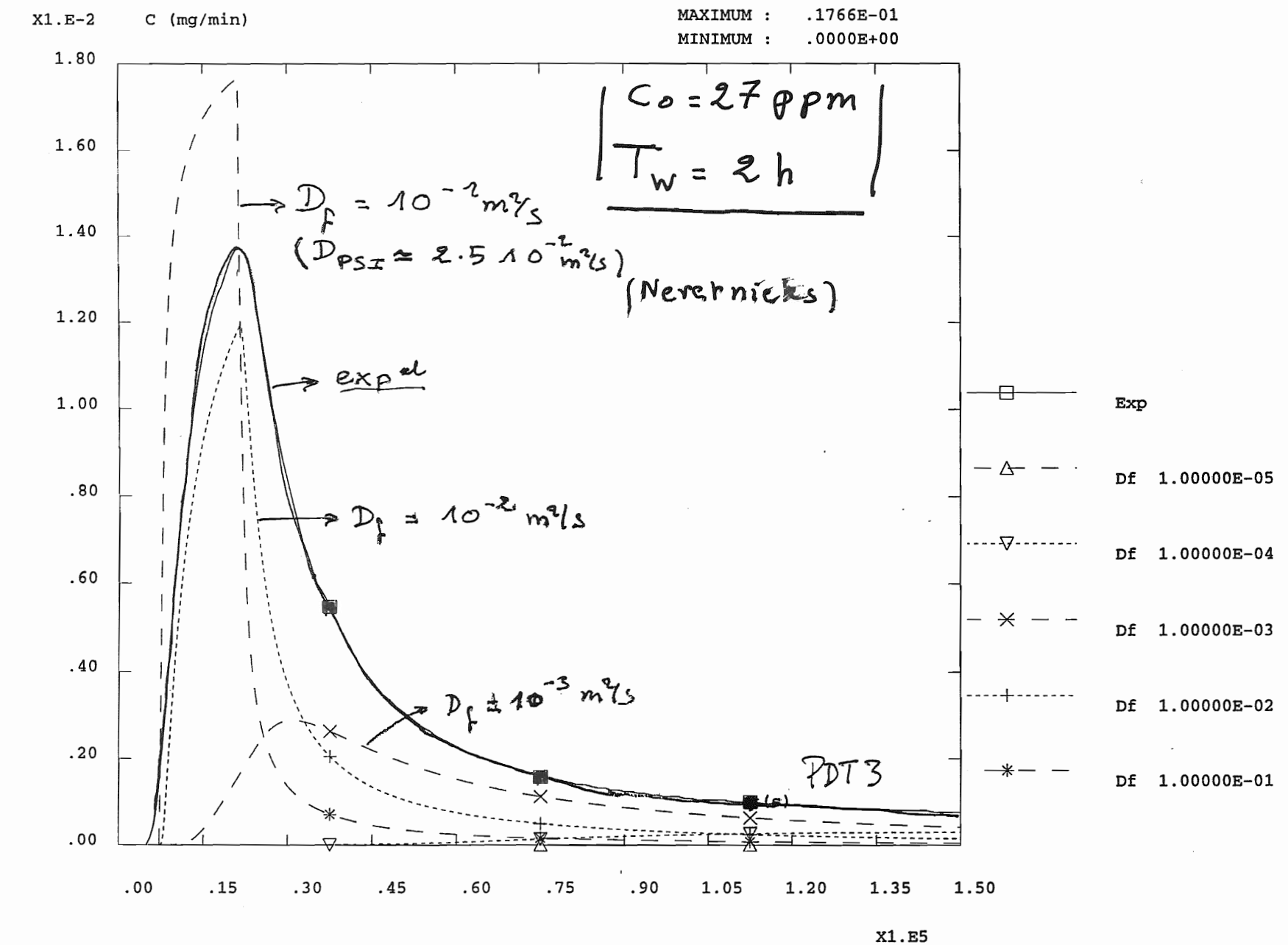

TITDESS

$t_w = 2\,h$, 27_{ppm}

Basic idea

- Fracture is composed of a channel as well as a fault gouge
- Modeled by multi-layered fractures or single fracture model

→ PSI model

PDT3

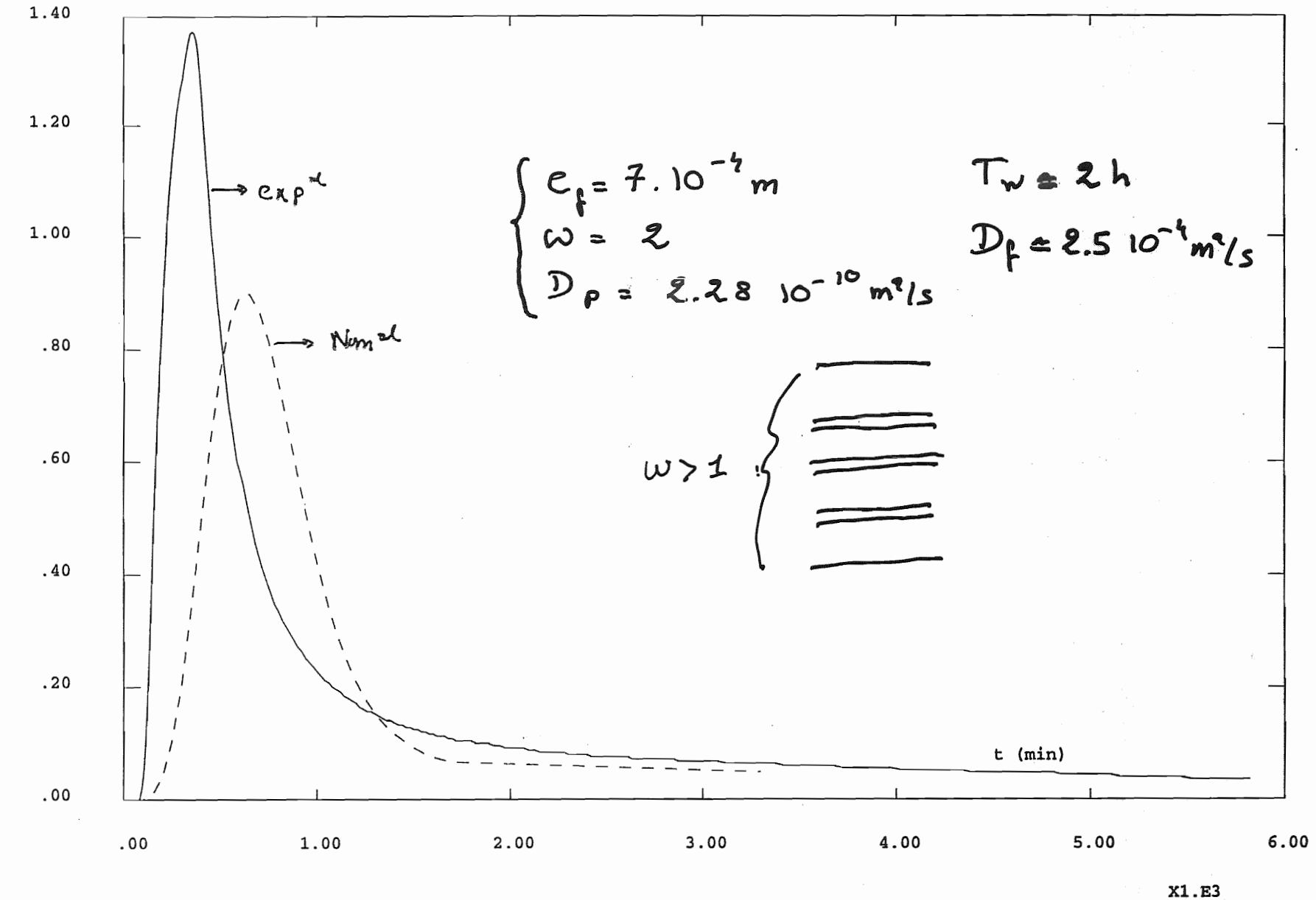

$\begin{cases} e_f = 7.10^{-4}\ m \\ \omega = 2 \\ D_p = 2.28\ 10^{-10}\ m^2/s \end{cases}$

$T_w \simeq 2\ h$

$D_f \simeq 2.5\ 10^{-4}\ m^2/s$

$\omega > 1$:

Derivees de la masse en fonction du temps Cas 12

PDT3 : Best fit

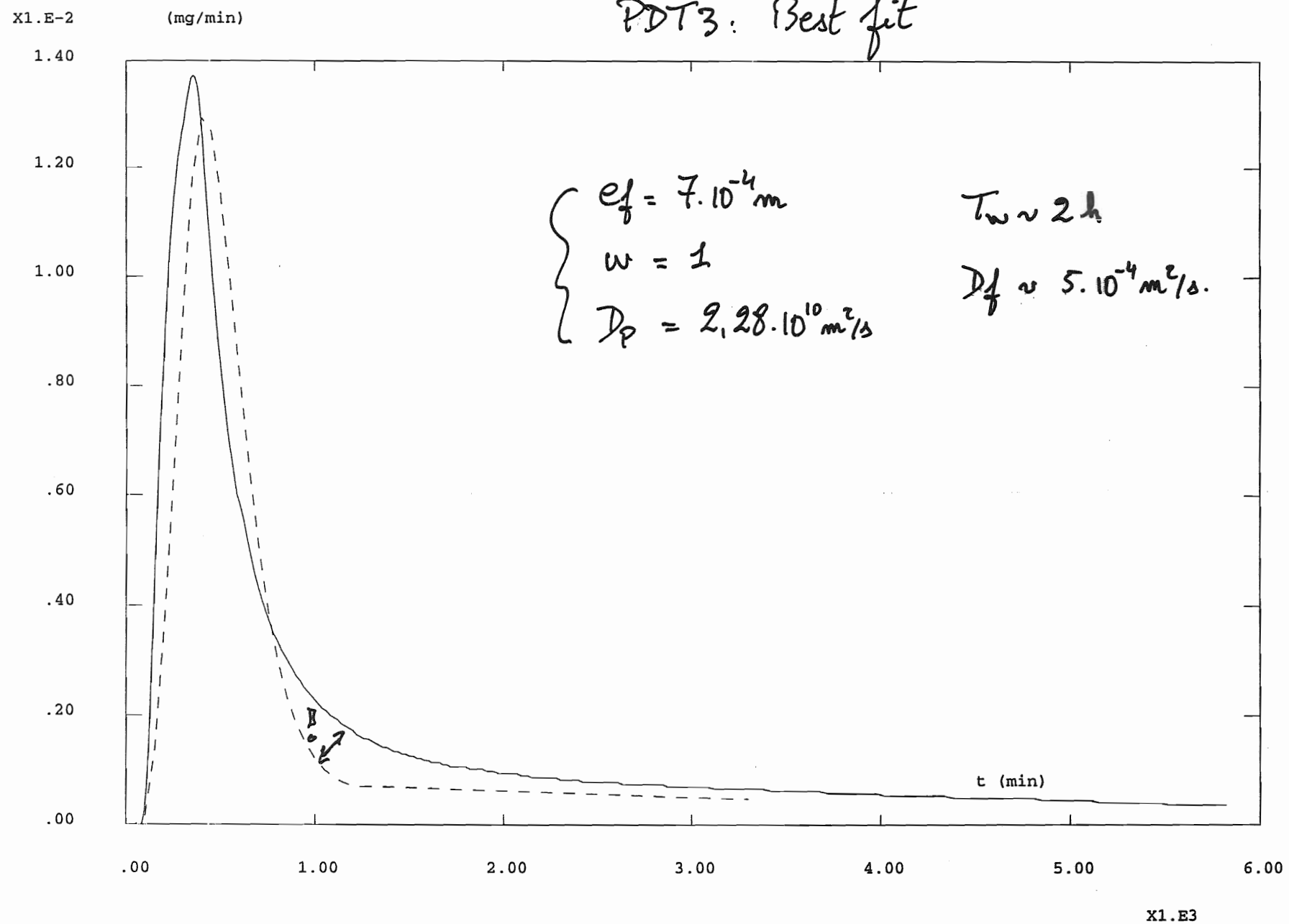

$$\begin{cases} e_f = 7.10^{-4}\,m \\ w = 1 \\ D_p = 2,28.10^{10}\,m^2/s \end{cases}$$

$T_w \sim 2\,h$

$D_f \sim 5.10^{-4}\,m^2/s.$

Derivees de la masse en fonction du temps

Cas 10

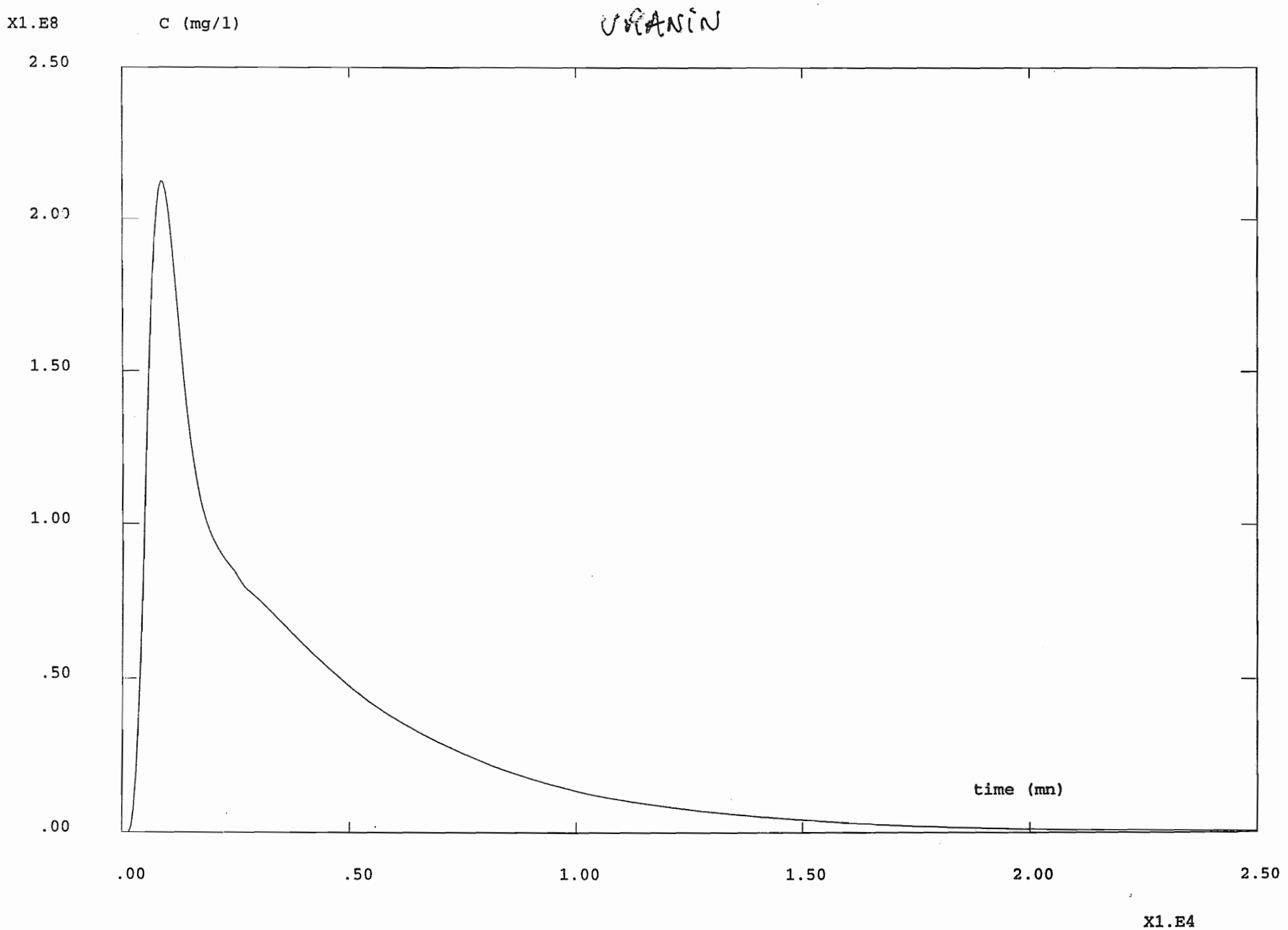

Concentration au pompage en fonction du temps

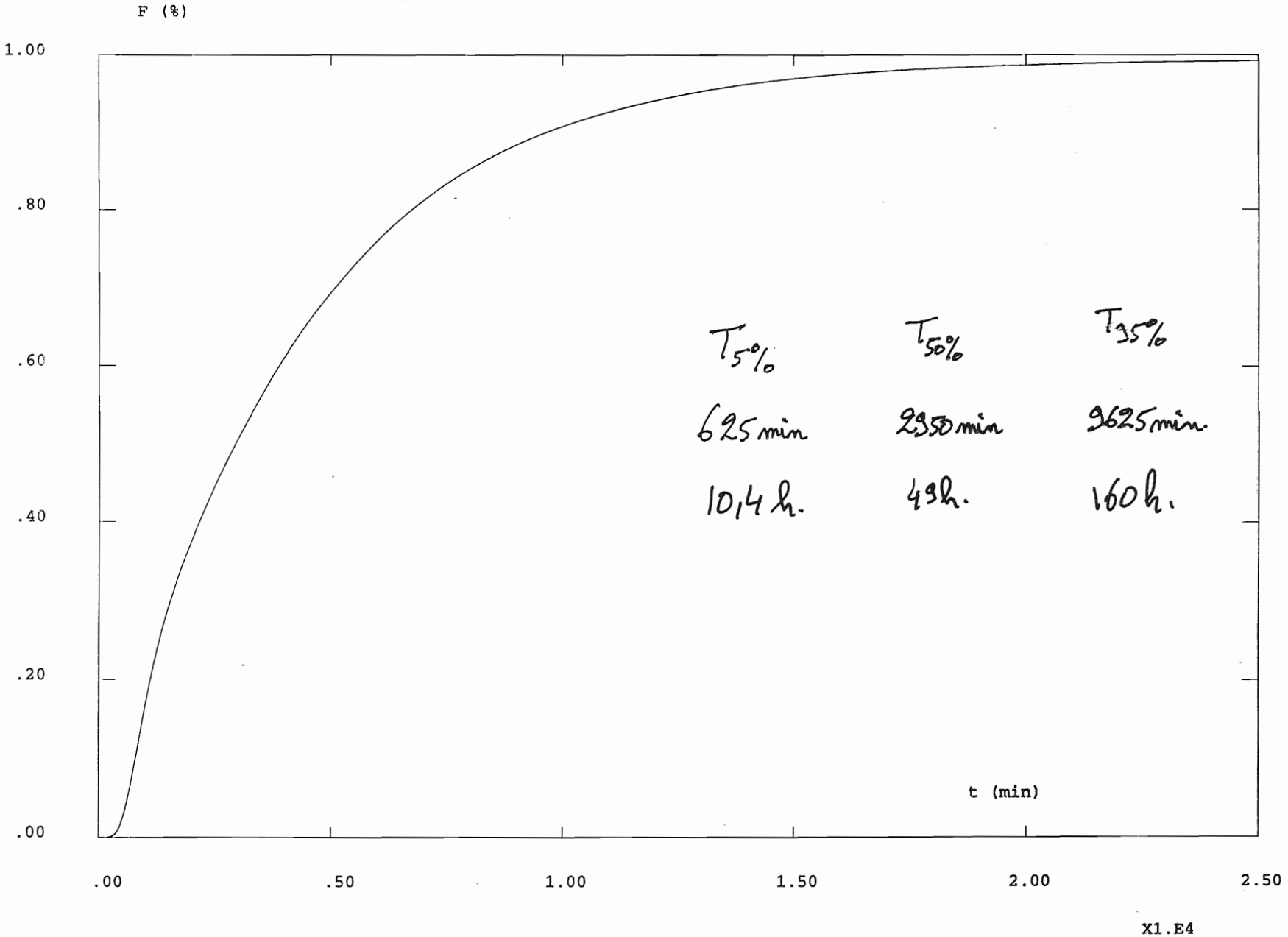

Mass recovery for Uranin vs time

URANIN

Modelling of STT1b and tracer tests and Predictive computations of STT2.

L. Moreno (SKB/KTH-KAT)

MODELLING OF THE SORBING TRACER TESTS

BY USING THE CHANNEL NETWORK MODEL

TASK 4F

L. Moreno

Department of Chemical Engineering and Technology
Royal Institute of Technology
Stockholm, Sweden

April 1999

ABSTRACT

The TRUE (Tracer Retention Understanding Experiments) experiment comprises a series of flow and transport experiments performed at different scales. The goal of these tracer tests is to give and develop a better understanding of radionuclide migration and retention in fractured rock. In earlier experiments and predictions, the transport of non-sorbing tracers was studied. Tracer tests with sorbing species have also been performed (STT1 and STT1b). Here, the tracer test with sorbing species STT2 is reported. This test comprises three non-sorbing species and 7 sorbing species.

1. INTRODUCTION

The first stage of the TRUE project at Äspö involved interference tests, dilution tests, flow loggings, pressure build-up tests and preliminary tracer tests. After this, a radially converging tracer test (RC-1) and a dipole experiment including four tests (DP 1-4) were performed. Later, in order to test eventual changes in the hydraulic conditions and refine the test design, several tracer tests with non-sorbing tracer were made previous to the experiments with sorbing species (RC-2, DP 5-6 and PDT 1-4).

The first set of experiments with sorbing tracers (STT1a) was performed with injection at KXTT4-R3 and extraction at KXTT3-R2. The extraction flow rate used was of 0.4 l/min. Due to the low recovery of Caesium, the collection of the tracers was maintained for a longer time. It was then decided to perform a new experiment with sorbing tracers (STT1b) with injection at KXTT1-R2 and extraction at the section KXTT3-R2.

The second set of tracer tests with sorbing species was carried out with injection in KXTT4-R3 and extraction at KXTT3-R2. This means the same injection and extraction section than in the test STT1a, but with an extraction flow rate of 0.2 l/min. The aim of this report is to present the results of the predictions of the tracer tests STT2.

2. MODEL CONCEPT

In the modelling of TRUE we have used the codes CHAN3D-flow and CHAN3D-transport, which both are based on the Channel Network model. First, the geometric information and boundary conditions were inserted to the flow model and the resulting flow distribution was then used in the transport model. A schematic picture of the features and the boreholes are shown in Figure 1.

2.2 The flow model

In the flow model, the tunnel with the niche, all the boreholes, the Feature A and the Feature B planes were included. The feature A was extended to the boundaries and the feature B fractures were treated as confined fracture planes. Regarding the boundary conditions, a given head was used on the top, on the bottom and on the right side of the rock block. No flow was assumed on the sides perpendicular to the tunnel. The head in the tunnel was taken as boundary condition on the left side, for the other region on this side, no flow condition was assumed. The withdrawal flow rate in the extraction section is also taken as a boundary condition. The conductances of the channels that connect the rock with the tunnel and the niche were reduced to simulate a skin effect. The size of the modelled rock volume was 30 x 30 x 40 meters in the direction longitudinal to the tunnel, the horizontal direction and the vertical direction respectively (Figure 1).

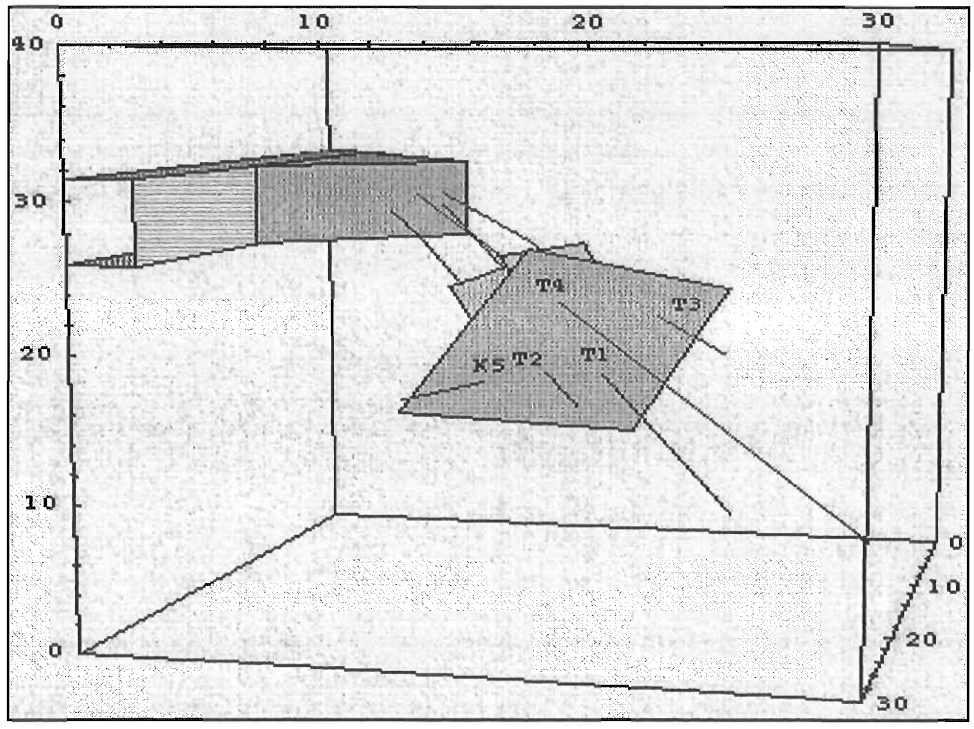

Figure 1. Feature A, the boreholes, the tunnel, and the niche. Behind feature A some of the feature B planes may be seen. For visualisation purposes the features are limited in extension. The feature A is extended to the borders of the model. The boreholes KXTT1, KXTT2, KXTT3, KXTT4 and KA3005A. are denoted as T1, T2, T3, T4 and K5, respectively.

The intersection points between Feature A and the boreholes were kept in the centre of the model to avoid the influence of the boundaries. The flow system was solved and the calculated flow field was used in the transport model. The mean transmissivity values for the different features were assigned from the experimental data. No conditioning of the transmissivity values around the intersection points was made.

2.3 The transport model

The transport in one channel member is by advection, but the solute in the channel, may diffuse into the rock matrix. No hydrodynamic dispersion is assumed in the channel. The dispersion of the solute is caused by the heterogeneity of the flow field when the solute is transported with different velocities in different channels in the network.

3. DESCRIPTION OF THE EXPERIMENTS

The tracer tests with sorbing species were carried out in a radially converging flow field. The experimental data is shown in Table 1. Three non-sorbing tracers were also injected together with the sorbing species, uranin, bromide, and HTO. The following weakly and intermediately sorbing tracers were used: Na^+, Sr^{2+}, Ca^{2+}, Ba^{2+}, Rb^+, and Cs^+. The radioactive species injected, the sorption constant and the effective diffusivity are shown in Table 2. All the values are corrected by decay.

Table 1. Experimental information for the tracer test STT2.

	STT2
Injection hole	KXTT4-R3
Injection-section volume, l	1.548
Sampling flow, ml/h	1.9
Pumping hole	KXTT3-R2
Pumping flow, l/min	0.200

Table 2. Half-life, sorption constant and effective diffusivity for the tracer used in the tracer tests.

Species	Radio-nuclide	Kd	De	Extraction time hrs
Uranin		-	1.20E-13	886
HTO	H-3	-	1.20E-13	641
Br^-	Br-82	-	-	234
Na^+	Na-22	1.40E-06	6.70E-14	3 078
Sr^{2+},	Sr-85	4.70E-06	4.00E-14	3 078
Rb^+	Rb-86	4.00E-04	1.00E-13	1 322
Ca^{2+}	Ca-47	5.20E-06	4.00E-14	458
Ba^{2+}	Ba-131	2.00E-04	4.20E-14	1 130
Ba^{2+}	Ba-133	2.00E-04	4.20E-14	3 078
Cs^+	Cs-134	6.00E-03	1.00E-13	3 078

4. PREDICTION OF THE SORBING TRACER TESTS.

4.1 Calibration

Since this tracer test was carried out at the same location than those used for STT1a, similar parameter values were used for these predictions.

The evaluation of the tracer test STT1a, and specifically the test with caesium shows that large differences are found between the predicted breakthrough times and the experimental times. The difference could be explained by a smaller flow rate in the paths from KXTT4 to KXTT3 (Appendix A). Based in these results, simulations were carried out using a flow rate 30 times smaller than the value calculated without conditioning.

4.2 Prediction results

The breakthrough curves for one realisation are shown in Figure 2 and 3. This realisation shows arrival times that are close to the respective medians. Figure 2 shows the breakthrough concentration expressed as the fraction of the activity (mass) of tracer injected per unit time (hour). Figure 3 shows the cumulative mass arriving to the extraction section. This is expressed in function of the mass of injected tracers.

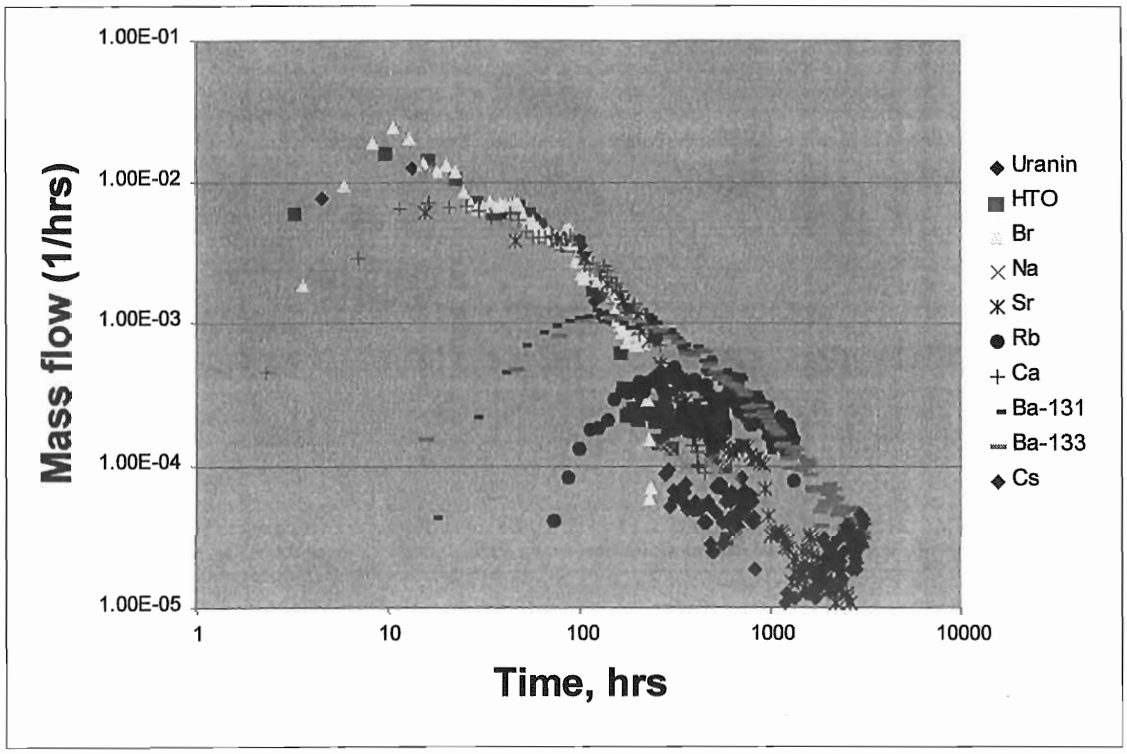

Figure 2 Mass flux into the extraction section for one realisation.

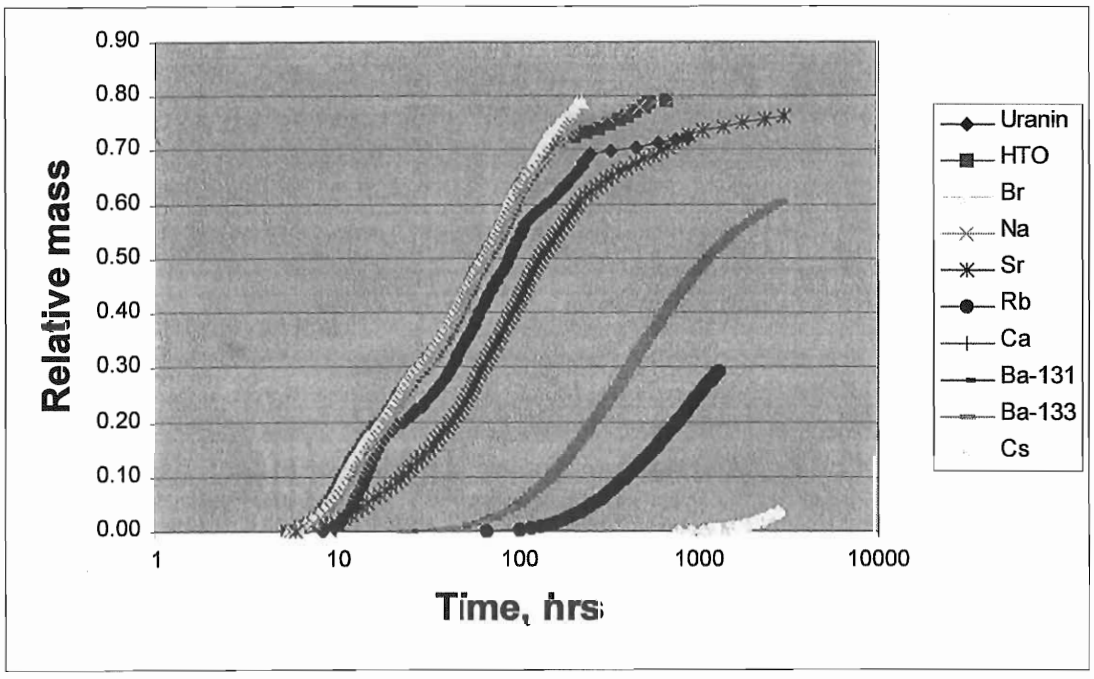

Figure 3 Cumulative mass arriving to the extraction section for one realisation.

4.3. Steady-state drawdown

The calculated steady-state drawdowns at the injection and extraction sections are shown in Table 3.

Table 3. The steady-state drawdown.

Section	S (5%), m	S (50%), m	S (95%), m
KXTT1-R2	1.5	1.7	1.9
KXTT2-R2	1.3	1.5	1.7
KXTT3-R2	4.3	5.7	8.3
KXTT4-R3	1.8	2.0	2.2
KA3005A-R3	1.1	1.2	1.4

4.4 Breakthrough times

The times to recover 5, 50 and 95 % of the injected mass are shown in Tables 4a, 4b and 4c, for the different tracers. All the injections were carried out in the section KXTT4-R3 and the extraction at the section KXTT3-R2.

Table 4a Times, T_5 [hr], for mass recovery.

Tracer test	T_5 (5%), hrs	T_5 (50%), hrs	T_5 (95%), hrs
Uranin	5.0	9.2	42.5
HTO	4.7	8.8	40.5
Br^-	4.7	8.7	38.2
Na^+	5.3	9.7	43.3
Sr^{2+},	6.2	15.1	168.7
Rb^+	63.2	310.3	-
Ca^{2+}	6.2	14.8	177.8
Ba^{2+}	25.0	111.4	-
Ba^{2+}	24.4	112.4	3068.3
Cs^+	728.3	3948.6	-

Table 4b Times, T_{50} (median) [hr], for mass recovery.

Tracer test	T_{50} (5%), hrs	T_{50} (50%), hrs	T_{50} (95%), hrs
Uranin	47.5	67.0	-
HTO	43.0	62.2	-
Br^-	39.3	58.9	-
Na^+	43.4	62.5	-
Sr^{2+},	64.9	148.0	-
Rb^+	555.3	-	-
Ca^{2+}	62.1	142.9	-
Ba^{2+}	250.4	1681.7	-
Ba^{2+}	251.9	1811.7	-
Cs^+	-	-	-

Table 4c Times, T_{95} [hr], for mass recovery.

Tracer test	T_{95} (5%), hrs	T_{95} (50%), hrs	T_{95} (95%), hrs
Uranin	244.1	-	-
HTO	377.5	-	-
Br^-	178.2	-	-
Na^+	265.1	-	-
Sr^{2+},	968.6	-	-
Rb^+	-	-	-
Ca^{2+}	959.3	-	-
Ba^{2+}	-	-	-
Ba^{2+}	-	-	-
Cs^+	-	-	-

4.5 Recovered mass

Table 5 shows the calculated recovered mass during the experiment. In the predictions the recovered mass was calculated for an observation time of 8000 hours.

Table 5 Recovered mass as a fraction of the injected mass (activity). A detection time of one year was used.

Tracer test	R(5%)	R(50%)	R(95%)
Uranin	0.25	0.83	1.00
HTO	0.24	0.83	1.00
Br^-	0.24	0.83	0.99
Na^+	0.24	0.83	1.00
Sr^{2+},	0.23	0.80	0.97
Rb^+	0.00	0.26	0.65
Ca^{2+}	0.14	0.70	0.93
Ba^{2+}	0.03	0.44	0.79
Ba^{2+}	0.07	0.59	0.86
Cs^+	0.00	0.05	0.35

4.6 Breakthrough times for a hypothetical pulse injection, Dirac pulse.

The times to recover 5, 50 and 95 % of the injected mass for a hypothetical pulse injection (Dirac pulse) are shown in Tables 6a, 6b and 6c, for the tracers used in the experiments. All the injections were carried out in the section KXTT1-R2 and the extraction at the section KXTT3-R2.

Table 6a Breakthrough curves, t_5 [hr] for pulse (Dirac) injection.

Tracer test	t_5 (5%), hrs	t_5 (50%), hrs	t_5 (95%), hrs
Uranin	2.2	5.3	16.7
HTO	2.2	5.3	16.7
Br^-	2.2	5.3	16.7
Na^+	2.2	5.3	17.2
Sr^{2+},	2.6	7.7	103.5
Rb^+	33.2	237.5	-
Ca^{2+}	2.5	7.7	123.9
Ba^{2+}	10.5	58.1	4337.0
Ba^{2+}	10.7	60.2	2935.4
Cs^+	485.6	3458.9	-

Table 6b Breakthrough curves, t_{50} [hr] for pulse (Dirac) injection.

Tracer test	t_{50} (5%), hrs	t_{50} (50%), hrs	t_{50} (95%), hrs
Uranin	3.2	9.4	-
HTO	3.2	9.7	-
Br^-	3.2	9.5	-
Na^+	3.2	9.6	-
Sr^{2+},	6.7	59.7	-
Rb^+	447.3	-	-
Ca^{2+}	7.0	65.4	-
Ba^{2+}	102.4	1572.2	-
Ba^{2+}	102.4	1694.0	-
Cs^+	-	-	-

Table 6c Breakthrough curves, t_{95} [hr] for pulse (Dirac) injection.

Tracer test	t_{95} (5%), hrs	t_{95} (50%), hrs	t_{95} (95%), hrs
Uranin	14.1	-	-
HTO	14.2	-	-
Br^-	14.0	-	-
Na^+	14.6	-	-
Sr^{2+},	865.8	-	-
Rb^+	-	-	-
Ca^{2+}	909.6	-	-
Ba^{2+}	-	-	-
Ba^{2+}	-	-	-
Cs^+	-	-	-

APPENDIX A

Interpretation of the caesium tracer test in STT1a

Background

In the tracer test STT1a, the tests carried out using sorbing solutes showed breakthrough times much longer than the predicted values. Here, we discuss the caesium tracer test, which showed the largest retardation. In these simulations, the values of sorption (matrix and surface) measured at the laboratory and delivered by SKB were used.

In order to discuss this tracer test, some important facts are summarised below.

The water residence time is about 10 hours.
Considering a distance between injection and extraction hole of 5 metres and an extraction flow rate of 0.2 l/min, the mean fracture aperture required to fit the travel time is

$$\delta_m = 3.0 \text{ mm}$$

Small or not at all surface sorption
Surface sorption (instantaneous) can not explain the larger retardation observed. This is shown in Figures 1 and 2, which show breakthrough curves for one realisation. An instantaneous sorption of the tracer on the fracture surface or on filling material is usually a fast reaction and equilibrium is established between the species in solution and the sorbed species. In this case the shape of the breakthrough curve is kept constant, it is only translated in the direction of longer times (see Figure 2).

Figure 2 shows breakthrough curves when the effect of surface sorption has been increased by 10 and 20 times. A greater effect of surface sorption may be due to a larger available surface for sorption; e.g. sorption on gauge, sorption on filling material or existence of several parallel fractures.

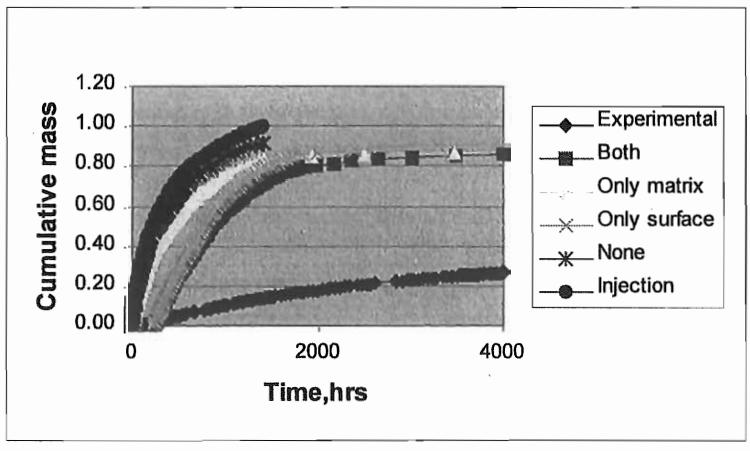

Figure 1. Cumulative mass as a function of the time

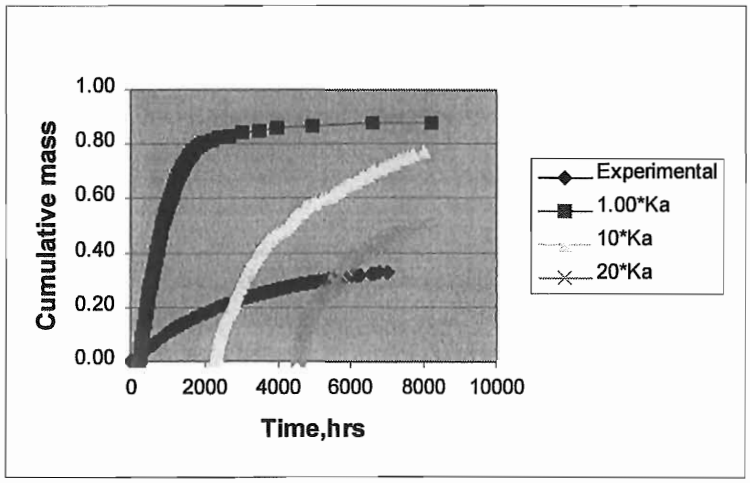

Figure 2. Cumulative mass for increasing surface sorption.

Hydraulic data

The transmissivity of the Feature A at the location where the boreholes meet the fracture is shown in Table 1. The values are in the interval 5.9E-9 to 2.1E-7, a ratio of about 35 between the largest and the lowest values. The experimental drawdowns measured in the tracer test RC1, where water was extracted at KXTT3 are shown also in Table 1. The recovered mass in these experiments was high for tracer injected in KXTT1 and KXTT4. The tracer injected in KXTT2 and KA3005 were not detected when an extraction flow rate of 0.2 litre/min was used.

Table 1. Some hydraulic data

Borehole	KXTT1	KXTT2	KXTT3	KXTT4	KA3005
Transmissivity, m2/s	8.3E-9	5.9E-9	2.1E-7	1.8E-8	2.7E-8
Drawdown, m	0.62	2.23	3.12	0.32	0.28
Recovered mass	high	zero	Extraction	high	zero

Difference between the experimental and simulated values

The retardation obtained in the simulations is significantly less than the experimental results. It is assumed that principally matrix diffusion and sorption within the matrix cause the retardation. The diffusion/sorption in the matrix is determined by a term that includes the effective diffusion (rock porosity), the volume sorption constant, the flow-wetted surface and the water flow rate.

$$\frac{(K_d \rho_p D_e)^{0.5}}{(t - t_o)} \frac{LW}{Q}$$

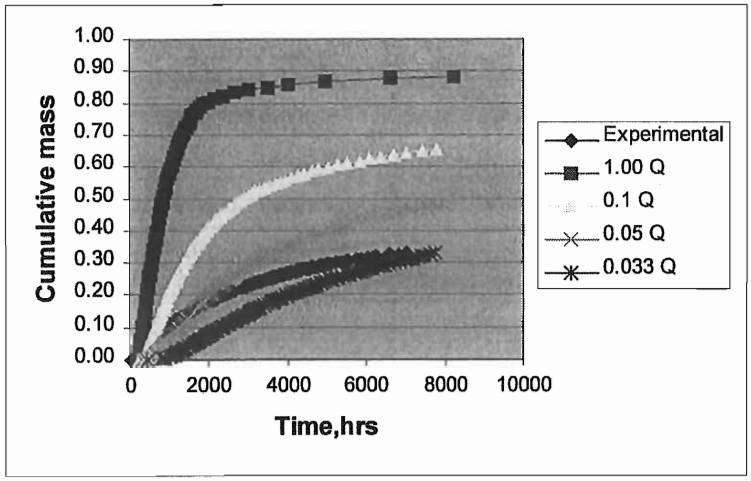

Figure 3. Breakthrough curves for different values of water flow rate.

Breakthrough curves for a realisation for different values of the water flow rate are shown in Figure 3. It is observed that in order to obtain a good agreement with the experimental results, the term would be increased by a factor of about 30. This increase may be obtained by different ways. Table 2 shows these different alternatives and the practical consequences of them.

Table 2. Parameter variation to fit the experimental results.

Parameter	Increase by	
Rock effective diffusion	900 times	No probable, too high porosity
Rock volume sorption	900 times	No probable, too high value
Flow wetted-surface	30 times	No probable. Need 30 parallel fractures
Water flow	30 times	Probable

Some possible causes of the difference between the experimental and simulated values

1. Lower flow rate between KXTT4 and KXTT3.

This is the most probable reason of the large difference between the experimental and simulated values. This is partially supported by

- Feature A shows large differences in transmisivity, the ratio between the largest and lowest is about 35. Moreover a zone with large transmissivity is found between the borehole KXTT3 and KXTT2. The extent of this zone is unknown and may acts as a sink for water from different parts.
- The large fracture aperture (mean value of 3 mm) needed to match the water residence time. If the fracture has filling material, the fracture aperture required would be about 10 mm, assuming a porosity of 0.30. These large values of fracture aperture are unusual in the field and they have not been observed in the cores taken from the Feature A. With a water flow rate 30 times smaller the fracture would be about 0.1 mm.

2. The fracture has filling material or coating close to the rock.
The water flow takes place through the fracture centre, where there is not filling material. The tracers transported by the flowing water may diffuse into the coating (or filling) and sorbed on it.

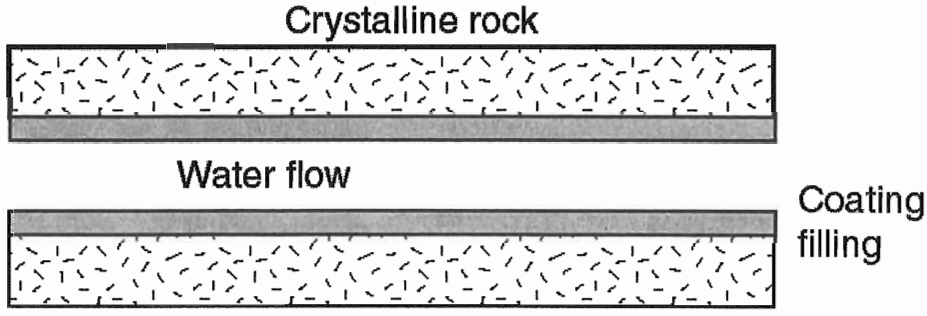

Figure 3. Schematic view of a fracture with coating/filling material

The porosity of the coating (filling material) may be high (0.20 - 0.30) implying a high effective diffusion. Compared with crystalline rock the effective diffusion may be 2-3 orders of magnitude greater. Moreover, if the coating (filling) is formed by very small particles, a larger value of the sorption constant would be expected due to the larger surface available for sorption. However, a free aperture of 3 mm for the water flow is required.

Evaluation of STT1 and Prediction of STT2.

V. Cvetkovic & H. Cheng (KTH-WRE), J-O. Selroos (SKB)

Evaluation of Sorbing Tracer Tests STT-1 and STT-1B in the First TRUE Stage

TASK 4E

Based on
TRUE-1 Final Report of the First Stage of the Tracer Retention Understanding Experiments (Winberg (ed.), in prep.)

TRUE MODELLING TEAM:
Vladimir Cvetkovic, Water Resources Eng., KTH
Hua Cheng, Water Resources Eng., KTH
Jan-Olof Selroos, SKB
April 1999

EXECUTIVE SUMMARY

We evaluated and interpreted the BTC-data for the sorbing tracers tests STT-1 and STT-1B using the LSAR framework (Cvetkovic et al. 1999). The observed BTCs for sorbing tracers exhibit significant kinetic effects, in particular for more strongly sorbing tracers; these are attributed to diffusion and sorption in the rock matrix, and to sorption in gouge material. It appears that the retention observed in the field cannot be predicted based on the laboratory data for κ alone. Calibration with a factor f, as well as with parameters K_d^g and α for gouge, was required for obtaining a close comparison between the modelled and observed BTCs. The calibration parameters f and K_d^g vary only mildly between different tracers, and for the different TRUE-1 tests.

INTRODUCTION

Predictions of breakthrough curves (BTCs) for sorbing tracers of STT-1 and STT-1B deviate from the experimental data. The objective of this evaluation is to provide a consistent interpretation of the measured BTCs with a minimum set of calibrated field-scale parameters. A comprehensive description of the theory, evaluation procedure and results is given in Cvetkovic et al. (in preparation).

STT-1 is performed in Feature A between boreholes KXTT4 R3 and KXTT3 R2 with a injection flow rate 400 ml/min, while STT-1B is also performed in Feature A, but between boreholes KXTT1 R2 and KXTT3 R2 with the same flow rate 400 ml/min.

Feature A is perceived as a planar fracture with a spatially variable aperture. A tracer injected in a borehole within feature A is advected and dispersed, and is subject to various mass transfer reactions. In particular, a tracer diffuses into the rock matrix and (if reactive) sorbs on internal surfaces of the rock; gouge (infill) material may be present and enhance sorption, i.e. retention.

EVALUATION FRAMEWORK

The Lagrangian stochastic advection-reaction (here abbreviated as LSAR) framework for reactive transport in rock fractures (Cvetkovic et al., 1999) is employed for the evaluation.

Solving the system of coupled transport equations for a single trajectory, a new parameter, β, was derived; β is a random quantity integrating the velocity-weighted variable aperture along a flow path. β controls surface sorption and diffusion/sorption into the rock matrix, and is related to the flow field. This result enables us to directly account for the effect of flow heterogeneity on the mass transfer reactions. The sorption in the gauge material is assumed to be a first-order kinetically controlled reaction, which is not influenced by β.

All mass transfer reactions considered in Cvetkovic et al. (1999) are assumed linear whereby the coupled effect is obtained by convolution. In particular, solutions for

individual mass transfer processes for pulse injection are convoluted with the input (tracer discharge vs time) in the injection borehole. To account for dispersive effects, the convoluted result for a single flow path is integrated over different flow paths described by a distribution of τ and β . τ and β have been shown to be significantly correlated both for generic conditions (Cvetkovic et al., 1999), and also for the flow conditions of feature A (Cvetkovic et al., in preparation). Based on these results, we establish an approximate linear (deterministic) relationship between τ and β using Monte Carlo simulations.

The water residence time distribution $g(\tau)$ (that accounts for dispersion effects due to advection variability) is contained in the breakthrough curves (BTCs) of HTO and Uranine, and is obtained through deconvolution of the measured HTO BTC.

KEY PARAMETERS

The two key parameter groups which control sorption and diffusion following Cvetkovic et al. (1999) are $K_a\beta$ for surface sorption, and $\beta\,\kappa$ for diffusion/sorption in the rock matrix. The parameter K_a and the parameter group κ have been determined in the laboratory for all tracers. The quantities τ (water residence time) and β are dependent on the flow conditions in the field and by definition cannot be determined in the laboratory.

Since measured BTCs indicate strong kinetic effects attributed to diffusion, we anticipate a comparatively small effect of surface sorption; hence we shall assume that the laboratory value of K_a is applicable in the field.

$\kappa = \theta[D(1+K_d^m)]^{1/2} = \theta(DR_m)^{1/2}$ where θ is the porosity of the rock matrix (note that we do not distinguish the "total porosity" from the "diffusion porosity"), D is the pore diffusivity in the rock matrix (θD is the effective diffusion coefficient in the rock matrix), and K_d^m is the sorption coefficient in the rock matrix. We found that κ, as determined in the laboratory, may not be applicable under field conditions. In other words, calibration may be required for the field-scale value. We define the field-scale κ as $f\kappa$, where $f>1$ is the *enhanced diffusion factor* to be calibrated on the BTC data. Using $\beta = k\,\tau$, we can write the parameter group controlling matrix diffusion/sorption as $f\,k\,\tau\,\theta(DR_m)^{1/2}$.

Two additional parameters to be considered in the evaluation are the distribution coefficient for the gouge K_d^g (once equilibrium is reached) and the kinetic rate (i.e. backward rate coefficient) α. The parameters K_d^g and α need to be inferred entirely from the measured BTC data since laboratory values are not available.

EVALUATION PROCEDURE

The evaluation procedure consists essentially of two steps:

1. We determine the water residence time distribution $g(\tau)$ by deconvoluting the HTO BTCs, accounting for diffusion into the matrix; the actual form of $g(\tau)$ is

assumed as inverse-gaussian, and the first two water residence time moments are calibrated.

2. We use $g(\tau)$ to model the reactive tracer BTCs by accounting for mass transfer processes, with parameters determined in the laboratory. If the modelled BTCs deviate from the observed BTCs, we enhance mass transfer by increasing the diffusion factor f (where $f\kappa$ is the calibrated value), and add sorption in gouge material.

Increasing κ by a factor f can imply larger values of the physical parameters (θ and D) and/or of the sorption coefficient K_d^m. If the calibrated value $f>1$ is due primarily to the physical factors, then f should be approximately constant for all tracers, irrespective of tracer sorption properties. If the calibrated value $f>1$ is primarily due to enhanced sorption properties (i.e. larger K_d^m in the field than measured in the laboratory), then f should be strongly dependent on tracer sorption properties. Furthermore, if $f>1$ is due to physical factors, then its impact has to be accounted for in the modelling of HTO BTCs. In other words, the above two steps become an iterative procedure, by which the moments of $g(\tau)$ are calibrated.

EVALUATION RESULTS

The BTC-data for TRUE-1 tests normalised with the total injected mass indicate that the sorptive tracers can be roughly classified into three groups: the weakly sorbing tracers Na and Sr, moderately sorbing tracers Ba and Rb, and strongly sorbing tracer Cs. The modelled BTCs for Na and Sr are more strongly influenced by the detailed form of the HTO BTC in comparison to the modelled BTCs for Ba, Rb and Cs.

The laboratory parameters and the field-scale parameters calibrated on measured BTCs are summarised in Tables 1 and 2 below. The calibrated temporal moments for HTO are mean=7h and variance=49h^2 for STT-1 and mean=5h and variance=1.5h^2 for STT-1B.

Tracer	K_a [m]	K_d^m [$m^3 kg^{-1}$]	D [m^2h^{-1}]	D_w [m^2h^{-1}]	$\kappa=\theta(DR_m)^{1/2}$ [$mh^{-1/2}$]
HTO	0.0	0.0	1.1E-7	8.4E-6	0.130E-5
Na	7.0E-7	1.4E-6	5.8E--8	4.8E-6	0.134E-5
Sr	8.0E-6	4.7E-6	3.6E-8	2.8E-6	0.155E-5
Ba	2.0E-4	2.0E-4	3.6E-8	3.0E-6	0.883E-5
Rb	5.0E-4	4.0E-4	9.0E-8	7.3E-6	1.968E-5
Cs	8.0E-3	6.0E-3	9.0E-8	7.3E-6	7.622E-5

Table 1: Laboratory parameters for HTO and sorbing tracers of the TRUE-1 tests. The parameters are defined in the Appendix. Additional laboratory values used in the evaluation are θ=0.004 and ρ=2700kg/m^3.

Tracer	Enhanced diffusion factor f		K_d^g [-] for gouge (α=0.3h^{-1})	
	STT-1	STT-1B	STT-1	STT-1B
HTO	40	32	-	-
Na-22	40	32	1.0	0.5
Sr-85	40	32	2.0	1.6
Ba-133	40	-	4.0	-
Rb-86	45	34	5.0	4.0
Cs-137	50	-	10.0	-

Table 2: Calibrated parameters for HTO and sorbing tracers of the TRUE-1 tests; note that only the tracers for which laboratory data is available within the TRUE programme are included. The slope of the linear relationship $\beta = k\,\tau$ is k=3400 m^{-1} .

REFERENCES

Cvetkovic, V., J.O. Selroos and H. Cheng, Transport of reactive solute in single fractures, *J. Fluid Mech.*, **318**, 335-356, 1999.

Cvetkovic, V., H. Cheng and J.O. Selroos, Evaluation of TRUE-1 sorbing tracer experiments at Äspö: Theory and applications, SKB International Cooperation Report (in preparation).

Prediction of Sorbing Tracer Tests STT-2

in the First TRUE Stage

TASK 4F

TRUE MODELLING TEAM:
Vladimir Cvetkovic, Water Resources Eng., KTH
Hua Cheng, Water Resources Eng., KTH
Jan-Olof Selroos, SKB
April 1999

Introduction

STT-2 was performed in the same path as in STT-1, but with a lower pumping rate of 200 ml/min. The tracers are injected in the borehole KXTT4 R3 and extracted in the borehole KXTT3 R2. The tracers used in STT-2 test are two conservative tracers (tratiated water and Br^{82}), and seven sorbing tracers (Na^{22}, Ca^{47}, Sr^{85}, Ba^{131}, Ba^{133}, Rb^{86} and Cs^{134}).

The injection section volume used is 1898 ml.

Conceptual and Mathematical Models

The same framework and models as in the evaluation of STT-1 and STT-1B are used.

The water residence time distribution $g(\tau)$ is assumed to have an inverse-Gaussian distribution. The moments of $g(\tau)$ are obtained by calibrating the calculated breakthrough against the experimental data from PDT2.

From the evaluation of STT-1, we found that the matrix diffusion needs to be increased by a factor f in order to explain the measured data, we also found the sorption in the gauge material may exist (Cvetkovic et al, 1999). STT-2 is performed in the same configuration as STT-1. Then the same factor f and parameters for the kinetic sorption in the gauge material from the evaluation of STT-1 are used for the prediction of STT-2. All other relevant parameters are laboratory values.

Flow and nonreactive Transport Results

Head value:

Tracer test Borehole section	$s_{(5\%)}{}^{c}$	$s_{(50\%)}{}^{c}$	$s_{(95\%)}{}^{c}$ (m)
***Q*=0.2 l/min**			
KXTT1	-62.7	-50.8	-47.7
KXTT2	-51.2	-47.5	-46.7
KXTT3	-48.2	-46.7	-46.4
KXTT4	-46.9	-46.5	-46.4
KA3005	-49.7	-47.6	-47.1

Sorbing Transport Results

The following tracer data has been used:

Tracer	K_a (m)	K_d (m^3/kg)	D (m^2/s)
HTO	0	0	3.0×10^{-11}
Br-82	0	0	3.0×10^{-11}
Na-22	7×10^{-7}	1.4×10^{-6}	1.6×10^{-11}
Ca-47	4×10^{-6}	5.2×10^{-6}	1.0×10^{-11}
Sr-85	8×10^{-6}	4.7×10^{-6}	1.0×10^{-11}
Ba-131	2×10^{-4}	2.0×10^{-4}	1.0×10^{-11}
Ba-133	2×10^{-4}	2.0×10^{-4}	1.0×10^{-11}
Rb-86	5×10^{-4}	4.0×10^{-4}	2.5×10^{-11}
Cs-134	8×10^{-3}	6.0×10^{-3}	2.5×10^{-11}

A matrix porosity of $\theta = 0.004$ and $\rho = 2700\ \mathrm{kg/m^3}$ based on Andersson et al. (1997) are used. The values of K_a, K_d^m and D are obtained from the laboratory. K_d^g and α are fitted values for gauge material; the same values of K_d^g and α are used as in the evaluation of Na, Sr and Rb in STT-1.

The resulting (deterministic) travel times (hours) and mass recoveries for pulse input are

Tracer	t_5	t_{50}	t_{95}	*Recovery*
HTO	4.8	12.3	330.1	0.97
Br-82	4.8	12.3	330.1	0.94
Na-22	6.1	20.9	336.5	0.99
Ca-47	7.6	27.2	436.8	0.95
Sr-85	8.6	30.3	414.8	0.99
Ba-131	32.6	164.4	9946.0	0.82
Ba-133	32.6	164.4	9946.0	0.90
Rb-86	88.4	745.2	46646.3	0.61
Cs-134	1318.7	15773.5	861787.5	0.16

The resulting (deterministic) travel times (hours) and mass recoveries for experimental input are

Tracer	t_5	t_{50}	t_{95}	*Recovery*
HTO	8.5	57.4	295.1	0.99
Br-82	8.3	52.4	231.3	0.95
Na-22	11.3	66.2	374.0	1.00
Ca-47	14.6	67.8	348.9	0.96
Sr-85	16.8	79.0	446.8	1.00
Ba-131	57.3	279.2	6389.4	0.83
Ba-133	56.8	283.1	6853.1	0.90
Rb-86	118.4	660.2	8715.7	0.67
Cs-134	1556.8	14304.3	459294.3	0.15

The recovery is calculated at the termination time provided by the Task Force Secretariate.

References

Andersson, P., et al., TRUE 1st stage tracer test programme, Experimental plan for tests with sorbing tracers at the TRUE-1 site, SKB Äspö HRL-97-07, 1997.

Cvetkovic, V., H. Cheng and J.O. Selroos, Evaluation of TRUE-1 sorbing tracer experiments at Äspö: Theory and applications, SKB International Cooperation Report (in preparation).

Analysis of STT1 and STT1b tests and Predictions of the breakthrough times in the STT2 test.

Antti Poteri (POSIVA/VTT)

TRUE STT2 TEST

Antti Poteri
VTT Energy

VTT ENERGY Antti Poteri

Conceptual model

- Single channel
- Large range of flow velocities
  - linear velocity profile [0, 2 mm/s]
- Advective field and molecular diffusion

VTT ENERGY Antti Poteri

Mathematical model

Advection & molecular diffusion

$$R_a \frac{\partial C}{\partial t} - D_w \left[\frac{\partial^2 C}{\partial x^2} + \frac{\partial^2 C}{\partial y^2} \right] + v_{\max} \left(1 - \frac{y}{a_{ch}} \right) \frac{\partial C}{\partial x} = 0$$

Matrix diffusion

$$\frac{\partial C(x,z,t)}{\partial t} = -v \frac{\partial C(x,z,t)}{\partial x} + D_e \frac{2}{2b_v} \frac{\partial C(x,z,t)}{\partial z}\Big|_{z=0}$$

$$R_p \frac{\partial C(x,z,t)}{\partial t} = \frac{D_e}{\varepsilon_p} \frac{\partial^2 C(x,z,t)}{\partial z^2}$$

VTT ENERGY Antti Poteri

Analysis of the STT1 test

- Injection flow rate

t < 10 h	36 ml/h
10 h < t < 70 h	42 ml/h
t > 70 h	33 ml/h

VTT ENERGY Antti Poteri

Analysis of the STT1 test

- Parameters for advection-dispersion calculation

Molecular diffusion coefficient, D_w	$2.4\ 10^{-9}$ m^2/s
Maximum flow velocity, v_{max}	$8.9\ 10^{-4}$ m/s
Channel width, a_{ch}	0.05 m
Channel length, X_{ch}	4.68 m
Retardation coefficient, Ra	

- Parameters for matrix diffusion

$$u = \sqrt{D_w \varepsilon R_p}\,\frac{WL}{Q}$$

Analysis of the STT1 test

- R_a estimated from the slopes of the first breakthrouhgs

Uranine	1
HTO	1
Cs	46
Na	1.1
Ca	1.4
Sr	1.1
Ba	3
Rb	8

Analysis of the STT1 test

Fitted breakthrough curves

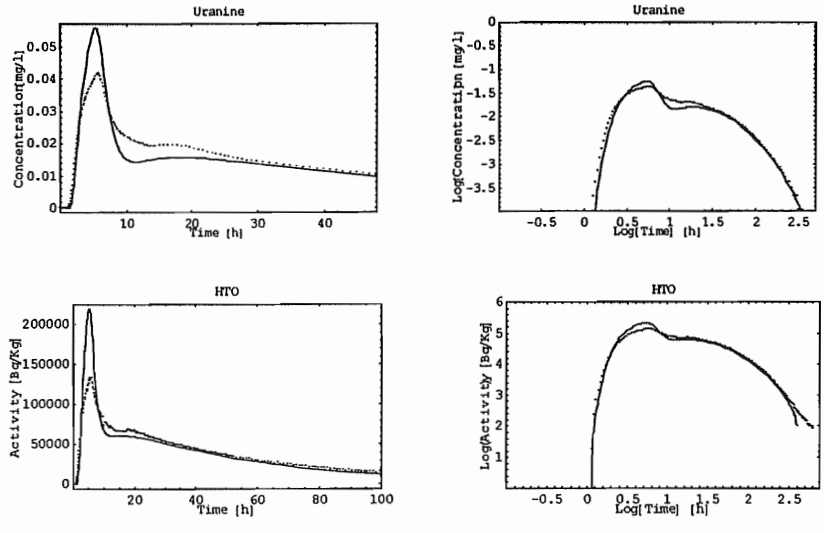

VTT ENERGY Antti Poteri

Analysis of the STT1 test

Fitted breakthrough curves

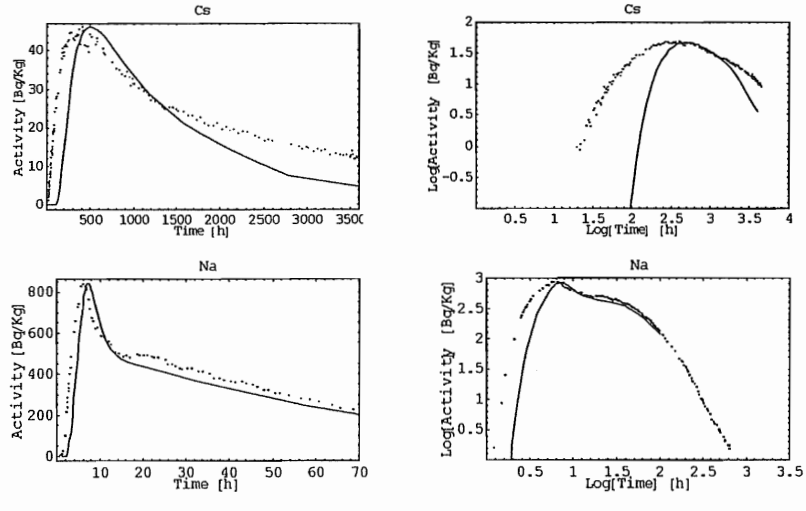

VTT ENERGY Antti Poteri

Analysis of the STT1 test

Fitted breakthrough curves

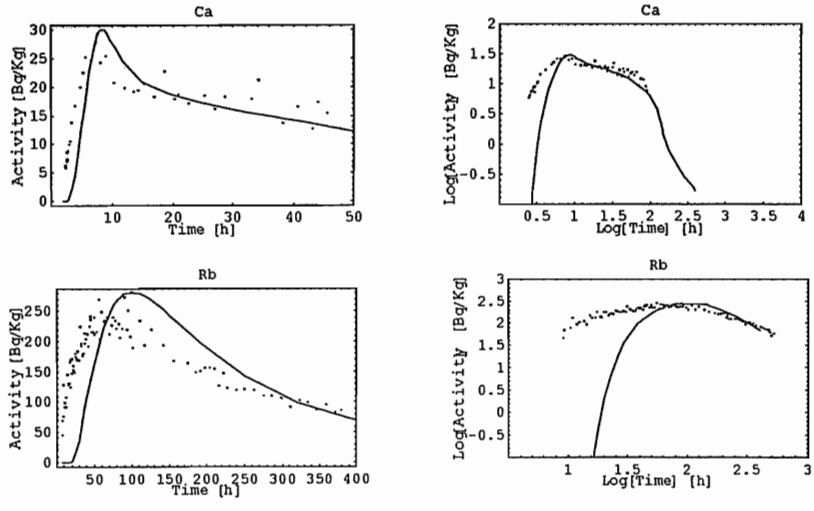

VTT ENERGY Antti Poteri

Analysis of the STT1 test

Fitted breakthrough curves

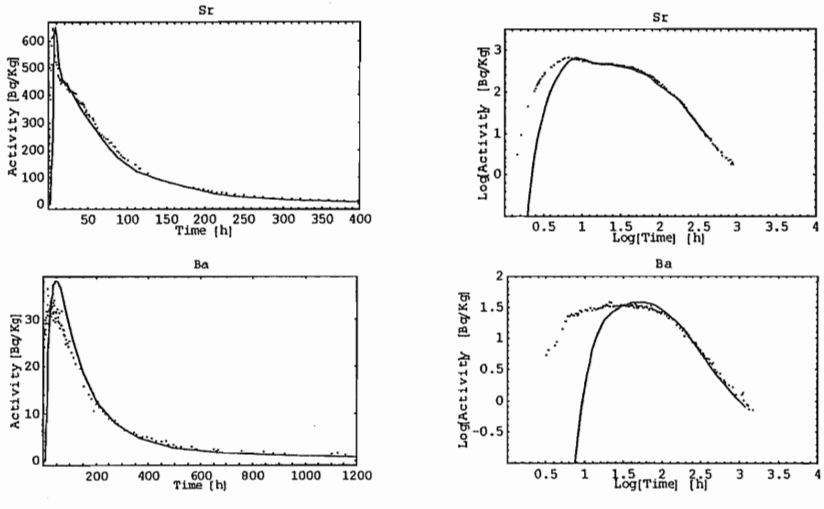

VTT ENERGY Antti Poteri

Fitted parameters

	u sqrt(h)	D (m2/h)	eps	rp	w/q (h/m)	l (m)	2bv (m)	q ml/h	chan. width (m)	v max (m/s)
HTO	0.172	8.6E-06	1	1	5.9E+01	4.68	5E-04	40	0.05	8.89E-04
Ur	0.172	8.6E-06	1	1	5.9E+01	4.68	5E-04	40	0.05	8.89E-04
Cs	13.0	8.6E-06	1	5715	5.9E+01	4.68	5E-04	40	0.05	8.89E-04
Na	1.10	8.6E-06	1	41	5.9E+01	4.68	5E-04	40	0.05	8.89E-04
Rb	6.0	8.6E-06	1	1217	5.9E+01	4.68	5E-04	40	0.05	8.89E-04
Ca	1.2	8.6E-06	1	49	5.9E+01	4.68	5E-04	40	0.05	8.89E-04
Sr	1.6	8.6E-06	1	87	5.9E+01	4.68	5E-04	40	0.05	8.89E-04
Ba	3.8	8.6E-06	1	488	5.9E+01	4.68	5E-04	40	0.05	8.89E-04

VTT ENERGY Anttl Poteri

Predictions of the STT2 test

- Parameters based on the STT1 test
- Injection flow rate from the Uranine injection curve

  $t < 20$ h 90 ml/h (based on the interval 0.5 h < t < 4 h)

  $t > 20$ h 25 ml/h

VTT ENERGY Anttl Poteri

Predictions of the STT2 test

- Calculated injected masses in Bq (Uranine mg)

Ba131	1.20119×10^{6}
Ba133	1.83574×10^{5}
Br	4.00979×10^{6}
Ca	2.44399×10^{5}
Cs	4.90308×10^{6}
HTO	1.15876×10^{8}
Na	1.19493×10^{6}
Rb	3.43682×10^{6}
Sr	3.68994×10^{6}
Ur	3.55978×10^{1}

VTT ENERGY Antti Poteri

Transport parameters

Based on the STT1 test

	u sqrt(h)	D (m2/h)	eps	rp	w/q (h/m)	l (m)	2bv (m)	q ml/h	chan. width (m)	v max (m/s)
HTO	0.275	8.6E-06	1	1	9.4E+01	4.68	5E-04	25	0.05	5.56E-04
Ur	0.275	8.6E-06	1	1	9.4E+01	4.68	5E-04	25	0.05	5.56E-04
Cs	20.8	8.6E-06	1	5715	9.4E+01	4.68	5E-04	25	0.05	5.56E-04
Na	1.76	8.6E-06	1	41	9.4E+01	4.68	5E-04	25	0.05	5.56E-04
Rb	9.6	8.6E-06	1	1217	9.4E+01	4.68	5E-04	25	0.05	5.56E-04
Ca	1.9	8.6E-06	1	49	9.4E+01	4.68	5E-04	25	0.05	5.56E-04
Sr	2.6	8.6E-06	1	87	9.4E+01	4.68	5E-04	25	0.05	5.56E-04
Ba	6.1	8.6E-06	1	488	9.4E+01	4.68	5E-04	25	0.05	5.56E-04

VTT ENERGY Antti Poteri

Breakthrough curves

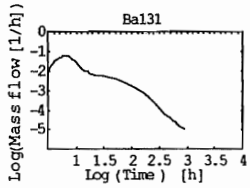

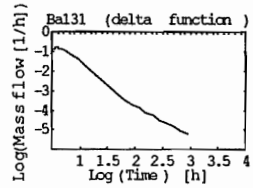

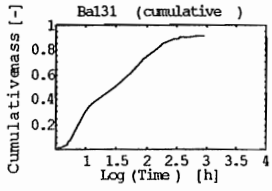

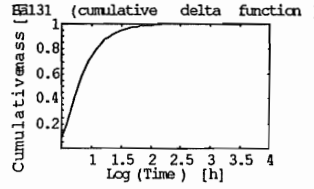

VTT ENERGY Antti Poteri

Breakthrough curves

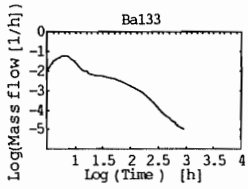

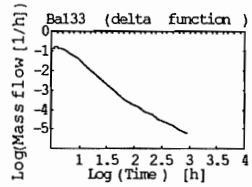

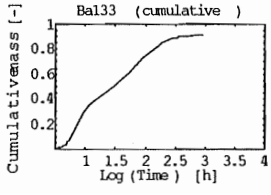

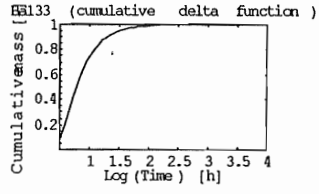

VTT ENERGY Antti Poteri

Breakthrough curves

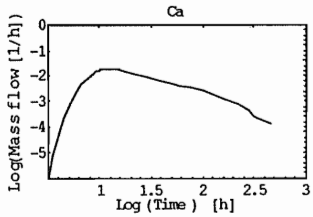

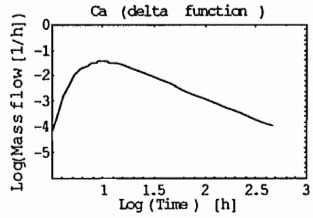

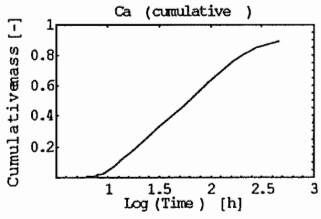

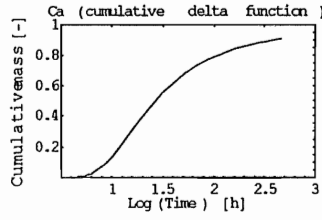

Breakthrough curves

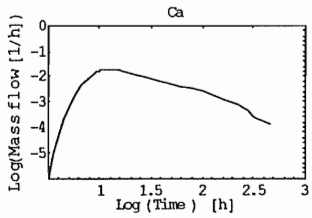

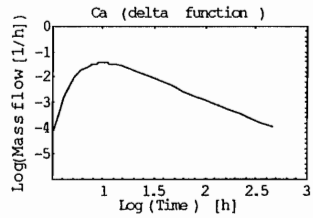

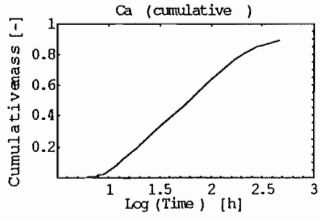

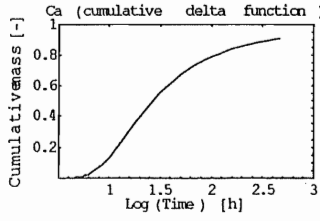

Breakthrough curves

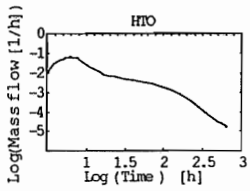

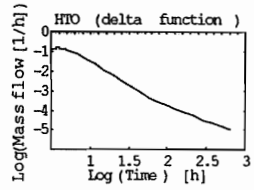

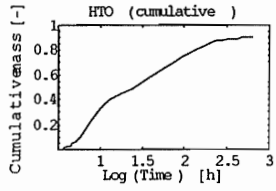

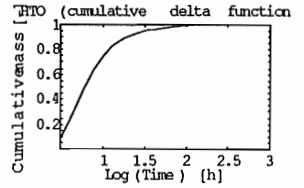

VTT ENERGY Antti Poteri

Breakthrough curves

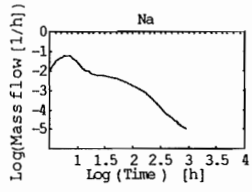

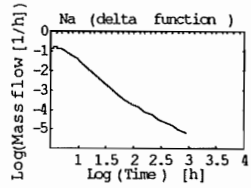

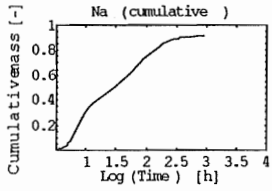

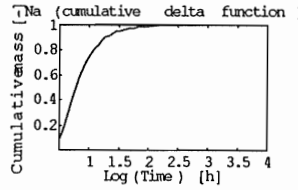

VTT ENERGY Antti Poteri

Breakthrough curves

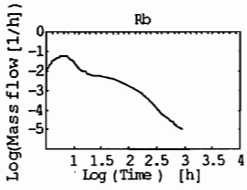

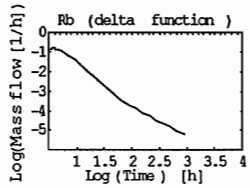

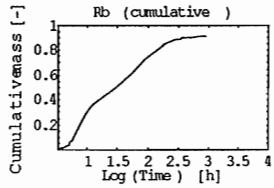

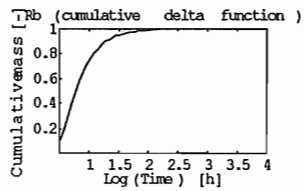

Breakthrough curves

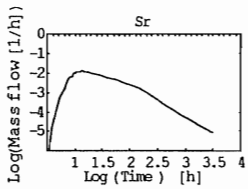

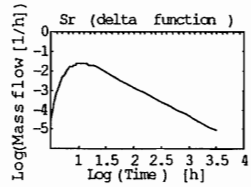

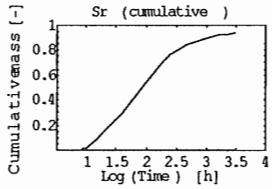

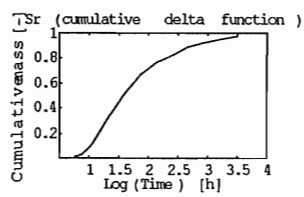

Breakthrough curves

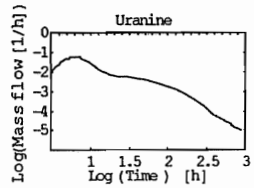

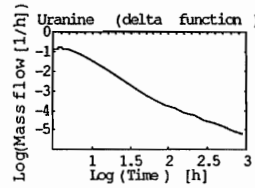

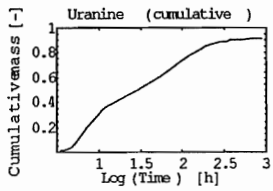

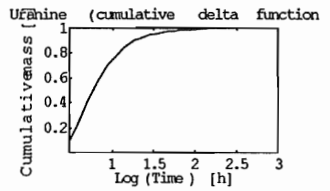

ENERGY Antti Poteri

Breakthrough curves

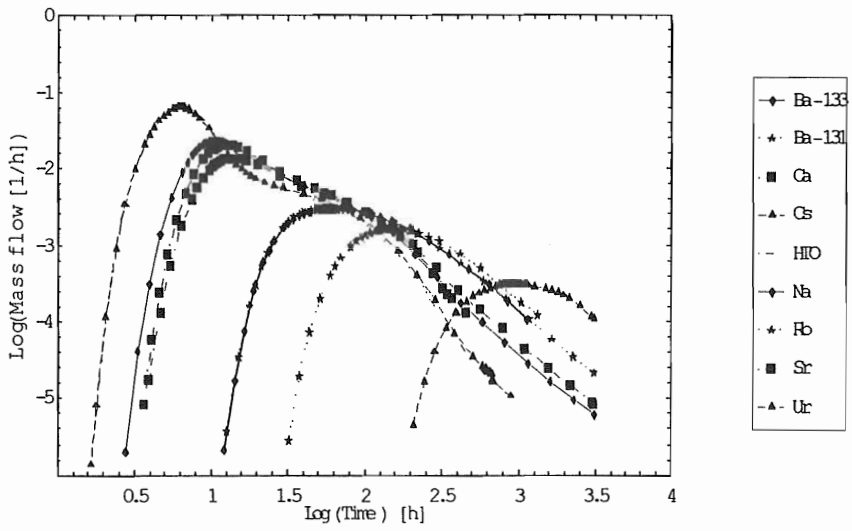

ENERGY Antti Poteri

Recoveries and breakthrough times

	t5 (h)	t50 (h)	t95 (h)	Recovery	
Ba-131	46	290		79 %	(1130 h)
Ba-133	46	280		90 %	(1130 h)
Ca	11	61		89 %	(458 h)
Cs	590	2400		60 %	(3078 h)
HTO	4.7	24		90 %	(641 h)
Na	9	58	1900	96 %	(3078 h)
Rb	107	523		71 %	(1322 h)
Sr	12	86		94 %	(3078 h)
Uranine	4.8	29		91 %	(886 h)

VTT ENERGY Antti Poteri

Task 4F analysis of STT2 blind predictions.

T.T. Cladouhos & W. Dershowitz (JNC/Golder), M. Uchida (JNC)

TRACER TESTS WITH SORBING TRACERS

Task 4F Analysis of STT-2 blind prediction

DRAFT

Trenton T. Cladouhos[1]
William S. Dershowitz[1]
Masahiro Uchida[2]

[1]Golder Associates, Inc., Redmond, WA, USA
[2]Japanese Nuclear Cycle Corporation, Tokai, Japan

April 15, 1999

EXECUTIVE SUMMARY

This report describes analysis of sorbing tracer experiments carried out within the Äspö TRUE-1 rock block for the Äspö Modeling Task Force (AMTF) meeting of April 19, 1999. Task 4f was a prediction of the SST-2 sorbing and non-sorbing tracer breakthrough based on an improved understanding of transport processes and parameters.

The STT-2 experiment was run at a pumping rate of 0.2 l/min between wells KTXX3 and KTXX4. As this is the same rate and geometry as PDT-2, the non-sorbing breakthrough curve of that test was used for pathway calibration. Calibration produced a nine path model. The average advective velocity, width, aperture, and length of the nine pathways was 0.4 m/s, 2.4 m, 0.23 mm, and 4.5 m, respectively. The model includes diffusion into matrix with 3% porosity and 1 cm diffusion depth in order to model the long breakthrough tails. This model is also capable of reproducing the non-sorbing breakthroughs at two different pumping rates (PDT-1 at 0.1 l/min and PDT-3 at 0.4 l/min).

The transport parameters for the sorbing tracers of STT-2 were calibrated to the STT-1 and STT-1b results. Surface and matrix sorption values were slightly adjusted from those used in STT-1 and STT-1b. Retardation values, which are dependent upon porosity and aperture, also changed for STT-2. Blind predictions for STT-2 are presented as log-log normalized mass flux breakthrough curves, cumulative mass curves, and values for t5, t50, t95, and percent mass recovery. Predictions based on a Dirac pulse injection, rather than the more complicated actual injection for STT-2 are also presented.

DRAFT

TABLE OF CONTENTS

LIST OF TABLES

LIST OF FIGURES

1. INTRODUCTION AND BACKGROUND

The Tracer Retention Understanding Experiments (TRUE) are part of a research program at Äspö, the Swedish Hard Rock Laboratory, designed to study the transport of radionuclides in crystalline rock. A series of tracer tests (TRUE-1) have been performed on a single fracture or fracture zone known as Feature A. The latest round of tests have included three non-sorbing tracers tests (PDT-1 , PDT-2, PDT-3, and PDT-4) and three sorbing tracer tests (STT-1, STT-1b, and STT-2). Task 4f, described in this report, involves blind prediction of the results of STT-2. STT-2, performed in the summer of 1998, involved the injection of a cocktail of ten tracers at KTXX4 and recovery at KTXX3 which was being pumped at a rate of 0.2 l/min. The combination of wells KTXX4 and KTXX3 have already been involved in several tracer tests including one, PDT-2, at the same pumping rate.

The primary goal of STT-2 wass to further investigate the effects of matrix diffusion by the use of a lower pumping rate. A secondary goal was to demonstrate the modeling of decay by using tracers with relatively short half lives. The tracers chosen for STT-2 included both conservative tracers, HTO, Uranine, and Br-82, and sorbing tracers, Na-22, Ca-47, Sr-85, Ba-131, Ba-133, Rb-134, and Cs-134. Ca-47, Br-82, Sr-85, Ba-131, and Rb-134 have half lives short enough that decay must also be modeled.

Throughout the TRUE-1 experiment the JNC/GOLDER modeling group has used stochastic discrete feature network (DFN) models to make predictions. Initially, for PDT-3 and STT-1, the DFN models were based upon multiple stochastic DFN realizations of a Feature A geologic conceptual model. This DFN model included three deterministic features, Feature A, Feature A', and Feature NW, and background fractures. Flow simulations of the DFN models provided simulated drawdowns and, via particle tracking, simulated non-sorbing tracer breakthrough curves. Acceptable models were chosen by comparing the measured drawdowns and breakthrough curves of PDT-3 to the model results. Accepted models were then used to predict STT-1 by calculating a retardation factor for each sorbing tracer.

As more information has been collected on the pathways between the injection and withdrawal boreholes, the need for a stochastic model has faded. The simple shape of the breakthrough curves in many of the tests indicates that models with relatively few transport paths are necessary. Therefore, in the latter part of TRUE-1, the JNC/Golder models have been pipe networks derived from the DFN. Pipe networks are better able to account for complex transport processes such as matrix diffusion and sorption and are computationally faster. For Task 4e:II and 4e:III, one path and two paths models were used to analyze STT-1 and predict STT-1b.

In this report, the results of the last blind prediction (STT-1b) are briefly reviewed to assess whether the transport processes are properly being modeled. Some changes in transport parameters are suggested. Then the DFN pipe network model is calibrated to non-sorbing breakthroughs of PDT-2 and the sorbing tracer tests modeled.

2. TASK 4F: PREDICTION OF STT-2

2.1 JNC/Golder strategy for Task 4f

The JNC/Golder strategy for this task closely followed that of the last two TRUE-1 tasks. We started with the geometric DFN model which includes Feature A, Feature A', Feature NW and intersecting background fractures (Dershowitz et al., 1997, Cladouhos et al., 1998). This basic model has remained unchanged since Task 4e (STT-1). From this 3D DFN model a pipe network approximation was generated using the PAWorks code. A similar procedure was performed for Task 4e:II and III; however, this time a 9 path approximation of the fracture model was retained rather than the more simplistic 1 or 2 path model that was used in the prediction of STT-1b.

Flow simulations using the 9 path model were performed and drawdowns calculated and compared to the drawdowns observed in PDT-2. No calibration was necessary to achieve acceptable drawdowns as the transmissivity of Feature A has been well-determined and already included in the model. Next, using the transport code LTG, the transport parameters of the 9 path model were calibrated to the non-sorbing tracer breakthrough of PDT-2. Fitting of the PDT-2 breakthrough required including a significant component of diffusion into stagnant immobile zones.

Prior to running simulation of sorbing tracer, we evaluated the results of the blind predictions STT-1b to ensure that the transport mechanisms were being properly modeled. Satisfied that STT1-b provided reasonable fits, sorption values were adjusted slightly and then the 9 pathway model was used to predict the STT-2 breakthrough curves.

2.2 Summary of Predictions

Table 1 STT-2 Tracer predictions

Tracer	t5 (h)	t50 (h)	t95 (h)	t100 (h)	Recovery
Uranine	9.7	65.3	247.9	886	100.0%
HTO	11.3	61.3	229.5	641	100.0%
Na-22	16.3	105.3	650.0	3078	100.0%
Ca-47	18.7	414.5	--	458	50.7%
Br-82	9.4	135.3	--	234	57.1%
Sr-85	22.7	170.6	--	3078	89.6%
Ba-131	162.7	1130.7	--	1130	18.3%
Ba-133	180.1	1106.6	--	3078	76.1%
Rb-134	533.5	--	--	1322	8.3%
Cs-134	1233.4	--	--	3078	16.8%

2.3 Dirac Pulse predictions

Table 2 STT2 Tracer predictions, Dirac pulse

Tracer	t5 (h)	t50 (h)	t95 (h)	t100 (h)	Recovery
Uranine	4.0	17.0	65.3	886	100.0%
HTO	5.3	20.3	61.3	641	100.0%
Na-22	7.3	44.3	224.0	3078	100.0%
Ca-47	8.3	147.3	--	458	48.6%
Br-82	4.0	27.3	--	234	57.9%
Sr-85	6.7	93.3	--	3078	88.0%
Ba-131	21.4	70.7	--	1130	75.7%
Ba-133	21.4	60.6	238.6	3078	98.5%
Rb-134	326.6	--	--	1322	10.6%
Cs-134	113.2	299.9	846.6	3078	98.9%

Äspö TRUE-1 Sorbing Tracer Experiment STT-2

Task 4F

JNC/Golder Team

April 19, 1999

JNC サイクル機構

Task 4F Approach

- Feature A with Intersecting Background Fractures
- PAWorks/LTG Pipe Transport Simulation in 3D DFN Model
- Calibrate transport mechanisms from STT-1b
- Calibrate transport pathways from PDT-2
- Calibrate drawdowns from PDT-2
- Predict STT-2 From STT-2 Injection with PDT-2 Pathways and STT-1b mechanisms

Transport mechanisms

- advection on multiple pathways
- longitudinal dispersion
- sorption to fracture surfaces
- diffusion into matrix or stagnant pools with sorption
- decay

3D DFN Model

- **Features NW, A, and A' and background fractures**

All 359 background fractures

5% background fractures

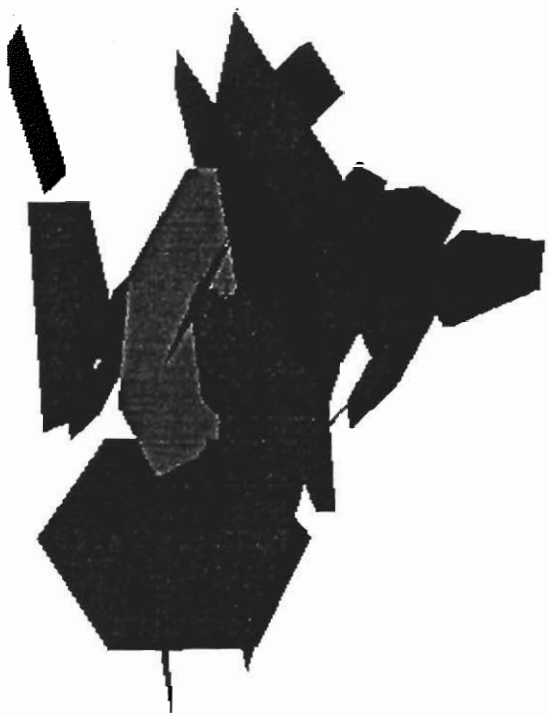

Test Geometries and Borehole Intersection Pattern

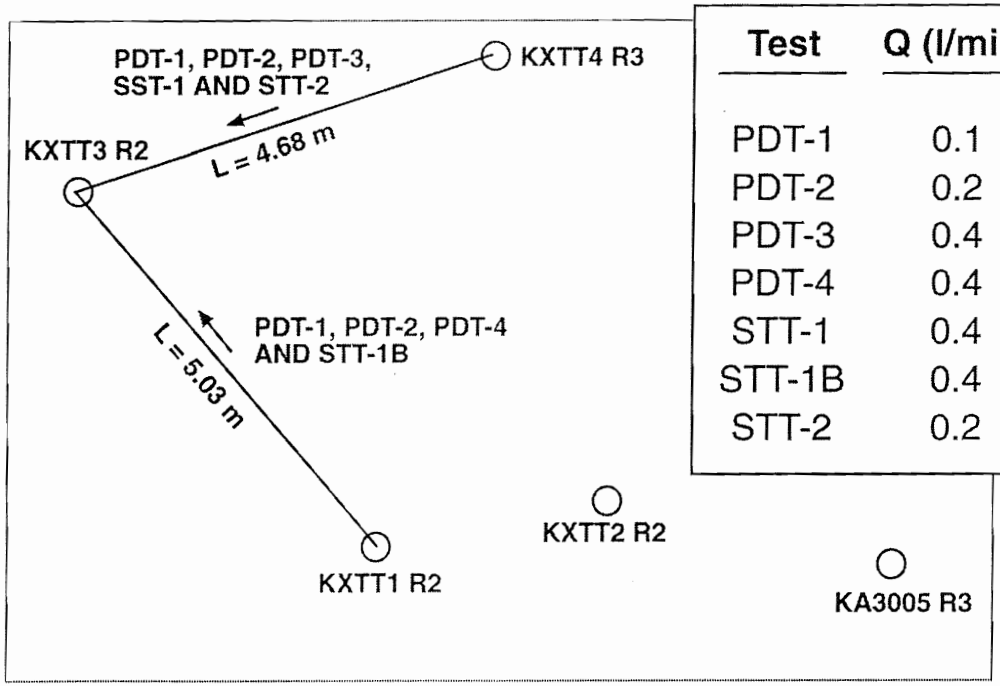

Test	Q (l/min)
PDT-1	0.1
PDT-2	0.2
PDT-3	0.4
PDT-4	0.4
STT-1	0.4
STT-1B	0.4
STT-2	0.2

Heads in Feature A

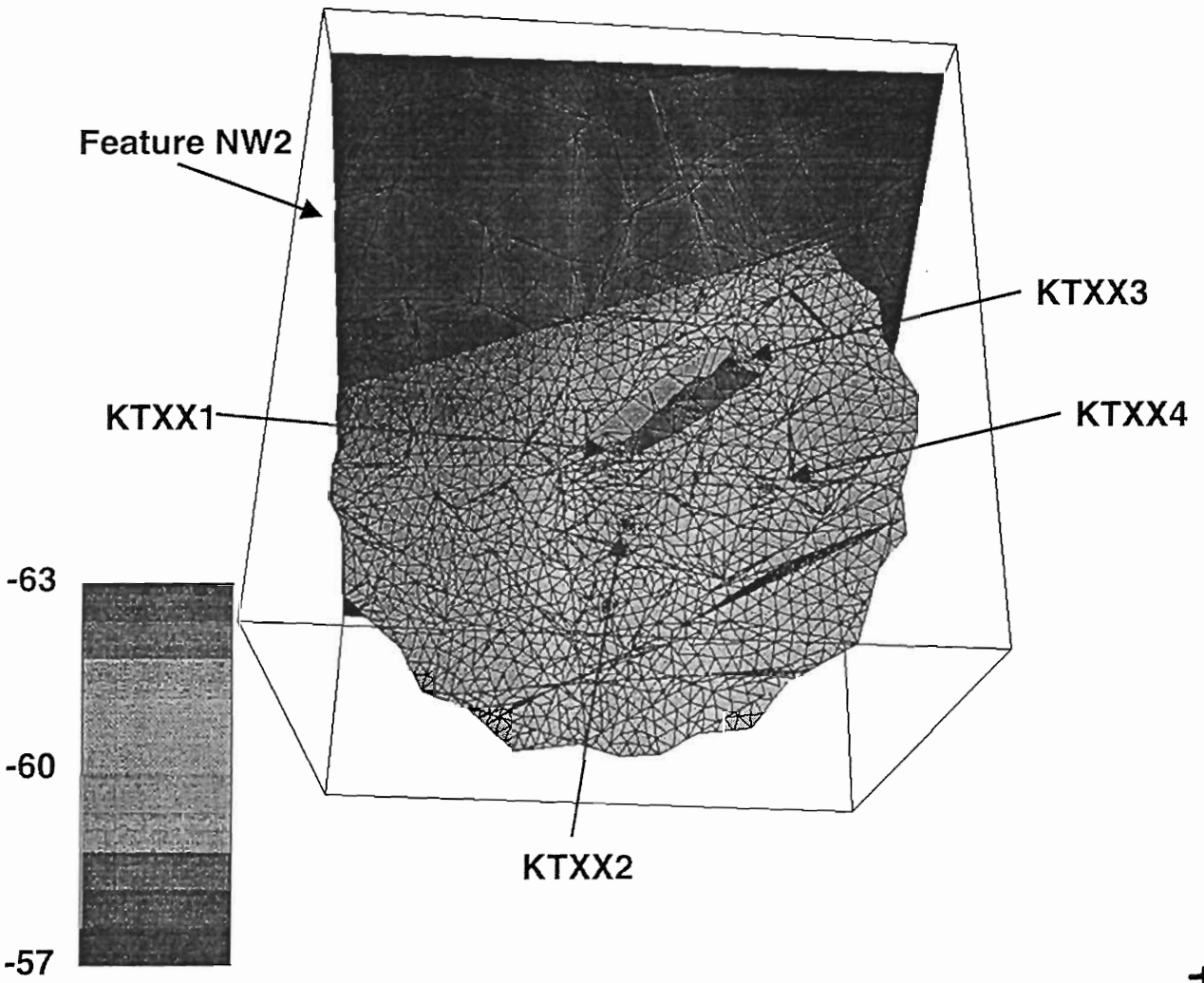

JNC サイクル機構

Drawdown Prediction from DFN Simulation

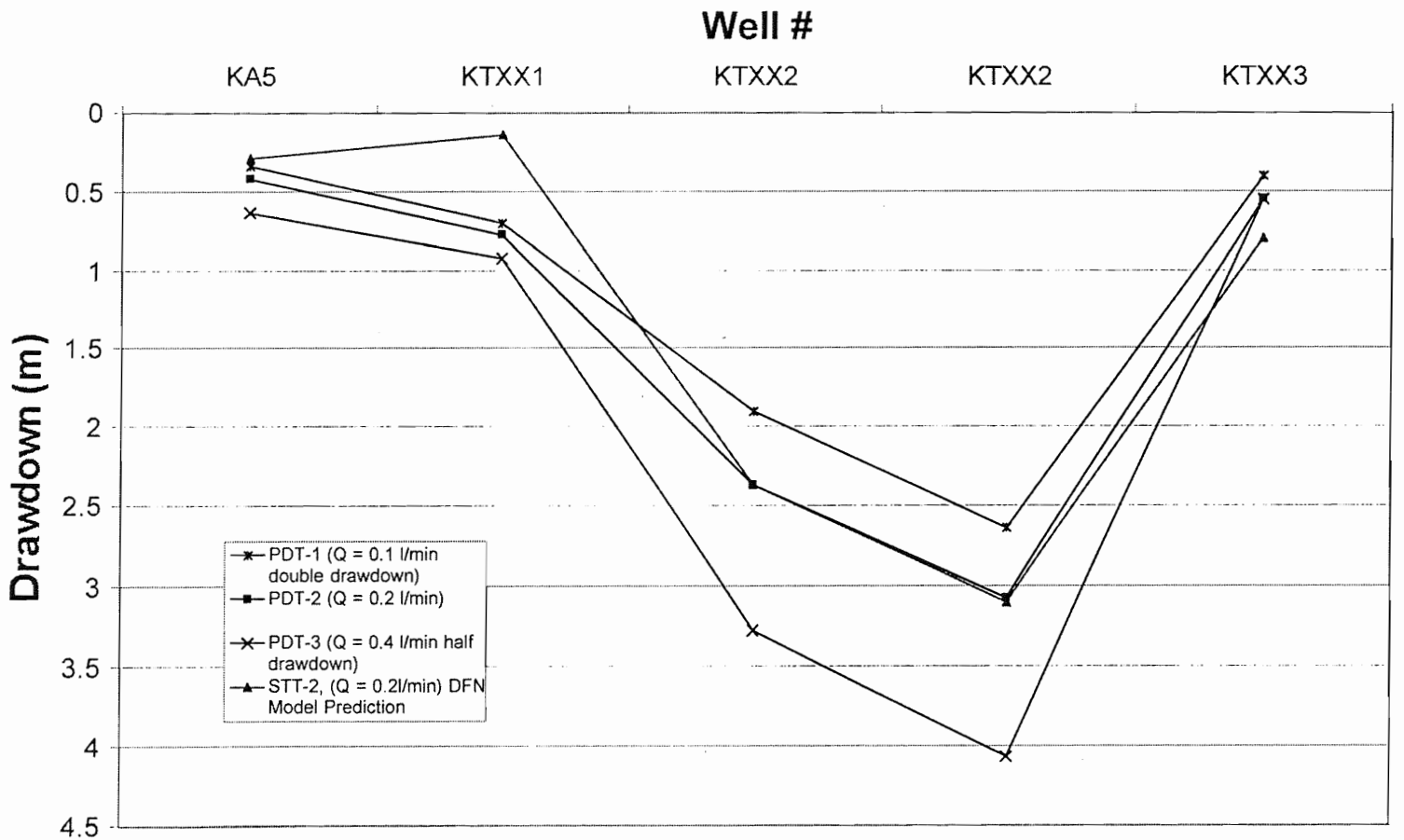

JNC サイクル機構

Drawdown predictions for STT-2

Well	STT-2 prediction (Q = 0.2 l/min)(m)	PDT-2 (Q = 0.2 l/min)(m)
KA5	0.29	0.42
KTXX1	0.14	0.77
KTXX2	2.37	2.37
KTXX2	3.1	3.08
KTXX3	0.8	0.55

Immobile zone concept

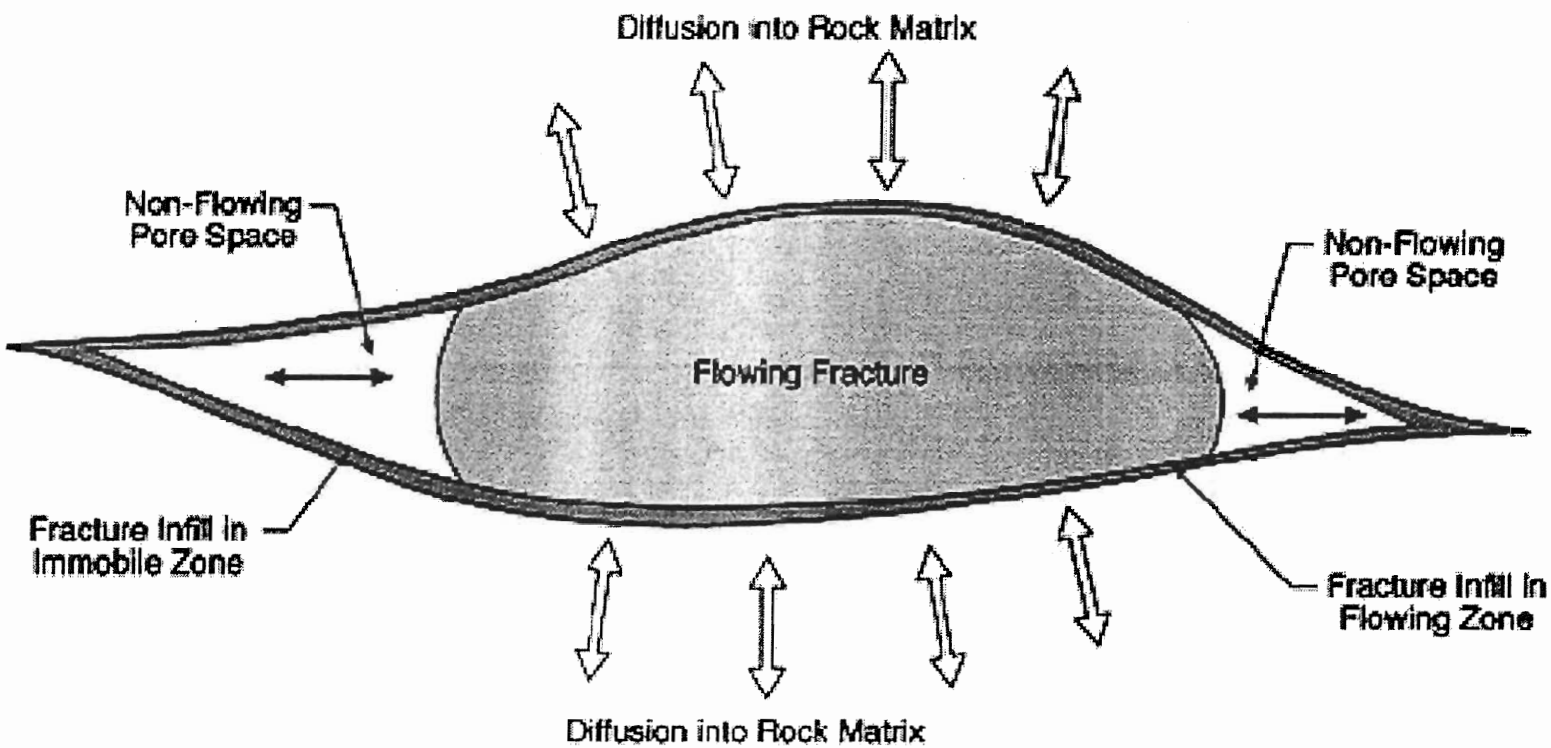

STT-1b Sorbing Tracer Breakthrough

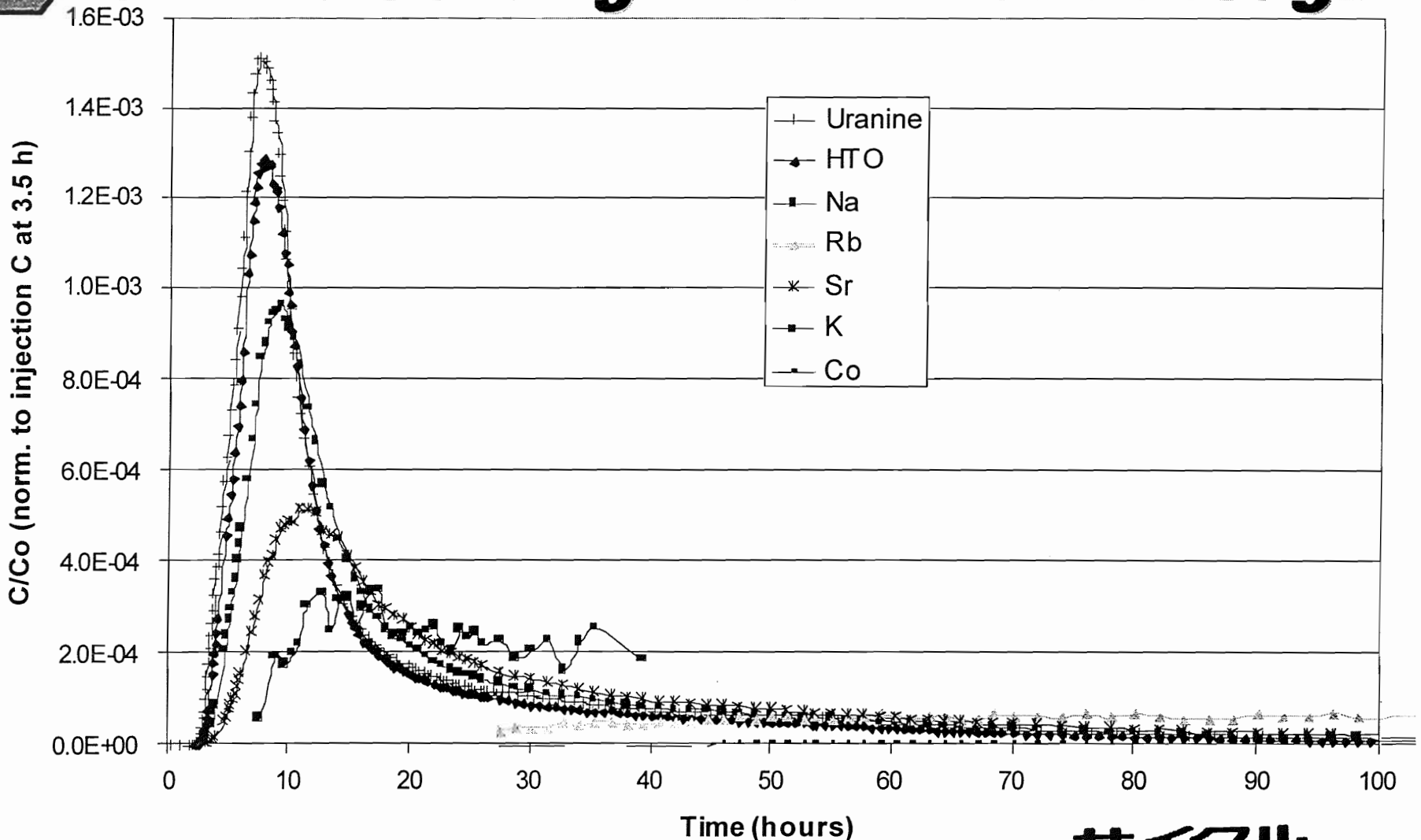

JNC サイクル機構

STT-1 Sorbing Tracer Breakthrough

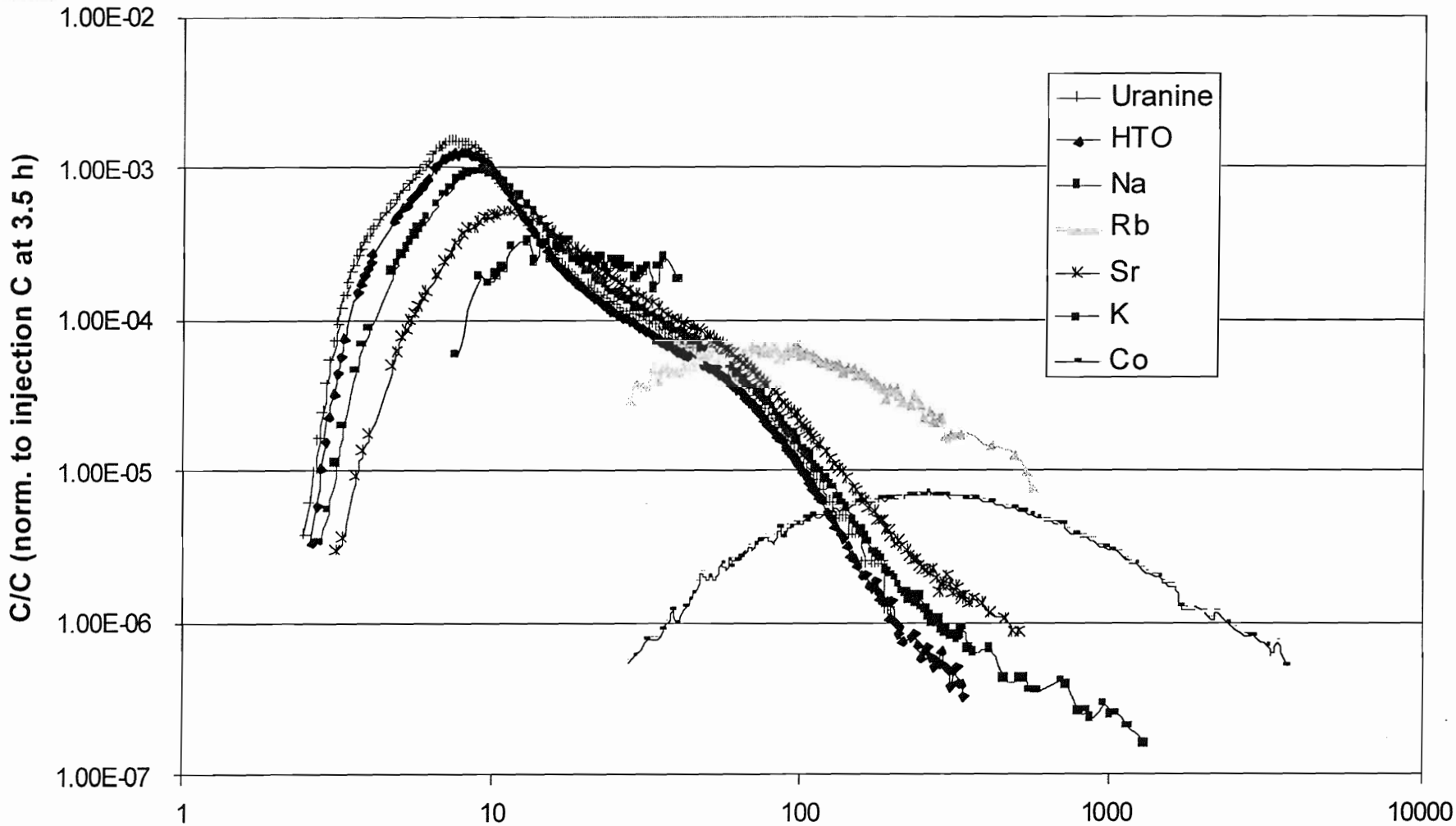

JNC サイクル機構

STT-1b Sr-86 prediction

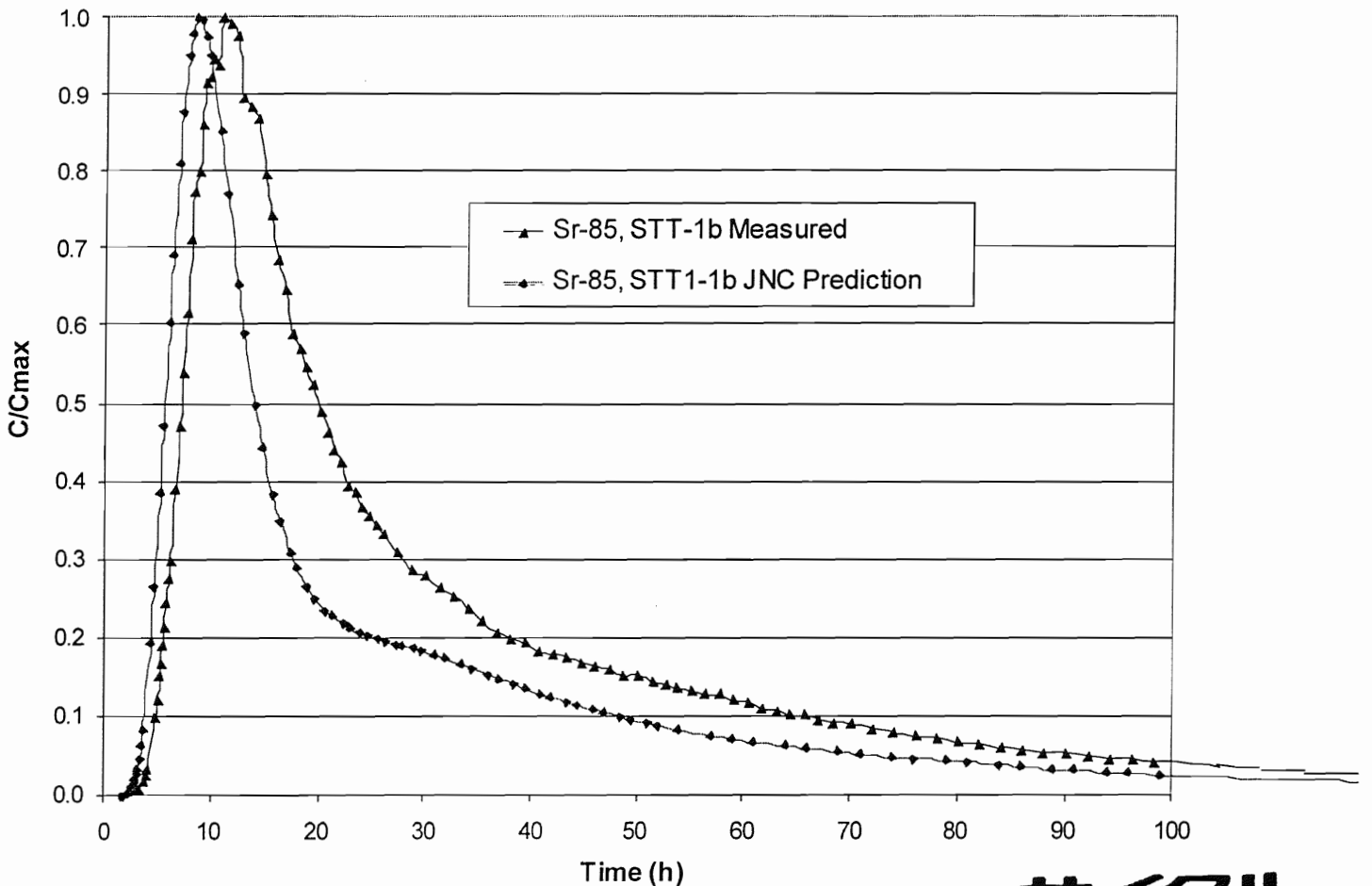

JNC サイクル機構

STT1b Rb prediction

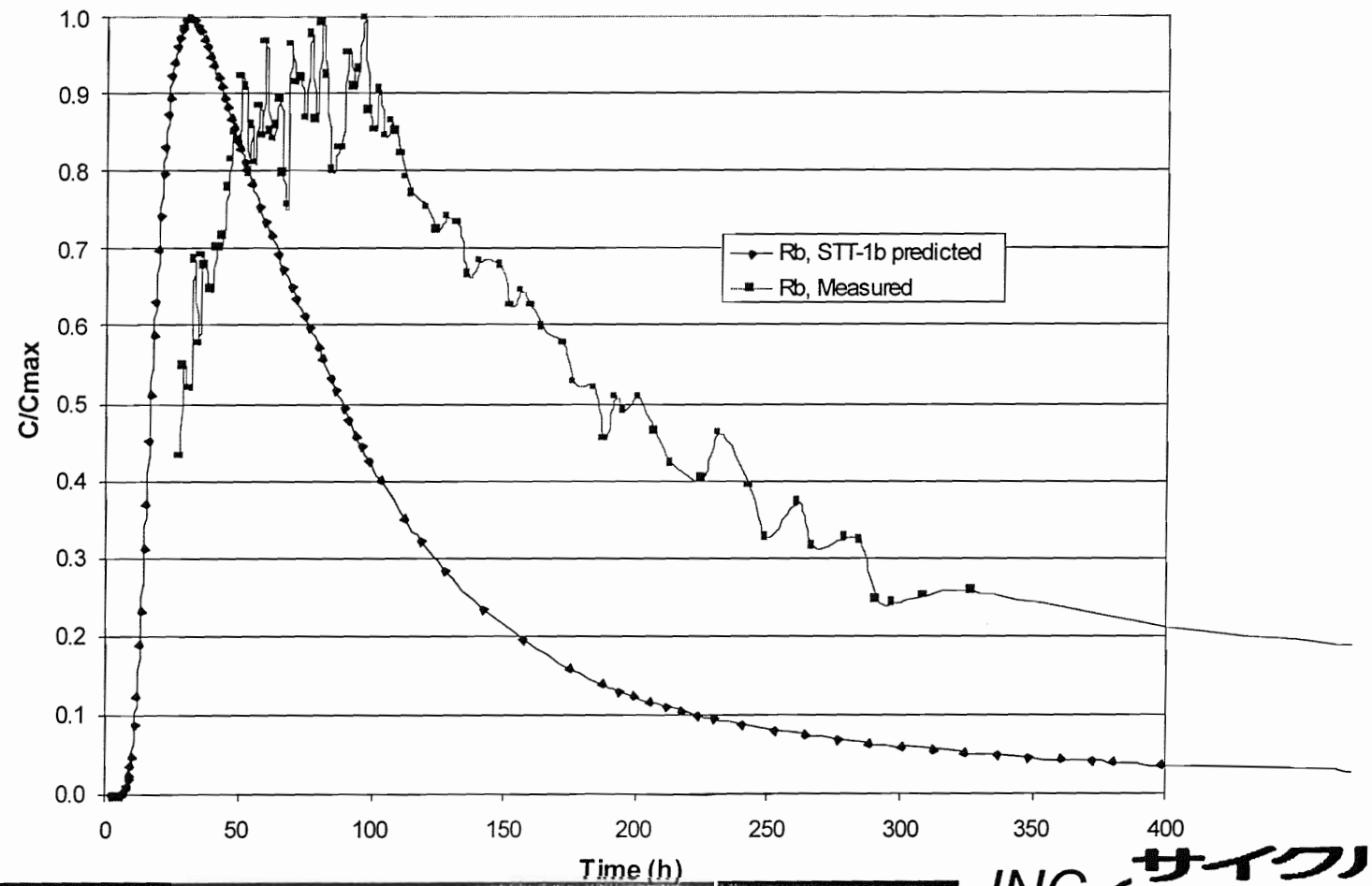

JNC サイクル機構

Transport Parameters for STT-1b

Parameter	one path	two path	
Velocity (m/hr)	0.75	0.75	0.4
Aperture (mm)	4	2	5
Width (m)	2.75	1.75	0.5
Length (m)	5.5	5.0	5.8
Travel Time (hr)	6.88	6.7	14.5
Dispersivity	0.4	0.5	0.2
Porosity	0.10	0.015	0.015

STT-1b Predictions and Measurement

		t5(h)	t50(h)	t95 (h)	t100 (h)	Rec. %
Ur	Predict.	5.2	12.3	83.3	195	97.9
	Meas.	5	11	80.5	0	100
HTO	Predict.	5	11.2	78.8	333	99.1
	Meas.	5	11.5	174	0	96
Na	Predict.	5	13.5	93.6	1292	100
	Predict.	6.5	17	900	0	96
K	Meas.	5.3	12.8	--	39.3	88.5
	Predict.	10.4	29.3	--	--	70
Sr	Meas.	5.8	19.5	229	505	96.9
	Predict.	8.3	35	229	0	81
Rb	Predict.	21.2	98.8	--	553	81.2
	Meas.	43	176	--	--	93
Co	Predict.	45.7	283	--	3620	89.6
	Meas.	273	--	--	--	30

Performance of STT-1b predictions

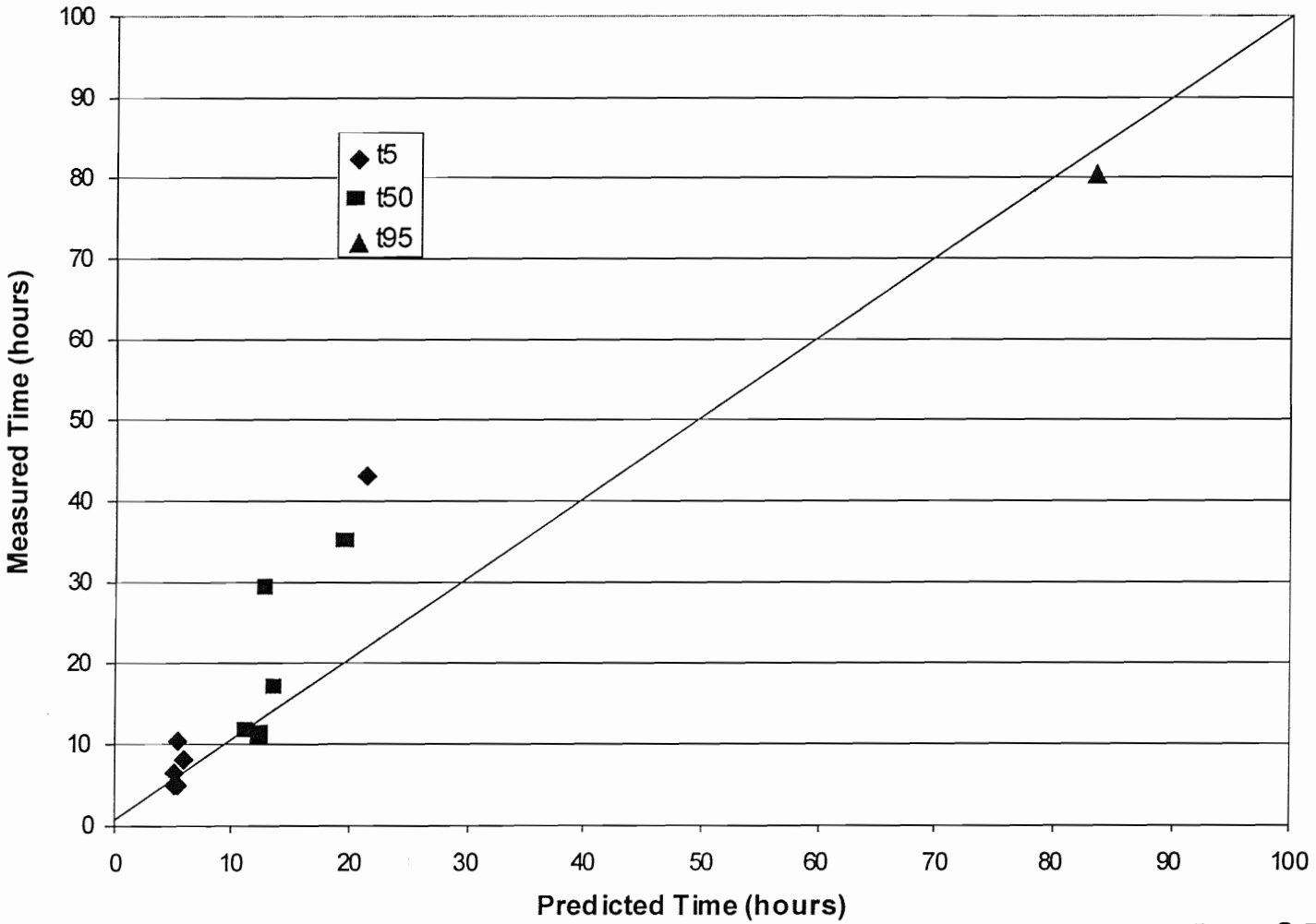

JNC サイクル機構

Performance of STT-1b predictions

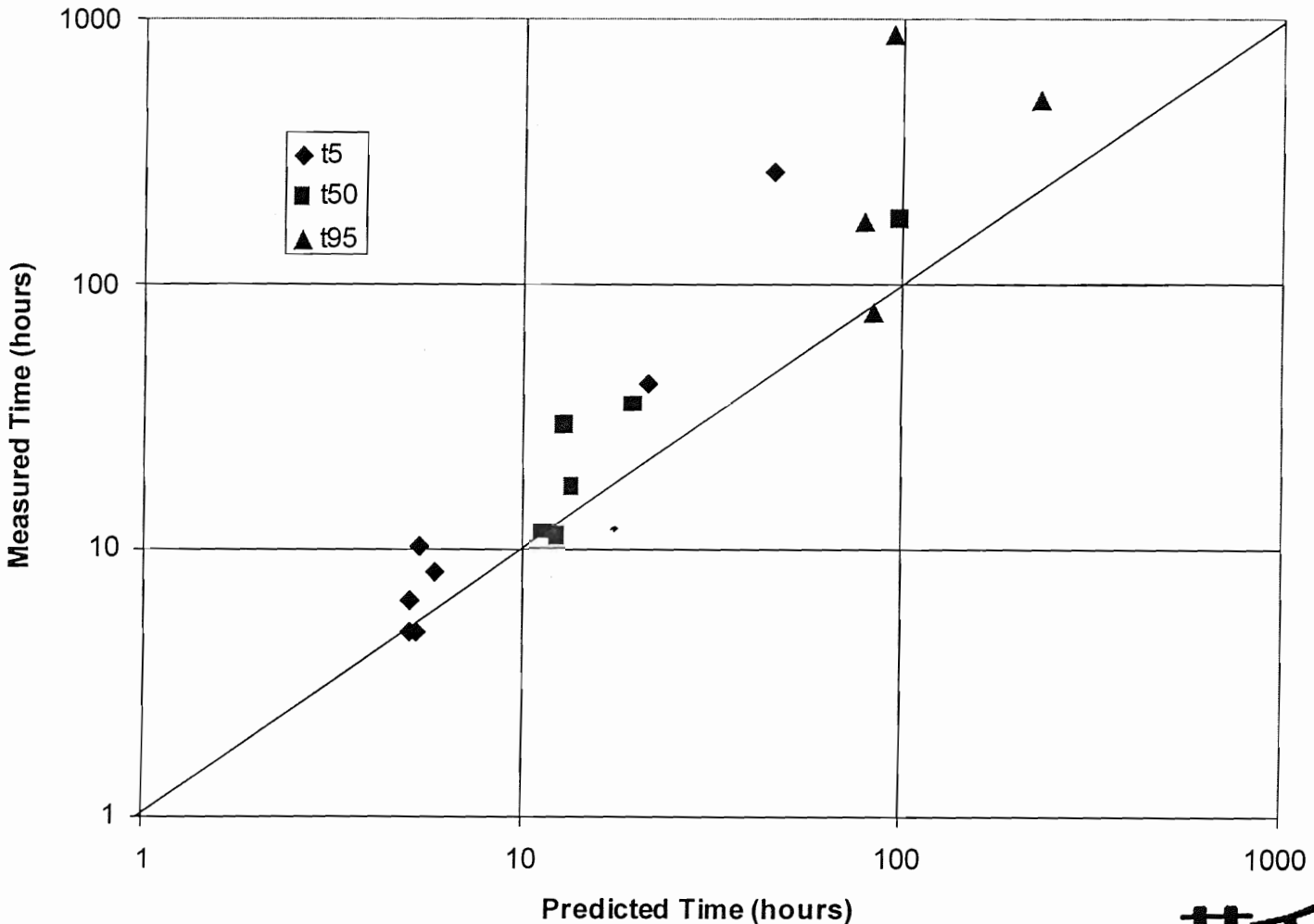

JNC サイクル機構

Performance of STT-1b recovery predictions

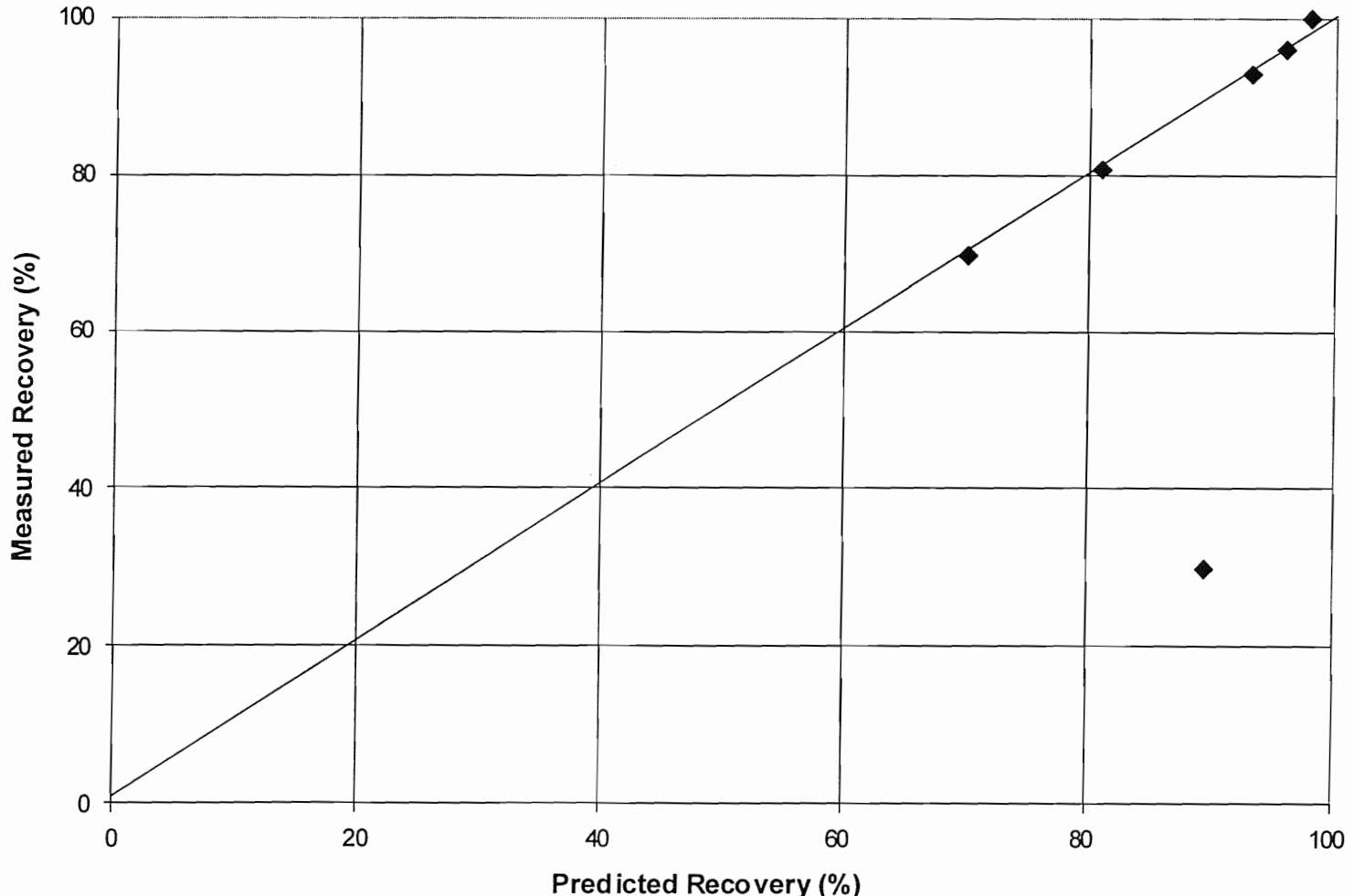

JNC サイクル機構

Transport Mechanisms based on STT-1b Results (Task 4E:III)

- t_{50} predictions were good. Transport aperture, surface sorption are OK
- t_{95} prediction requires even more matrix sorption processes (i.e. Rb)
- possible advective immobile zone process ?
- large surface area of multiple transport paths required by large tails

Transport Pathways Based on PDT-2

- Pathway Search through DFN Model with Background Fractures, Features A and A'
- Calibrate to Drawdown
- Aperture Calibrated to Mean Breakthrough
- Matrix Porosity, Thickness, and Surface Area of Immobile Zone Calibrated to Tail

Pathways through DFN Model found using PAWorks

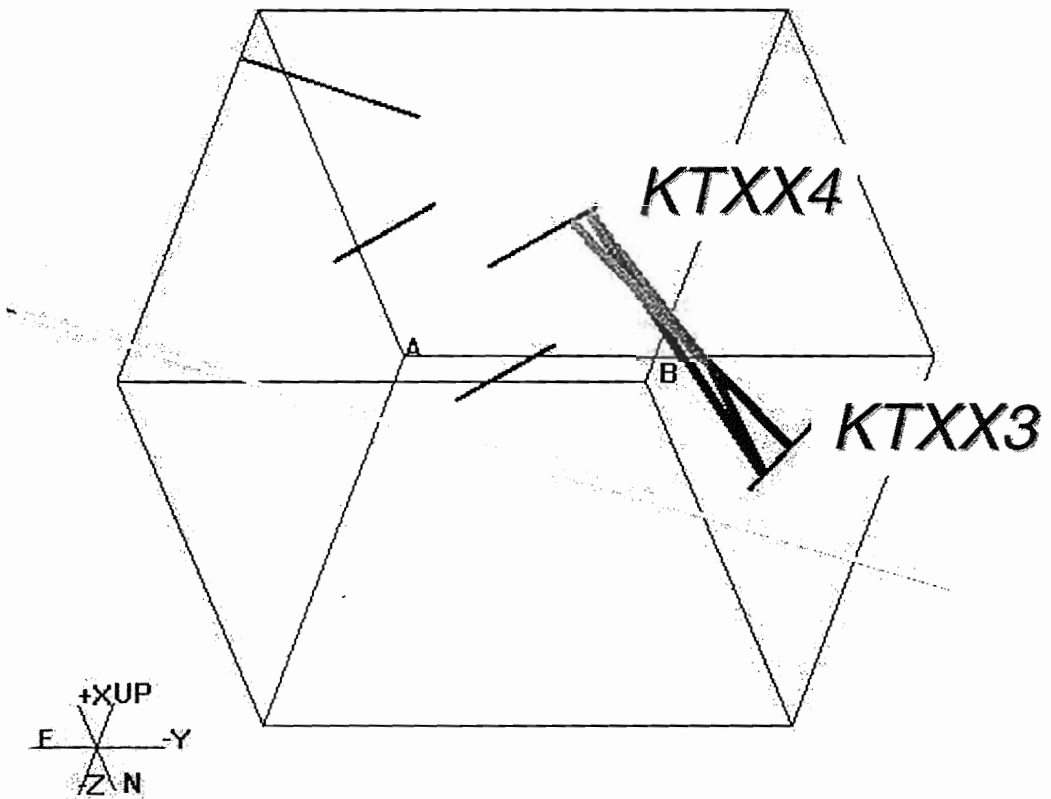

Pathways with background fractures

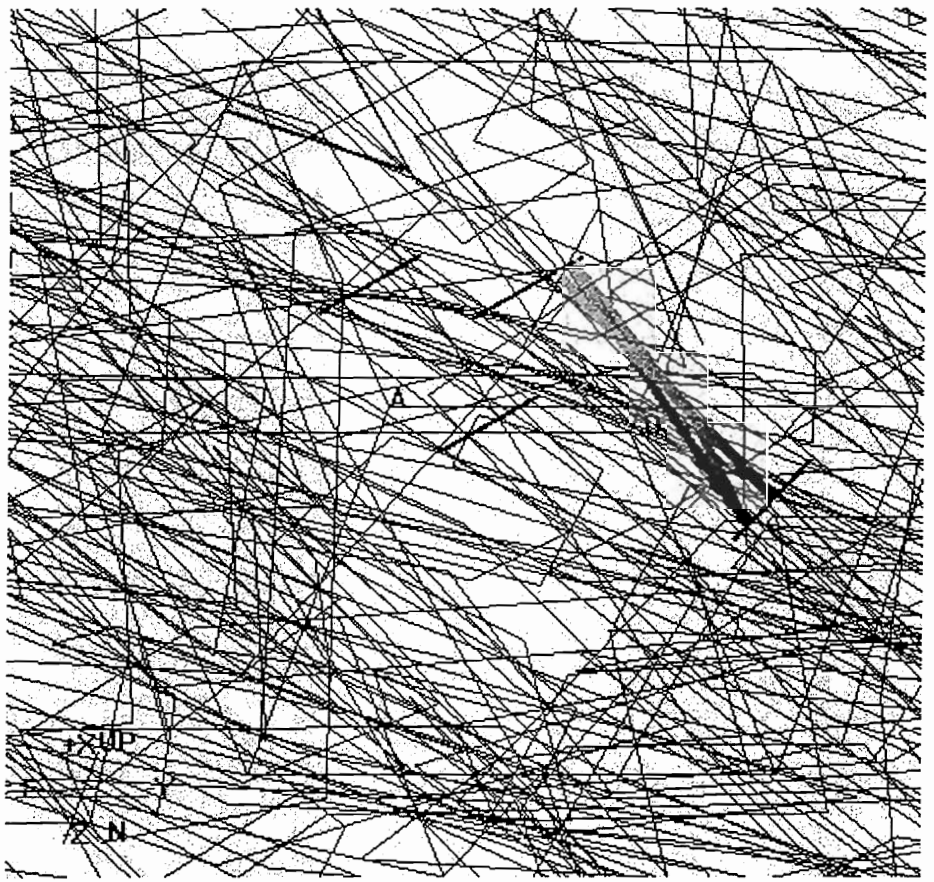

JNC サイクル機構

PDT-2 and STT-2 injection curves

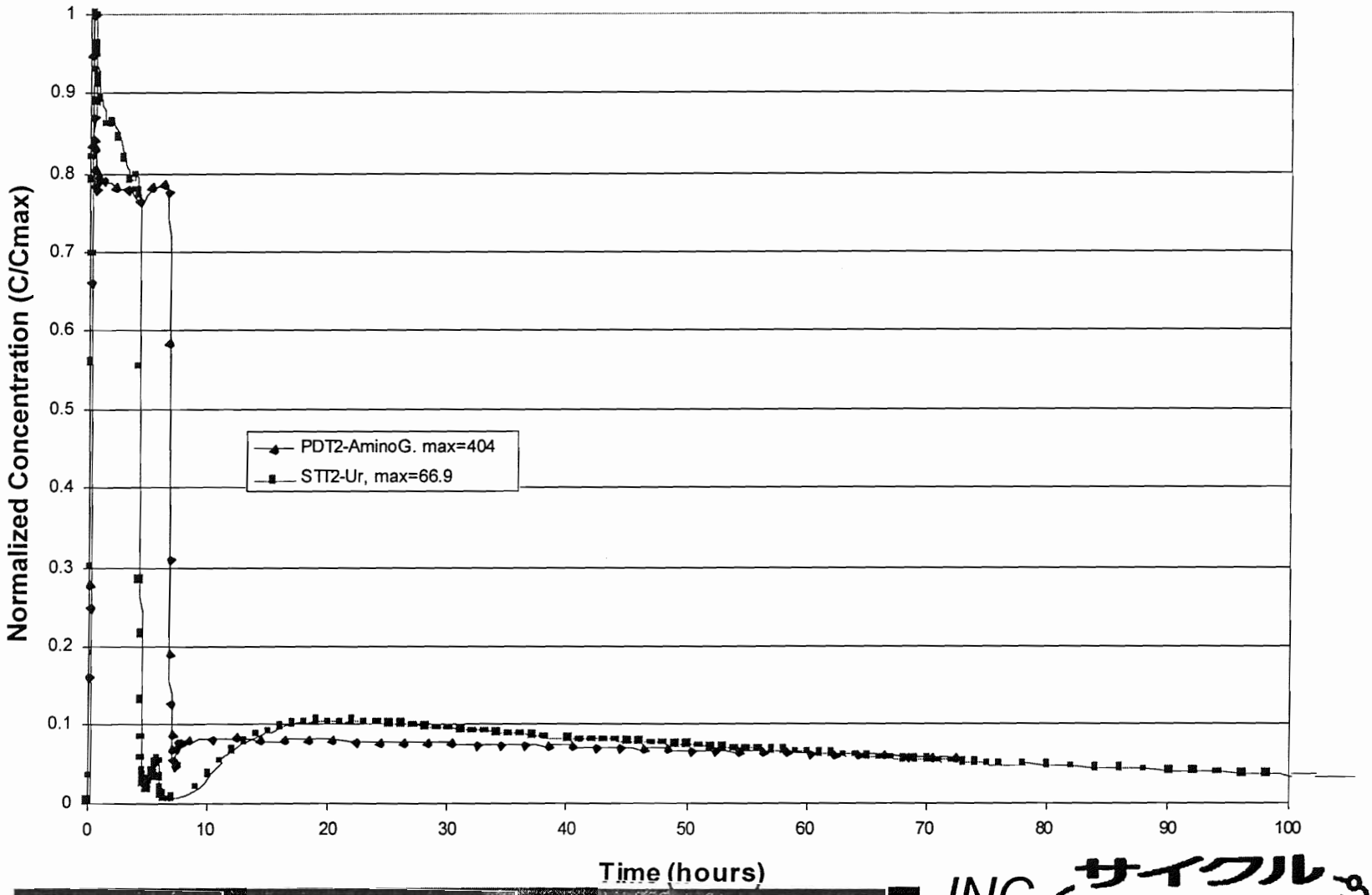

JNC サイクル機構

PDT-2 calibration

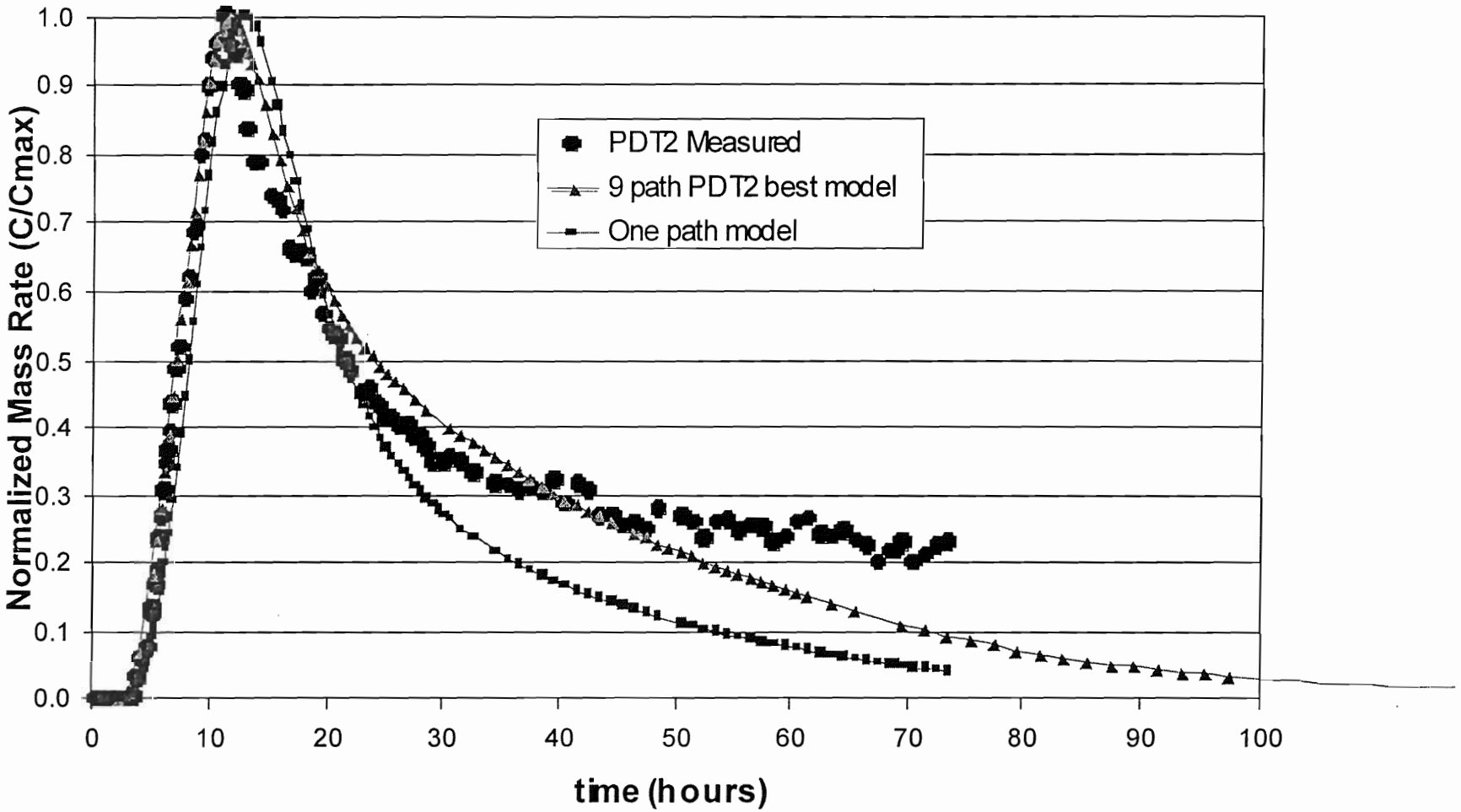

JNC サイクル機構

Transport Pathways in DFN Model by Calibration to PDT-2 Breakthrough

Parameter	9 path preferred model			1 path model
	min	max	mean	
Velocity (m/hr)	0.14	1.1	0.4	0.4
Aperture (mm)	0.10	0.29	0.23	0.23
Width (m)	0.02	2.9	2.4	13.5
Length (m)	4.2	4.7	4.5	4.5
Travel Time (hr)	4.3	29.3	11.4	11.3

Statistics from 9 Pathways
2 of 7 pipes extend out of Feature A
Mean travel time is flux weighted

Comparison of PDT-2 and STT-1b Pathways

Parameter	STT-1b (one path)	STT-1b (two path)	PDT-2 mean
Velocity (m/hr)	0.75	0.75 & 0.4	0.4
Aperture (mm)	4	2, 5	0.23
Width (m)	2.75	1.75 & 0.5	2.4
Length (m)	5.5	5.0 & 5.8	4.5
Travel Time (hr)	6.88	6.7 & 14.5	11.4

DFN model and other Well 4 to 3 non-sorbing tracer tests

Injection curves and pumping rate adjusted for each test

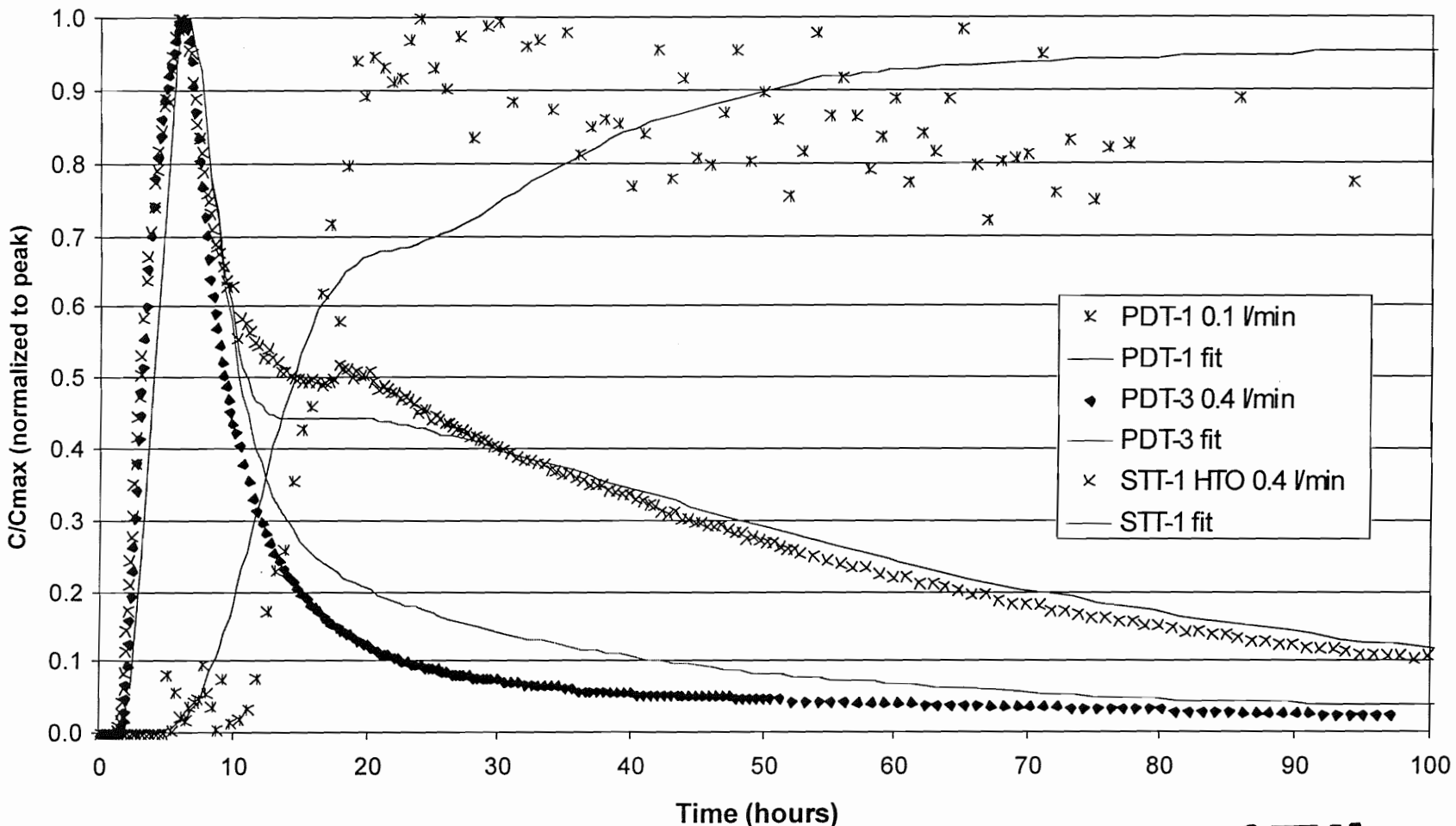

JNC サイクル機構

Effect of Matrix diffusion on PDT-2

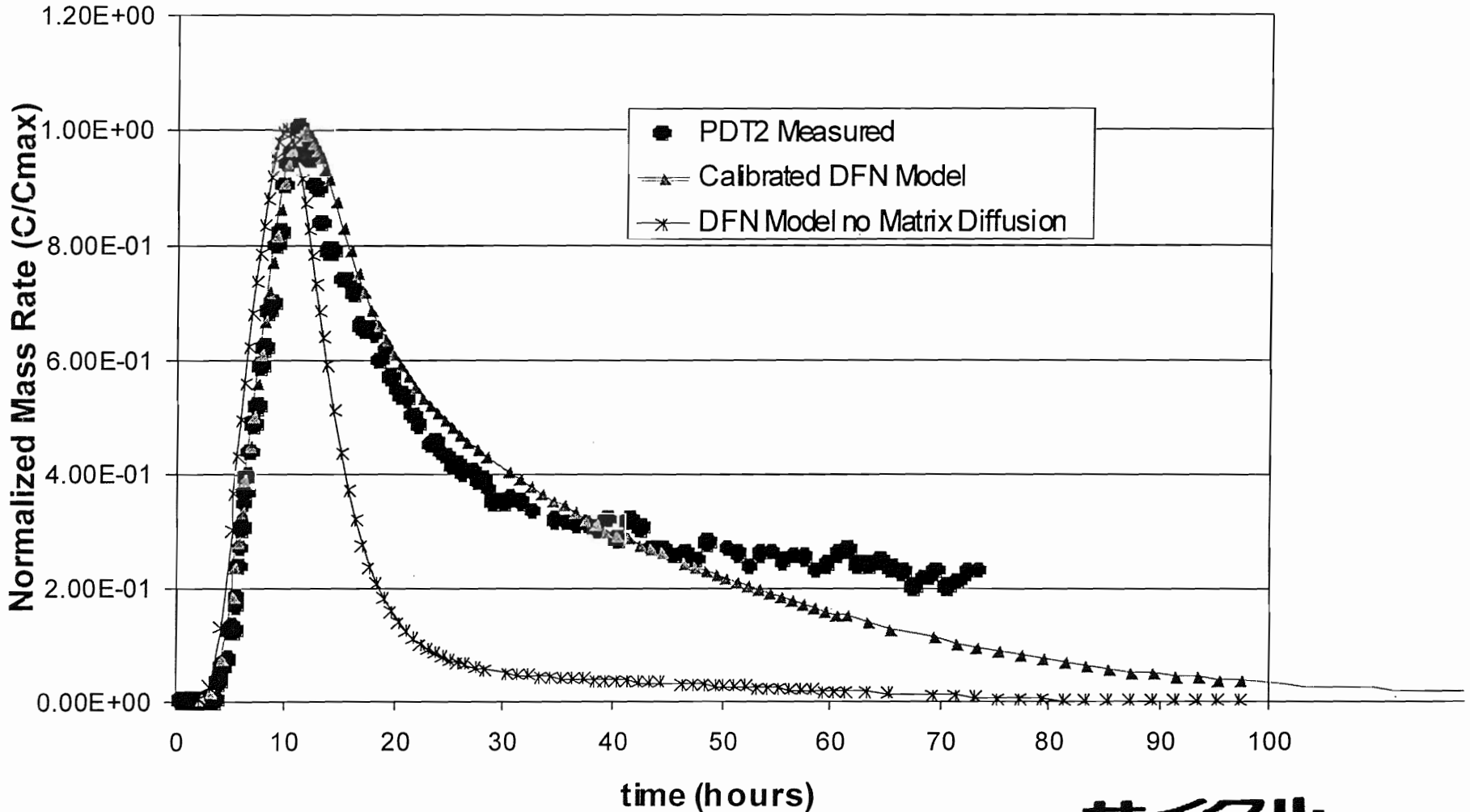

JNC サイクル機構

Effect of multiple paths and fracture perimeter

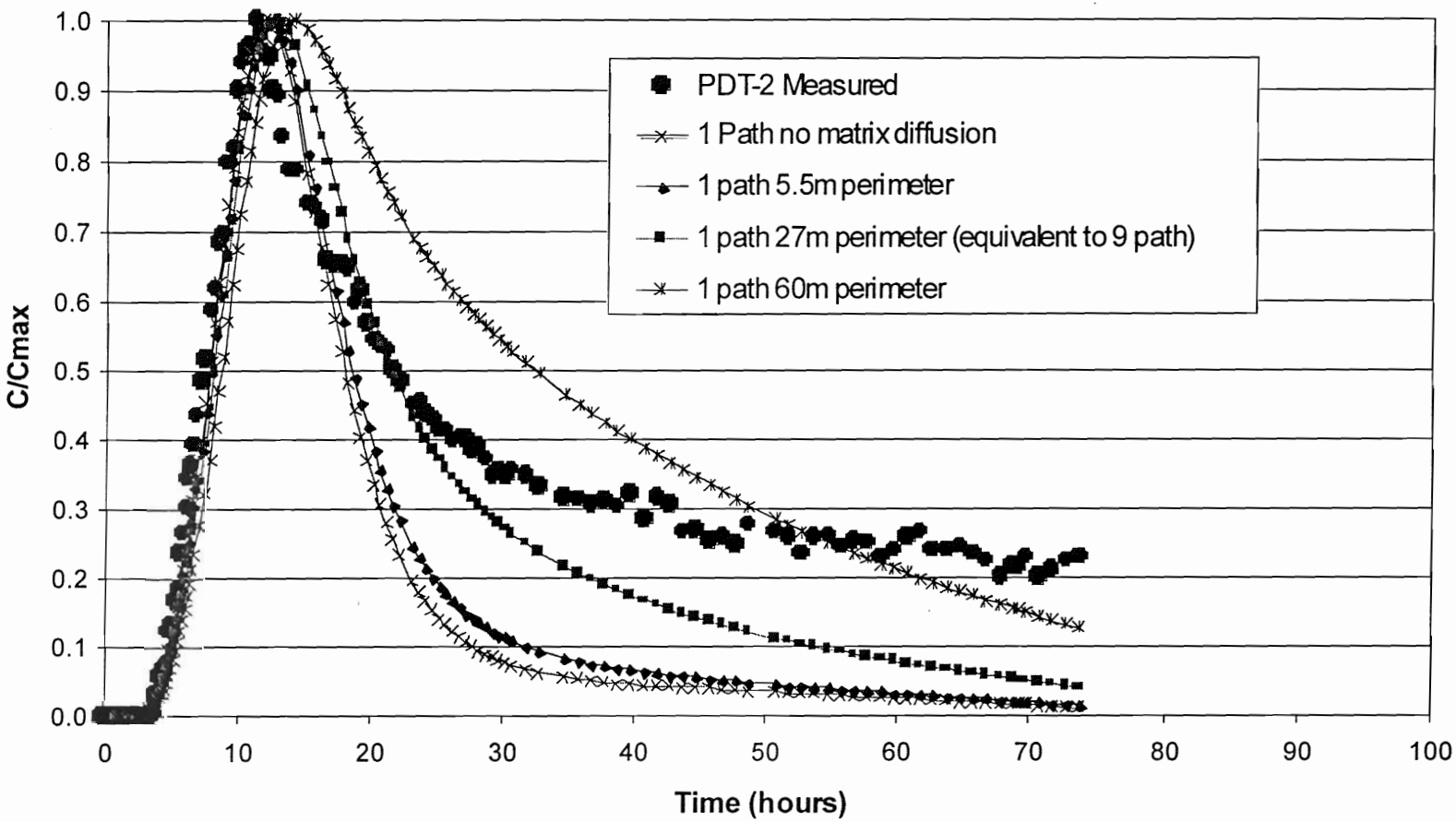

JNC サイクル機構

Pathways Transport Parameters Derived from PDT2 DFN Calibration

- Aperture = 1 * $T^{1/2}$
  - 0.3 mm on Feature A,
  - ~0.1 mm mean on background
- Matrix (immobile zone)
  - perimeter = 27 m
  - Porosity = 3%, and thickness = 1 cm,
  - OR porosity = 1%,and thickness = 3 cm

Sorption, diffusivity, and half lives for STT-1b and STT-2 datasets

Tracer	Surface Sorption, Ka (m)	Diffusivity (m/yr)	HalfLife	Source
Uranine	0	0.032	NA	HRL 97-07
HTO	0	0.076	12.3 y	HRL 97-07
Na-22	1.3E-05	0.042	2.6 y	STT1b
Ca-47	3.0E-05	0.025	4.5 d	HRL 97-07
Br-82	0	0.032	35 h	HRL 97-07
Sr-85	5.0E-05	0.025	65 d	STT1b
Ba-131	6.0E-04	0.026	12 d	Ohlsson & Neretnieks
Ba-133	6.0E-04	0.026	10.5 y	
Rb-96	1.0E-03	0.064	19 d	STT1b
Cs-134	4.0E-03	0.064	2.1 y	HRL 97-07

Retardations

	Ka (m)	Kd (m^3/kg) = Ka/ρ x 150	Surface retardation e = 0.29 mm	Matrix retardation n = 3%
Ur, HTO, Br	0	0	1	1
Na-22	1.3E-05	2.7E-05	1.09	3.25
Ca-47	3.0E-05	6.3E-05	1.21	6.2
Sr-85	5.0E-05	1.0E-04	1.34	9.7
Ba-131 -133	6.0E-04	1.3E-03	5.1	105
Rb-96	1.0E-03	5.2E-03	7.6	168
Cs-134	4.0E-03	1.67E-03	28	693

STT-1b vs. STT-2 transport parameters

Tracer and Test	Ka (m)	Kd (m3/kg)	Surface retardation	Matrix retardation
Na-22 STT-2*	1.3E-05	2.7E-05	1.09	3.25
Na-22 STT-1b**	5.0E-06	2.8E-05	1.04	2.00
Sr-85 STT-2	5.0E-05	1.0E-04	1.34	9.7
Sr-85 STT-1b	2.0E-05	2.3E-04	1.14	12
Rb-96 STT-2	2.5E-03	5.2E-03	18.1	434
Rb-96 STT-1b	1.0E-03	1.4E-03	8.1	20

* STT-2 based on nine path models, e=0.29 mm, n=3%

**STT-1b based on one path models, e=4 mm, n=10%

STT-2 Injection Curves

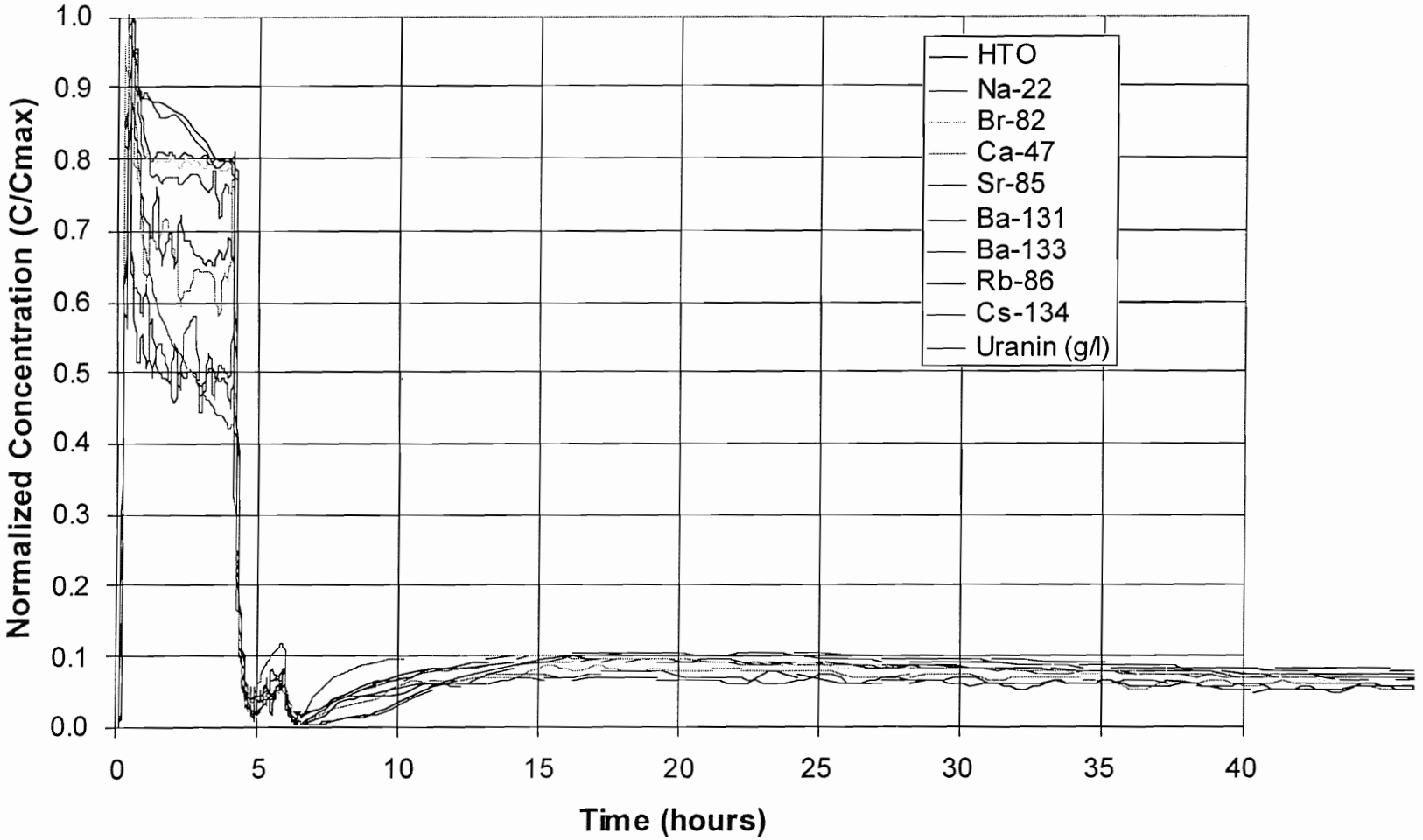

JNC サイクル機構

Injected Masses

Uranine	21.85	mg
HTO	69.45	MBq
Na	0.91	MBq
Br	2.87	MBq
Ca	0.19	MBq
Sr	2.75	MBq
Ba-131	1.12	MBq
Ba-133	0.08	MBq
Rb	3.51	MBq
Cs	4.14	MBq

Calculated at 26.6 ml/hr flow rate at injecting well

STT-2 Predictions, mass rate, to 100 h

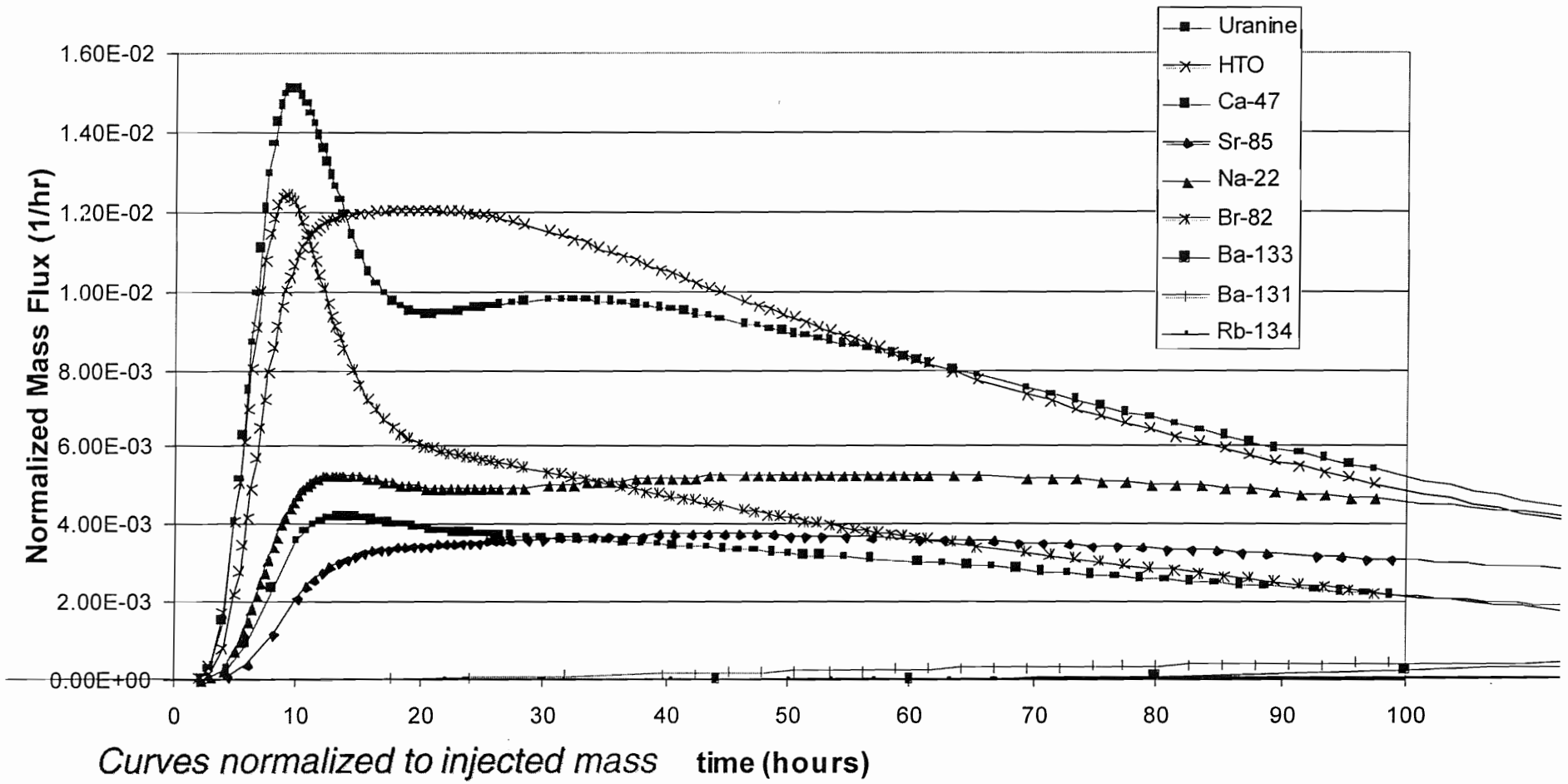

JNC サイクル機構

STT-2 Predictions, mass rate, to 3000 h

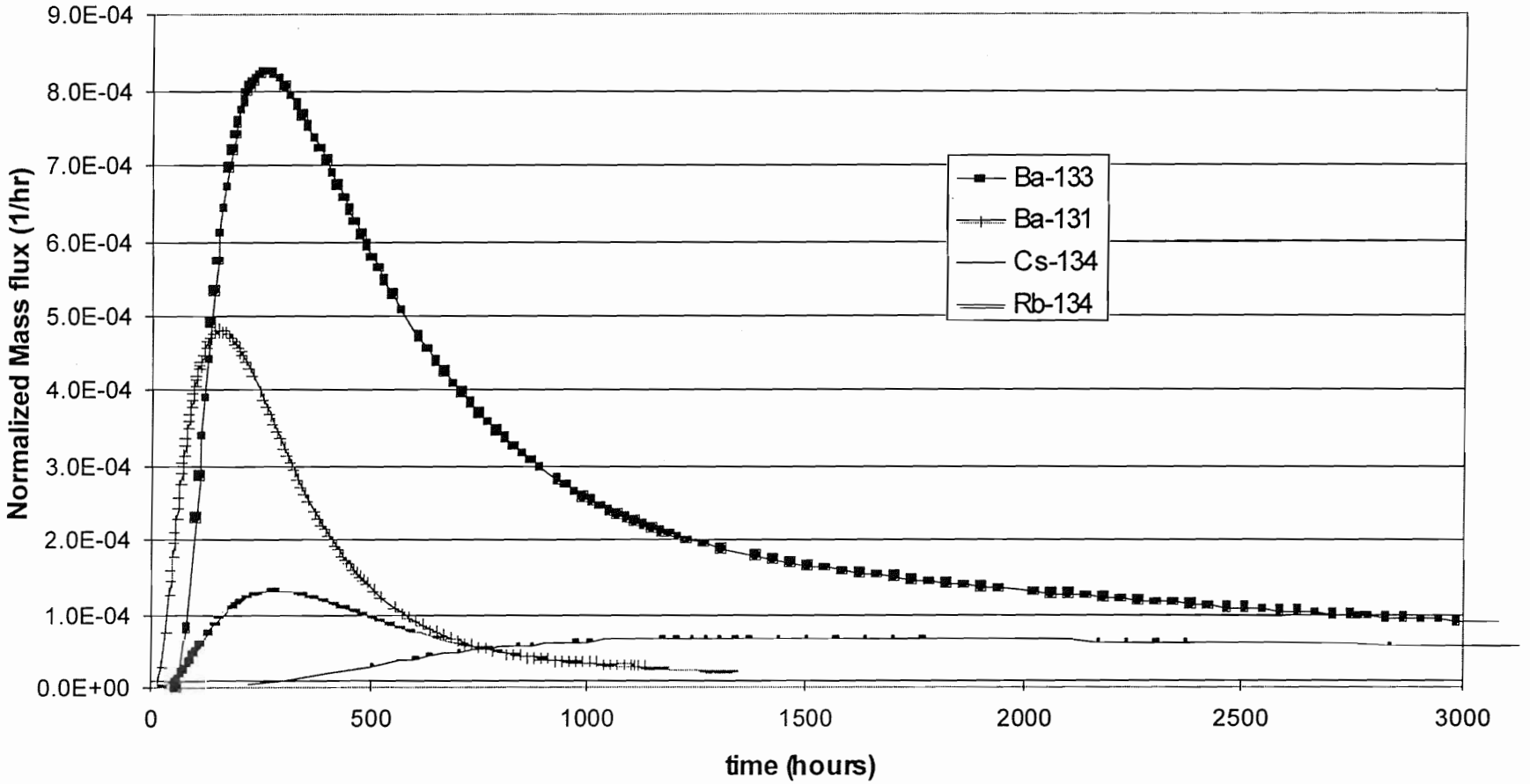

JNC サイクル機構

Effect of decay, Br-82, 35 h half life

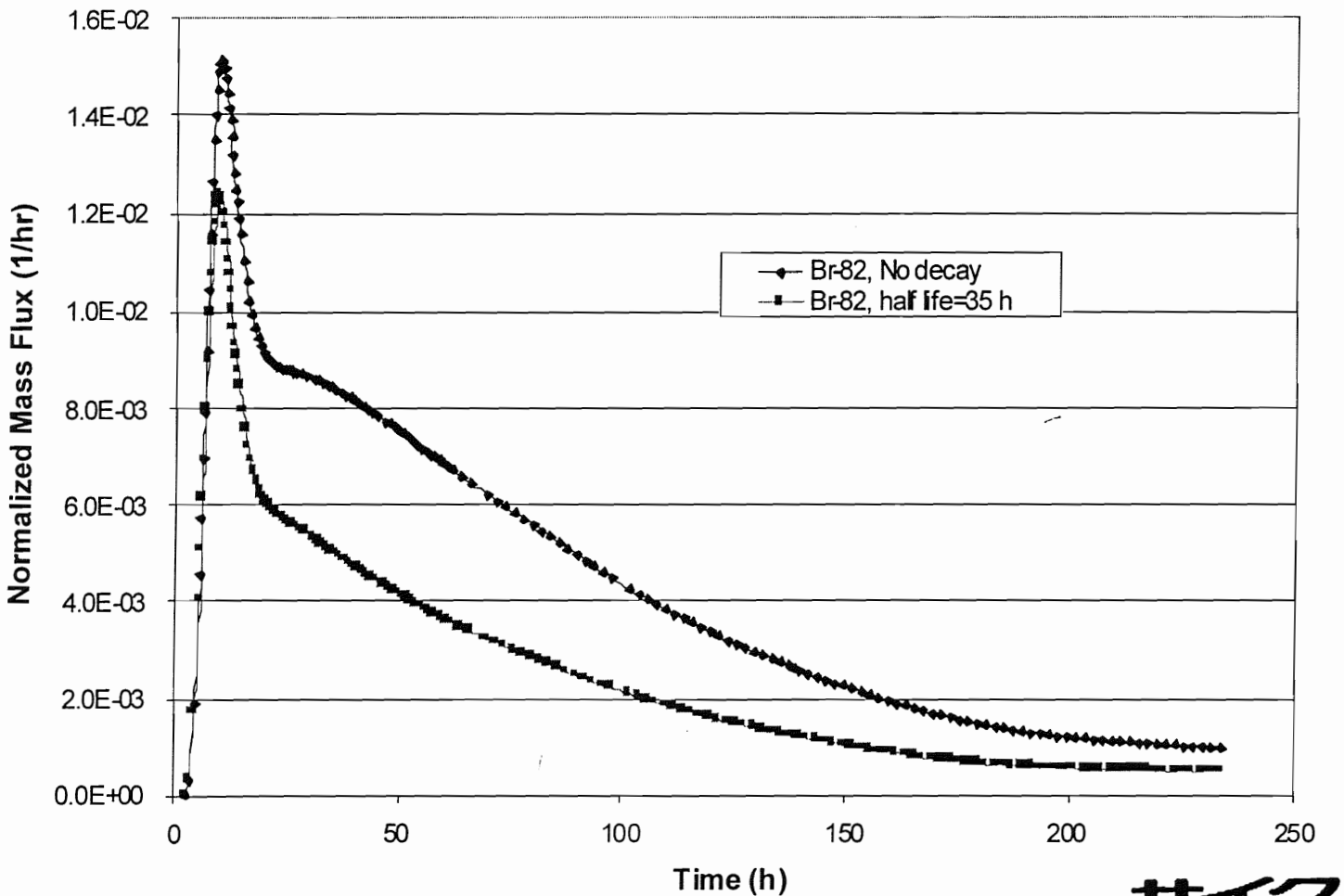

JNC サイクル機構

Effect of decay, Rb-96, 19 d half life

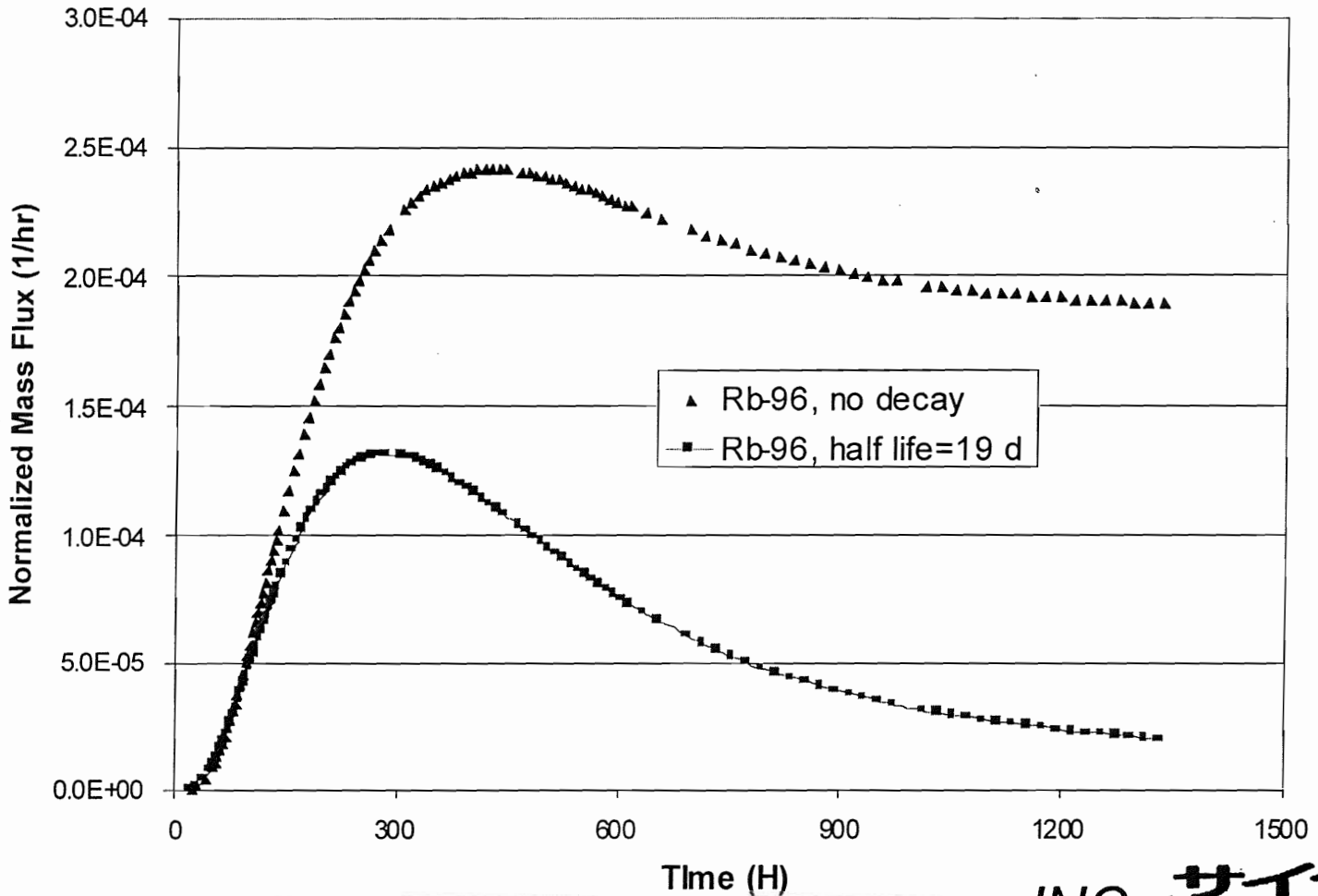

JNC サイクル機構

Mass Flux predictions, STT-2

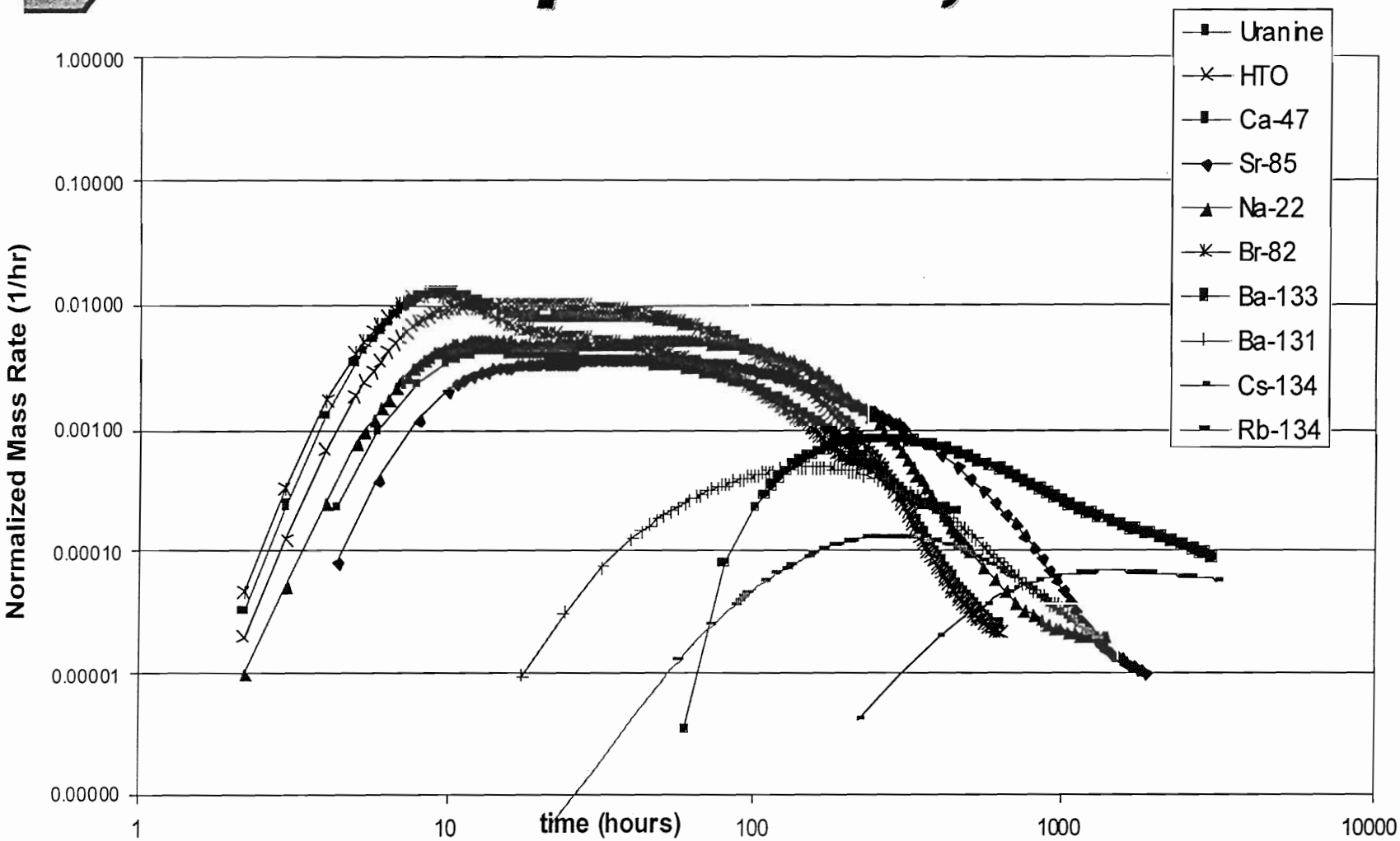

Official Scale

JNC サイクル機構

Cumulative Mass Prediction, STT-2

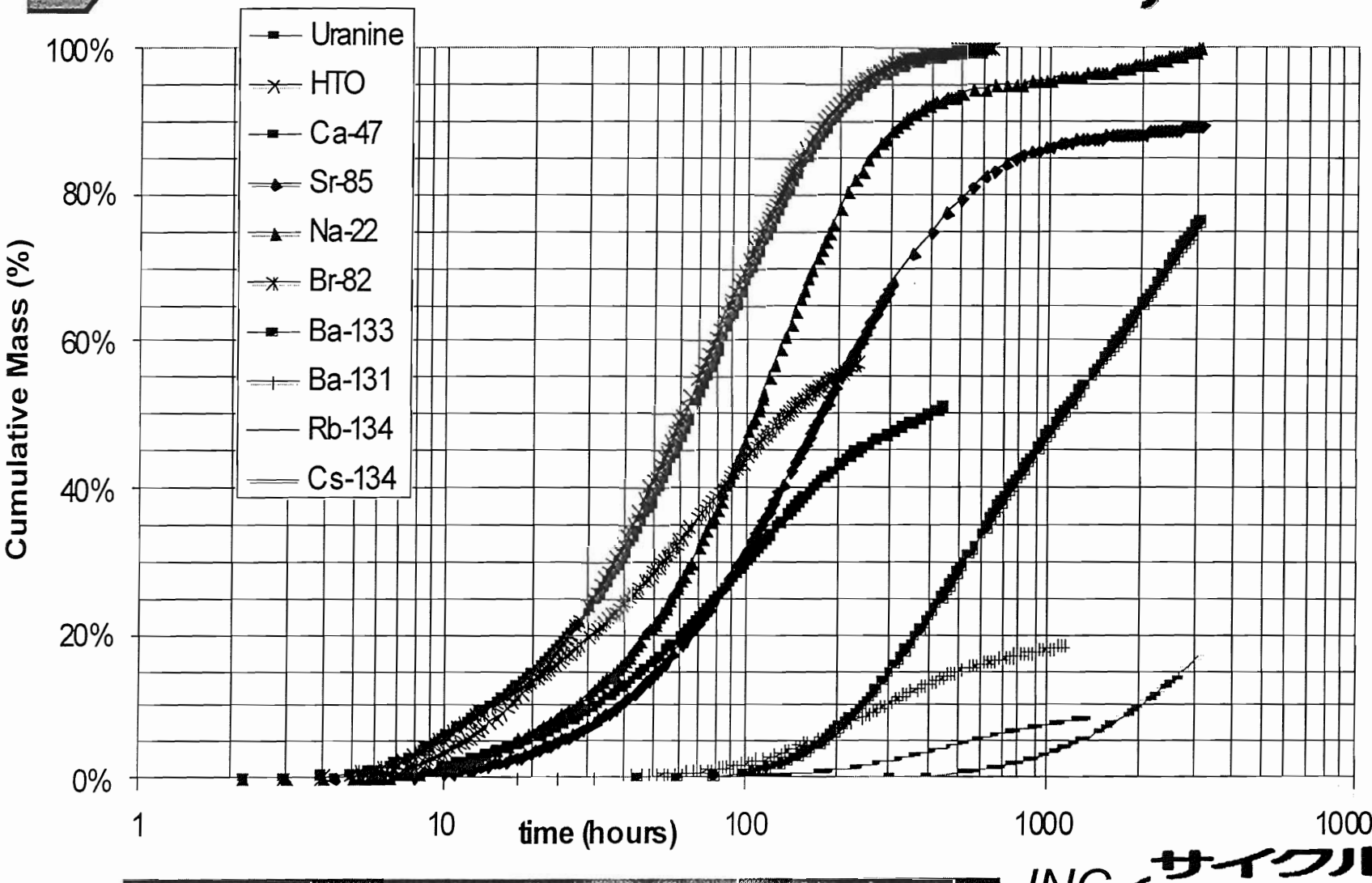

Official Scale

JNC サイクル機構

STT-2 predictions

Tracer	t5 (h)	t50 (h)	t95 (h)	t100 (h)	Recovery
Uranine	9.7	65.3	247.9	886	100.0%
HTO	11.3	61.3	229.5	641	100.0%
Na-22	16.3	105.3	650.0	3078	100.0%
Ca-47	18.7	414.5	--	458	50.7%
Br-82	9.4	135.3	--	234	57.1%
Sr-85	22.7	170.6	--	3078	89.6%
Ba-131	162.7	1130.7	--	1130	18.3%
Ba-133	180.1	1106.6	--	3078	76.1%
Rb-134	533.5	--	--	1322	8.3%
Cs-134	1233.4	--	--	3078	16.8%

Mass Flux, STT-2, Dirac Pulse

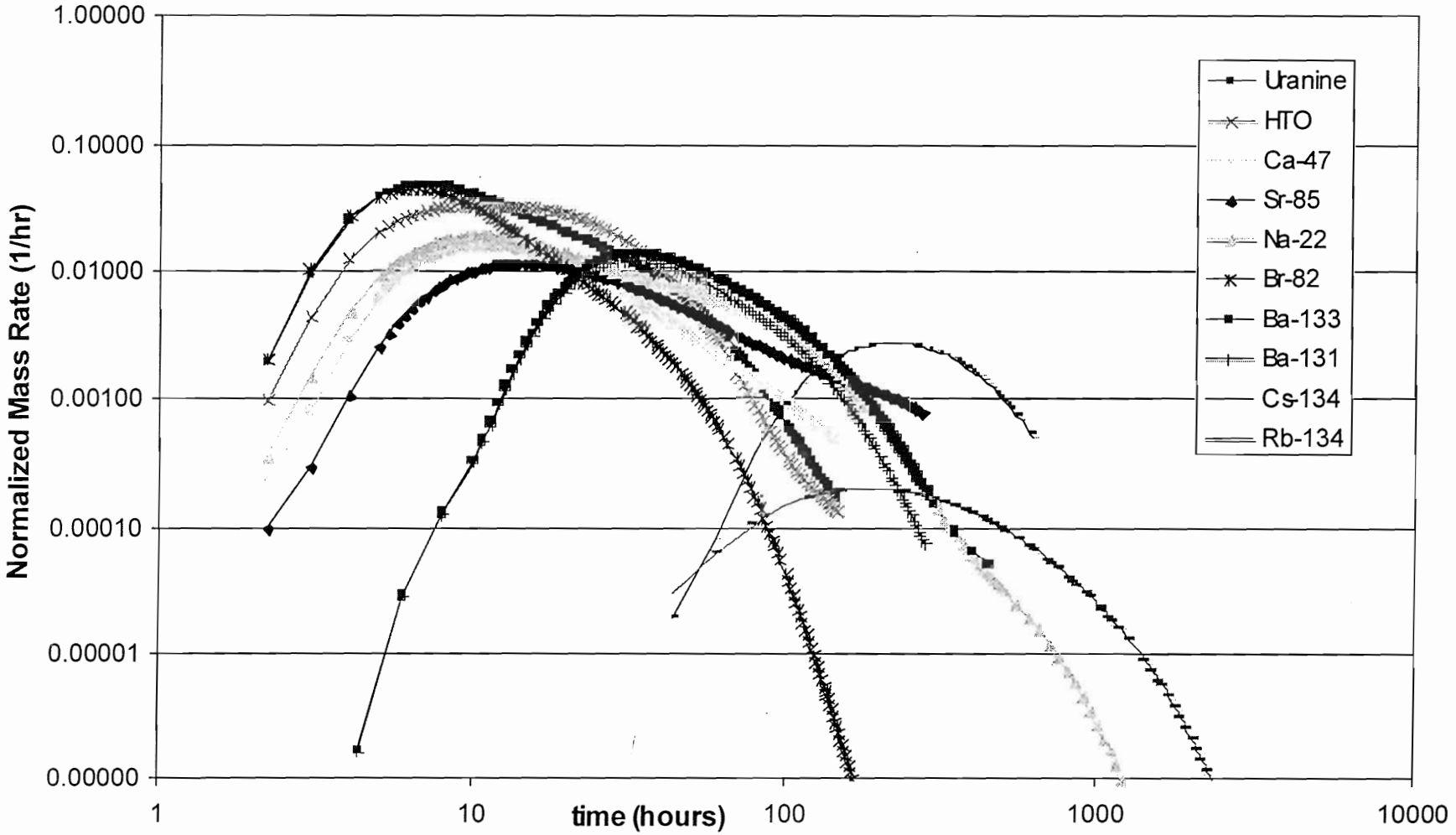

Official Scale

JNC サイクル機構

Cumulative Mass, Dirac Pulse

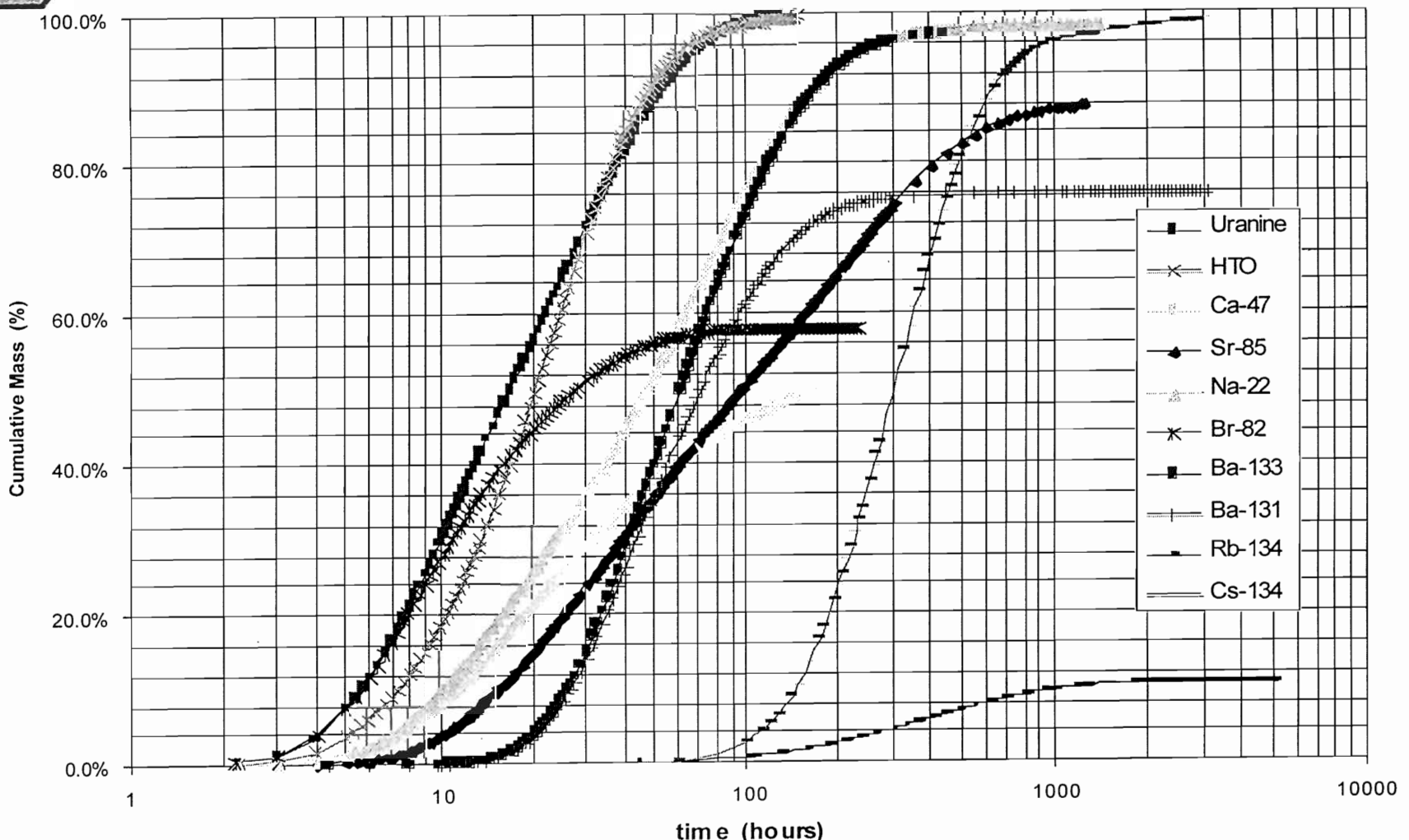

Official Scale

JNC サイクル機構

STT2 Dirac Pulse predictions

Tracer	t5 (h)	t50 (h)	t95 (h)	t100 (h)	Recovery
Uranine	4.0	17.0	65.3	886	100.0%
HTO	5.3	20.3	61.3	641	100.0%
Na-22	7.3	44.3	224.0	3078	100.0%
Ca-47	8.3	147.3	--	458	48.6%
Br-82	4.0	27.3	--	234	57.9%
Sr-85	6.7	93.3	--	3078	88.0%
Ba-131	21.4	70.7	--	1130	75.7%
Ba-133	21.4	60.6	238.6	3078	98.5%
Rb-134	326.6	--	--	1322	10.6%
Cs-134	113.2	299.9	846.6	3078	98.9%

Conclusions

- STT-2 accesses multiple pathways through network
- STT-2 lower flux is expected to increase diffusion effect on tail significantly, highlight difference between Ur and HTO
- Drawdown pattern is not expected to change significantly from PDT-2
- All tracers are expected to be recovered

Numerical analysis with FEGM/FERM for TRUE-1 sorbing tracer tests.

Y. Tanaka, T. Igarashi, M. Kawanishi (CRIEPI)

NUMERICAL ANALYSIS WITH FEGM/FERM FOR TRUE-1 SORBING TRACER TESTS

Yasuharu Tanaka
Toshifumi Igarashi
Motoi Kawanishi

Abiko Research Laboratory,
Central Research Institute
of Electric Power Industry,
Abiko, Japan

April 1999

Keywords: numerical analysis, tracer test, fracture, sorption, dispersion, radionuclide, pumping, transmissivity, drawdown

1. Introduction

In this study, we performed numerical analyses for STT-2 by using our developed groundwater and transport models, FEGM/FERM. Before the analyses for STT-2, we calibrated our model of Feature A on basis of the data of the previous tracer tests. First the spatial distribution of transmissivity in Feature A was estimated by kriging from drawdowns observed in the previous tracer tests. Secondly the average hydraulic gradient under the natural condition was estimated from the hydraulic heads observed prior to start of PDT-3 in order to determine the hydraulic boundary conditions. Thirdly the fluid flux through the tracer injection sections were estimated from the tracer concentration curves in the sections in order to calculate the mass flux of the tracers injected into Feature A. Fourthly simulations of the tracer migration were performed for Uranine during STT-1a and Amino G Acid during PDT-2 so that the aperture of Feature A and the longitudinal dispersivity were estimated through the simulations by try and error. Furthermore simulations of the tracer migration were performed for STT-1 and the surface related sorption coefficients, the matrix sorption coefficients and the diffusivities were identified through the simulations. Finally simulations for STT-2 were performed by using the above mentioned conditions.

2 SIMULATION METHOD

2.1 NUMERICAL MODEL

We applied the groundwater and transport models, FEGM/FERM (Igarashi *et al.*, 1994 and Kawanishi *et al.*, 1987), to this analysis.

The governing equation for groundwater flow in fracture and rock matrix under steady state are expressed as follow respectively;

$$\frac{\partial}{\partial x_i}\left(T\frac{\partial h}{\partial x_i}\right)+Q+\Gamma_w=0 \qquad \text{(in fracture)} \qquad 2\text{-}1$$

$$\frac{\partial}{\partial x_i}\left(k\frac{\partial h}{\partial x_i}\right)+q-\Gamma_w=0 \qquad \text{(in rock matrix)} \qquad 2\text{-}2$$

where T is the transmissivity of fracture, k the hydraulic conductivity of rock matrix, h the hydraulic head, Q, q the sink/source of the fluid and Γ_w the water inflow from the rock matrix into the fracture.

In this study, we do not consider decay of the radioactive tracers. Therefore the governing equations for solute migration are expressed as follow;

$$b\left(1+\frac{2K_a}{b}\right)\frac{\partial C}{\partial t}+\frac{\partial V_i C}{\partial x_i}-\frac{\partial}{\partial x_i}\left(D_{ij}\frac{\partial C}{\partial x_j}\right)-M-\Gamma_m=0 \qquad \text{(in fracture)} \qquad 2\text{-}3$$

$$n\left(1+\frac{1}{n}\rho_d K_d\right)\frac{\partial C}{\partial t}+\frac{\partial V_i C}{\partial x_i}-\frac{\partial}{\partial x_i}\left(nD_{ij}\frac{\partial C}{\partial x_j}\right)-m+\Gamma_m=0$$

(in rock matrix) 2-4

where b is the fracture aperture, n the porosity of the rock matrix K_a the surface related sorption coefficient, K_d the matrix sorption coefficient, ρ_s the dry density of rock matrix, C the concentration of the solute, V_i the component of the darcian velocity in the direction x_i and M, m the sink/ source of the solute and Γ_m, the mass flux of the solute from the rock matrix into the fracture. And D_{ij} is the tensor of dispersion coefficient of which the ij-th component is expressed as follows;

$$nD_{ij} = \alpha_T |V| \delta_{ij} + (\alpha_L - \alpha_T) \frac{V_i V_j}{|V|} + D_e \delta_{ij} \qquad 2\text{-}5$$

where α_T is the longitudinal dispersivity, α_L the transverse one, δ_{ij} Kronecker delta V the darcian velocity vector and D_e diffusivity of the rock matrix.

2.2 MODELING OF FEATURE A

In this study, Feature A was represented by discrete fracture model as a single flat square of which the length of the side was 30 meters. And the rock matrix of 10-cm thickness on each side of Feature A was represented by porous media model. Figure 2-1 shows the finite element mesh on one side of Feature A used in the analysis. The figure is drawn on the different reduced scales between the length and the thickness. The boreholes were expressed as cavities. The total numbers of fracture and porous media element are 3,855 and 19,275 respectively.

No groundwater flow was assumed on the boundary of rock matrix on the opposite side of Feature A and the hydraulic heads were fixed on the other surrounding boundaries of the model. No flux of the tracers was assumed to cross the boundaries. The time-varying mass flux of the tracers was prescribed at the injection boreholes.

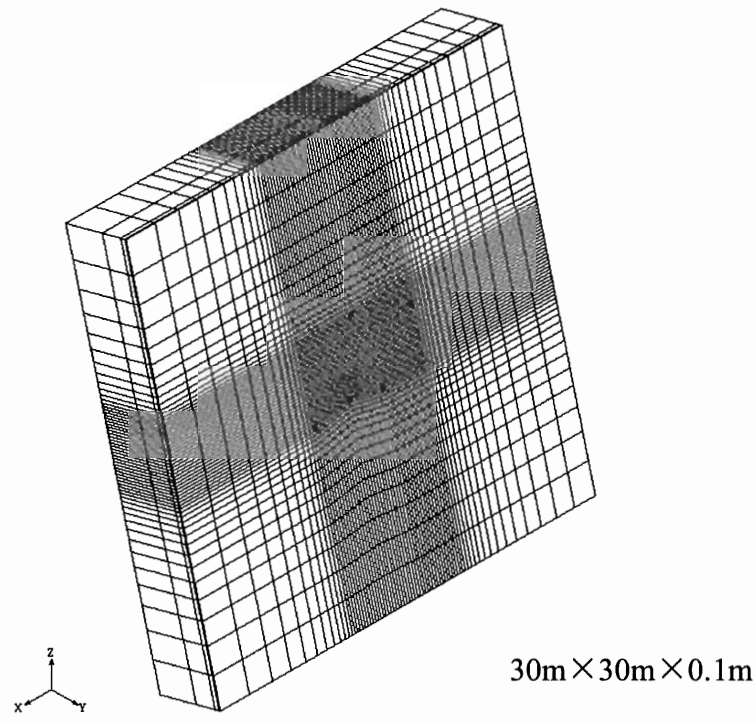

Figure 2-1. *Finite element mesh for the numerical analysis.*

2.3 TRANSMISSIVITY IN FEATURE A

Transimissivities in Feature A were assumed to show a normal distribution in the logarithmic scale and to be distributed spatially with correlation. The spatial distribution of the transmissivity in Feature A was estimated by kriging on the basis of the transmissivities at the five borehole sections.

By kriging method, the estimation at the point $\boldsymbol{x}$, T^*, can be obtained as the linear sum of the values at the measurement point $\boldsymbol{x}_i$, T_i (de Marsily, 1986).

$$T^*(\boldsymbol{x}) = \sum_{i=1}^{n} \lambda^i(\boldsymbol{x}) \cdot T_i \qquad 2\text{-}6$$

where n is the number of the measurement points and $\lambda_i(\boldsymbol{x})$ the weights of the kriging estimator. The following condition is required in order to have an unbiased estimator.

$$\sum_i \lambda^i(\boldsymbol{x}) = 1 \qquad 2\text{-}7$$

And the errors of estimation must be minimal so that the estimator is optimal.

$$E\left[\left\{T^*(\boldsymbol{x}) - T(\boldsymbol{x})\right\}^2\right] \text{ minimum} \qquad 2\text{-}8$$

where E represents the expectation of the value in parenthesis. The values of $\lambda_i(\mathbf{x})$ which satisfy the conditions 2-5 and 2-6 can be obtained by solving the following simultaneous equations.

$$\begin{aligned} &\sum_j \lambda^j(\boldsymbol{x})\gamma(\boldsymbol{x}_i - \boldsymbol{x}_j) + \mu = \gamma(\boldsymbol{x}_i - \boldsymbol{x}_0) \quad i = 1, \cdots, n \\ &\sum_i \lambda^i(\boldsymbol{x}) = 1 \end{aligned} \qquad 2\text{-}9$$

where μ is an unknown, called a Lagrange multiplier. And γ is the variogram defined by the following equation.

$$\gamma(\boldsymbol{h}) = \frac{1}{2}\text{var}[Y(\boldsymbol{x}+\boldsymbol{h}) - Y(\boldsymbol{x})] \qquad 2\text{-}10$$

where var represents the variance of the value in parenthesis. In this study, the following exponential model was used to express variogram.

$$\gamma(h)=\sigma^2\cdot\left\{1-exp\left(-\frac{h}{a}\right)\right\} \qquad 2\text{-}11$$

where σ^2 is the variance of the logarithmic transmissivity, h the distance and a the correlation length.

3 CALIBRATION OF MODEL

3.1 TRANSMISSIVITY IN FEATURE A

The transmissivities at all the borehole sections except for KA3005A R3 were identified so that the sum of the squares of normalized errors between the calculated drawdowns and the observed ones, S_d, would be minimal.

$$S_d = \sum_{i=1}^{17} \left(\frac{\Delta h^i_{cal} - \Delta h^i_{obs}}{\Delta h^i_{obs}} \right)^2 \qquad 3\text{-}1$$

where Δh^i_{obs} is the i-th observed drawdown at the withdrawal or injection section. And Δh^i_{cal} is the i-th drawdown calculated by using the spatial distribution of transimissivity in Feature A which is estimated by kriging on basis of the transmissivities at the five borehole sections. The correlation length was assumed to be 1 meter and the value determined from the flow- and pressure build-up test (Winberg, 1996) was used as the transmissivity at KA3005A R3. The rock matrix was not taken into consideration in this identification analysis for the transmissivity in Feature A, that is, the single fracture model was used.

The identified transmissivities are given in Table 3-1. And Figure 3-1 shows the spatial distribution of transmissivity in Feature A estimated on basis of the identified section transmissivities. The drawdowns calculated by using the estimated transmissivity distribution are given in Table 3-2. In this study, we used this estimated transmissivity distribution as the spatial distribution of transmissivity in Feature A.

3.2 HYDRAULIC BOUNDARY CONDITION

No groundwater flow was assumed on the boundary of rock matrix on the opposite side of Feature A and the hydraulic heads were fixed on the other surrounding boundaries of the model as mentioned in 2.2. The hydraulic heads on the boundaries were identified so that the sum of the squares of normalized errors between the calculated heads and the observed ones at the five borehole sections under the natural condition, S_h, would be minimal.

$$S_h = \sum_{i=1}^{5} \left(\frac{h^i_{cal} - h^i_{obs}}{h^i_{obs}} \right)^2 \qquad 3\text{-}2$$

where h^i_{obs} is the observed hydraulic head at the i-th section under the natural condition and h^i_{cal} the calculated one. The rock matrix was ignored in this identification analysis for the hydraulic heads on the boundaries, that is, the single fracture model was used.

The identified parameters were the hydraulic head at the point A, h_A, the magnitude of the average hydraulic gradient, I, and the angle between the direction of the average hydraulic gradient and the side AB, θ, *see* Figure 3-2. Table 3-3 gives the identified values of these parameters for the hydraulic head prior to start of PDT-3.

3.3 MASS FLUX AT INJECTION SECTION

The fluid flux through the tracer injection section, Q_{bh}, is obtained theoretically by the following equation (Winberg, 1996 and Andersson, 1996).

$$Q_{bh} = -\frac{V}{t} ln(C/C_0) - Q_{sam} \qquad 3\text{-}3$$

where V is the volume of the tracer injection section, t the elapsed time, C_0 the initial concentration of the tracer in the injection section, C the concentration at the time t and Q_{sam} the sampling flow rate.

Figure 3-3 to 3-5 show the measured concentration of Uranine or Amino G Acid at the injection section, KXTT4 R3, and the straight lines for approximation during STT-1a, PDT-2 and STT-2 respectively. Table 3-4 shows the fluid flux through the injection section estimated by using the equation 3-3 from the slope of the straight lines. In this calculation, the borehole volume of KXTT4 R3 was supposed to be 2154 ml (Andersson et al., 1998). The pumping rate during STT-2 was the same as during PDT-2. But the fluid flux through the injection section during STT-2 was about three times that during PDT-2. The natural hydraulic gradient or the transmissvity of Feature A probably changed.

The product of the tracer concentration and the fluid flux was used as the mass flux of the tracer injected into Feature A for the tracer migration analysis of each tracer test. The fluid flux for Uranine or Amino G Acid were used for the calculation of the mass flux.

3.4 APERTURE AND DISPERSIVITY

Simulations for the migration of Uranine and Amino G Acid in Feature A were performed for STT-1a and PDT-2 on basis of the above-mentioned conditions. In the simulations, the rock matrix was ignored, that is, the

single fracture model was used. The aperture of Feature A, b, and the longitudinal dispersivity, α_L, along the travel path in each tracer test were estimated through the simulations. The ratio of longitudinal dispersivity to transverse one was fixed at 10 to 1 in the simulations.

The best-fit run for each test is shown in Figure 3-6 and 3-7 respectively. The identified aperture of Feature A and the longitudinal dispersivity are shown in Table 3-5. The calculated breakthrough curves agreed approximately with the measured ones. The following factors are considered to cause the slight difference between the calculated result and the experimental one. First the concentration values measured in the injection section in the early stage of the experiment were not accurate due to delay and dispersion in the sampling line (Andersson, 1996). Accordingly the input tracer flux in the early stage used in the simulation might be different from the one in the experiment. Secondly the natural hydraulic gradient was estimated on basis of the hydraulic heads at only five borehole sections. So the hydraulic boundary condition used in the simulations might be different from the one in the experiments. Thirdly the transmissivities at the five borehole sections were identified so that they would satisfy the drawdowns observed in all the tracer tests properly at the same time. Consequently the calculated drawdowns did not exactly agree with all the observed ones, see Table 3-2.

3.5 SORPTION COEFFICIENT

Simulations for migration of the radioactive tracers were performed for STT-1a on basis of the above-mentioned conditions. The three-dimensional model including the rock matrix was used in the simulations. The porosity and hydraulic conductivity of the rock matrix were assumed to be 0.001 and $1x10^{-11}$ m/sec respectively. The effective diffusivities for the tracers were quoted from Winberg *et al.*(1998). Other transport parameters were identified through the simulations by try and error.

Figure 3-8 shows the results of the best-fit runs. The simulated results agree well with the measured ones except for Cs-137. Table 3-6 shows the values of the transport parameters for each tracer used in the best-fit runs. The longitudinal and transverse dispersivity of 5 meters and 2.5 meters respectively gave good simulated results although these values seemed very large.

Table 3-1. Transmissivities at borehole sections identified on basis of drawdowns at borehole sections during tracer tests.

Borehole Section	Transmissivity (m^2/s)
KXTT1 R2	9.40×10^{-9}
KXTT2 R2	3.81×10^{-9}
KXTT3 R2	6.59×10^{-2}
KXTT4 R3	2.26×10^{-8}
KA3005A R3	$4.20\times10^{-8*}$

* Not identified but determined from flow- and pressure build-up tests

Table 3-2. Drawdowns at injection and withdrawal sections calculated by using the estimated spatial distribution of transmissivity in Feature A.

Test#	Injection section		Withdrawal section	
	Observed	Calculated	Observed	Calculated
RC-1			3.1	2.71
DP-1	-4.6	-6.02	1.2	1.31
DP-2	-18	-15.4	40	25.9
DP-3	-5	-5.32	44.5	26.0
DP-4	-15	-15.6	11	12.1
DP-5	-2	-2.06	1.1	1.30
DP-6	-0.8	-0.71	3.2	2.67
RC-2			27	32.4
PDT-1			1.3	1.37
PDT-2			3.1	2.73
PDT-3			8.2	5.44

Unit:mH_2O

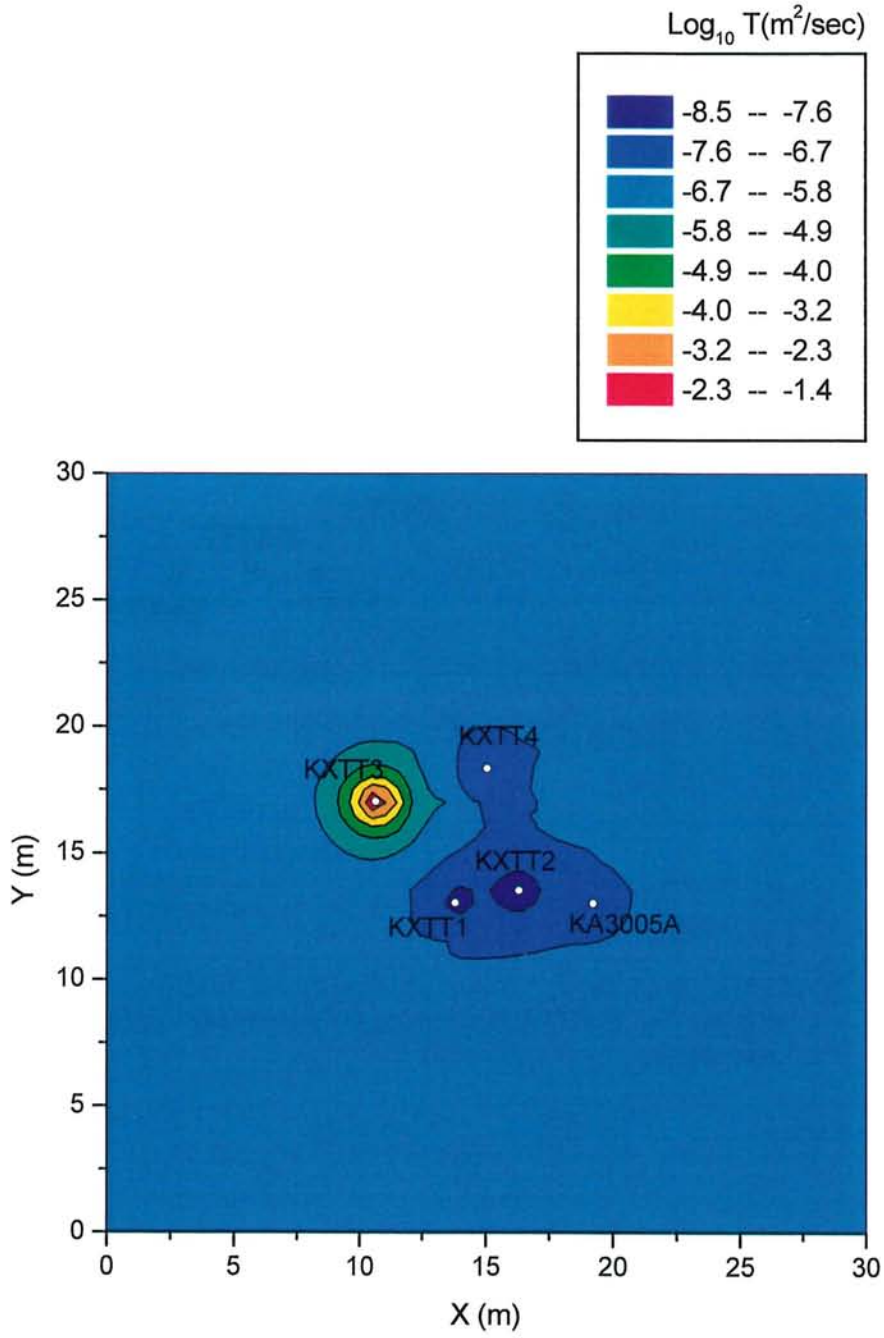

Figure 3-1. *Spatial distribution of logarithmic transmissivitiy in Feature A estimated by kriging on basis of the identified transmissivities at the five borehole sections. (KXTT1 R2:(X,Y)=(13.78, 13.04), KXTT2 R2:(16.32, 13.53), KXTT3 R2:(10.63, 17.04), KXTT4 R3:(15.06, 18.35), KA3005A R3:(19.22, 13.03))*

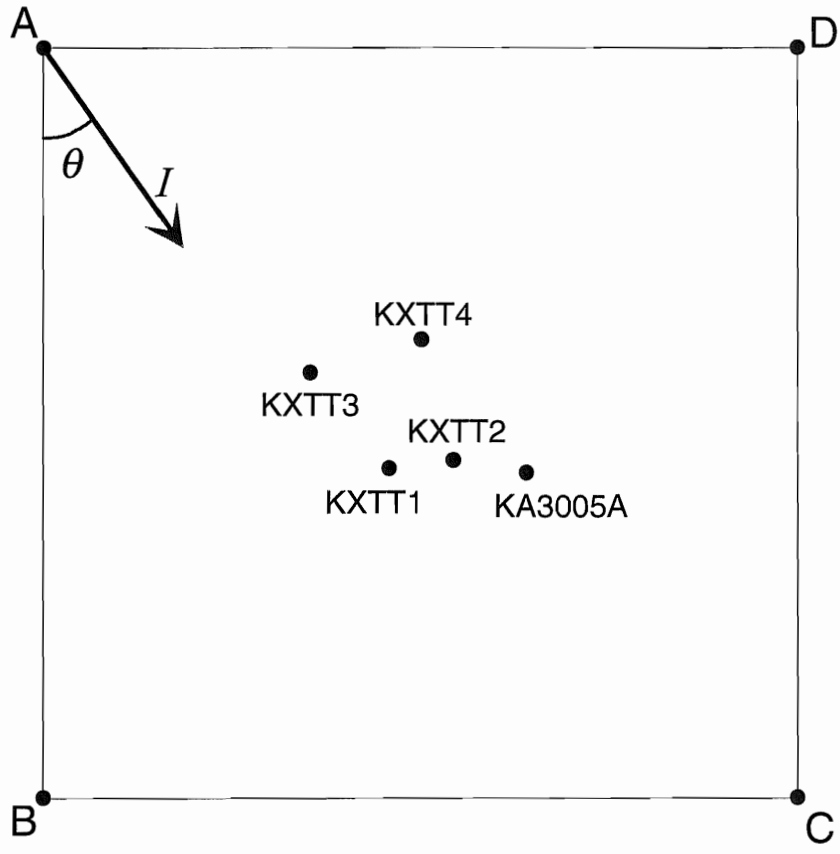

Figure 3-2. *Schematic diagram for parameters defining hydraulic boundary conditions.*

Table 3-3. Identified values of parameters for natural hydraulic head prior to start of the Preliminary Design Test, PDT-3.

Parameters	Identified value
Hydraulic head, h_A	-51.7mH_2O
Magnitude of hydraulic gradient, I	0.124
Direction of hydraulic gradient, θ	57.8°

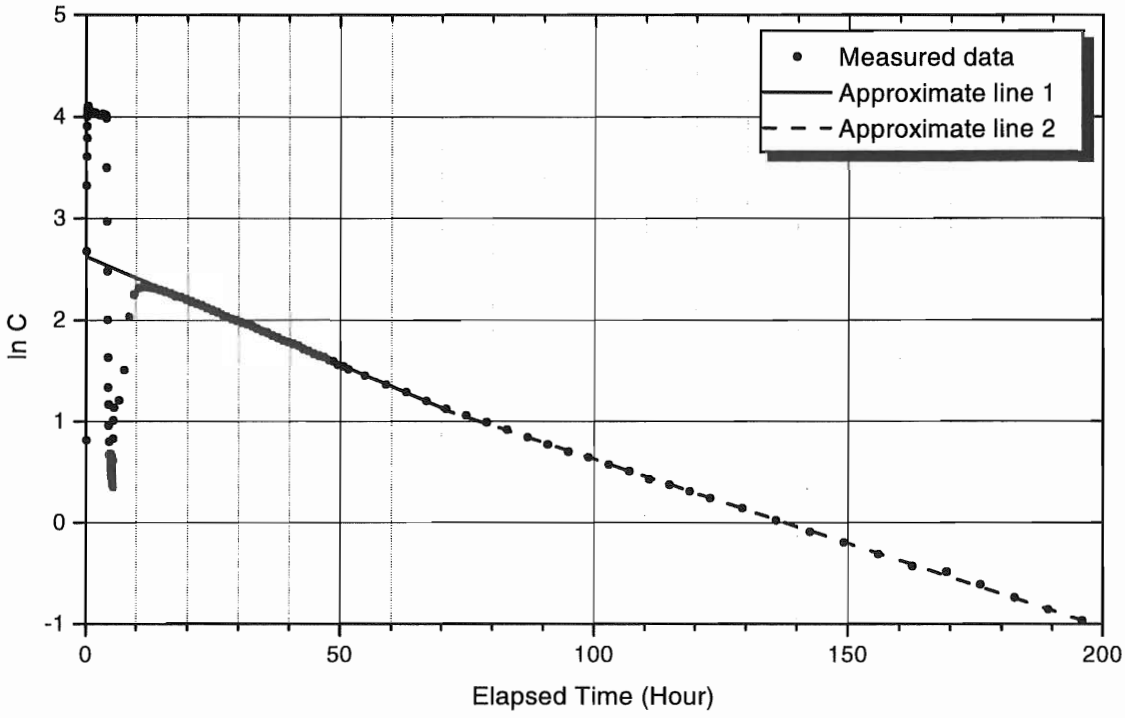

Figure 3-3. *Injected concentration of Uranine (ln C) in KXTT4 R3 during STT-1a.*

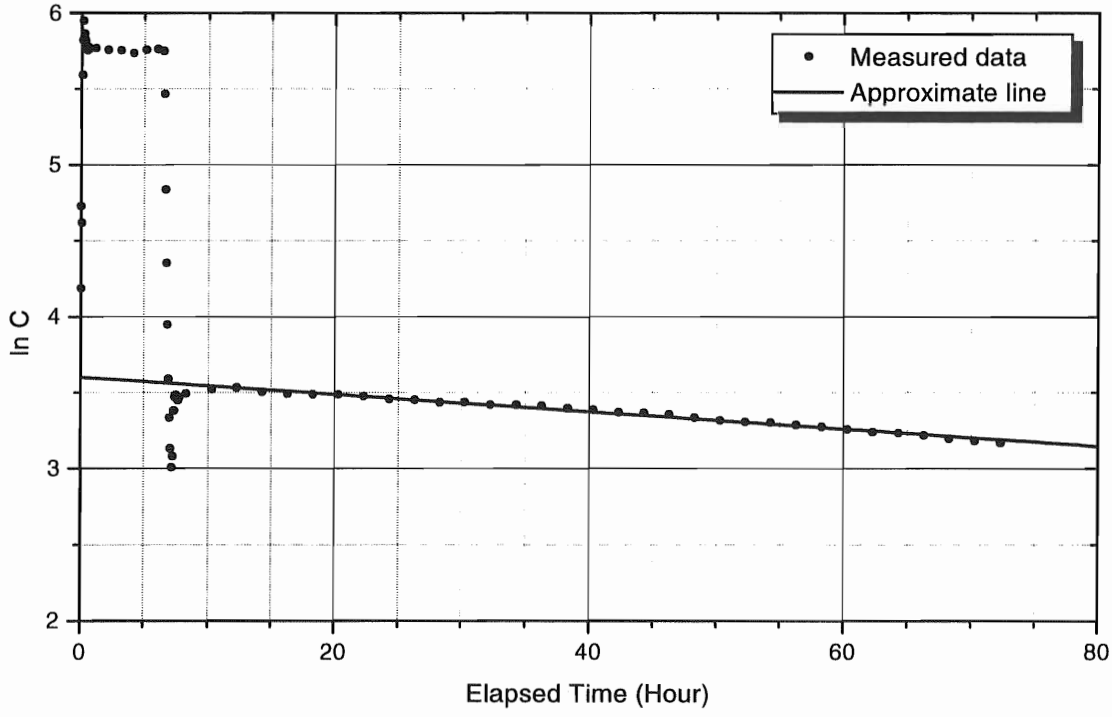

Figure 3-4. *Injected concentration of Amino G Acid (ln C) in KXTT4 R3 during PDT-2.*

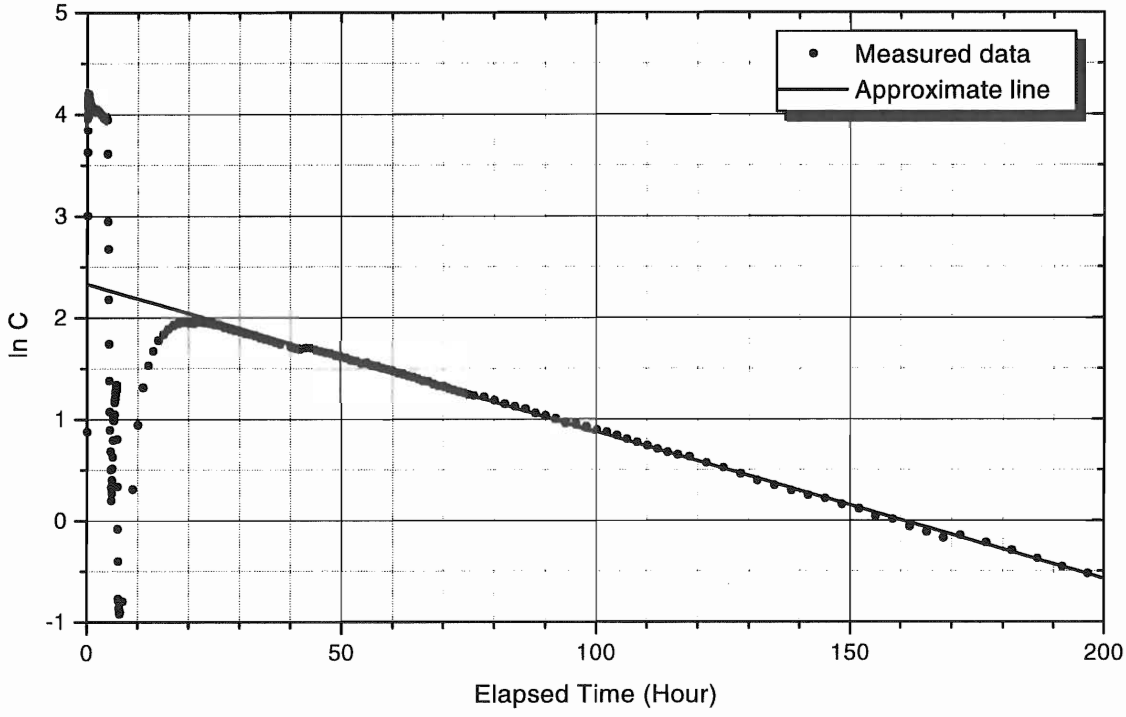

Figure 3-5. Injected concentration of Uranine (ln C) in KXTT1 R2 during STT-2.

Table 3-4. Fluid flux through the tracer injection section during PDT-2, STT-1a and STT-2 estimated from the dilution of Uranine, HTO and Amino G Acid.

Test#	Inj. section	Tracer	Elapsed time (h)	Fluid flux (ml/min)
STT-1a	KXTT4 R3	Uranine	20-70	0.720
			70-200	0.550
		HTO	20-70	0.698
			70-200	0.544
PDT-2	KXTT4 R3	Amino G Acid	10-72.3	0.151
STT-2	KXTT4 R3	Uranine	25-200	0.478
		HTO	25-200	0.486

Table 3-5. Aperture of Feature A, b, and longitudinal dispersivity, α_L, between KXTT3 R2 and KXTT4 R3 identified through simulations for STT-1a and PDT-2.

Test#	Injection section	Withdrawal section	b (mm)	α_L (m)
STT-1a	KXTT4 R3	KXTT3 R2	0.58	1.92
PDT-2	KXTT4 R3	KXTT3 R2	0.528	1.42

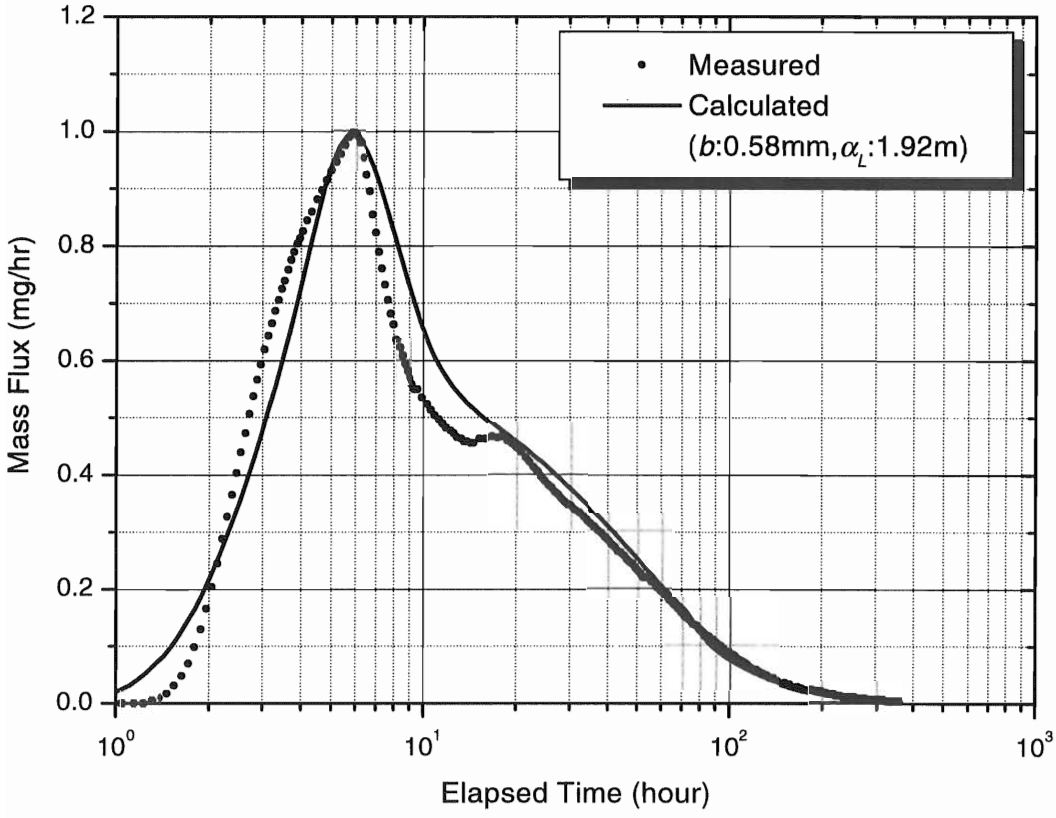

Figure 3-6. *Measured breakthrough curve of Uranine in pumping section during STT-1a and result of the best-fit run.*

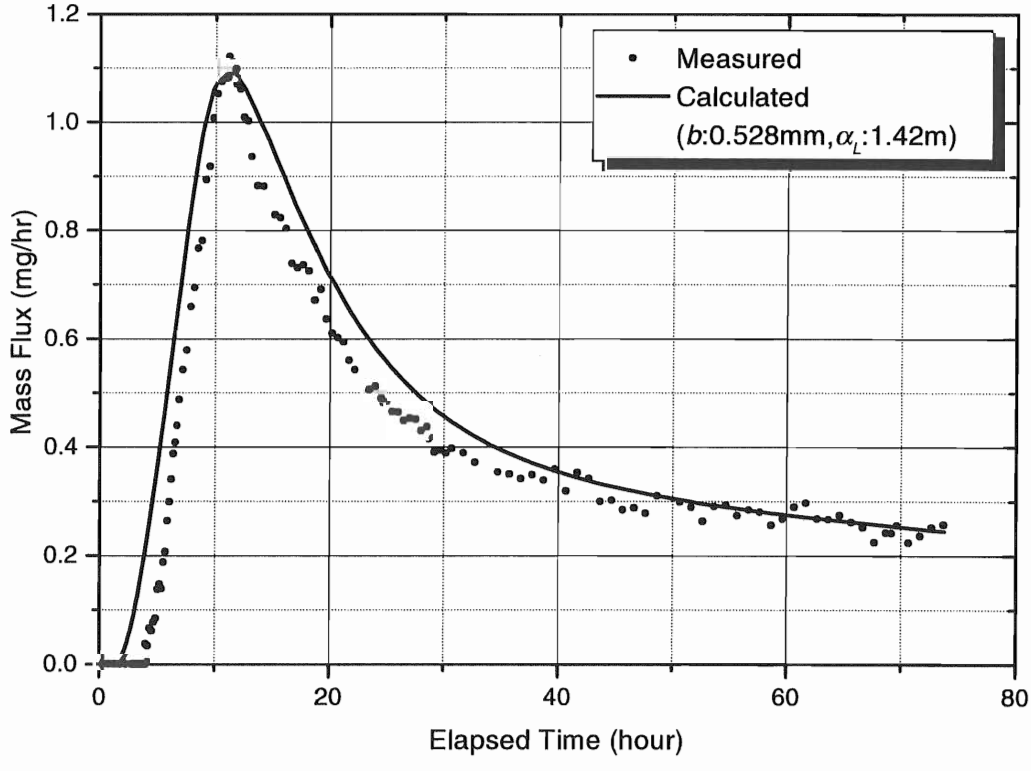

Figure 3-7. *Measured breakthrough curve of Amino G Acid in pumping section during PDT-2 and result of the best-fit run.*

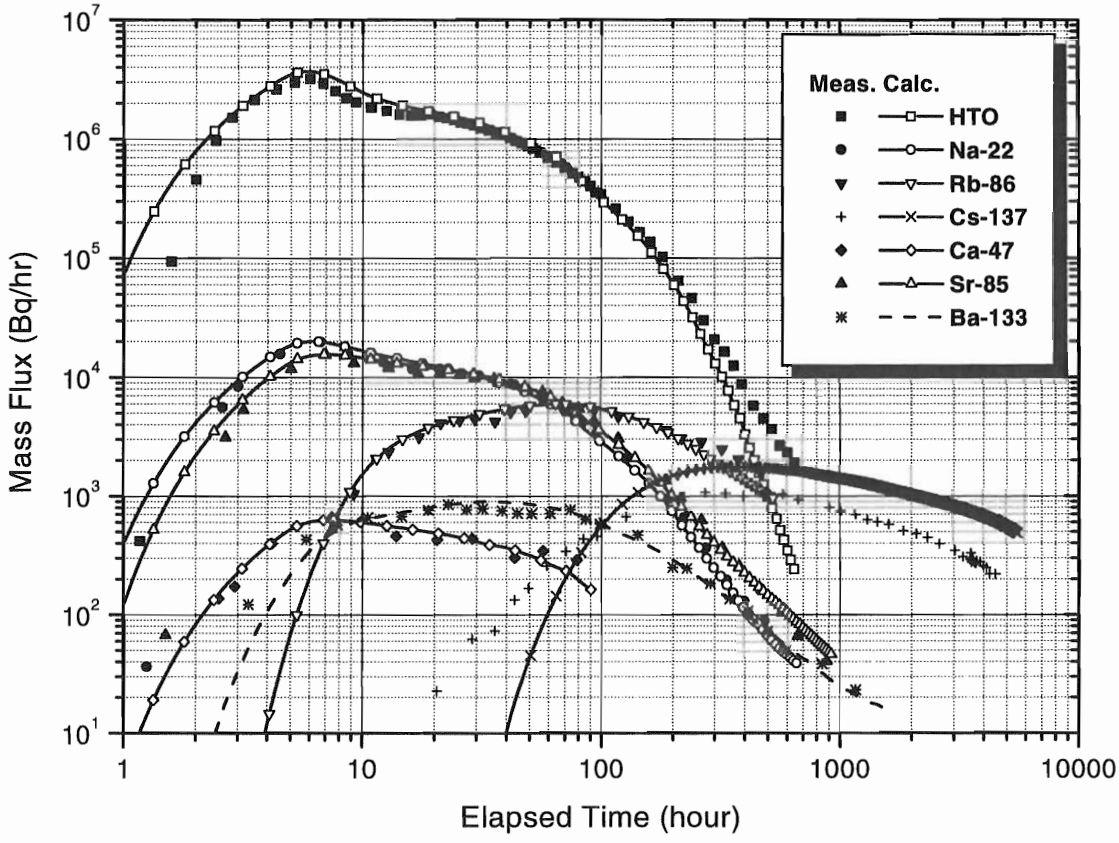

Figure 3-8. *Measured breakthrough curves of radioactive tracers in pumping section during STT-1a and results of the best-fit run.*

Table 3-6. Surface related sorption coefficients, matrix sorption coefficients and diffusivities used for best-fit runs for STT-1a.

Tracer	K_a (m)	K_d (m^3/kg)	D_e (m^2/s)
HTO	-	-	4×10^{-14}
Na-22	4.0×10^{-5}	2.60×10^{-5}	2.2×10^{-14}
Rb-86	1.5×10^{-3}	2.80×10^{-3}	3×10^{-14}
Cs-137	4.5×10^{-3}	6.00×10^{-2}	3×10^{-14}
Ca-47	1.5×10^{-4}	4.16×10^{-5}	1.3×10^{-14}
Sr-85	1.2×10^{-4}	8.00×10^{-5}	1.3×10^{-14}
Ba-133	6.53×10^{-4}	8.00×10^{-4}	1.4×10^{-14}

4 SIMULATED RESULTS

Simulations were performed for STT-2. Firstly, the drawdown was calculated. The transmissivity distribution shown in Figure 3-1 was used in the calculation. The parameter values for the natural hydraulic head were assumed to be identical to the ones given in Table 3-3. The calculated drawdowns at the five boreholes are shown in Table 4-1.

Secondly the tracer migration was simulated for the pulse input. The values for PDT-2 in Table 3-5 were used as the aperture of Feature A and the longitudinal dispersivity. The surface related sorption coefficients, matrix sorption coefficients and diffusivities were assumed to be identical to the ones in Table 3-6. Only in the simulation for Uranine, the rock matrix was ignored and the single fracture model was used. In the simulations for the other tracers, three-dimensional model including the rock matrix was used. Figure 4-1 and 4-2 show the calculated mass flow and cumulative mass in the pumping section respectively. These values are normalized to the injected mass. Table 4-2 gives the tracer travel times, t_5, t_{50} and t_{95}, defined as times when 5, 50 and 95 % of the injected mass respectively had arrived. And Table 4-3 gives the tracer recoveries at the time of termination of monitoring. The maximum mass flow becomes small with increasing sorption coefficient.

Finally the tracer migration was simulated for the measured input. The products of the tracer concentration in the injection section and the fluid flux for Uranine in Table 3-4 were used as the mass flux of the tracers injected into Feature A. Figure 4-3 and 4-4 show the normalized mass flow and cumulative mass respectively. Table 4-4 and 4-5 give the tracer travel times and the tracer recoveries.

Table 4-1. Calculated drawdons at five boreholes during STT-2.

Borehole Section	Drawdown (mH_2O)
KXTT1 R2	1.77
KXTT2 R2	1.16
KXTT3 R2	2.73
KXTT4 R3	1.83
KA3005A R3	0.56

Table 4-2. Calculated tracer travel times for pulse input in STT-2.

Tracer	t_5	t_{50}	t_{95}
Uranine	3.52	11.93	41.93
HTO	3.57	12.43	48.04
Na-22	4.67	21.98	504.33
Rb-86	49.00	622.55	-
Cs-134	505.75	-	-
Ca-47	6.41	31.21	458.00
Sr-85	6.45	37.53	1688.33
Ba-131	20.55	201.24	-
Ba-133	20.55	201.24	-

Unit : hour

Table 4-3. Calculated tracer recoveries at the time, t_t, for pulse input of STT-2. t_t represents the time of termination of monitoring.

Tracer	t_t (hour)	Recovery (%)
Uranine	886	100.00
HTO	641	100.00
Na-22	3078	98.95
Rb-86	1322	62.64
Cs-134	3078	28.22
Ca-47	458	92.39
Sr-85	3078	96.64
Ba-131	1130	78.26
Ba-133	3078	86.43

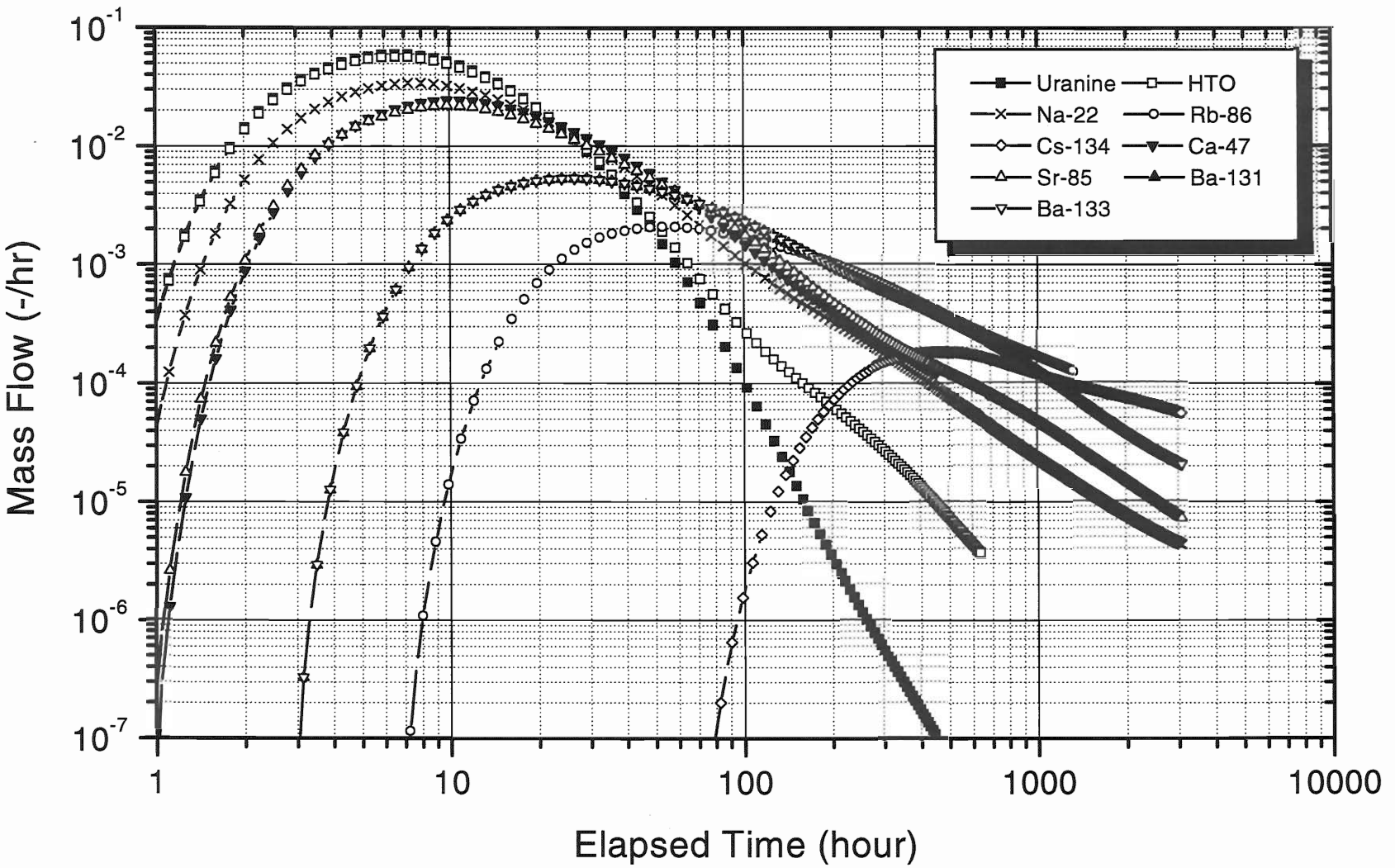

Figure 4-1. Calculated mass flow in pumping section for pulse input in STT-2.

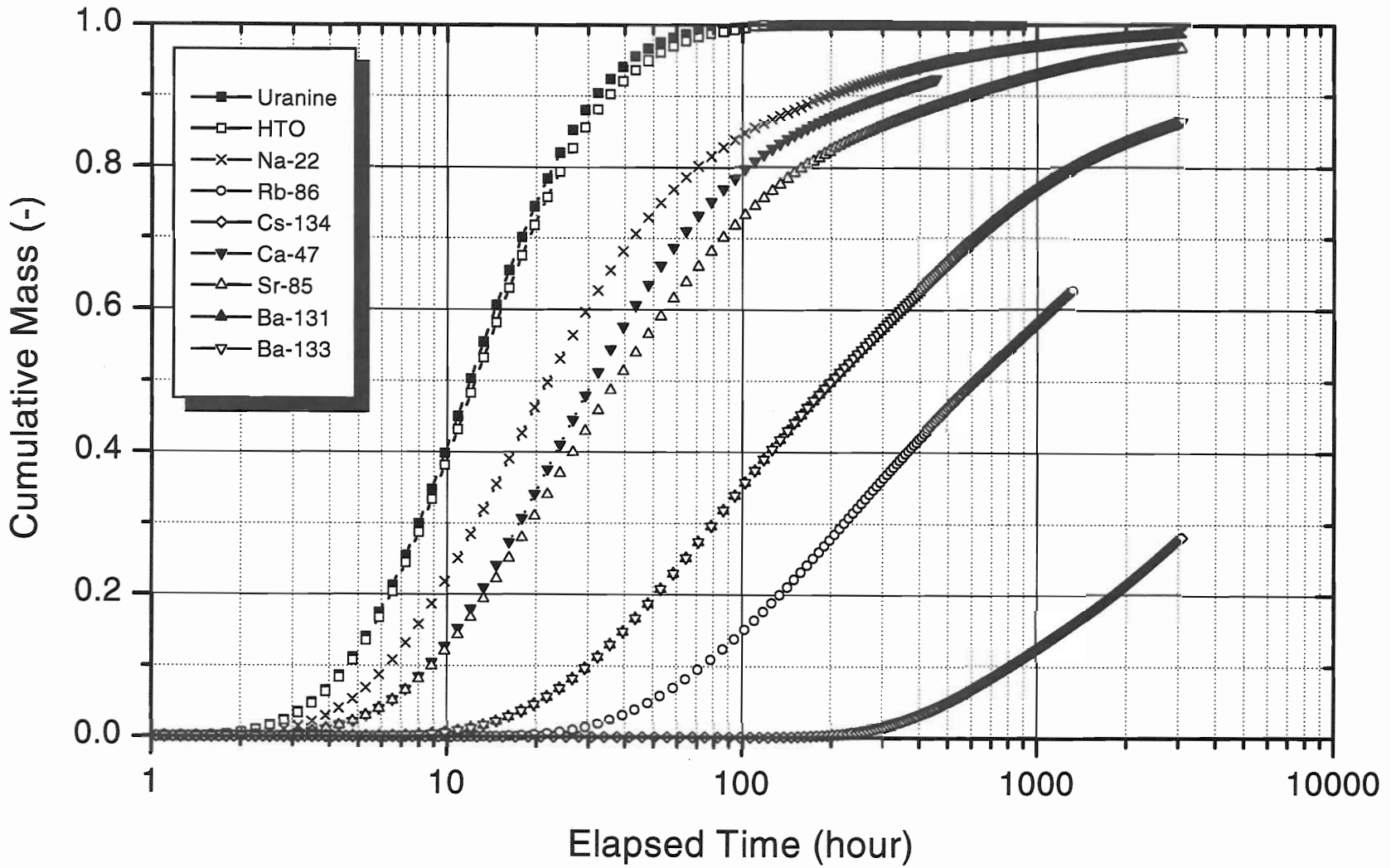

Figure 4-2. Calculated cumulative mass in pumping section for pulse input in STT-2.

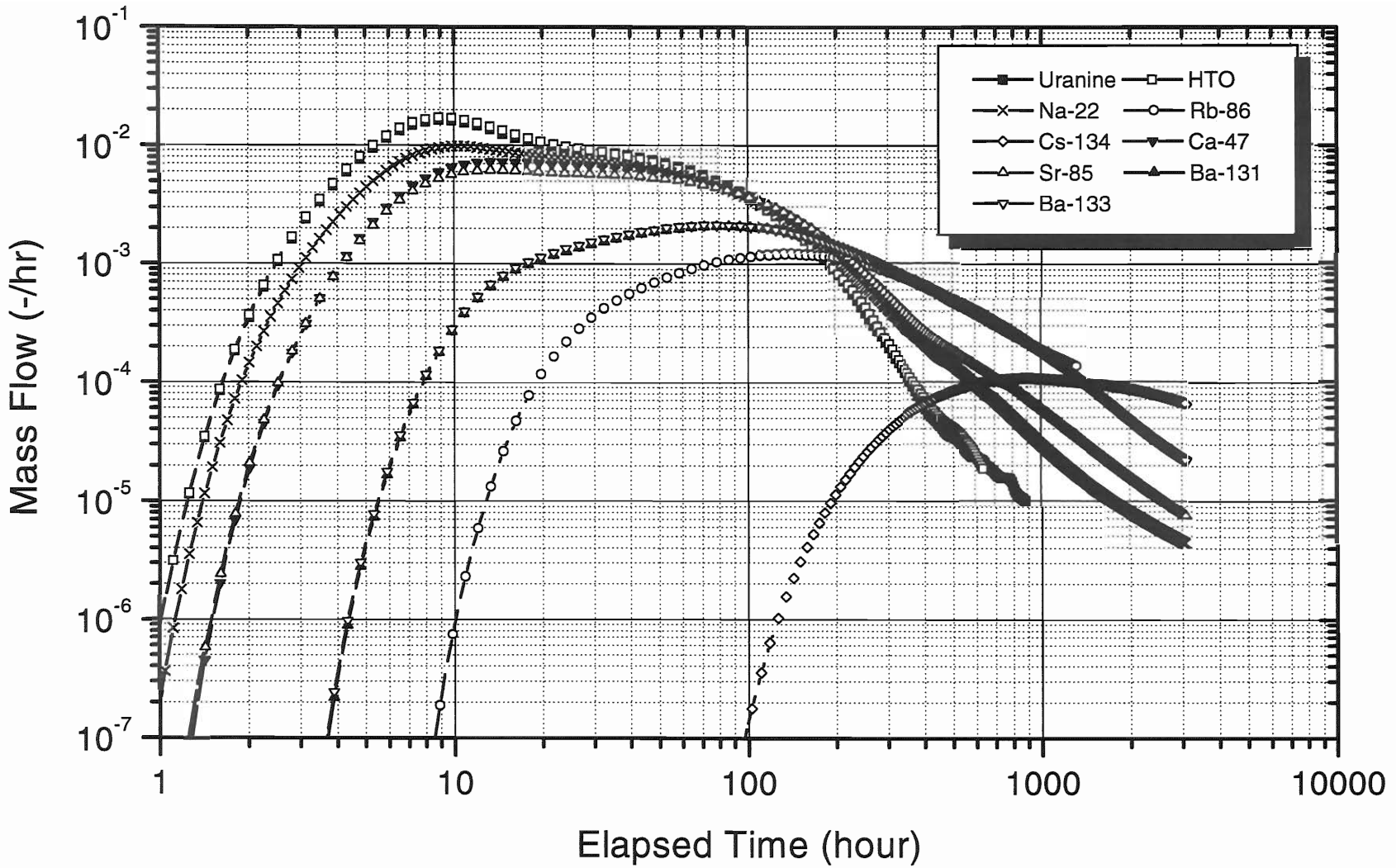

Figure 4-3. Calculated mass flow in pumping section for measured input in STT-2.

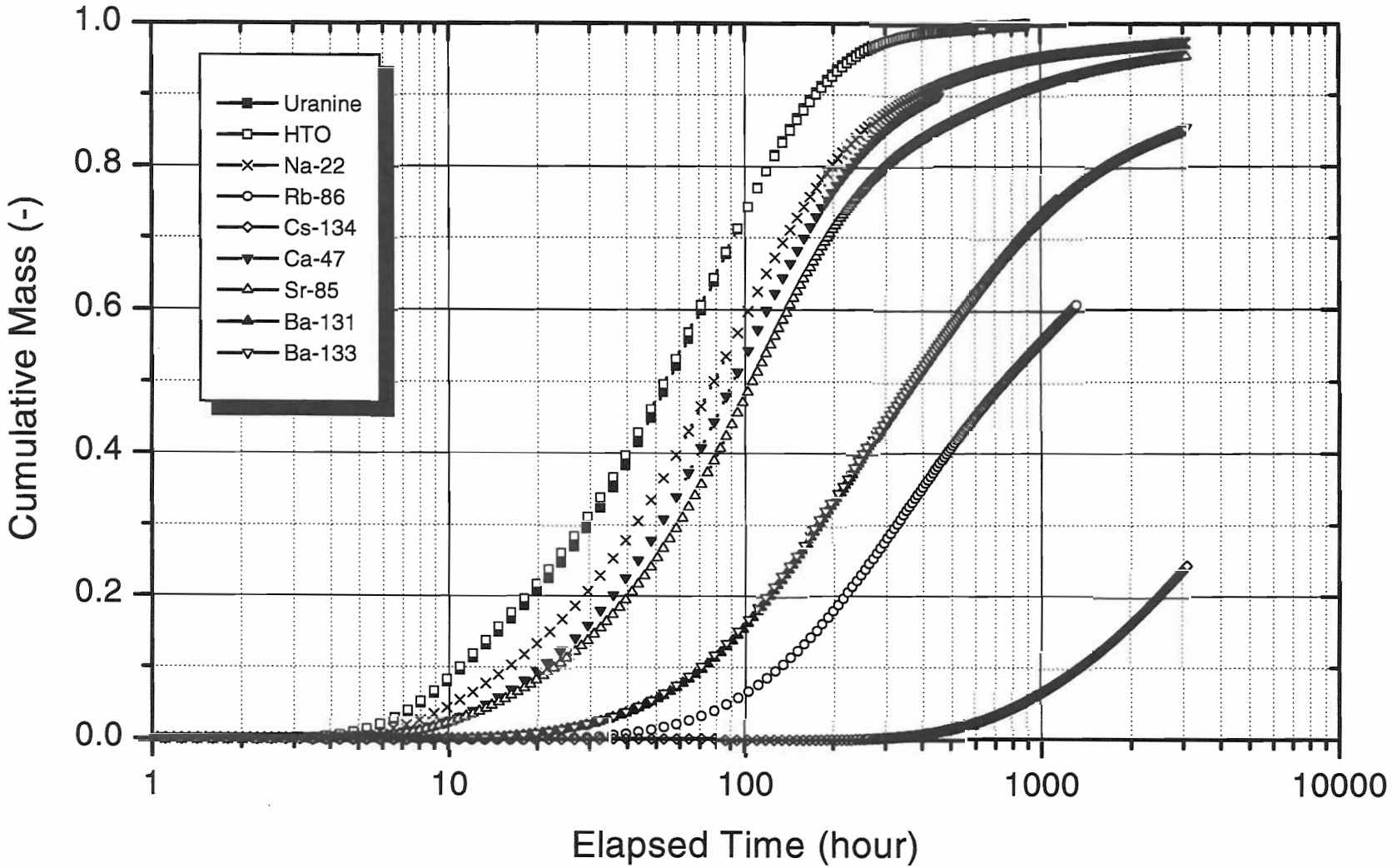

Figure 4-4. Calculated cumulative mass in pumping section for measured input in STT-2.

REFERENCES

Igarashi T, Tanaka Y, Kawanishi M, 1994. Application of three-dimensional smeared fracture model to the groundwater flow and the solute migration of LPT-2 experiment. SKB International Cooperation Report ICR 94-08.

Kawanishi M, Igarashi T, Mahara Y, Komada H, Maki Y, 1987. Computer models for safety assessment on land disposal of low-level wastes. Waste Management '87, 3, Tucson, Arizona, pp. 175-180.

de Marsily G, 1986. Quantitative Hydrogeology. Academic Press, INC..

Winberg A, 1996. Descriptive structural-hydraulic models on block and detailed scales of the TRUE-1 site. SKB International Cooperation Report ICR 94-08.

Andersson P, 1996, TRUE 1st stage tracer test program. Experimental data and preliminary evaluation of the TRUE-1 radially converging tracer test (RC-1). Äspö Hard Rock Laboratory Progress Report HRL-96-24.

Andersson P, Nordqvist R, Jönsson S, 1997. TRUE 1st stage tracer test program. Experimental data and preliminary evaluation of the TRUE-1 dipole tracer tests (DP-1 – DP-4). Äspö Hard Rock Laboratory Progress Report HRL-97-13.

Andersson P, Byegård J, Cvetkovic V, Johansson H, Nordqvist R, Selroos J, Winberg A, 1997. TRUE 1st stage tracer test program. Experimental plan for tests with sorbing tracers at the TRUE-1 site. Äspö Hard Rock Laboratory Progress Report HRL-97-07.

Andersson P, Johansson H, Nordqvist R, Skarnemark G, Skålberg M, Wass E, 1998. TRUE 1st stage tracer test program. Tracer tests with sorbing tracers, STT-1. Experimental description and preliminary evaluation.

Winberg A, Andersson P, Hermanson J, Byegård J, 1998. First TRUE stage. Updated structural model of the TRUE-1 block and detailed description of Feature A. A technical memorandum prepared for the Äspö Task Force, Tasks 4E/4F. Final Draft.

Table 4-4. Calculated tracer travel times for measured input of STT-2.

Tracer	t_5	t_{50}	t_{95}
Uranine	8.01	55.12	226.96
HTO	7.87	53.50	230.98
Na-22	10.46	78.36	859.20
Rb-86	88.23	746.96	-
Cs-134	849.01	-	-
Ca-47	13.57	91.18	458.00
Sr-85	14.51	106.47	2334.41
Ba-131	47.20	368.93	-
Ba-133	46.03	366.43	-

Unit : hour

Table 4-5. Calculated tracer recoveries at the time, t_t, for measured input of STT-2. t_t represents the time of termination of monitoring.

Tracer	t_t (hour)	Recovery (%)
Uranine	886	99.97
HTO	641	99.81
Na-22	3078	97.61
Rb-86	1322	60.87
Cs-134	3078	24.31
Ca-47	458	90.14
Sr-85	3078	95.70
Ba-131	1130	75.46
Ba-133	3078	85.42

Estimation of STT1b and STT1, and Blind prediction of the STT-1 tracer tests with multiple rates of mass transfer.

S. McKenna (DOE/Sandia)

Solute Transport Modeling of the Äspö STT-1 Tracer Tests with Multiple Rates of Mass Transfer

Äspö Task Force on Modelling of Groundwater Flow and Transport of Solutes

Sean A. McKenna

Geohydrology Department
Sandia National Laboratories
PO Box 5800 MS 0735
Albuquerque, New Mexico 87185-0735

April 16th, 1999

Abstract

A solute transport model employing multiple rates of mass transfer is applied to the STT-1 tracer test data. Observed data from all eight tracers can be explained using a single, one-dimensional transport pathway with negligible longitudinal dispersion. Three parameters are estimated for each tracer: the total capacity, and the mean and standard deviation of a log-normal distribution of mass-transfer rate coefficients. Seven of the eight tracers can be estimated by fixing the fracture surface retardation to zero (Rm = 1.0). For the Cs-137 data, it is necessary to invoke surface sorption to adequately match the observed data. Estimates of the total capacity of the transport system are used to calculate values of K_d. These calculated values are higher than previously reported, laboratory-derived values and also span a smaller absolute range than the previously reported values. The fraction of the rock matrix that acts as a seemingly infinte sink for solute is determined through a Damkohler calculation and is shown to be less than 0.5

1 Introduction

The data set available for the STT-1 estimations are reviewed and a weighted average injection rate is determined using data available from Andersson et al. (1998). The flow and transport parameters estimated by the multirate model are defined. The standard error about each estimated parameter can be used to determine the precision of the estimated values.

1.1 Available Data

The STT-1 tracer tests were conducted in Feature A of the Aspo Hard Rock Laboratory. A detailed geologic description of Feature A is given by Winberg, 1999. The STT-1 tracers were injected in borehole KXTT4 R3 and extracted from borehole KXTT4 R2. The pumping rate in borehole KXTT3 R2 was held constant at 400 ml/min (6.67E-06 m^3/s). The straight-line distance between boreholes KXTT4 R3 and KXTT4 R3 is 4.68 m (Andersson et al., 1998).

The concentration history at the injection borehole and the observed breakthrough curve at the pumping well are available for eight different tracers. These tracers, in order of increasing sorptivity, are: Uranine, HTO, Na22, Ca47, Sr85, Ba133, Rb86 and Cs137. For the radioactive tracers (all eight tracers excepting uranine), values of activity in Bq/kg are provided. For uranine, the concentrations are modeled in units of kg/m^3. Both the injection and the breakthrough curve activity values have been corrected for radioactive decay.

1.2 Determination of Injection Rate

The tracer injection rate, Q_{inj}, is a necessary parameter for understanding tracer transport in Feature A. The value of Q_{inj} is the denominator of the dilution factor parameter in the

multirate model employed here (see above). However, the exact value of Q_{inj} is highly uncertain (Andersson, et al., 1998). The value of Q_{inj} is determined as:

$$Q_{inj} = V \cdot \Delta(\ln(C/Co)/t) \qquad (1\text{-}1)$$

where V is the volume of the packed off borehole section and the remaining parameters in equation 1-1 represent the decrease in *ln* tracer concentration, normalized by the maximum concentration, as a function of time, t. Using the conservative tracers, HTO and uranine, and adjusting the value of V to get 100 percent mass recovery, Andersson et al. (1998) were able to determine values of Q_{inj} for three distinct injection periods: 0-4, 10-70 and 70-200 hours. The time weighted average injection rate for these three periods, based on the HTO results in Table 3-3 of Andersson et al. (1998), is calculated to be 36.13 ml/hour (1.004x10-08 m^3/s). The values used in this calculation are given in Table 1-1.

Table 1-1. Determination of Q_{inj} as a weighted average. The sum of column four divided by the total injection time, 200 hours, gives a weighted average Q_{inj} of 36.13 ml/h (1.004E-08 m^3/s).

Time Period	Flow Rate (ml/h) (from Table 3-3 of Andersson et al., 1998)	Weight (hours)	Weighted Volume (ml)
0-4	36.0	4	144.0
4-10	42.3	6	253.8
10-70	42.3	60	2538.0
70-200	33.0	130	4290.0

Note that there is no injection rate calculated for the time period 4-10 hours. The injection rate determined for the time period 10-70 hours was assumed to be representative of the injection rate during the 4-10 hour period for the weighted average calculation. Using the time weighted average injection rate and the pumping rate of 400 ml/hour gives a dilution factor of 664.0. This value of the dilution factor is compared to the value derived from parameter estimation of the HTO breakthrough curve data below.

1.3 Multirate Model

The mathematics behind the multirate model have been presented previously (Haggerty and Gorelick, 1995; Haggerty and Gorelick, 1998). McKenna (in review) has given a fairly concise description of the application of multirate theory to fractured rocks. A description of the multirate model is not repeated here, and the reader is referred to the above references for better understanding of the details of the multirate model.

1.4 Parameter Estimation

The parameter estimation for the STT-1 data is essentially the same as was done for the STT-1b data. This section is taken from (McKenna, in review) with one minor change: the definition of *Rm* is based directly on fracture surface area and fracture volume.

The parameter values are estimated through a least-squares algorithm that minimizes the difference between the observed and modeled data. In the current version of STAMMT-L (v1.10) used for the modeling presented in this report, it is possible to estimate a total of seven different parameters. These parameters are denoted as: β_{tot}, μ, σ, *Rm*, *rP*, *dilute*, and v_x. A brief explanation of each parameter is provided below.

The total capacity for mass uptake within the aquifer is defined as β_{tot}:

$$\beta_{tot} = \frac{R_{im}\phi_{im}}{R_m\phi_m}. \tag{1-2}$$

where *Rim* and *Rm* represent the retardation factors for the immobile (non-advecting) and mobile (advecting) portions of the aquifer respectively. At equilibrium conditions, the concentrations of mass are evenly distributed for a diffusing solute. In this situation, there is no concentration gradient between the mobile, or advective, and immobile, or diffusive, portions of the aquifer, and β_{tot} is simply the ratio of the immobile zone to mobile zone porosities : ϕ_{im}/ϕ_m. In the case of a sorbing and diffusing solute, the ratio of mobile to immobile zone concentrations at equilibrium includes the retardation factors, R_{im} and R_m for the mobile and immobile zones respectively.

In the work presented here, a lognormal distribution of mass-transfer rate coefficients is employed to model mass-transfer between the mobile and immobile zones. The estimated parameters, μ and σ, define the first and second moments of the *ln* mass-transfer rate coefficient distribution. In the case of a sorbing tracer, μ can be decomposed into diffusing and sorbing components describing mass-transfer to the immobile zone:

$$\alpha_d^* = \frac{D_{aq}\tau}{R_{im}l^2} \tag{1-3}$$

where Daq is the free-water diffusion coefficient, t is the tortuosity, and l is the distance from the fracture matrix interface to the center of the matrix block. Taking the natural log of both sides of equation 1-3 and separating terms gives:

$$\ln(\alpha_d^*) = \ln\left(\frac{D_{aq}\tau}{R_{im}l^2}\right) \Rightarrow \ln\left(\frac{D_{aq}\tau}{l^2}\right) - \ln(R_{im}). \tag{1-4}$$

This separation of terms allows the determination of the immobile zone retardation factor for the matrix block length, *l*, corresponding to the diffusion rate coefficient.

The retardation factor for the mobile zone is defined as:

$$R_m = 1 + \frac{A_d}{V_f} K_a \tag{1-5}$$

where A_d is the surface area of the fractured rock, V_f is the fracture volume and K_a is the distribution coefficient for sorption onto the fracture walls. The mobile zone retardation factor is obtained by parameter estimation.

The Peclet number for the transport system is defined as:

$$rP = \frac{L_s}{\alpha_L} \tag{1-6}$$

where L_s is a user-defined system length. In order to avoid numerical error problems within STAMMT-L, L_s should be set as longer than the actual transport path. In this study, L_s is set to 10.0 meters and the transport pathway, L_o, is set to the distance between the injection and withdrawal wells (4.68m).

A dilution factor is also estimated. For the TRUE tracer tests, the dilution factor is conceptualized as the ratio of pumping to injection rates:

$$dillute = \frac{Q_p}{Q_{inj}}. \tag{1-7}$$

Using the value of Q_{inj} calculated above and the pumping rate of 400 ml/min, the value of the dilution factor is 664. Equation 1-7 assumes that 100 percent of the injected mass is recovered in the pumping well. In the case of the more strongly sorbing tracers, this is not the case, and this less than full recovery will impact the value of the dilution factor. This behavior can be conceptualized as irreversible sorption with respect to the time scale of the tracer test. In these cases, *dilute* is conceptualized as:

$$dillute = \frac{Q_p}{Q_{inj}} * \frac{1}{RF} \tag{1-8}$$

where RF is the mass fraction of the tracer recovered in the pumping well.

The practice of parameter estimation can be thought of as a process for using the available data to uncover some information regarding a much larger data base, or population. Under this framework, the gathering of information from experiments falls into the realm of the statistics of sampling theory (Harr, 1987). Each estimated parameter, as introduced above, can be thought of as a random variable with an expected value (mean) and a standard deviation. It can be shown that the value of the estimated

parameter is a sample mean derived from the available data. Furthermore, this sample mean is an unbiased estimator of the underlying population mean.

In order to determine a measure of the expected error about the estimated parameter value, it is possible to determine the standard deviation of the expected value (see Harr, 1987, p. 229). It is noted that this standard deviation is not equal to the standard deviation of the sampled data. Under the assumption of uncorrelated errors, the standard deviation of the estimated parameter value is given by:

$$\sigma(P) = \frac{1}{\sqrt{N}}\sigma(x_i) \tag{1-9}$$

where N is the number of samples and $\sigma(x_i)$ is the standard deviation of those samples. The standard deviation of the estimate is also known as the *standard error* and the standard error will be used to determine confidence intervals about the estimated parameters in this report.

2 Estimation of STT-1 Breakthrough Curves

The approach used here is to try and estimate the STT-1 breakthrough curves by fixing as many parameters as possible. The values of the flow parameters, α_L, v_x and *dilute* are determined by estimating the HTO data with *Rm* fixed at 1.00 are then used as fixed parameters for all other tracers. Values of the transport parameters: β_{tot}, μ and σ are estimated independently for each tracer. For the Cs-137 data, it is also necessary to estimate values or *Rm* and *dilute*.

2.1 Modeling of the HTO Data

As a first step in the modeling process, the HTO data are used to estimate values of parameters defining the flow system in the STT-1 tracer tests. It is assumed that, as a component of water, the HTO breakthrough data are representative of non-reactive transport through Feature A and the flow parameters, α_L, v_x and *dilute*, estimated using the HTO data can be applied to the other tracers as well. The transport parameters, *Rm*, βtot, μ, σ are tracer dependent and must be modeled separately. For the HTO data, *Rm* is fixed at 1.00 and the remaining 6 parameters are estimated by the model. The results of this estimation are shown in the top row of Table 2-1. The flowpath velocity estimated with the HTO data is 1.853×10^{-03} m/s, with the lower and upper bounds of the 95 percent confidence interval being 1.79×10^{-03} and 1.91×10^{-03} m/s respectively. This velocity value is held constant for all other parameter estimations for all tracers.

Parameters estimated for the HTO data by the multirate model are shown n the first row of Table 2-1. It is interesting to note that the value of the dilution factor estimated with the HTO data, 607, is lower than that estimated above, 664, using the injection rates calculated in Andersson et al. (1998). The value estimated from the multirate code is approximately 91 percent of that determined above using the concentration decay in the injection borehole. A dilution factor of 607 corresponds to an injection rate of 39.5 ml/hour, slightly higher than the value of 36.1 ml/hour calculated above.

Another interesting result of the HTO estimation is the extremely large value of the Peclet numbr, *rP*. This corresponds to an extremely small dispersivity of 1.63×10^{-05} meters (top row of Table 2-1).

2.2 Three Parameter Estimation

A set of inverse model runs was conducted by fixing the values of v_x, *dilute*, and α_L. Additionally, the amount of surface sorption in Feature A is tested by fixing the value of *Rm* to 1.0 for all tracers. Although this is theoretically incorrect as several of the tracers are known to be moderately to strongly sorbing from laboratory testing, it is not clear that the laboratory derived values are representative of the sorption processes acting within Feature A. Results of modeling the tracer breakthrough curves are shown in Figure 2-1

and 2-2. The values of the parameters obtained by fitting the breakthrough curve data are given in Table 2-1.

Table 2-1. Parameter values and goodness of fit measures (RMSE) for the eight tracers modeled with the multirate model. Only 3 parameters were estimated for each tracer: β_{tot}, μ and σ. All other parameters, including the velocity, are held constant across the suite of tracers.

Tracer	β_{tot}	μ	σ	*Rm*	*rP*	*dilute*	RMSE
HTO	77.4	-16.7	3.35	1.00	6.14E+05	607.0	0.114
Uranine	36.1	-15.4	3.51	1.00	6.14E+05	607.0	0.116
Na22	110.3	-15.9	2.38	1.00	6.14E+05	607.0	0.090
Ca47	33.8	-12.0	0.22	1.00	6.14E+05	607.0	0.118
Sr85	286.4	-17.5	2.43	1.00	6.14E+05	607.0	0.079
Ba133	566.0	-16.7	1.11	1.00	6.14E+05	607.0	0.292
Rb86	704.3	-16.0	0.09	1.00	6.14E+05	607.0	0.122
Cs137	13,502	-19.9	3.46E-07	1.00	6.14E+05	607.0	0.752

Examination of Figures 2-1 and 2-2, show that it is possible to adequately model the tracer data by estimating only three parameters. The Cs-137 and Ba-133 data are exceptions to this statement, and these two tracers will be examined in more detail below. The RMSE values in Table 2-1 show that the model fits to all tracers are reasonable (RMSE near 0.10) with the exceptions of Ba-133 and Cs-137.

The tracers in Table 2-1 are listed in order of increasing sorptivity from top to bottom. Given the definition of total capacity in Equation 1-2, for a constant ratio of porosities, the capacity of the rock to store the tracer will increase with increasing sorptivity. The values in Table 2-1 indicate that, in general, this trend applies to the STT-1 data. The exceptions to this trend are uranine and Ca-47. Results of the STT-1b modeling showed that uranine may in fact be more "non-reactive" than HTO due to anion exclusion processes. If this is the case, then uranine also fits the general model of increasing capacity with increasing sorptivity. The model results of uranine will be explored further below. The Ca-47 results also do not fit the model of increasing capacity with increasing sorptivity. It is difficult to determine if these results are significant or just an artifact of the relatively short Ca-47 data set. Compared to the length of the other data sets, the Ca-47 data is especially short (see lower image, Figure 2-1) and it may be prudent to discount any results obtained with the Ca-47 data.

Computing the standard error about the estimate (see Equations 1-9) can be used to check the precision of the parameter estimates obtained from the multirate model. An approximate 95 percent confidence interval can be constructed as +/- 2 standard errors about the estimated value. The bounds of these confidence intervals are also shown in Tables 2-2, 2-3, and 2-4.

Table 2-2. Estimates of β_{tot} with approximate 95 percent interval bounds.

Tracer	Estimate	Estimate - 2 Std. Error	Estimate +2 Std. Error
HTO	77.4	63.10	94.90
Uranine	36.1	34.40	37.97
Na22	110.3	90.555	134.44
Ca47	33.8	30.72	37.14
Sr85	286.4	236.89	346.21
Ba133	566.0	397.59	805.75
Rb86	704.3	663.10	747.99
Cs137	13,502	11444.1	15930.7

Table 2-3. Estimates of μ with approximate 95 percent interval bounds.

Tracer	Estimate	Estimate - 2 Std. Error	Estimate +2 Std. Error
HTO	-16.7	-17.6	-15.8
Uranine	-15.4	-15.4	-15.3
Na22	-15.9	-16.6	-15.1
Ca47	-12.0	-12.2	-11.7
Sr85	-17.5	-18.1	-16.9
Ba133	-16.7	-17.7	-15.6
Rb86	-16.0	-16.1	-15.8
Cs137	-19.9	-20.6	-19.2

Table 2-4. Estimates of σ with approximate 95 percent interval bounds.

Tracer	Estimate	Estimate + 2 Std. Error	Estimate –2 Std. Error
HTO	3.35	3.044	3.678
Uranine	3.51	3.435	3.584
Na22	2.38	2.133	2.656
Ca47	0.22	0.174	0.269
Sr85	2.43	2.296	2.575
Ba133	1.11	0.550	2.261
Rb86	0.09	0.075	0.106
Cs137	3.46E-07	0	NAN

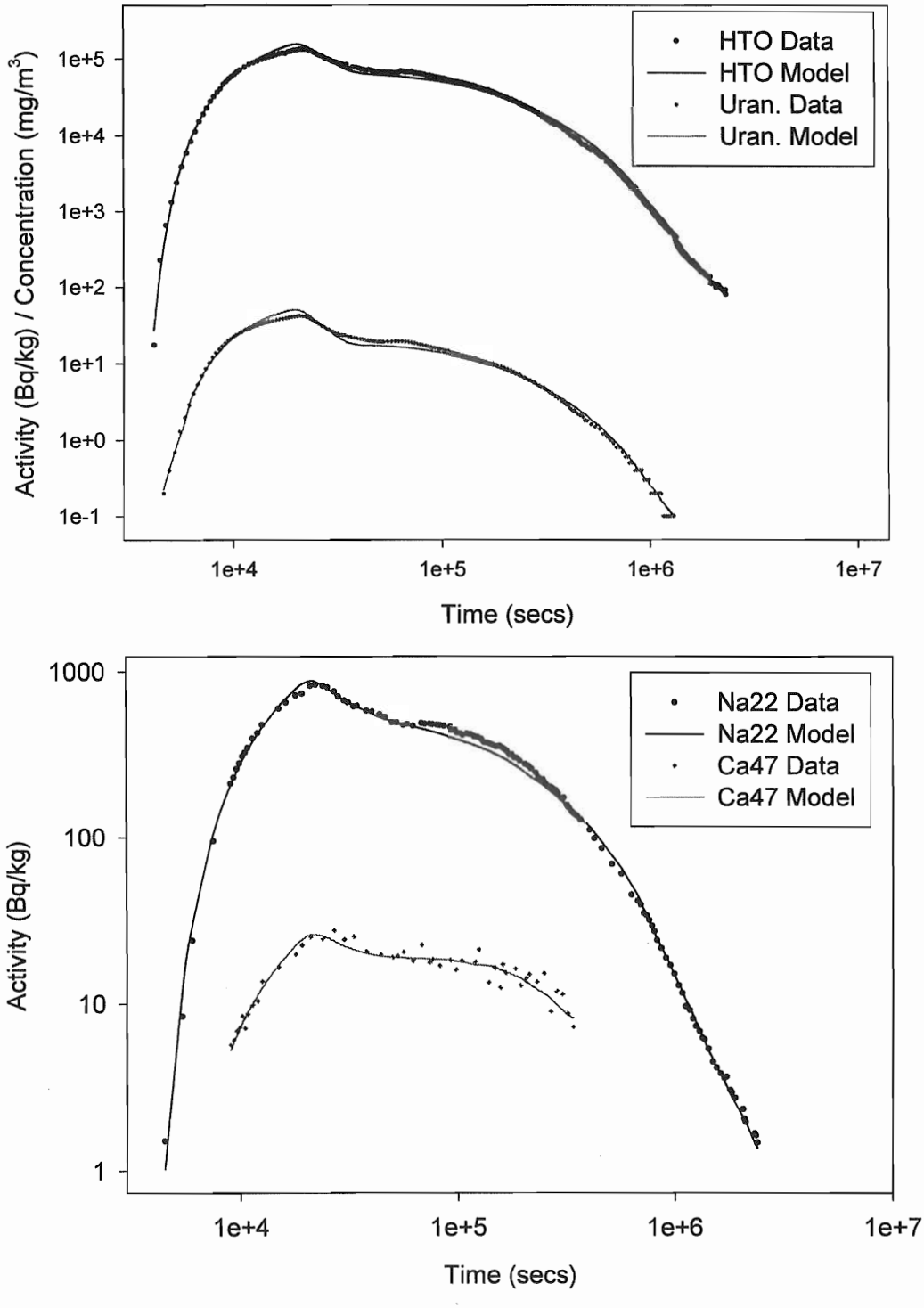

Figure 2-1. Multirate model fits to observed data obtained by estimating β_{tot}, μ, and σ with *Rm* fixed at 1.0. The upper image shows the results for HTO and uranine, the lower image shows results for Na22 and Ca47. Parameter values are listed in Table 2-1.

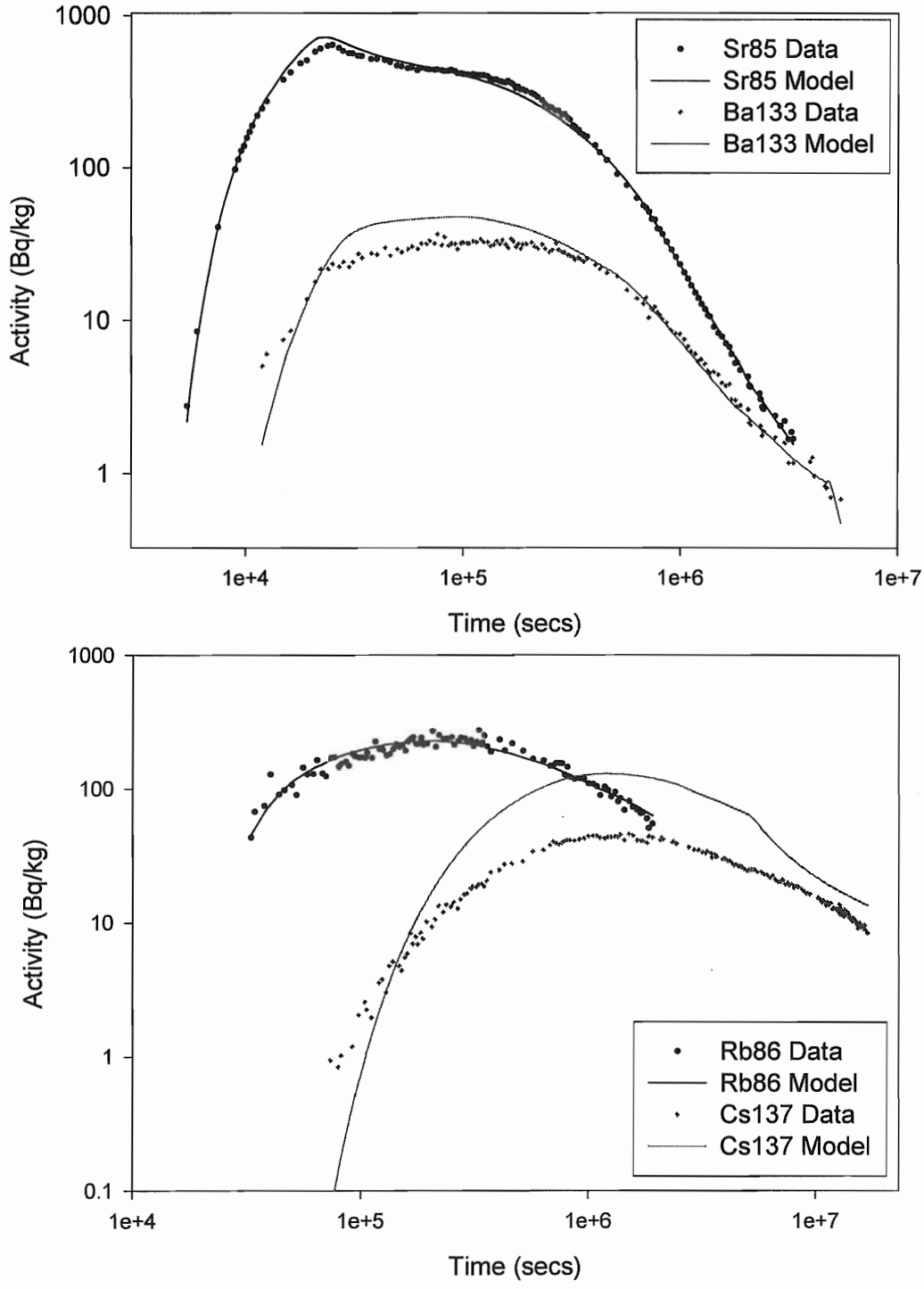

Figure 2-2. Multirate model fits to observed data obtained by estimating β_{tot}, μ, and σ with *Rm* fixed at 1.0. The upper image shows the results for Sr85 and Ba133, the lower image shows results for Rb86 and Cs137. Parameter values are listed in Table 2-1.

3 Additional Simulations

Several additional estimations are conducted for the Cs-137, Ba-133 and unraine data sets. The goal of these additional simulations is to improve the model fit to the observed data and gain a better understanding of the processes controlling mass-transfer within Feature A.

3.1 Cs137 and Ba133

Parameter estimation done with the multirate model uses the RMSE between the natural log of the observed and modeled activities/concentrations as an objective criteria to adjust parameter values. This procedure is constrained to the injection history, but does not explicitly take into account the amount of mass under the observed breakthrough curve. Examination of Figures 2-2 shows that the Ba-133 and Cs-137 multirate models overestimate the amount of mass in the breakthrough curve. Relative to the other tracers, these results suggest that the amount of mass contained in the Ba-133 and Cs-137 breakthrough curves is significantly less than the amount of mass injected.

Estimates of the recovered mass of each tracer were calculated using two different techniques and are given by Andersson et al. (1998, see table 3-8). For Cs-137, only 26 or 22 percent of the injected mass was recovered depending on the method of calculation. For situations of less than 100 percent mass recovery, the dilution factor can be interpreted as:

$$dilute = \frac{Q_p}{Q_i} * \frac{1}{RF}$$

where RF is the fraction of recovered mass. The 26 percent mass recovery given by Andersson et al. (1998) is used to recalculate the dilution factor. The new dilution factor for Cs137 is 2336.95. This new value of the dilution factor is used in an additional simulation of the Cs-137 data. This additional simulation is done estimating four parameters: βtot, μ, σ, and Rm. The values of α_L, v_x and *dilute* are fixed. Results of this simulation are shown in Figure 3-1 and the estimated and fixed parameters are given in Table 3-1.

Table 3-1. Values of parameters used in additional estimations. In all cases, v_x is held at 1.85×10^{-03} m/sec and α_L is held at 1.63×10^{-05} m.

Tracer	Number of Estimated Parameters	β_{tot}	μ	σ	*Rm*	*dilute*	RMSE
Ba133	4	2077.1	-15.0	0.441	0.14	740.5	0.179
Cs137	4	525.0	-17.4	0.024	5.25	2336.9	0.192
Cs137	5	2942.7	-17.6	0.032	1.16	1982.1	0.117
Uranine	4	44.1	-15.6	3.793	0.843	607.0	0.115

The four parameter estimation of the Cs-137 breakthrough curve using the dilution factor based on the fraction of recovered mass determined by Andersson et al. (1998) provides a significantly better fit to the data than did the three parameter estimation. However, the RMSE of the model fit to the data is still larger than the RMSE values for the three parameter fits to the other tracers (see Tables 2-1 and 3-1). A final attempt to fit the Cs-137 data was done by estimating five parameters: *βtot*, μ, σ, *Rm,* and *dilute* in order to see what value of dilution factor would be estimated by the multirate model. The results of this five-parameter estimation are also shown in Figure 3-1 and Table 3-1.

Estimation of five parameters gives the best fit to the observed Cs-137 data (RMSE = 0.117). The estimated value of the dilution factor is 1982.1. By using the definition of the dilution factor in equation 1-8 and the original value of the dilution factor obtained from the HTO data, the estimated fraction of the mass that was recovered in the breakthrough curve can be determined. The fraction of recovered mass given the dilution factor of 1982.1 is 0.306 or approximately 31 percent. This value is in line with the 26 percent mass recovery estimated by Andersson et al. (1998).

Reestimation of the Ba-133 data is done using a similar approach to that taken above for Cs-137. The fraction of recovered mass for Ba-133 calculated by Anderssson et al. (1998) is either 82 or 55 percent depending on the calculation technique. Using the value of 82 percent gives a dilution factor of 740.54. This dilution factor is used to reestimate the Ba-133 breakthrough curve. The results of this reestimation are presented in Figure 3-1 (lower) and the estimated and fixed parameters are given in Table 3-1.

Examination of the lower image in Figure 3-1 shows that the fit to the Ba-133 data is greatly improved by the four parameter model with the dilution factor based on the data from Andersson et al. (1998). The RMSE has dropped from 0.292 to 0.179 (see Tables 2-1 and 3-1). However, the model still has difficulty in fitting the fairly broad peak of the observed data and the estimated value of the *Rm* is an unrealistic 0.14 (see Table 3-1).

An additional simulation was attempted for the Ba-133 data in which the value of *dilute* was estimated by the multirate model. The value of *Rm* was fixed at 1.00, as was done in the original simulation, such that only four parameters are estimated. The simulation could not converge to a solution for this estimation.

3.2 Uranine

Previous work on estimating the STT-1b tracer tests (McKenna, in review) showed that relative to the other tracers, uranine appeared to be extremely non-reactive. These results were attributed to the anion exclusion process where the negative charge of the uranine keeps the tracer from having any significant interaction with the fracture walls and/or the matrix. Values of Rm estimated using the STT-1b data (McKenna, in review) were often less than 1.0. While these values are physically unrealistic, they do suggest an extreme "non-sorptivity" of uranine along the STT-1b transport pathway.

The sorptivity of uranine is examined along the STT-1 transport pathway with a four parameter estimation where βtot, μ, σ, and *Rm* are all estimated by the multirate model. Results of this estimation are given in Table 3-1. The parameter estimates in Table 3-1 show that the results of the four parameter model are very similar to those obtained with the three parameter model (Table 2-1). The RMSE value for the four parameter model is 0.115, only slightly lower than the three parameter model RMSE of 0.116. The estimated value of *Rm* does drop below 1.0 to 0.84, but the estimated values of the other three parameters are all similar to those estimated with the three parameter model. These results indicate that uranine may be less reactive than HTO, but that the actual fit to the STT-1 observed data is not extremely sensitive to the value of *Rm*. The estimated values from the original three parameter model fit to the uranine data are retained for further analysis and prediction of the STT-2 tracer test.

3.3 Summary

Examination of the original three parameter simulations and the additional four and five parameter simulations, leads to selection of the final set of simulations that best represent the observed data. The final set of simulations includes the three parameter simulations for HTO, uranine, Na-22, Ca-47, Sr-85, Ba-133, and Rb-86. The parameters used for these seven tracers are tabulated in Table 2-1. The best simulation for the Ba-133 data in terms of RMSE is the four-parameter simulation conducted with a dilution factor based on the fraction of mass recovered as determined by Andersson et al. (1998). However, the estimated value of *Rm* in this simulation is 0.14 and these results are deemed unrealistic. The five-parameter simulation for Cs-137 is retained as the simulation most representative of the Cs-137 data. The parameters defining this simulation are tabulated in the 3rd row of Table 3-1.

In summary, seven of the eight tracers are best fit by simulations that only optimized three parameters. For these seven tracers, the retardation factor for the fracture surfaces is set to 1.0 indicating negligible surface sorption occurring within Feature A along the STT-1 transport pathway. For Cs-137, it is necessary to increase the dilution factor to account for the majority of the mass not being recovered during the tracer experiment, and it is also necessary to use an *Rm* value greater than 1.0. It is also noted that all tracers can be modeled with an extremely small dispersivity (approximately 2×10^{-05} meters).

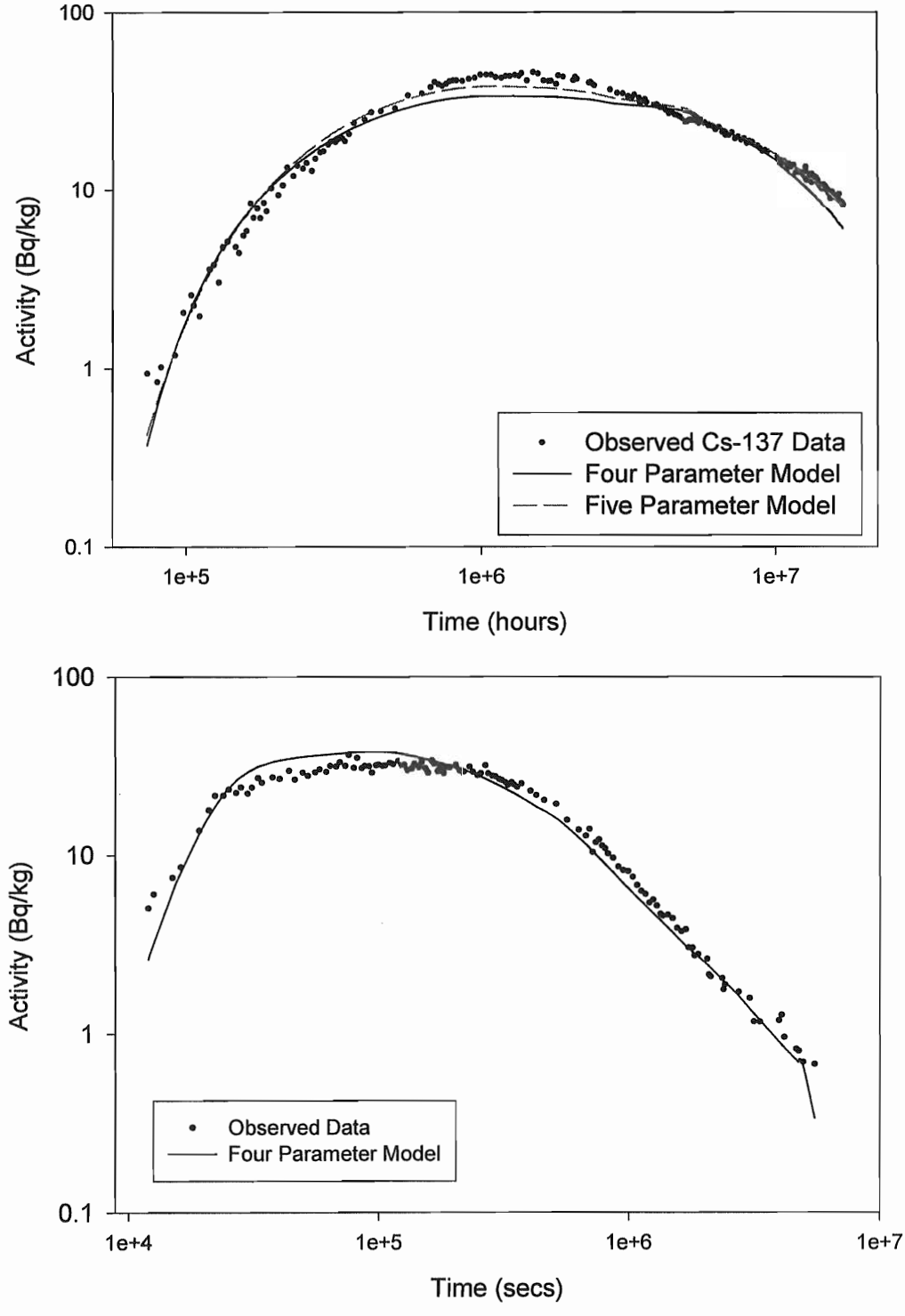

Figure 3-1. Four and five parameter estimations for the Cs-137 data (upper image) and four parameter estimation for the Ba-133 data (lower image).

4 Examination of Results

Results of the modeling presented above are examined further by determining the values of *Rim* and K_d for the sorbing tracers and by calculating the Damkohler numbers for the mass-transfer rate coefficient distributions. The values of K_d are compared to those reported in Winberg et al. (1998). The Damkohler calculations allow for determination of the fraction of the immobile zone capacity in different states of equilibrium/non-equilibrium with the solute concentrations in the mobile zone.

4.1 Calculation of K_d

Given the estimates of β_{tot} in Tables 2-1 and 3-1, it is possible to calculate estimated values of the immobile zone retardation coefficient for each tracer. These calculations require some assumptions regarding the porosity of the mobile and immobile zones. By making an additional assumption regarding the bulk density of the Äspö diorite, it is also possible to estimate a distribution coefficient, K_d, for each tracer.

Equation 1-2 can be rearranged to solve for Rim given the estimated value of β_{tot}. For these calculations, ϕ_{im} is assumed to be 0.004 (average reported by Byegard, et al., 1998), and ϕ_m is assumed to be 0.015. The results of the R_{im} calculations are given in Table 4-1. With additional information on the bulk density of the rock, ρ_b, values of K_d can also be estimated as:

$$K_d = (R_{im} - 1)\frac{\phi_{im}}{\rho_b} \qquad (4\text{-}1)$$

A representative value for the bulk density of diorite is 2800 kg/m^3 (Best, 1982). Using this value in equation 4-1 with the assumed porosities given above, produces the K_d values given in Table 4-1.

Table 4-1. Estimated values of *Rim* and K_d based on the estimates of βtot and assumed values of porosity and bulk density.

Tracer	β_{tot}	*Rm*	*Rim*	K_d (m^3/kg)
Na22	110.3	1.0	413.6	5.895E-04
Ca47	33.8	1.0	126.8	1.796E-04
Sr85	286.4	1.0	1074.0	1.533E-03
Ba133	566	1.0	2122.5	3.031E-03
Rb86	704.3	1.0	2641.1	3.772E-03
Cs137	2,943	1.16	12800.	1.829E-02

The range of estimated K_d values shown in Table 4-1 is roughly 1.5 orders of magnitude. This range is less than that reported by Winberg et al. (1998; Table 5-1), where the Kd values measured in the laboratory covered a range of approximately 2.5 orders of

magnitude. The values in Table 4-1 are considerably higher than those reported by Winberg, et al. (1998) that range from $1.4x10^{-06}$ m^3/kg for Na-22 to $6x10^{-03}$ m^3/kg for Cs-137. If the assumed value of mobile zone (fracture) porosity was changed from 0.015 to a value in the range of 0.001 to 0.0005, the estimated K_d values would decrease to the range of those reported by Winberg et al. (1998). This same range of K_d values could also be achieved by smaller decreases in the mobile zone porosity coupled with increases in the immobile zone porosity. The reported porosity of the diorite (0.004) may be an unrealistically low estimate of the mylonite and fault gouge found in Feature A.

4.2 Damkohler Calculations

Calculation of the Damkohler number for the STT-1b results proved useful in gaining a better understanding of the sorptive and diffusive capacity of Feature A. Those calculations are repeated here using the results of the models for each of the eight tracers. The Damkohler number is defined for mass-transfer into layer shaped blocks as:

$$DaI = 3.0 * \alpha_i (1.0 + \beta_i) \frac{LRm}{v_x} \qquad (4\text{-}2)$$

Where a_i and b_i refer to the mass transfer rates and associated capacities across the multirate distribution. The other parameters are as defined previously. Using the modeling results for each tracer, the Damkohler number is calculated for every point on the multirate distribution. Rather than display all of these results, the Damkohler number is used her to determine the fraction of the mass-transfer distribution that is within one of three critical regions: 1) saturated immobile zone, 2) finite immobile zone, and 3) seemingly infinite mobile zone. These three regimes correspond to Da > 100, 100 > DaI > 0.01 and DaI < 0.01 respectively. The results of these calculations are given in Table 4-2.

Table 4-2. Fraction of immobile zone within each mass-transfer regime for each tracer in the STT-1 test.

Tracer	Fraction Saturated (*DaI* > 100.0)	Fraction of finite immobile volume (100 > *DaI* > 0.01)	Fraction of infinite immobile volume (*DaI* < 0.01)
HTO	0.009	0.541	0.45
Uranine	0.017	0.583	0.40
Na22	0.002	0.688	0.31
Ca47	0.000	0.000	1.00
Sr85	0.001	0.619	0.38
Ba133	0.000	0.865	0.135
Rb86	0.000	0.980	0.02
Cs137	0.000	0.009	0.991

The results shown in Table 4-2 indicate that only a small fraction of the immobile zone capacity has come to equilibrium with the tracer concentrations in the fracture. This interpretation is based on the small fraction of the capacity that is saturated during the course of the tracer test (Table 4-2). The saturated fraction ranges from zero to 1.7 percent.

Results for the STT-1b tracer test obtained by McKenna (in review) showed that the majority of the immobile zone capacity was still acting as a seemingly infinite source for solute. In contrast to those results, the STT-1 results in Table 4-2 show a significant portion of the capacity to be responding as finite capacity blocks of immobile zone for all but two of the tracers. This portion of the immobile zone capacity can be conceptualized as matrix blocks that are small enough such that the concentration at the center of the blocks increases above zero. This arrival of solute at the center of the matrix/mylonite/gouge blocks decreases the concentration gradient driving solute into these blocks. Relative to the STT-1b pathway, these results may indicate a more developed rubble zone along the STT-1 pathway, or the presence of more fault gouge. With the exertion of Ca-47 and Cs-137, less than half of the immobile zone capacity behaves as an infinite sink for solute. This result is in sharp contrast to results obtained along the STT-1b pathway.

5 Summary

The results in this report show that the multirate model is capable of matching the observed breakthrough curves for the STT-1 tracer test. All tracers can be modeled with an extremely small, almost negligible, longitudinal dispersivity value. Also, it is not necessary to invoke multiple flowpaths from the injection to the extraction borehole in order to explain the observed data. For all tracers, with the exception of Ba-133 and Cs-137, it is possible to model the observed breakthrough curves without any retardation along the fracture walls ($K_A = 0.0$).

These results demonstrate a model of the observed data that regards all variability in transport within Feature A to be due to mass transfer processes. The efects of variability in advection is virtually ignored in these models. While the exact nature of the flow and transport processes acting within Feature A is unknown, it is likely a combination of both variable flow and mass-transfer rates that create the observed breakthrough curves. However, the results of this work show that given the current knowledge base, a transport model based strictly on variability in mass-transfer rates cannot be disregarded. At this point, the conceptual model presented herein, is as valid as any other model and should be considered in performance assessment calculations.

The results of the STT-1 estimations will next be used in a blind prediction of the data collected in the STT-2 tracer test.

References

Andersson, P., H. Johansson, R. Nordqvist, G. Skarnemark, M. Skalberg, E. Wass, 1998, TRUE 1st Stage Tracer Test Programme: Tracer Tests with Sorbing Tracers, STT-1: Experimental Description and Preliminary Evaluation, Grap 97 077, GEOSIGMA, Uppsala, Sweden, 34 pp.

Best, M.G., 1982, *Igneous and Metamorphic Petrology*, W.H. Freeman and Company, New York, 630 pp.

Byegard, J., H. Johansson and M. Skalberg, 1998, The Interaction of Sorbing and Non-sorbing Tracers with Different Aspo Rock Types, SKB Technical Report TR-98-18, SKB, Stockholm, Sweden, 105 pp.

Haggerty, R. and S.M. Gorelick, 1995, Mulitple rate mass-transfer for modeling diffusion and surface reactions in media with pore-scale heterogeneity, *Water Resour. Res.*, *31* (10), 2383-2400.

Haggerty, R. and S.M. Gorelick, 1998, Modeling mass transfer processes in soil columns with pore-scale heterogeneity, *Soil Sci. Soc. Am. J.*, *62* (1), 62-74.

McKenna, S.A., (in review), Solute Transport Modeling of the Äspö STT-1b Tracer Tests with Multiple Rates of Mass Transfer, Äspö Task Force Delivery, Feb. 1999.

Winberg, A., P. Andersson, J. Hermanson and J. Byegard, (in press) Updated Structural Model of the TRUE-1 Block and Detailed Description of Feature A, Technical Memorandum, Final Draft, December, 23rd, 1998, 27 pp.

PREDICTION OF STT-2 TRACER TESTS

APPLICATION OF THE MULTIRATE MODEL

Sean A. McKenna

Geohydrology Department
Sandia National Laboratories
PO Box 5800 MS 0735
Albuquerque, New Mexico 87185-0735

October 12th, 1999

Keywords: Solute Transport, STT-2, Multirate Mass Transfer

Abstract

The STT-2 tracer test will be conducted along the same transport pathway as was the STT-1 tracer test, albeit at a lower pumping rate. Results of the STT-1 tracer test estimation are used as a basis for blind prediction of the STT-2 tracer test results. STT-1 parameters are modified to account for the lower pumping rate of the STT-2 test. Cumulative mass recovery and normalized mass flow are calculated using the measured injection concentrations and also a Dirac input pulse. The time to 0.05, 0.50 and 0.95 mass recovery are calculated for the STT-2 predictions and tabulated for all tracers. Differences in time to a given mass recovery between the measured input and the Dirac pulse are greatest for small mass fraction arrivals.

Contents

List of Figures

List of Tables

1. Introduction

This report describes the blind prediction of the STT-2 tracer tests using the multirate mass transfer model. The blind predictions are based on results of estimations done for the STT-1 tracer tests as described in McKenna (in review). The resulting predictions of the STT-2 tracer tests are given in the form of cumulative mass breakthrough and mass flow rate, both as a function of time. Also the times to 0.05, 0.50 and 0.95 mass recovery are given for each tracer along with the mass recovery, F, at the termination times provided by SKB. Note that the modelling approach employed here does not explicitly calculate a head field; therefore, results for steady-state drawdowns in the injection and extraction boreholes are not provided.

1.1 Approach

Blind prediction of the STT-2 results is accomplished by using the parameters estimated previously (McKenna, in review) on the STT-1 data set with a reduced velocity along the transport path to reflect the lower pumping rate in STT-2 relative to STT-1. The dilution factor is also decreased to reflect the lower pumping rate. Predictions of several tracers that were not estimated in STT-1 are necessary. For each of these tracers, parameters from an STT-1 proxy tracer are used for the predictive modelling.

1.2 Review of STT-1 Results

The STT-2 tracer test is conducted along the same transport pathway as the STT-1 tracer test. Many of the same tracers used in STT-1 are also used in STT-2. Also, three additional tracers not used in STT-1 are to be used in STT-2. Results obtained through estimation of the STT-1 test serve as the basis for the STT-2 predictions (McKenna, in review). Those results are reviewed briefly here.

For the majority of the tracers run in the STT-1 test, a good match to the breakthrough curve could be obtained by using fixed values for the longitudinal dispersivity, α_L, the mobile-zone retardation factor, R_m, the dilution factor, *dilute,* and the advective velocity, v_x. Three parameters were estimated using inverse parameter estimation: the total capacity, β_{tot}, and the mean, μ, and standard deviation, σ, of the log-normal distribution of mass-transfer rate coefficients. This approach produced very good matches to the observed breakthrough curves for 6 of the 8 tracers. The matches to the Ba-133 and Cs-137 data were not as good. It was possible to get a much better match to the Cs-137 data by also estimating the dilution factor and the mobile zone retardation factor, R_m. It was not possible to obtain a better match to the Ba-133 data by estimating a greater number of parameters.

The final set of parameters obtained from the STT-1 estimations is given in Table 1-1. Note that the advective velocity value, v_x, for the STT-2 predictions is held constant at 9.27×10^{-4} m/s (half of the value estimated in the STT-1 tests) and the longitudinal dispersivity is held constant at 1.63×10^{-5} m for all tracers. These two parameters were estimated from the conservative HTO results in the STT-1 tests. The parameter values resulting from the STT-1 modelling, as shown in Table 1-1, provide the basis for the STT-2 predictions.

Table 1-1 Final parameters estimated for STT-1 and used as the basis for the STT-2 predictions.

Tracer	β_{tot}	μ	σ	*Dilute*	*Rm*
HTO	77.4	-16.7	3.35	607.0	1.00
Uranine	36.1	-15.4	3.51	607.0	1.00
Na22	110.3	-15.9	2.38	607.0	1.00
Ca47	33.8	-12.0	0.22	607.0	1.00
Sr85	286.4	-17.5	2.43	607.0	1.00
Ba133	566.0	-16.7	1.11	607.0	1.00
Rb86	704.3	-16.0	0.09	607.0	1.00
Cs137	2942.7	-17.6	0.032	1982.1	1.16

1.3 Modifications to STT-1 Parameters

Several of the parameters estimated in the STT-1 test must be modified for use in the STT-2 predictions. The pumping rate in borehole KXTT3 was 400 ml/min for the STT-1 test and it is to be lowered to 200 ml/min for the STT-2 test (Winberg, et al., 1998). This decrease in pumping rate decreases the velocity along the transport pathway, assuming the transport pathway remains constant, and also decreases the value of the dilution factor relative to the STT-1 value. For the STT-2 predictions, the values of velocity and dilution factor are simply decreased by a factor of 2.0 relative to the STT-1 values. The values of velocity and dilution factor used in the STT-2 predictions are: 9.27×10^{-04} m/s and 303.5 respectively. This decrease makes the implicit assumption that the injection rate of 1.099×10^{-8} m^3/s estimated for the STT-1 tracer tests is also used in the STT-2 tracer tests. Actual values of the injection rate for STT-2 are not yet available from SKB

Three of the tracers used in the STT-2 test were not examined in the STT-1 test: Br-82, Ba-131 and Cs-134. It is necessary to assign transport parameters to these tracers in order to predict the STT-2 results. The tracer parameters estimated for Ba-133 and Cs-137 in the STT-1 estimations are assigned to the Ba-131 and Cs-134 tracers respectively. Br-82 is relatively non-reactive and is also an anion. For the STT-2 predictions, the parameters estimated for HTO are used as a proxy for unknown Br-82 transport parameters. The parameters used for the STT-2 blind predictions are shown in Table 1-2.

Table 1-2 Final parameters used for the STT-2 predictions ($v_x = 9.27\text{x}10^{-04}$ m/s and $\alpha_L = 1.63\text{x}10^{-05}$ m).

Tracer	β_{tot}	μ	σ	*dilute*	*Rm*
HTO	77.4	-16.7	3.35	305.5	1.00
Uranine	36.1	-15.4	3.51	305.5	1.00
Na22	110.3	-15.9	2.38	305.5	1.00
Br82	77.4	-16.7	3.35	305.5	1.00
Ca47	33.8	-12.0	0.22	305.5	1.00
Sr85	286.4	-17.5	2.43	305.5	1.00
Ba131	566.0	-16.7	1.11	305.5	1.00
Ba133	566.0	-16.7	1.11	305.5	1.00
Rb86	704.3	-16.0	0.09	305.5	1.00
Cs134	2942.7	-17.6	0.032	991.05	1.16

2. Results

The observed STT-2 concentration histories in the injection borehole are used as input to the multirate model with the flow and transport parameters described in the previous section. A forward run of the model is done for each tracer and the results are tabulated and shown as cumulative mass arrival and mass flow curves. As requested of the Task Force participants, a set of forward model runs are also done with a Dirac input pulse. The Dirac input is scaled such that each tracer has the same amount of total activity as the observed injection history.

2.1 Measured Concentration Input

Results of the STT-2 predictions done with the measured injection concentrations are given in Tables 2-1 and 2-2 and in Figures 2-1 through 2-4. Table 2-1 shows the times to 0.05, 0.50, and 0.95 mass recovery. To obtain these results, the models were run to times beyond the termination times as specified by SKB for each tracer.

Table 2-1 Predicted times to 0.05, 0.50 and 0.95 mass recovery for observed input.

Tracer	T5 (hours)	T50 (hours)	T95 (hours)
HTO	9.25	71.43	373.9
Uranine	8.48	62.68	293.0
Na-22	14.22	94.54	577.6
Br-82	9.83	67.4	304.1
Ca-47	23.56	84.95	223.2
Sr-85	19.89	128.2	1217.7
Ba-131	50.37	320.96	3467.5
Ba-133	49.74	326.97	3466.3
Rb-86	150.0	864.5	2670.9
Cs-134	876.5	4354.8	11,927.4

The mass recovery, F, for each tracer is given in Table 2-2. The mass recovery is the fraction of the injected mass recovered at the termination time specified by SKB. Figures 2-1 and 2-2 show the cumulative mass recovery as a function of time. Cumulative mass recovery is shown for only five tracers in each figure to keep the figures readable. Figures 2-3 and 2-4 show the normalized mass flow, $(M/M_{inj})/\Delta t$, as a function of time. Results for the same five tracers as shown in Figures 2-1 and 2-2 are shown in Figures 2-3 and 2-4 respectively. Note that in

Figures 2-1 through 2-4, results are only shown up to the termination times specified by SKB.

Table 2-2 Predicted mass recovery at termination time for measured injection.

Tracer	$T_{termination}$ (hours)	Mass Recovery (F)
HTO	641	0.978
Uranine	886	0.994
Na-22	3078	0.994
Br-82	234	0.925
Ca-47	458	1.00
Sr-85	3078	0.981
Ba-131	1130	0.818
Ba-133	3078	0.941
Rb-86	1322	0.700
Cs-134	3078	0.337

2.2 Dirac Pulse Input

In order to correctly scale the Dirac pulse, it is necessary to know the total activity injected for each tracer. The activity for a given time interval is calculated as the product of the measured activity in Bq/kg and the mass of the fluid (water) injected during that same time interval. The mass of the injected water for a given time interval, of length Δt, is the volume of the water injected, Q_{inj}, multiplied by the water density, ρ_w. For the calculations done here, both Q_{inj} and ρ_w are assumed constant across all time intervals. The total activity is the sum of the individual activity values, A_i, across all N time intervals:

$$A_{tot} = Q_{inj} \cdot \rho_w \sum_{i=1}^{N} A_i \Delta t_i$$

The total injected activity is calculated for each tracer and is shown in Table 2-3. The calculation of injected activity is done for all times given in the injection history spreadsheet provided by SKB.

Table 2-3 The calculated total injected activity/mass for each tracer.

Tracer	Total Activity (Bq or kg)
HTO	1.0253E+08
Uranine	3.2812E-02
Na-22	1.0938E+06
Br-82	3.5974E+06
Ca-47	2.2116E+05
Sr-85	3.4485E+06
Ba-131	1.2383E+06
Ba-133	1.8908E+05
Rb-86	3.4652E+06
Cs-134	2.2174E+06

Results of the STT-2 predictions done with the scaled Dirac pulse injections are given in Tables 2-4 and 2-5 and in Figures 2-5 through 2-8. Table 2-4 shows the times to 0.05. 0.50 and 0.95 mass recovery. To obtain these results, the models were run to times beyond the termination times as specified by SKB for each tracer.

Table 2-4 Predicted times to 0.05, 0.50 and 0.95 mass recovery for Dirac input.

Tracer	T5 (hours)	T50 (hours)	T95 (hours)
HTO	4.19	19.0	254.7
Uranine	4.42	12.24	117.3
Na-22	7.10	34.15	475.19
Br-82	5.17	18.24	240.4
Ca-47	12.95	43.69	102.1
Sr-85	9.65	56.79	1143.5
Ba-131	24.70	193.7	3363.3
Ba-133	24.70	193.6	3353.6
Rb-86	95.42	783.7	2587.2
Cs-134	604.3	4028.9	11,589.9

The mass recovery, F, for each tracer is given in Table 2-5. The mass recovery is the fraction of the mass injected as a Dirac pulse recovered at the termination time specified by SKB. Figures 2-5 and 2-6 show the cumulative mass recovery as a function of time. Cumulative mass recovery is shown for only five tracers in each figure to keep the figures readable. Figures 2-7 and 2-8 show the normalized mass flow, $(M_i/M_{inj})/\Delta t$, as a function of time. Results for the same five tracers as shown in Figures 2-5 and 2-6 are shown in Figures 2-7 and 2-8 respectively. Note that in Figures 2-5 through 2-8, results are only shown up to the termination times specified by SKB.

Table 2-5 Predicted mass recovery at termination time for Dirac injection pulse.

Tracer	$T_{termination}$ (hours)	Mass Recovery (F)
HTO	641	0.980
Uranine	886	0.994
Na-22	3078	0.995
Br-82	234	0.949
Ca-47	458	1.00
Sr-85	3078	0.982
Ba-131	1130	0.833
Ba-133	3078	0.944
Rb-86	1322	0.728
Cs-134	3078	0.380

3 Summary

Blind predictions of the results of the STT-2 tracer tests are produced by using the flow and transport parameters estimated on the STT-1 data set. The velocity along the transport pathway and the dilution factor as estimated on the STT-1 data are decreased by a factor of two to account for the lower pumping rate in the STT-2 tracer test. Tracers not estimated in STT-1 (Br-82, Ba-131 and Cs-134) are assigned transport parameters for the STT-2 prediction based on the similarity of these tracers with other tracers estimated on the STT-1 data set. Predictions of the STT-2 transport results are made using both the measured injection concentrations and a Dirac pulse injection.

Results show that the time to recover 0.05, 0.50 and 0.95 of the injected mass varies over two orders of magnitude. The non-reactive and marginally reactive tracers (HTO, uranine, Br-82 and Na-22) have the shortest recovery times and the most reactive tracer, Cs-134, has the longest mass recovery times. These results are valid for both the measured injection concentrations as well as the Dirac pulse input models.

Use of the observed injection concentrations versus the Dirac input does create differences in the times to recover 0.05, 0.50 and 0.95 of the injected mass. These differences are most consistent for the non-reactive and weakly sorbing tracers. The Dirac input always produces shorter times for each mass recovery metric. These differences are greatest at early times (times to 0.05 mass recovery) due to the instantaneous nature of the Dirac input and the more drawn out injection of the observed data. At later times (times to 0.50 and 0.95 mass recovery), the differences between the measured input and the Dirac pulse are less significant. This is especially true for the more reactive tracers.

The mass recovery, F, at the termination times specified by SKB varies from 1.00 to 0.33 for the observed injection histories and from 1.00 to 0.38 for the Dirac input. Assuming these termination times are based on the length of the actual STT-2 tracer test, these mass recoveries should be representative of the amount of mass recovered for each tracer. Differences in mass recovery between the measured injection histories and the Dirac pulse injections are negligible for all tracers except Cs-134.

It is noted that the exact same capacities and mass transfer rate distributions used in STT-1 are also used in the STT-2 predictions. It may be possible to calculate more accurate predictions of the STT-2 results by scaling the β_{tot} and μ parameters to account for the decreased velocity along the flowpath. Previous work with the multirate model has shown that slower flow rates may decrease the estimated value of μ and increase the estimated value of β_{tot}. These results are due to slower mass-transfer rates and greater immobile zone capacity being sampled in the relatively longer test interval. The actual approach used to accurately scale the values of β_{tot} and μ to those representative of the time scales of the slower/longer tracer test are still under investigation

4 References

McKenna, S.A., (in review), Solute Transport Modeling of the Äspö STT-1 Tracer Tests with Multiple rates of Mass-Transfer, Äspö Task Force deliverable, 19 pp.

Winberg, A., P. Andersson, J. Hermanson and J. Byegard, (in press) Updated Structural Model of the TRUE-1 Block and Detailed Description of Feature A, Technical Memorandum, Final Draft, December, 23rd, 1998, 27 pp.

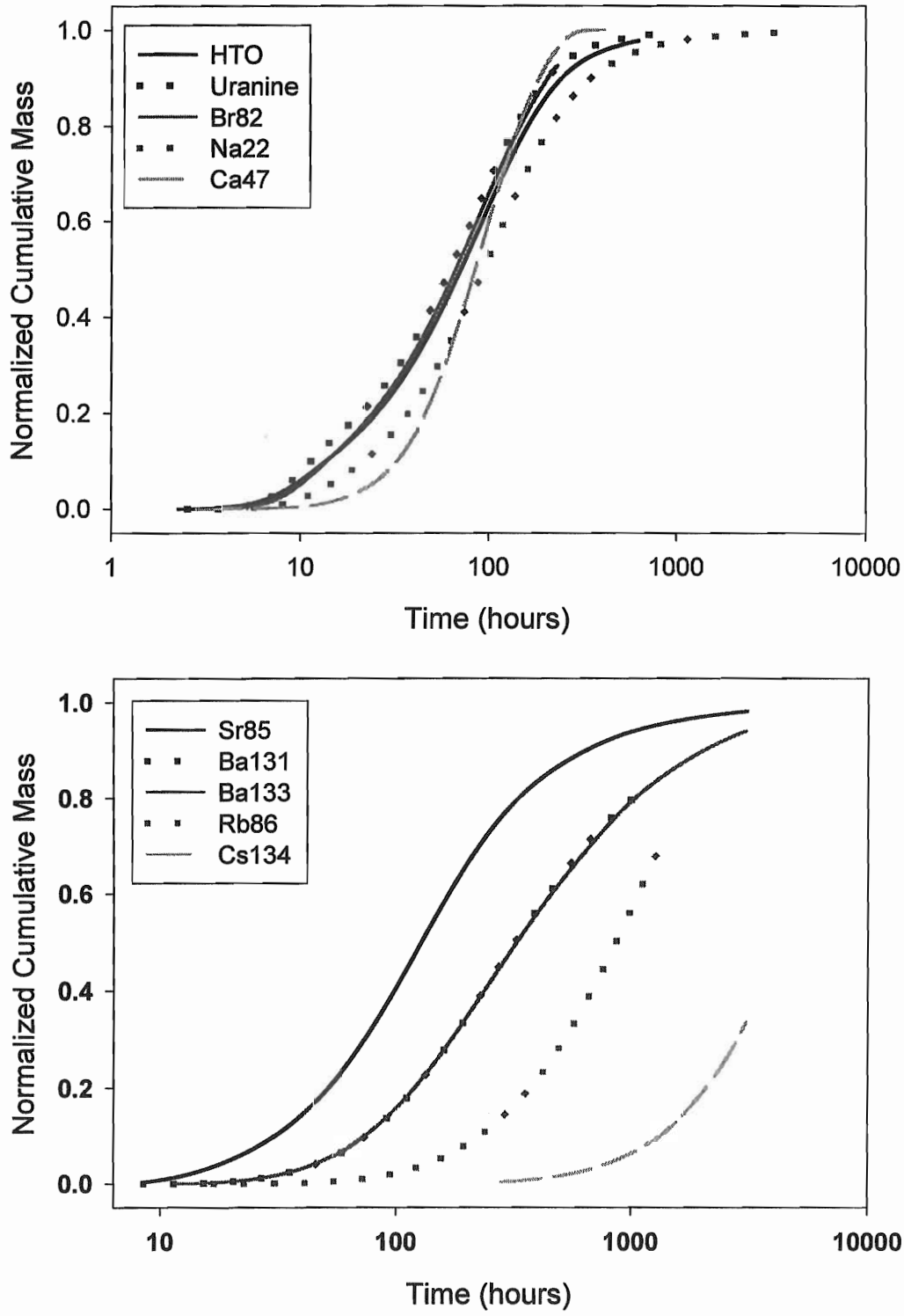

Figure 1. Cumulative mass recovery predictions for the STT-2 tracer tests using observed injection histories.

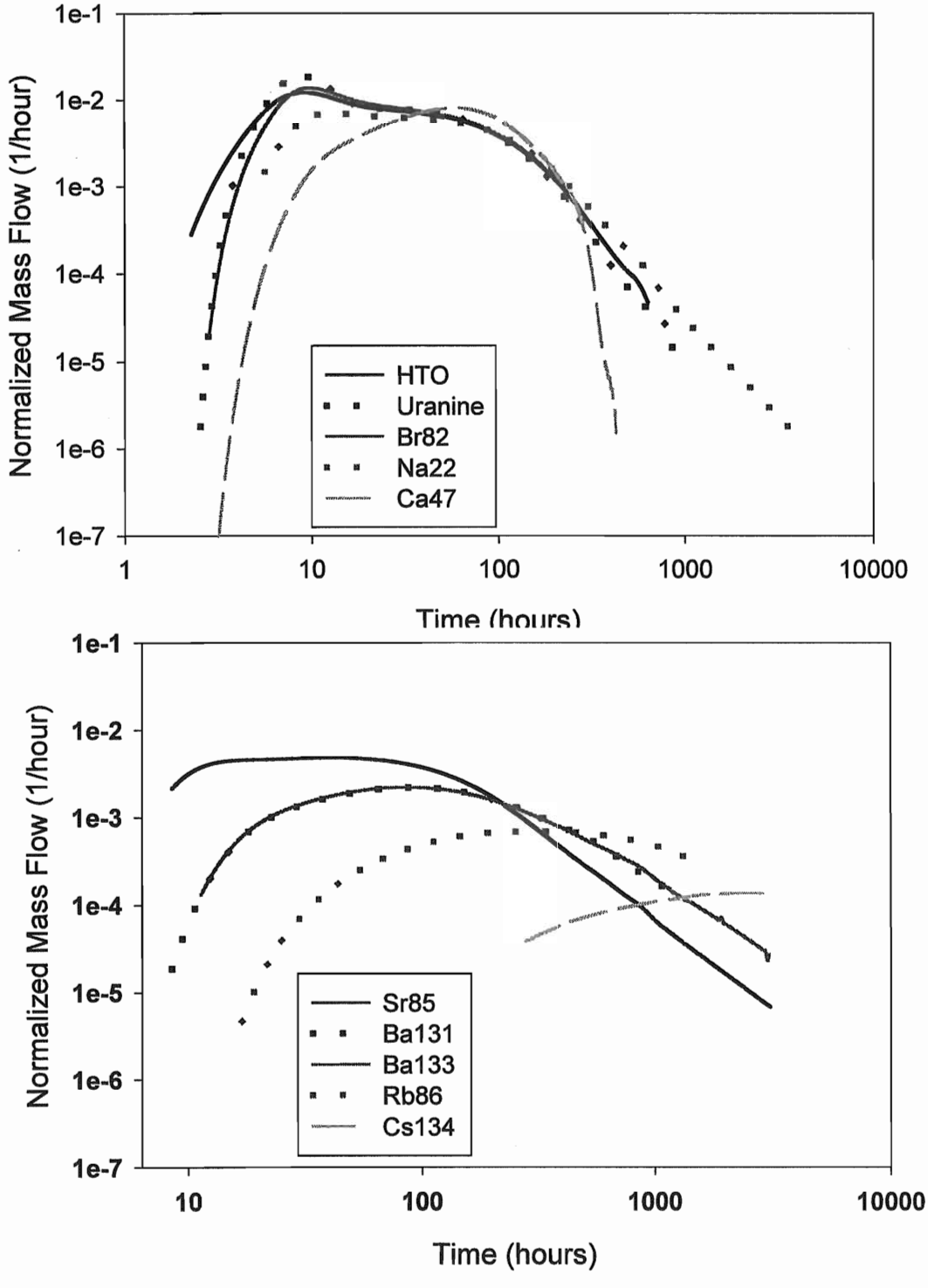

Figure 2. Mass flow rate predictions for the STT-2 tracer tests using observed injection histories.

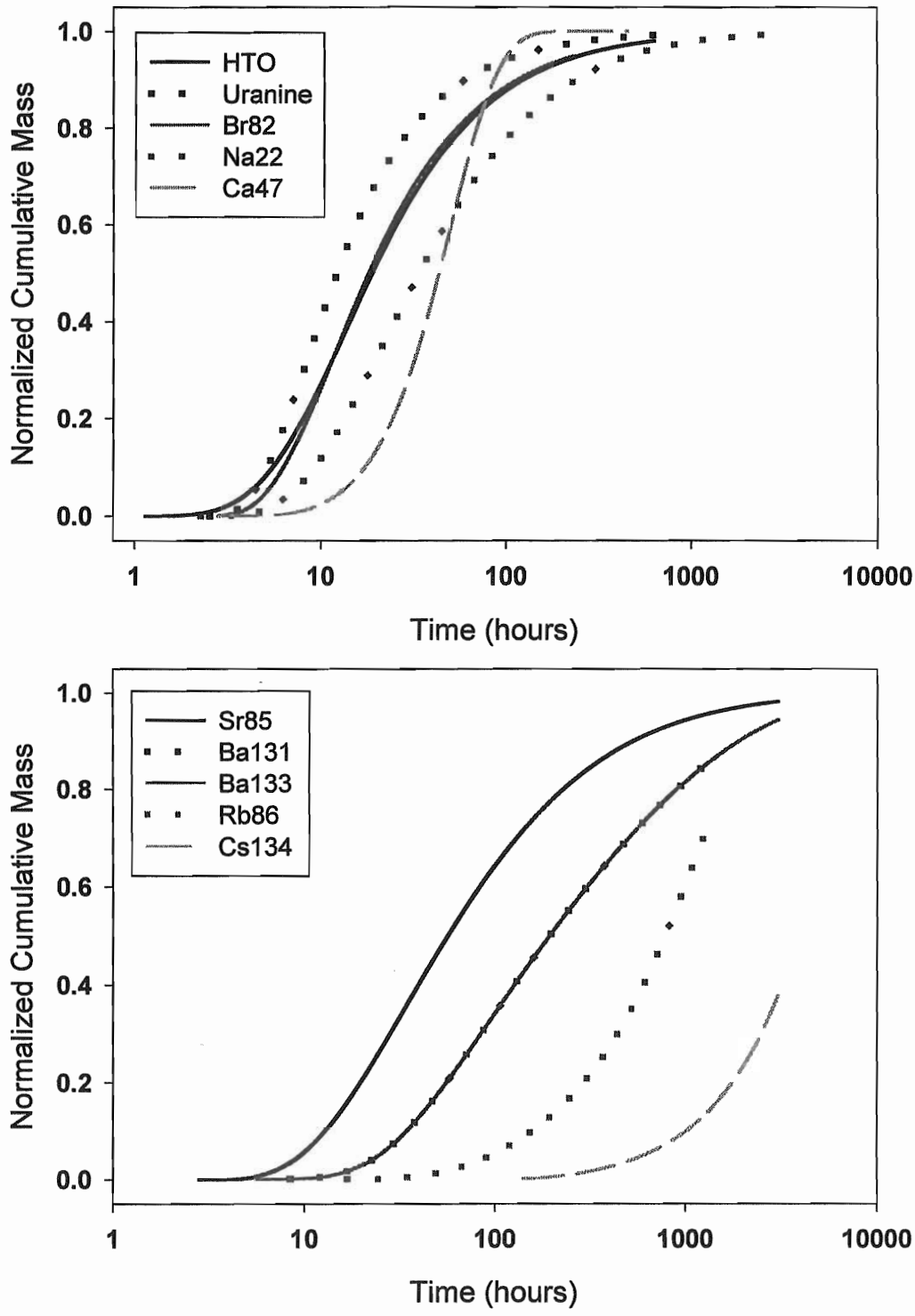

Figure 3. Cumulative mass recovery predictions for the STT-2 tracer tests using a Dirac pulse injection.

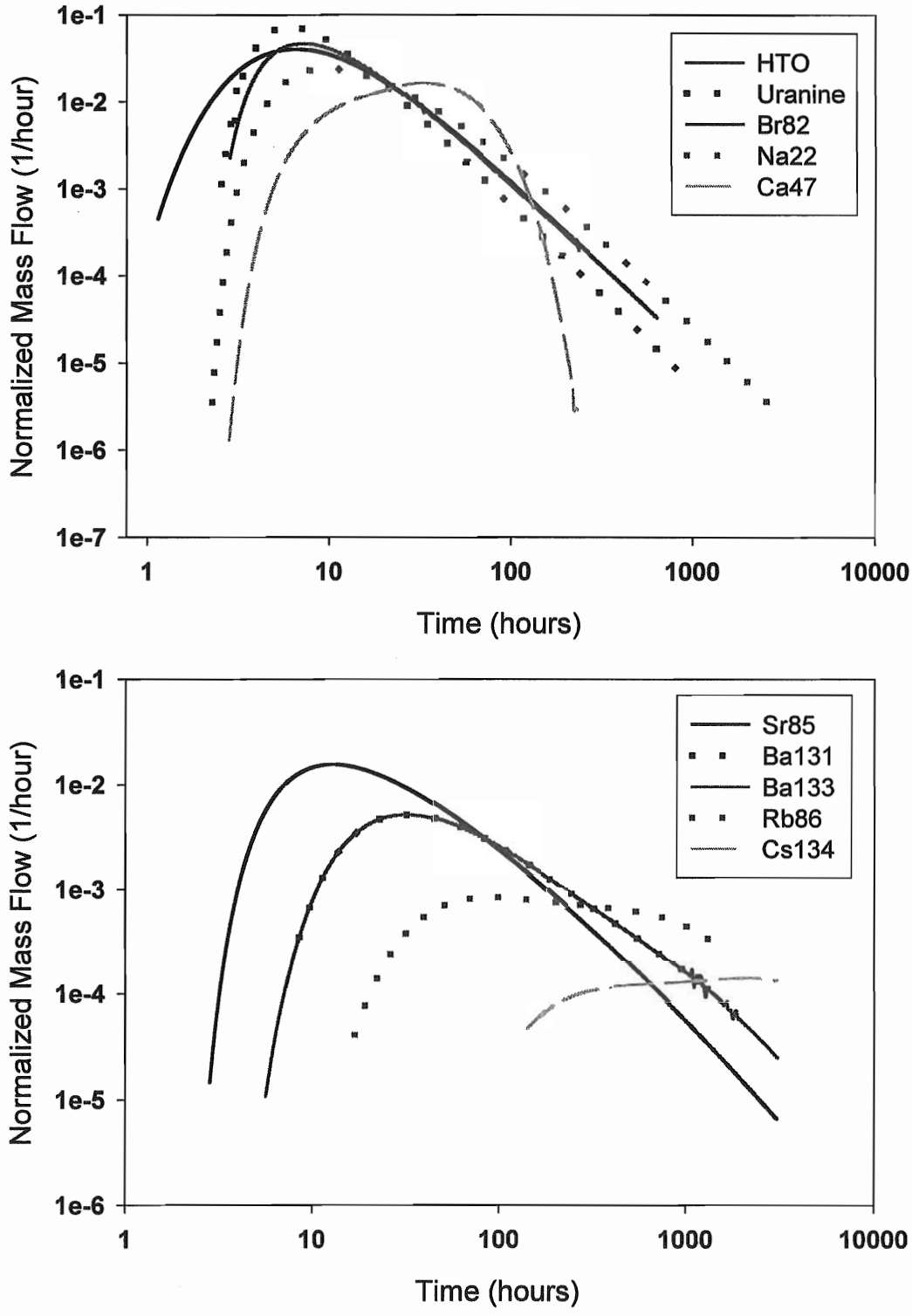

Figure 4. Mass flow rate predictions for the STT-2 tracer tests using a Dirac pulse injection.

Blind-predictions for the Task 4F (STT2) tracer migration experiment at the Äspö TRUE-1 site

A. Jacob and W. Heer (NAGRA/PSI)

Blind-predictions for the Task 4F (STT2) tracer migration experiment at the Äspö TRUE-1 site

Andreas Jakob, Walter Heer
Paul Scherrer Institute PSI, Switzerland
April 1999

Table of contents

1. Introduction

The primary purpose of the TRUE project is to exchange information in order to develop an increased understanding of radionuclide migration and retention in fractured crystalline rock, and to increase the confidence in the models for flow and transport used for an adequate description of the experimental data. The Äspö Task Force was initiated in 1992 by the Swedish Nuclear Fuel and Waste Management Company (SKB) to serve as a forum for organisations from different countries to interact in the area of modelling of groundwater flow and solute transport.

In 1997 the PSI-modelling team joined the Äspö Task Force to participate in the international modelling effort of the Task 4E comprehensive tracer transport experiments. Our objectives are:

- To apply our simple model, which was successfully applied to the modelling of the Grimsel migration experiments, to other types of crystalline rock with different transport properties.
- To explore how information obtained from structural geological investigations can be considered in our model.
- To examine whether values for the transport parameters obtained in small-scale laboratory measurements can be used for modelling field tracer tests. If so, how are they best scaled up?
- To obtain information regarding the advantages and disadvantages of competing models, especially those models including more sophisticated descriptions of the hydrology than ours.
- Finally, to test and further develop our model for groundwater flow and nuclide transport.

This report briefly summarises the modelling approach used by PSI to predict the breakthrough curves of various radioactive tracers, corresponding to the STT2 tracer test of Task 4F of the TRUE-1 program.

During the last two years, blind-predictions of the STT1 and STT1b tracer test were made. Further details concerning modelling flow and transport are outlined in [1] and [2] and values for the nuclide-dependent transport parameters applied for the blind-predictions for these tracer tests are also specified therein. A comprehensive modelling report is in preparation.
After the release of the measurement data, these blind-predictions were complemented by subsequent analysis and inverse modelling of the breakthrough curves. This was done to improve our understanding of the major geometrical aspects of the flow domain, of the transport mechanisms and led to a refinement of the model.
With the updated model, together with best-fit values for the transport parameters from inverse modelling of the STT1 tracer tests, blind-predictions for the STT2 migration experiments have been performed.

2. Procedure for the blind-predictions of the STT2 tracer test

2.1. Our model

For the sake of completeness a brief overview about our modelling methodology for the STT2 tracer tests is presented. Further details can be found in [1] and [2].
Due to the special experimental conditions at the TRUE-1 site at Äspö (an extreme narrow and fast flow field) our model is strongly based on the one applied to successfully model the Grimsel migration experiments.

For the blind-predictions of the STT2 tracer test the hydrological part of the model is based on a 2D-streamline/streamtube formalism with underlying homogeneous and isotropic transmissivity field. In addition, an averaged and uniform natural background flow field is taken into account.

Geometry of flow paths: From modelling of the trailing edge of the breakthrough curve of the conservative tracer uranine-PDT3 [1] we obtained strong evidence for matrix diffusion having a strong influence on tracer breakthrough. This was in strong contradiction to the small values for the diffusion accessible porosity (roughly 0.1%) as pointed out in [3]. The suspicion that, as observed in Grimsel, the existence of fault gouge could cause such large effects from matrix diffusion, was confirmed by observations by Mazurek et al. [4] on bore cores taken from a fracture system close to Feature A. Consequently our concept for the blind-predictions for the STT1 experiment was based on one single fracture family, on the presence of a fault gouge zone, characterised by a relative large porosity, and the structures on the cm-scale described by these authors. A detailed lithological interpretation of borehole intersections of Feature A and further details concerning the existence of fault gouge can also be found in [5]. However, in the subsequent analysis of the STT1 tracer tests we were obliged to refine the geometry of the transport model by including a second independent flow path family but bounded now, nor by a zone of fault gouge, but by a less porous cataclasite as indicated in Figure 1. Only by using the refined geometry for the transport part it was possible to reproduce the observed early tracer breakthrough of the sorbing tracers of the STT1 tracer test [2].

Tracer transport is performed in the frame of a dual porosity medium approach with averaged and constant transport parameters. Matrix diffusion occurs in the model into a limited porous zone adjacent to the fracture and sorption processes are described by linear isotherms.

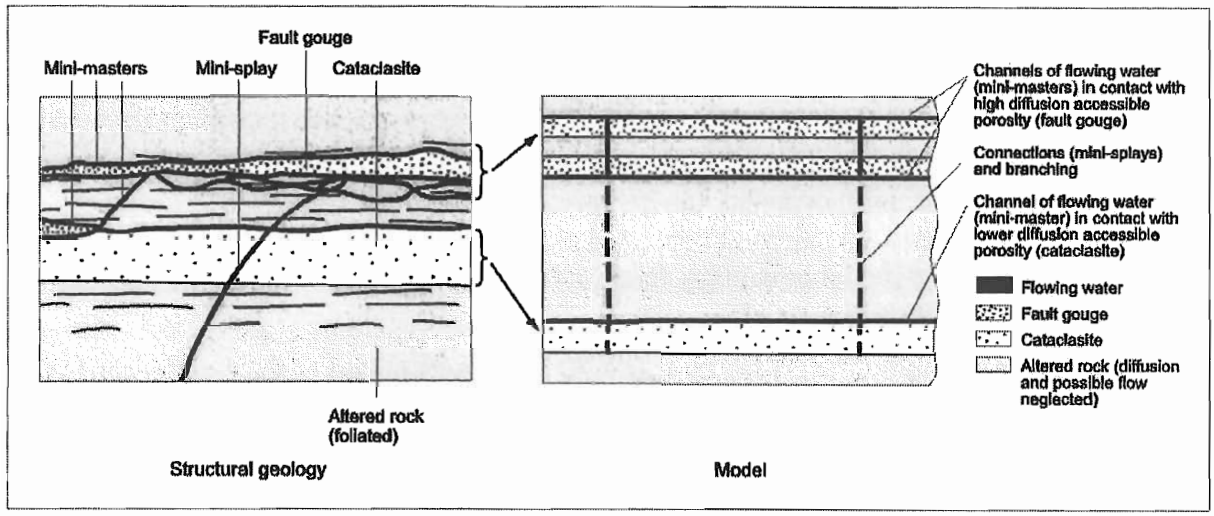

Figure 1: Sketch of the refined geometry for flow and transport after the analysis of the STT1 tracer breakthrough curves. The sketch on the left illustrates some important aspects of the fracture as they were identified in structural geological investigations [4]. The figure on the right shows the transformations into a relatively simple geometry which was the basis for the subsequent blind-predictions of the STT2 tracer test. The blind-predictions were performed in the frame of the dual porosity medium approach.

3. Blind-predictions for the STT2 tracer test

3.1. The flow field and its parameter values

To guarantee full tracer recovery a rigid flow field was installed with an essentially passive injection and strong pumping at the extraction borehole. From the decaying part of the injection distribution for the uranine test of the STT2 experiment, a constant flow rate of 0.456 ml/min was determined. Correcting for the sampling flow rate of $4.33 \cdot 10^{-2}$ ml/min (2.6 ml/hour) and adjusting by a correction factor ($f = 1.31$) which accounts for the mass balance of the STT1 tracer test, a final value for the injection flow rate of Q_i = 0.541 ml/min was obtained and used for all ten tracers in STT2. A fixed pumping rate Q_w of about 200 ml/min was installed as the downstream boundary; hence, the ratio Q_w / Q_i = 370 generated a practically monopole-like flow field.
Due to these conditions the flow domain remains very restricted for all tracers. The flow field was discretised using a 2D-streamtube formalism. In addition, the natural background flow was treated as being uniform and time-independent. Its strength and direction were determined from the head distribution in Feature A measured on December 15th 1998 and using kriging.

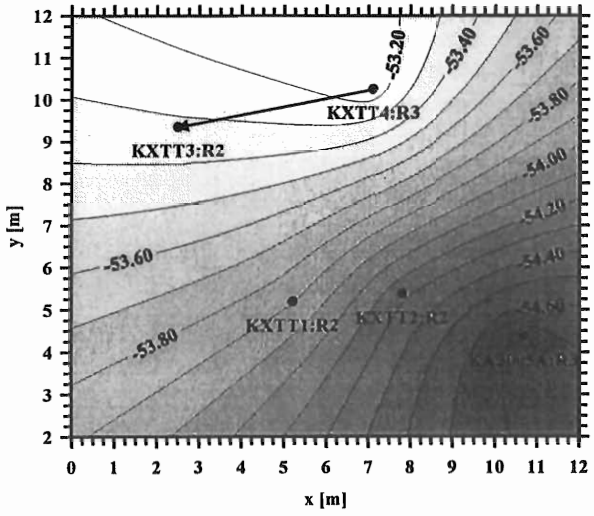

Figure 2: Hydraulic head distribution in the domain of interest of Feature A on December 15th 1998. The head isolines [m] are drawn using kriging. The STT2 tracer test is performed between the two boreholes KXTT4:R3 (injection) and KXTT3:R2 (pumping) as indicated in the figure.

For the head gradient $\left|\vec{\nabla}\Phi\right|$ we determined a value of about $3.85 \cdot 10^{-2}$ m/m and using a value for the fracture conductivity of $K_{fr} = 7.1 \cdot 10^{-4}$ m/s [6] we obtain for the strength of the mean natural background flow field $|v_0| = 2.7 \cdot 10^{-5}$ m/s. Concerning its direction an angle of -71° with respect to the line connecting the injection and extraction borehole was estimated. In figures 3 and 4 the flow field used for the subsequent tracer transport modelling is plotted.

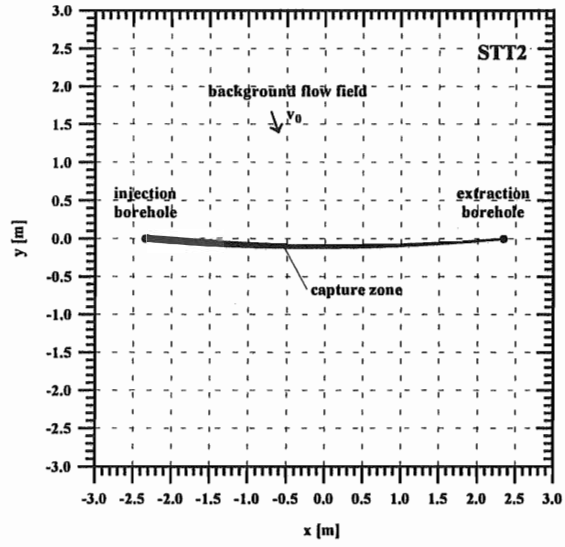

Figure 3: Flow domain for the STT2 tracer tests. The injection borehole is KXTT4:R3, the extraction borehole is KXTT3:R2. Ten streamlines of the capture zone [1] are shown along which all fluid flow and transport calculations were performed. Due to a weak background flow-field the water flow in the capture zone is slightly weakened.

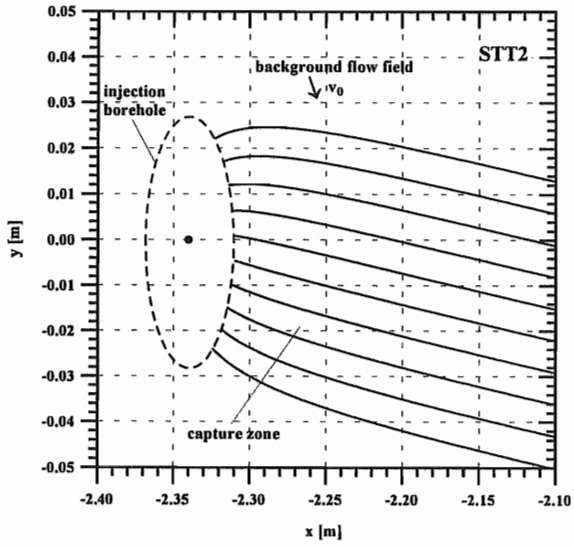

Figure 4: Magnification of a part of the flow domain from Figure 3 close to the injection borehole. Again ten streamlines are shown which start at the borehole/rock interface. Due to the strong pumping at the downstream boundary and passive injection, the capture zone is very narrow and has a width of only a few centimetres. (Note the different scales in both directions.)

[1] Regions of interflow between a recharge and a pumping well within a flow domain are denoted as the capture zone.

3.2. Final values of the transport parameters used for the blind-predictions

The model parameters derived from inverse modelling of the STT1 tracer tests and applied without further changes are:

$L = 4.61$ m	Mean travel distance between the boreholes
$B \cdot \varepsilon_f = 0.55 \cdot 10^{-3}$ m	Total flow width of all the channels (B = aquifer thickness, ε_f = flow porosity),
$v_f = 1.36 \cdot 10^{4}$ m/y	Mean water velocity
$a_L = 0.11$ m	Longitudinal dispersion length ($Pe = 42.4$),
$1/b = 2.19 \cdot 10^{4}$ m^{-1}	Specific interface area.
$\varepsilon_p^{(1)} = 0.17$	Porosity of the fault gouge,
$\varepsilon_p^{(2)} = 0.027$	Porosity of the cataclasite,
$\varepsilon_f^{(1)} / \varepsilon_f = 0.75$	Relative flow porosity of the first fracture family (bounded by a zone of fault gouge),
$\varepsilon_f^{(2)} / \varepsilon_f = 0.25$	Relative flow porosity of the second fracture family, (bounded by a zone of cataclasite)
$\Delta x = 5 \cdot 10^{-3}$ m	Thickness of the fault gouge and of the cataclasite,

Tracer	Fault gouge and cataclasite		Fracture surface
	D_p [m^2/s]	K_d [m^3/kg]	K_a [m]
Uranine	$4.45 \cdot 10^{-11}$	---	---
HTO	$7.32 \cdot 10^{-11}$	---	---
^{82}Br [2]	$12.9 \cdot 10^{-11}$	---	---
^{22}Na	$7.39 \cdot 10^{-11}$	$3.15 \cdot 10^{-5}$	$7.0 \cdot 10^{-6}$
^{85}Sr	$11.2 \cdot 10^{-11}$	$4.46 \cdot 10^{-5}$	$2.5 \cdot 10^{-5}$
^{47}Ca	$5.85 \cdot 10^{-11}$	$1.04 \cdot 10^{-4}$	$1.0 \cdot 10^{-5}$
^{131}Ba	$4.61 \cdot 10^{-11}$	$1.10 \cdot 10^{-3}$	---
^{133}Ba	$4.61 \cdot 10^{-11}$	$1.10 \cdot 10^{-3}$	---
^{86}Rb	$11.3 \cdot 10^{-11}$	$1.31 \cdot 10^{-3}$	$6.9 \cdot 10^{-5}$
^{134}Cs [3]	$5.60 \cdot 10^{-11}$	$2.52 \cdot 10^{-2}$	$2.0 \cdot 10^{-4}$

Table 1: Values for the tracer dependent transport parameters.

[2] For further information: see appendix.

[3] Assuming half of the injected Cs mass get lost.

3.3. Predictions for the recovery of all ten tracers

In the following table we have compiled the tracer recovery times t_5, t_{50}, t_{95} and $t_{99.9}$ for all ten tracers. The tracer recovery time t_i is defined as the actual time needed to recover i = 5, 50, 95 or 99.9 % of the total injected and decay-corrected activity or mass.

Tracer	t_5 [hour]	t_{50} [hour]	t_{95} [hour]	$t_{99.9}$ [hour]
Uranine	6.7	78	320	812
HTO	7.1	80	280	596
^{82}Br	8.2	81	227	512
^{22}Na	10	98	364	824
^{85}Sr	15	117	378	939
^{47}Ca	13	115	545	2190
^{131}Ba	47	378	3670	24600
^{133}Ba	46	387	3680	25400
^{86}Rb	94	719	3370	16200
^{134}Cs [4]	1150	[5]	---	---

Table 2: Calculated tracer recovery times **for the measured tracer injection distribution.**

Tracer	t_5 [hour]	t_{50} [hour]	t_{95} [hour]	$t_{99.9}$ [hour]
Uranine	2.8	15	197	500
HTO	3.0	23	165	372
^{82}Br	3.2	33	138	275
^{22}Na	4.2	34	252	652
^{85}Sr	6.2	54	252	633
^{47}Ca	5.4	48	484	1940
^{131}Ba	18	245	3540	21800
^{133}Ba	18	245	3540	21800
^{86}Rb	50	635	3280	14400
^{134}Cs [4]	740	[6]	---	---

Table 3: Calculated tracer recovery times **for Dirac delta-input.**

[4] Assuming half of the injected Cs mass is sorbed irreversibly in the fracture system and/or in the equipment.

[5] $t_{49\%}$ = 114000 h (13.0 years)

[6] $t_{49\%}$ = 113000 h (12.9 years)

		Calculated tracer recovery [-]	
Tracer	t_{end} [hour]	**Exp. Injection**	**Delta injection**
Uranine	886	1.000	1.000
HTO	641	1.000	1.000
^{82}Br	234	0.957	0.996
^{22}Na	3078	1.000	1.000
^{85}Sr	3078	1.000	1.000
^{47}Ca	458	0.924	0.944
^{131}Ba	1130	0.754	0.771
^{133}Ba	3078	0.930	0.935
^{86}Rb	1322	0.710	0.731
^{134}Cs [4]	3078	0.155	0.173

Table 4: Calculated tracer recovery $F = M_{ext}(t_{end}) / M_{inj}$. [-] at $t = t_{end}$, the time of termination of monitoring for all ten tracers and for the experimental injection distribution as well as for a Dirac delta injection.

On the following pages we have plotted our blind-predictions for the flow normalised to the total injected mass, and the tracer recovery versus time for all ten tracers for both the measured injection distribution and a Dirac delta pulse-input. In order to determine absolute values for the STT2 tracer flow we also present the calculated values for the total injected tracer masses m_{tot}. From the injection flow rate Q_i specified in sub-section 3.1 and the time integrals of the injection distributions of all the tracers the following values for the total injected tracer masses can be deduced:

Tracer	m_{tot}	**Unit**
Uranine	26.92	mg
HTO	$8.413 \cdot 10^7$	Bq
^{82}Br	$2.952 \cdot 10^6$	Bq
^{22}Na	$8.975 \cdot 10^5$	Bq
^{85}Sr	$2.830 \cdot 10^6$	Bq
^{47}Ca	$1.815 \cdot 10^5$	Bq
^{131}Ba	$1.016 \cdot 10^6$	Bq
^{133}Ba	$1.551 \cdot 10^5$	Bq
^{86}Rb	$2.843 \cdot 10^6$	Bq
^{134}Cs	$5.669 \cdot 10^6$	Bq

Table 5: Calculated total injected tracer masses for all ten tracers of STT2.

3.4. Predictions for uranine

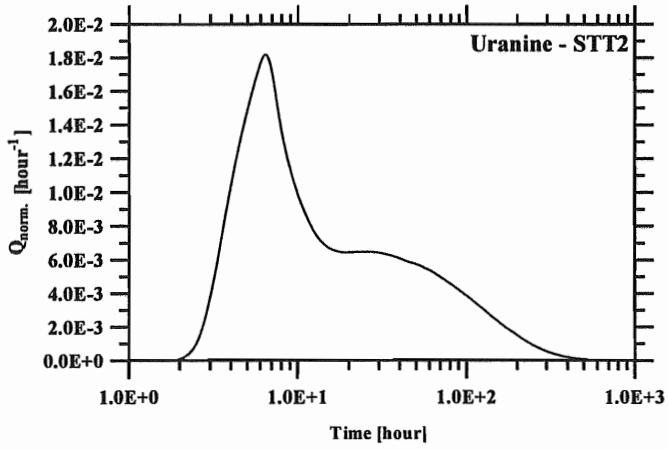

Figure 5: Flow of uranine [hour $^{-1}$] versus time [hour].

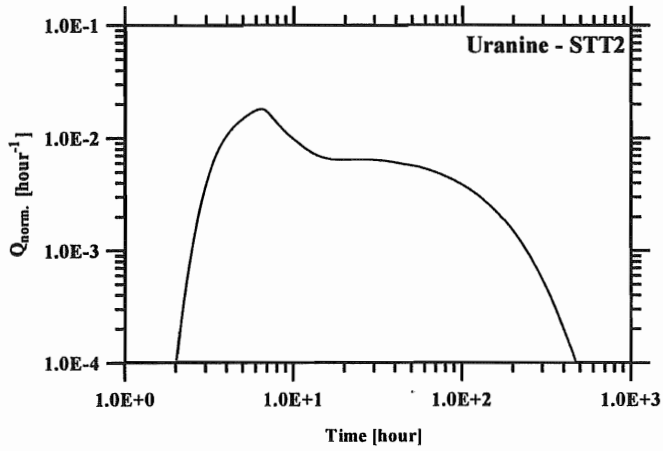

Figure 6: Flow of uranine [hour $^{-1}$] versus time [hour].

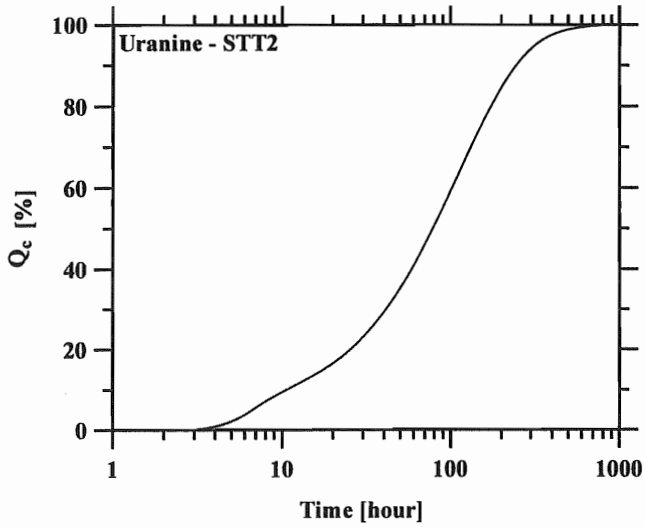

Figure 7: Tracer recovery [%] for uranine versus time.

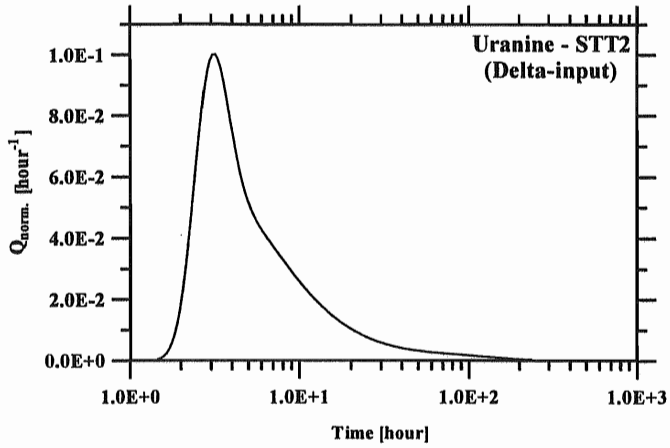

Figure 8: Flow of uranine [hour $^{-1}$] versus time [hour] for **delta-input**.

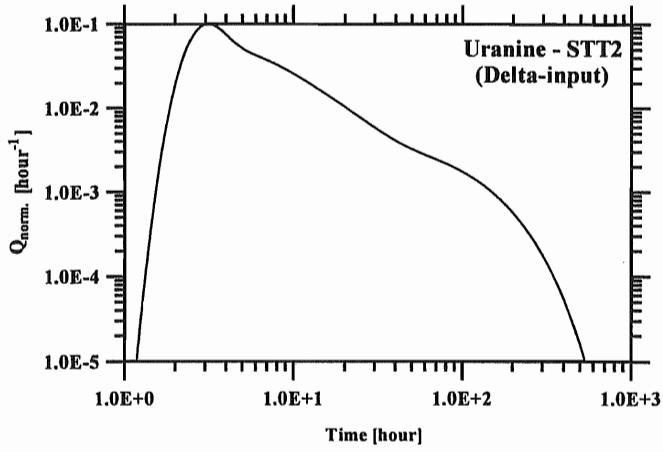

Figure 9: Flow of uranine [hour $^{-1}$] versus time [hour] for **delta-input**.

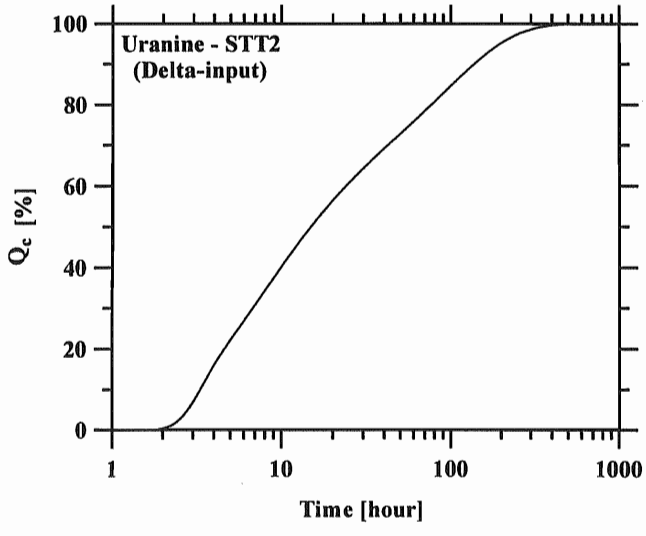

Figure 10: Tracer recovery [%] for uranine versus time for **delta-input**.

3.5. Predictions for tritium (HTO)

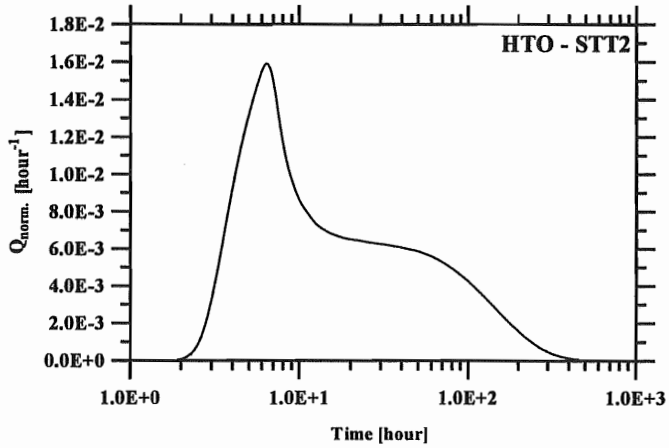

Figure 11: Flow of HTO [hour $^{-1}$] versus time [hour].

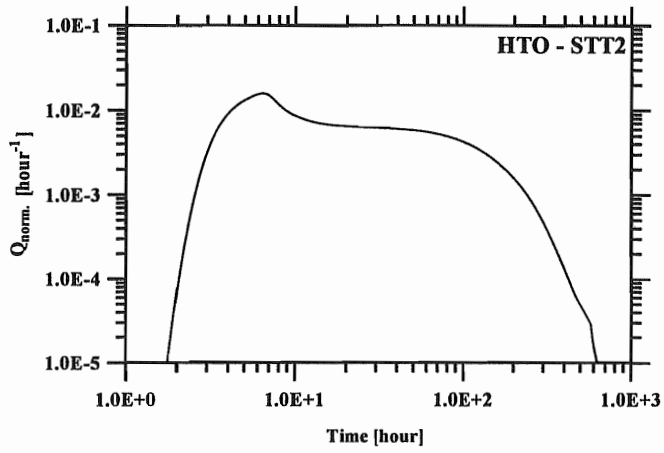

Figure 12: Flow of HTO [hour $^{-1}$] versus time [hour].

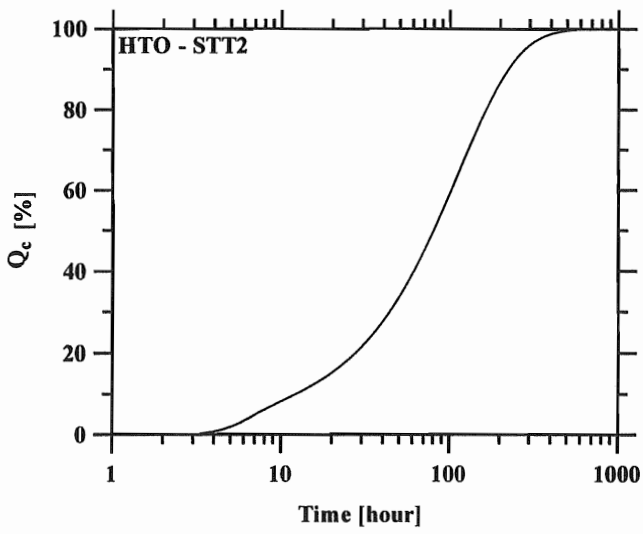

Figure 13: Tracer recovery [%] for HTO versus time.

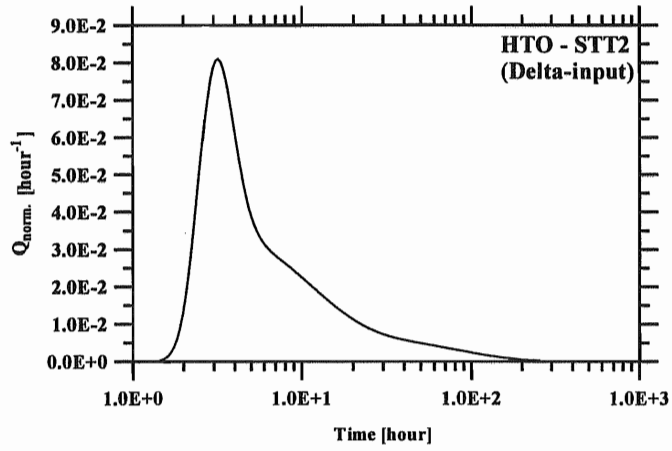

Figure 14: Flow of HTO [hour $^{-1}$] versus time [hour] for **delta-input**.

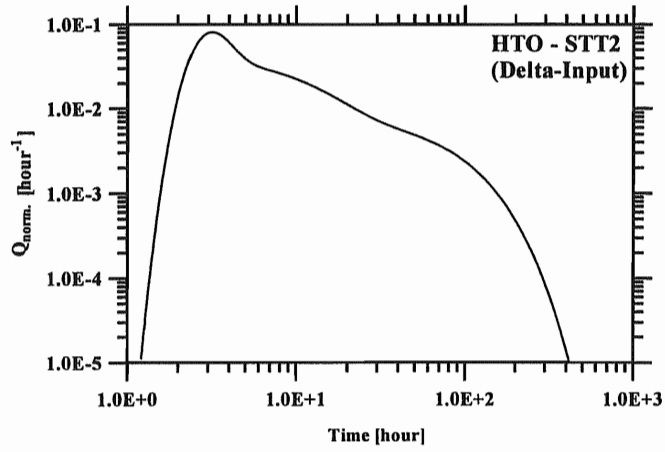

Figure 15: Flow of HTO [hour $^{-1}$] versus time [hour] for **delta-input**.

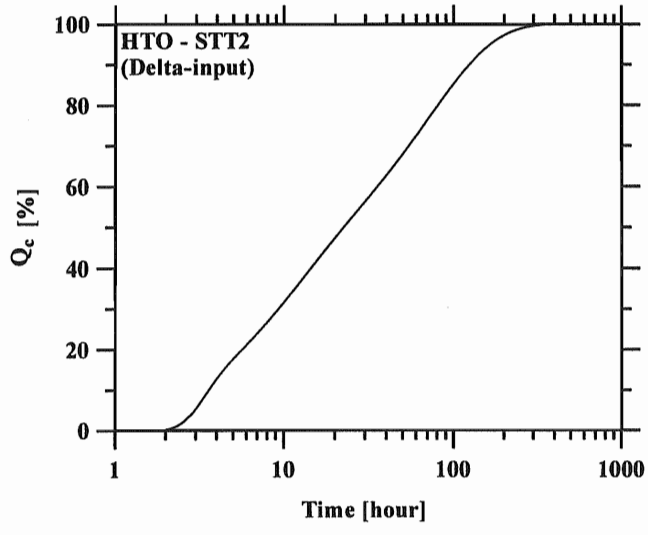

Figure 16: Tracer recovery [%] for HTO versus time for **delta-input**.

3.6. Predictions for bromine

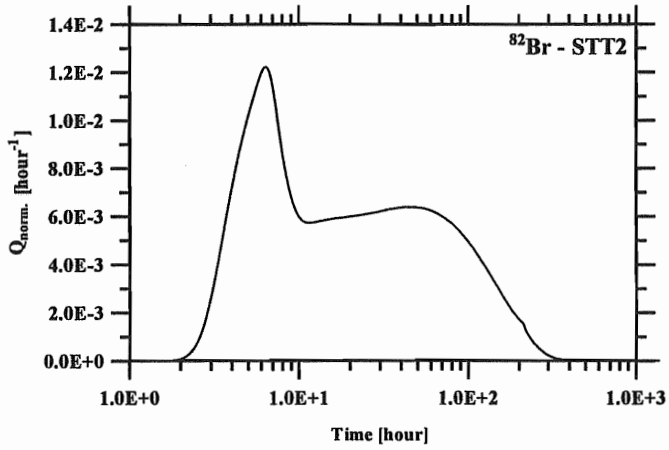

Figure 17: Flow of bromine [hour $^{-1}$] versus time [hour].

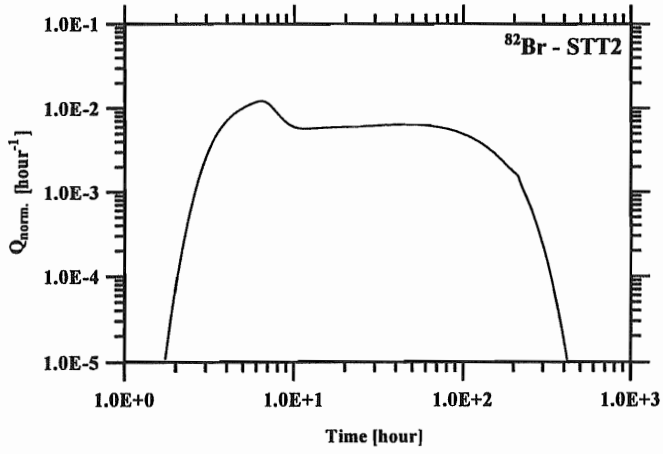

Figure 18: Flow of bromine [hour $^{-1}$] versus time [hour].

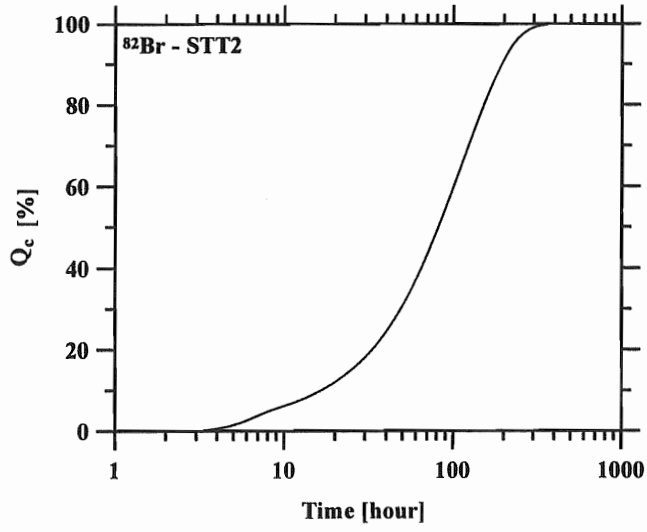

Figure 19: Tracer recovery [%] for bromine versus time.

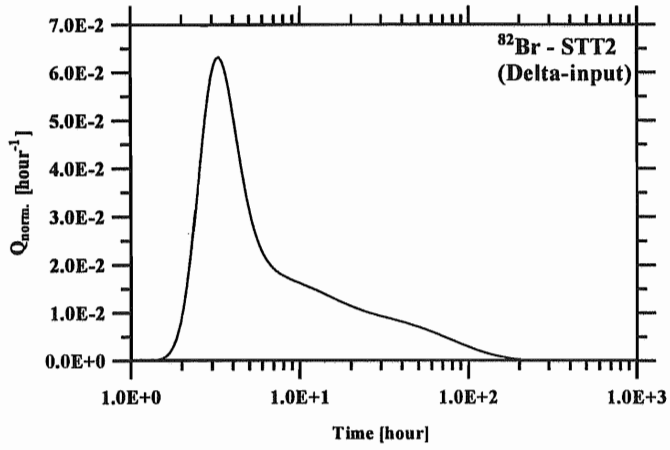

Figure 20: Flow of bromine [hour $^{-1}$] versus time [hour] for **delta-input**.

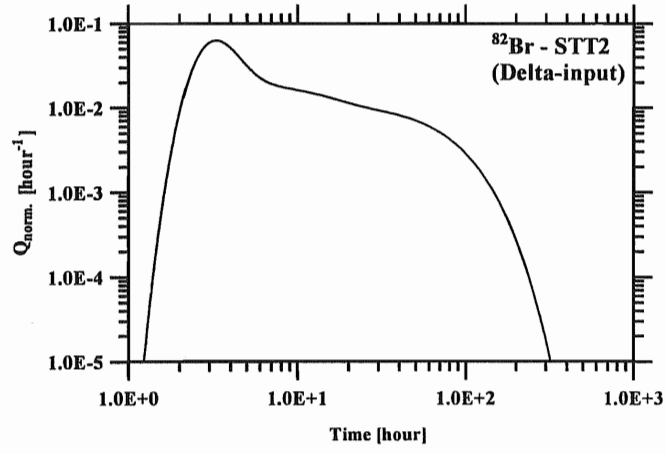

Figure 21: Flow of bromine [hour $^{-1}$] versus time [hour] for **delta-input**.

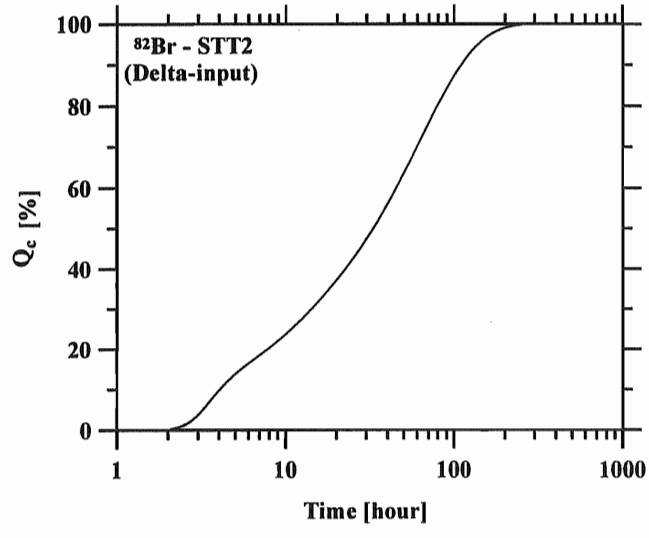

Figure 22: Tracer recovery [%] for bromine versus time for **delta-input**.

3.7. Predictions for sodium

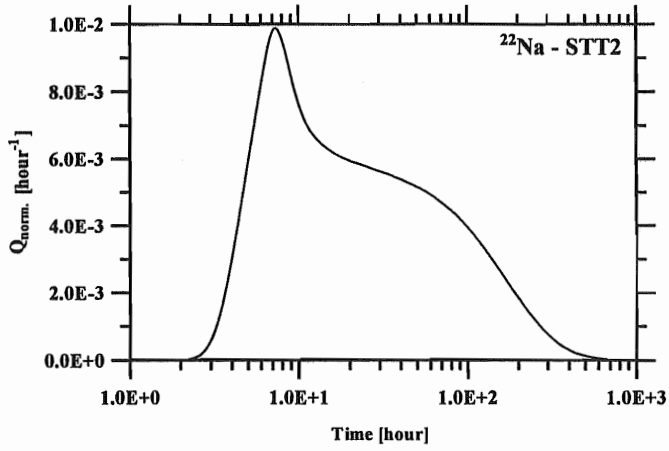

Figure 23: Flow of sodium [hour $^{-1}$] versus time [hour].

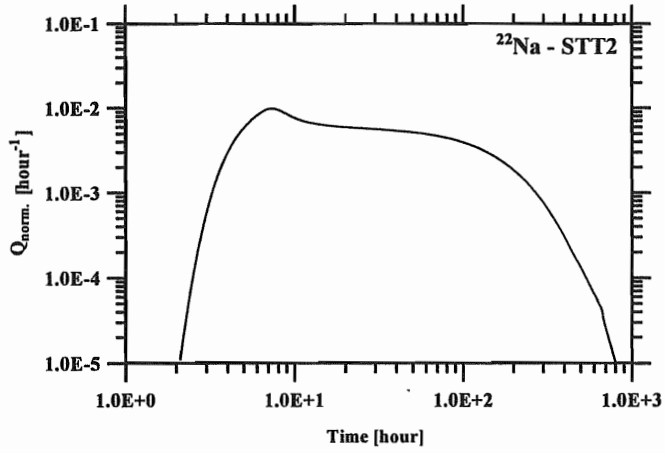

Figure 24: Flow of sodium [hour $^{-1}$] versus time [hour].

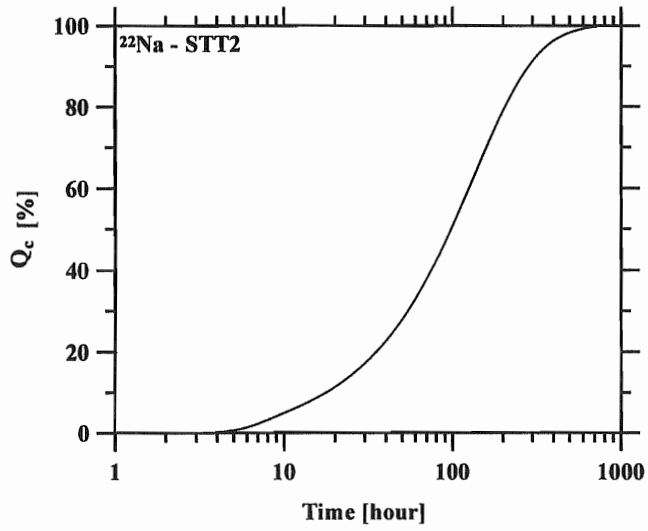

Figure 25: Tracer recovery [%] for sodium versus time.

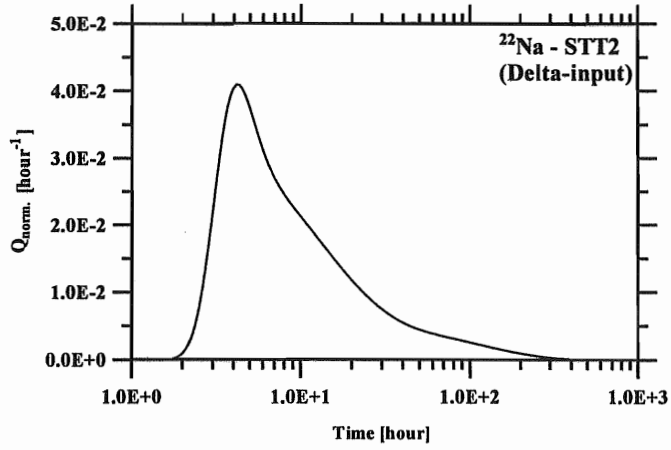

Figure 26: Flow of sodium [hour $^{-1}$] versus time [hour] for **delta-input**.

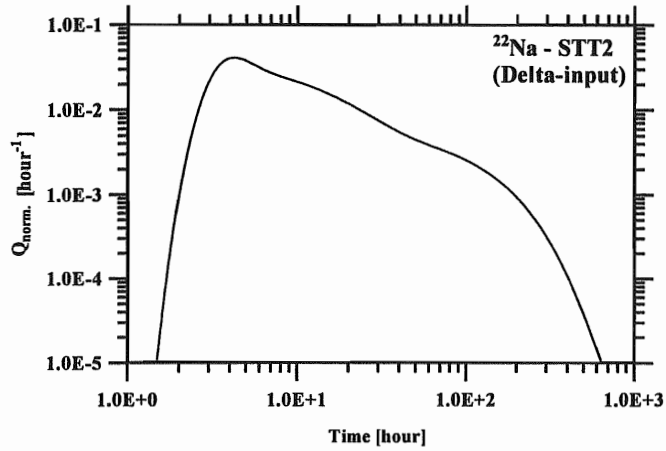

Figure 27: Flow of sodium [hour $^{-1}$] versus time [hour] for **delta-input**.

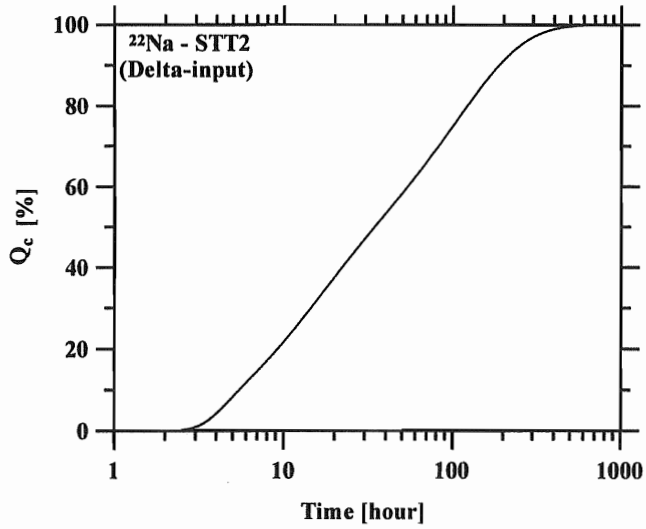

Figure 28: Tracer recovery [%] for sodium versus time for **delta-input**.

3.8. Predictions for strontium

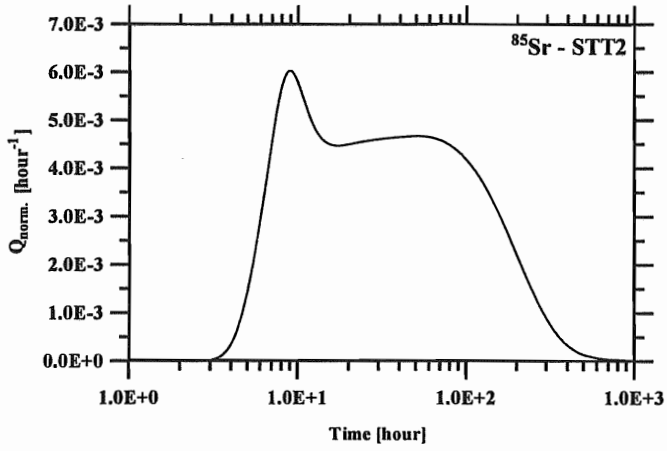

Figure 29: Flow of strontium [hour $^{-1}$] versus time [hour].

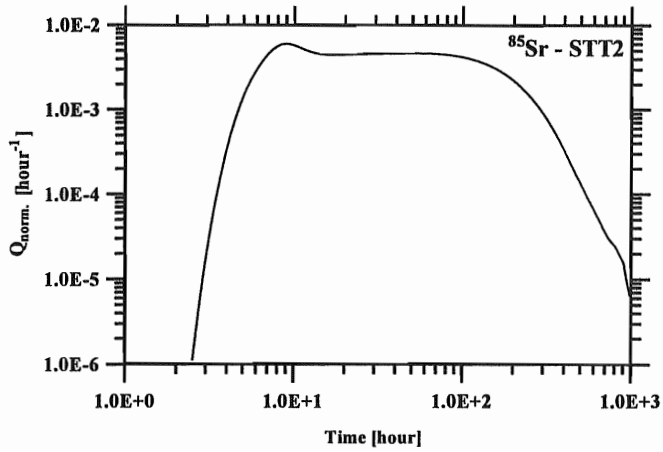

Figure 30: Flow of strontium [hour $^{-1}$] versus time [hour].

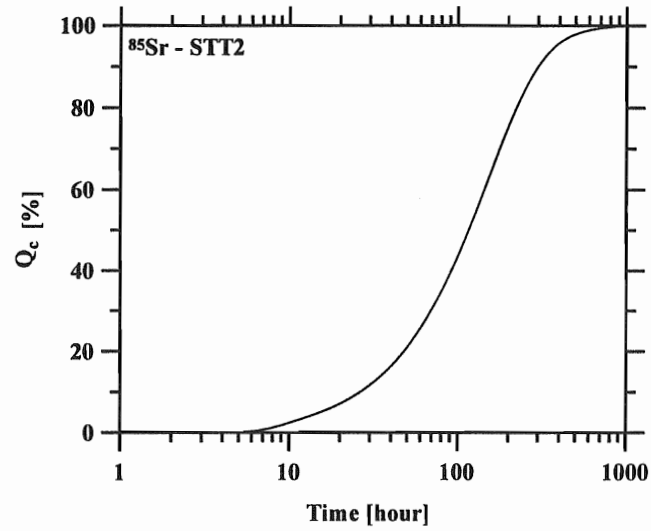

Figure 31: Tracer recovery [%] for strontium versus time.

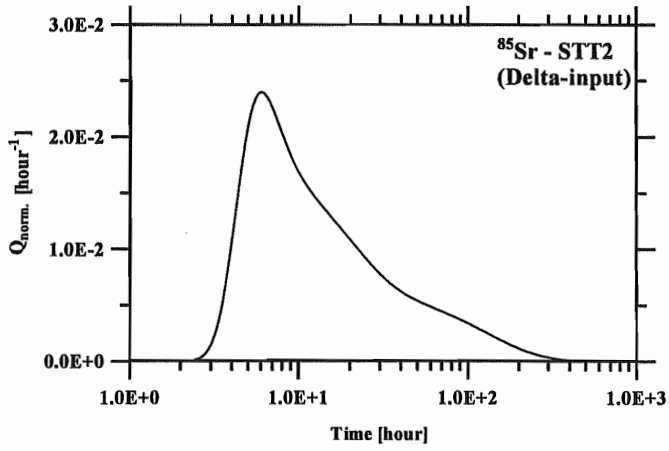

Figure 32: Flow of strontium [hour $^{-1}$] versus time [hour] for **delta-input**.

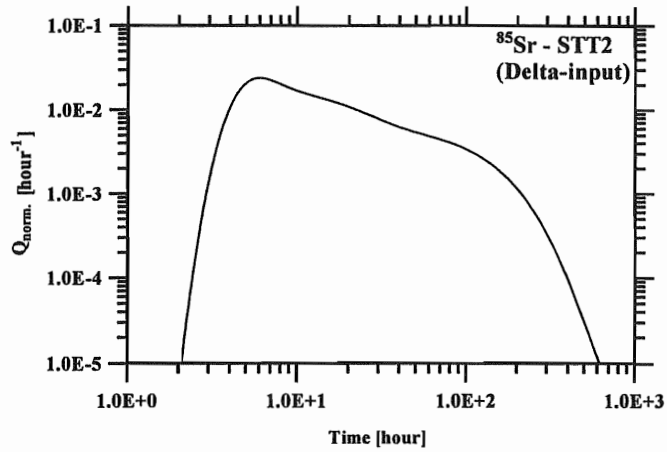

Figure 33: Flow of strontium [hour $^{-1}$] versus time [hour] for **delta-input**.

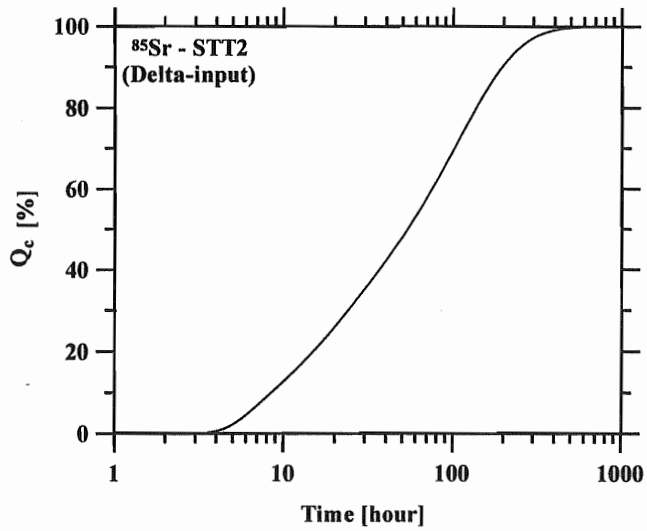

Figure 34: Tracer recovery [%] for strontium versus time for **delta-input**.

3.9. Predictions for calcium

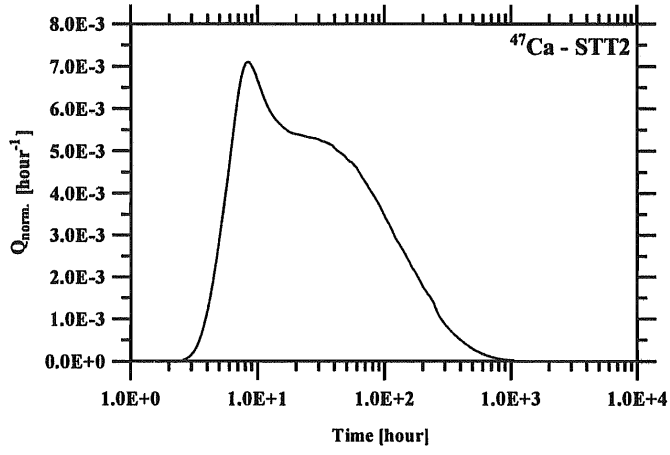

Figure 35: Flow of calcium [hour $^{-1}$] versus time [hour].

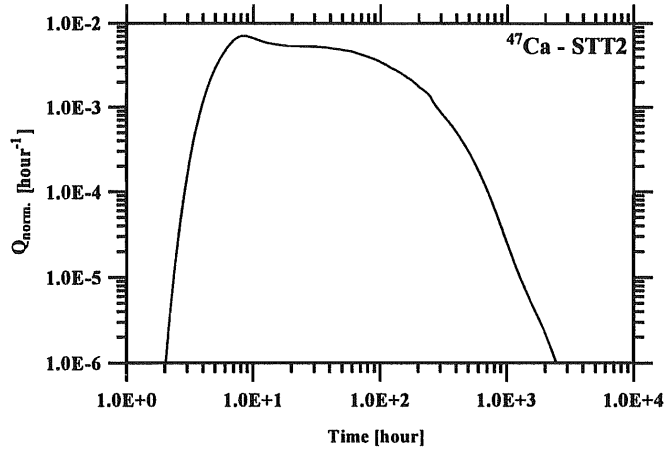

Figure 36: Flow of calcium [hour $^{-1}$] versus time [hour].

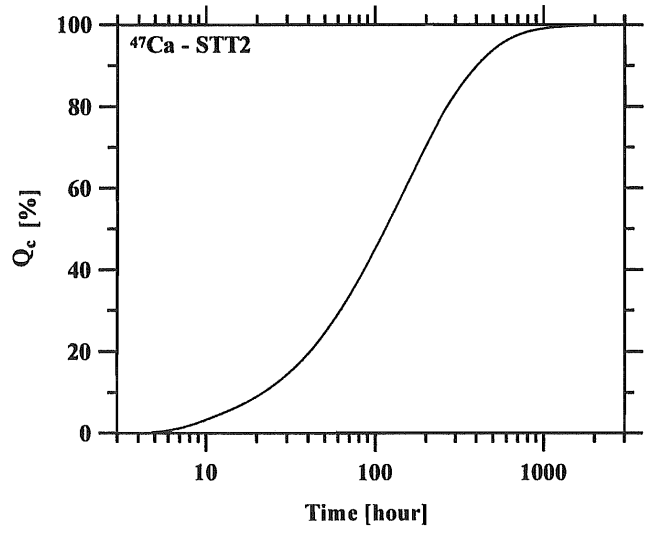

Figure 37: Tracer recovery [%] for calcium versus time.

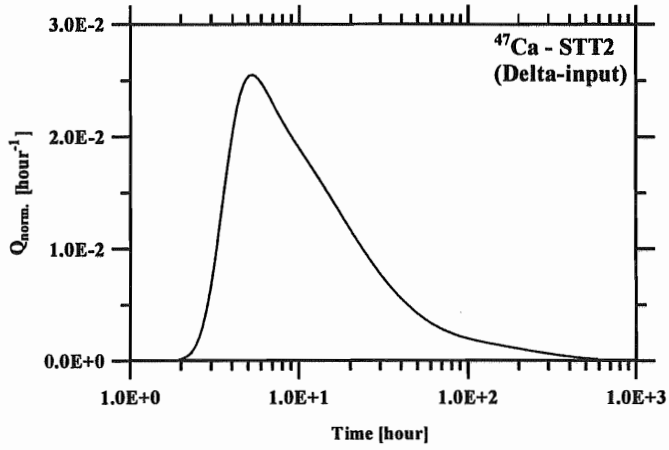

Figure 38: Flow of calcium [hour $^{-1}$] versus time [hour] for **delta-input**.

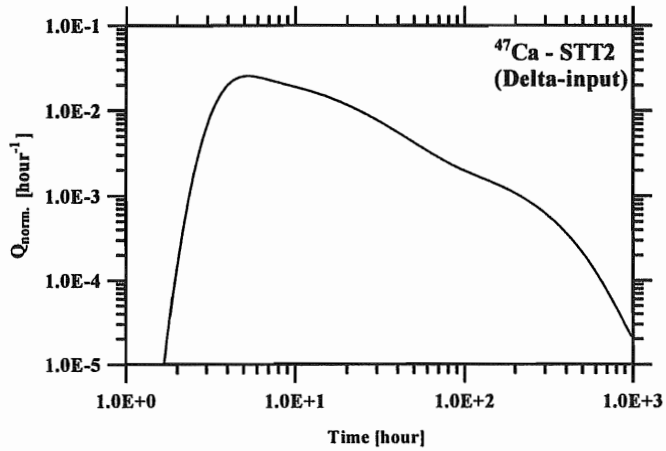

Figure 39: Flow of calcium [hour $^{-1}$] versus time [hour] for **delta-input**.

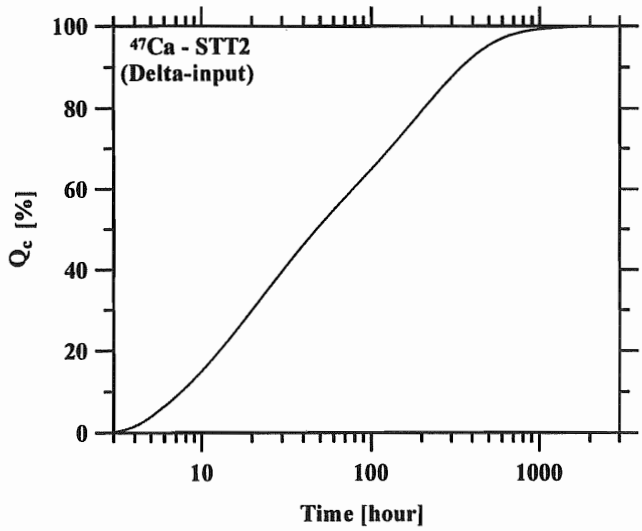

Figure 40: Tracer recovery [%] for calcium versus time for **delta-input**.

3.10. Predictions for barium-131

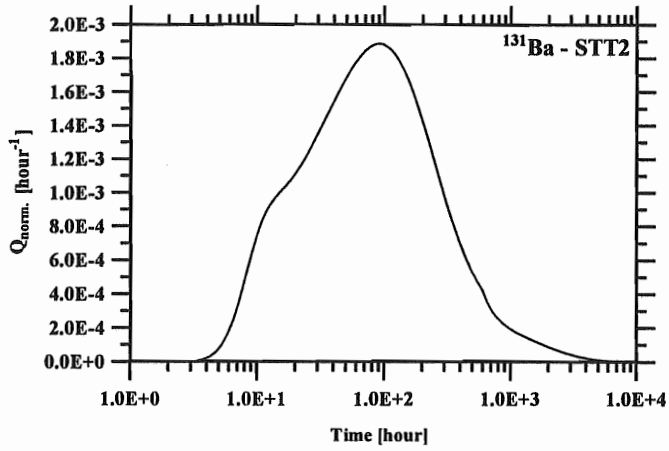

Figure 41: Flow of barium-131 [hour $^{-1}$] versus time [hour].

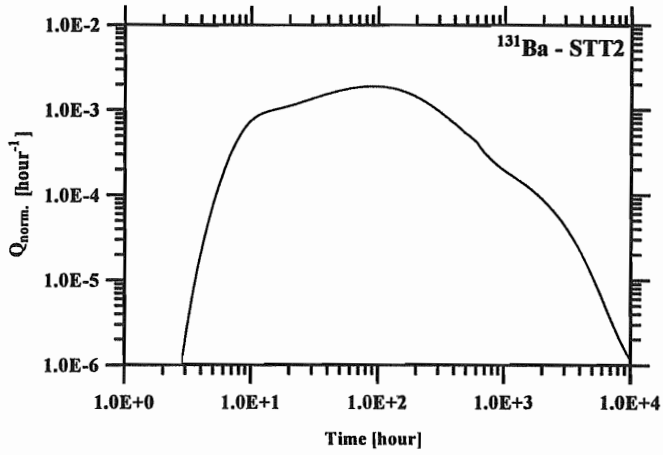

Figure 42: Flow of barium-131 [hour $^{-1}$] versus time [hour].

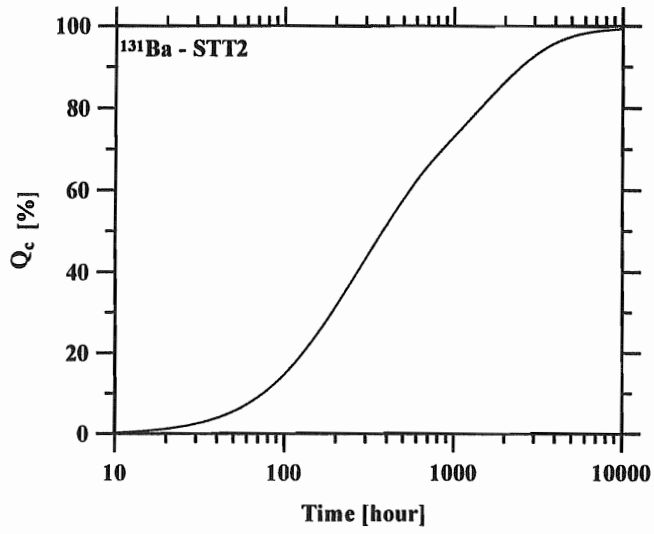

Figure 43: Tracer recovery [%] for barium-131 versus time.

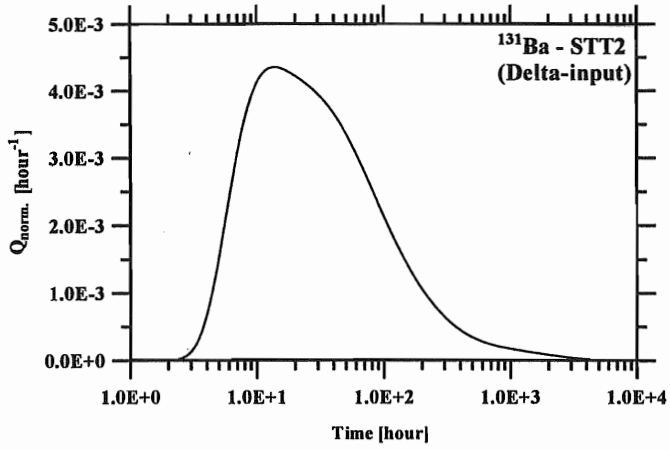

Figure 44: Flow of barium-131 [hour $^{-1}$] versus time [hour] for **delta-input**.

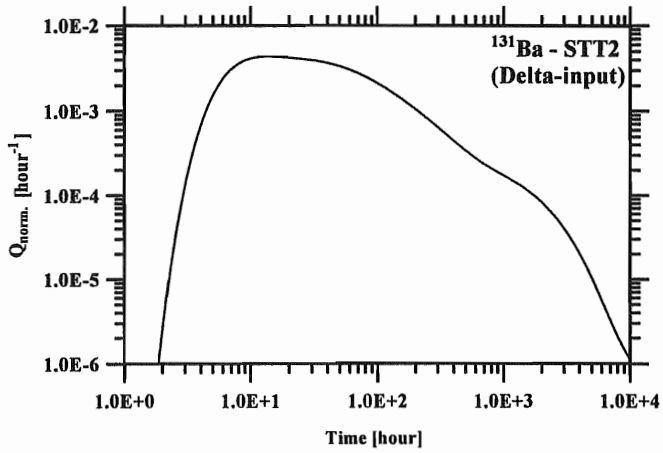

Figure 45: Flow of barium-131 [hour $^{-1}$] versus time [hour] for **delta-input**.

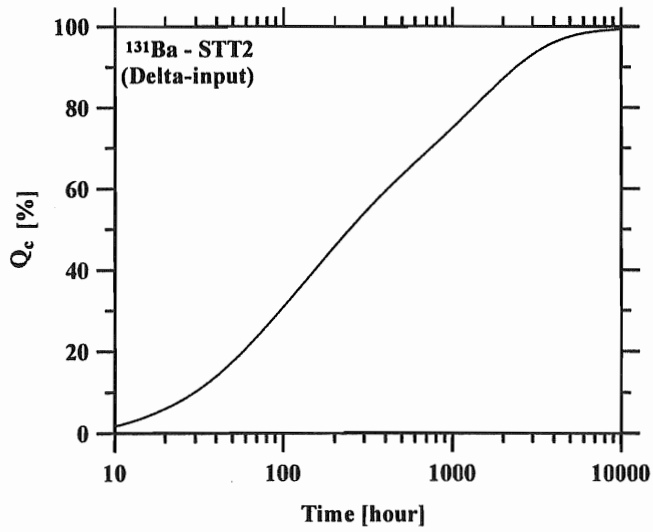

Figure 46: Tracer recovery [%] for barium-131 versus time for **delta-input**.

3.11. Predictions for barium-133

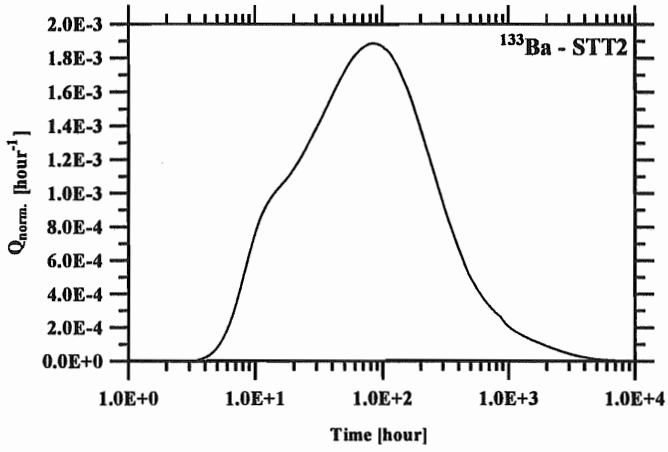

Figure 47: Flow of barium-133 [hour $^{-1}$] versus time [hour].

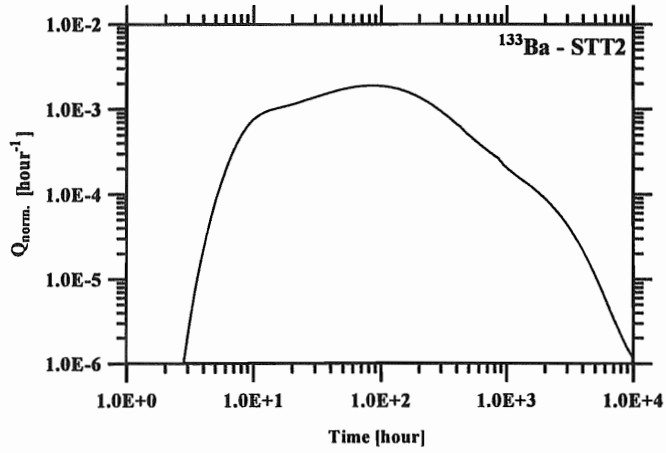

Figure 48: Flow of barium-133 [hour $^{-1}$] versus time [hour].

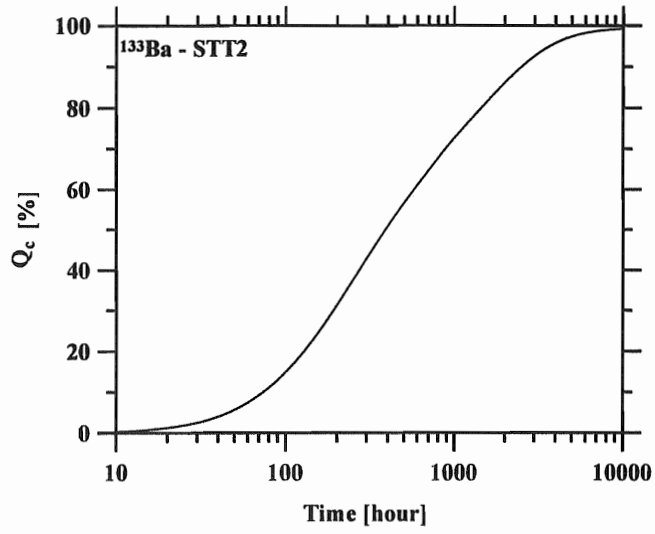

Figure 49: Tracer recovery [%] for barium-133 versus time.

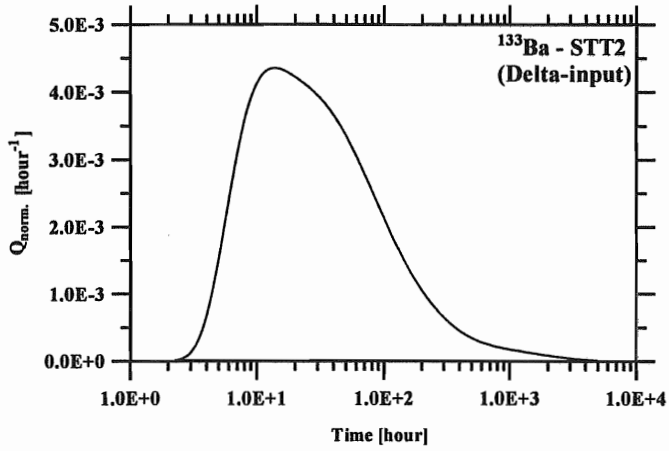

Figure 50: Flow of barium-133 [hour $^{-1}$] versus time [hour] for **delta-input**.

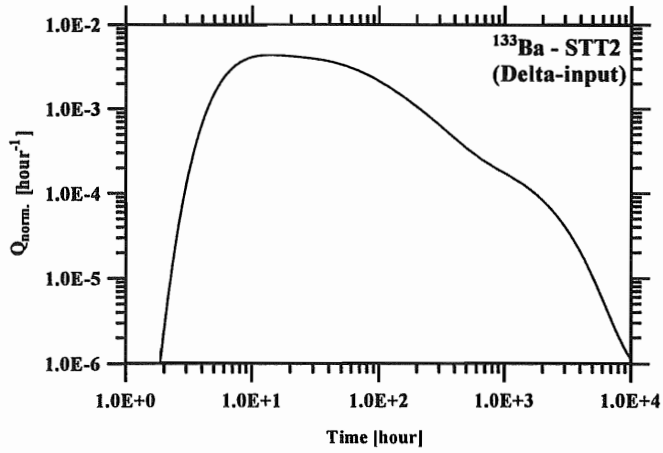

Figure 51: Flow of barium-133 [hour $^{-1}$] versus time [hour] for **delta-input**.

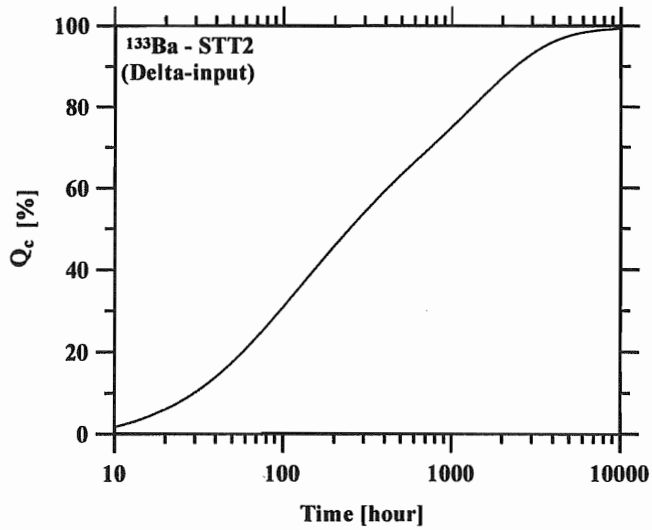

Figure 52: Tracer recovery [%] for barium-133 versus time for **delta-input**.

3.12. Predictions for rubidium

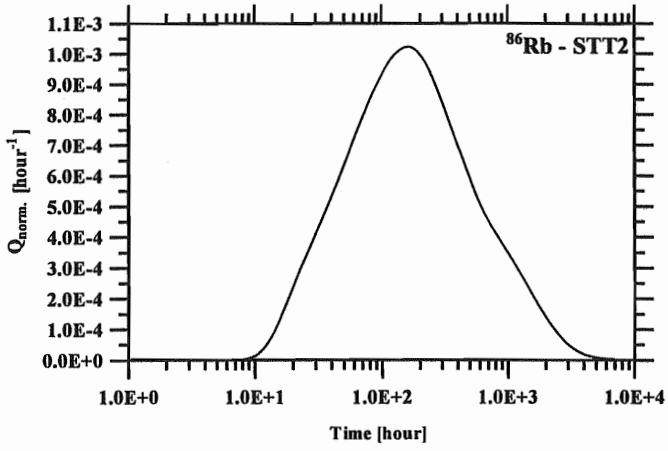

Figure 53: Flow of rubidium [hour $^{-1}$] versus time [hour].

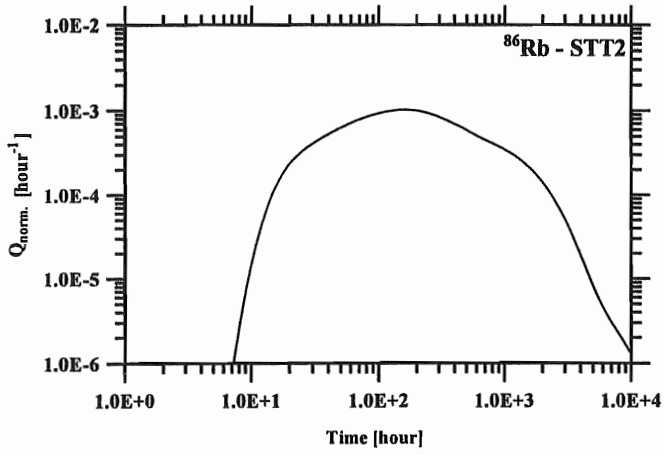

Figure 54: Flow of rubidium [hour $^{-1}$] versus time [hour].

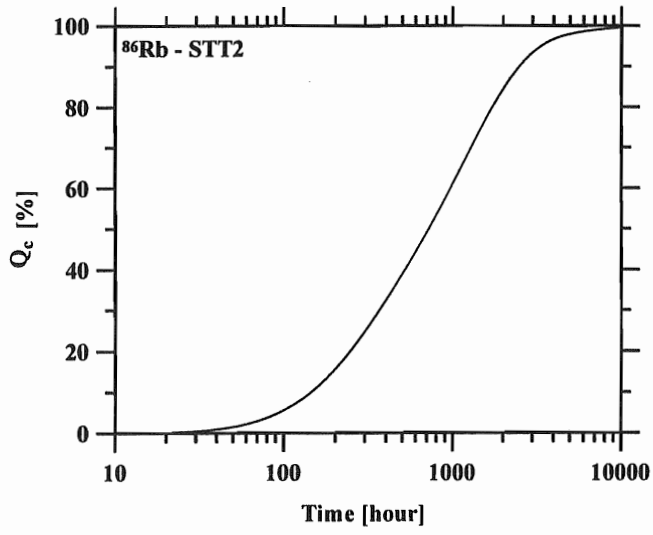

Figure 55: Tracer recovery [%] for rubidium versus time.

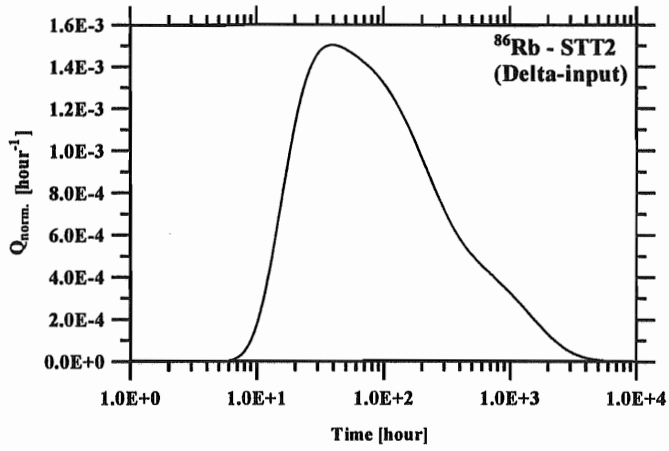

Figure 56: Flow of rubidium [hour $^{-1}$] versus time [hour] for **delta-input**.

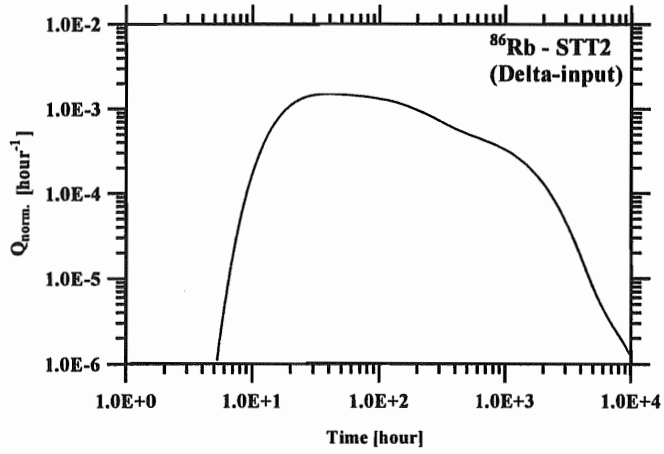

Figure 57: Flow of rubidium [hour $^{-1}$] versus time [hour] for **delta-input**.

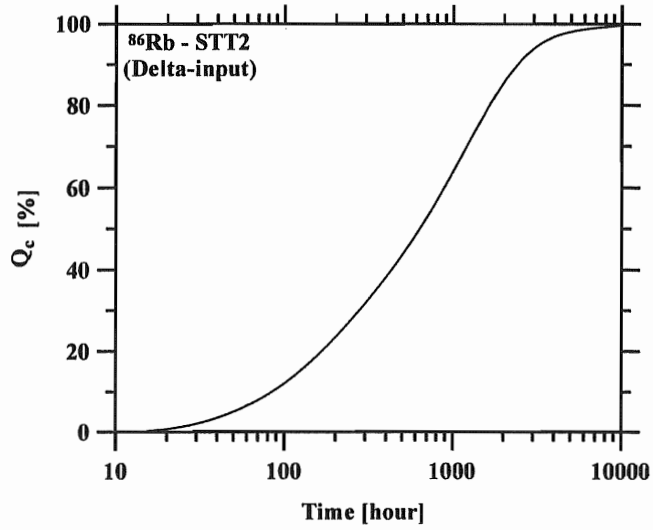

Figure 58: Tracer recovery [%] for rubidium versus time for **delta-input**.

3.13. Predictions for caesium

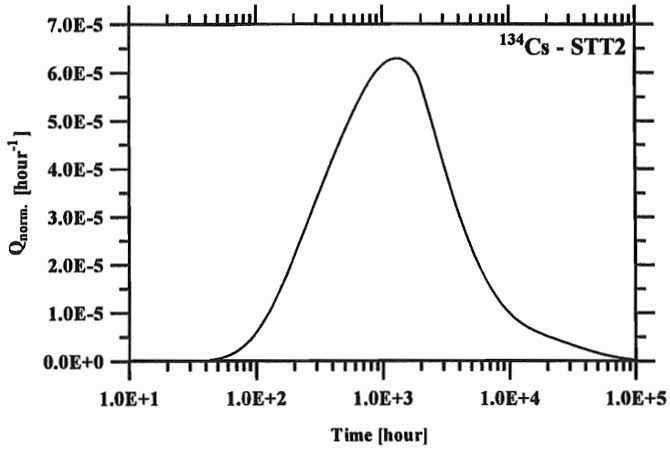

Figure 59: Flow of caesium [hour $^{-1}$] versus time [hour].

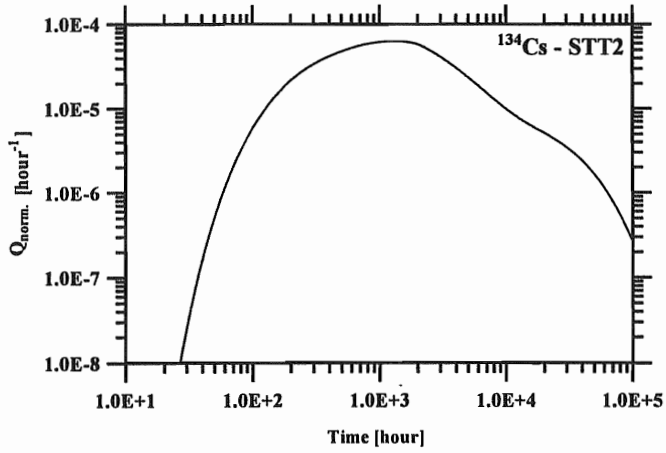

Figure 60: Flow of caesium [hour $^{-1}$] versus time [hour].

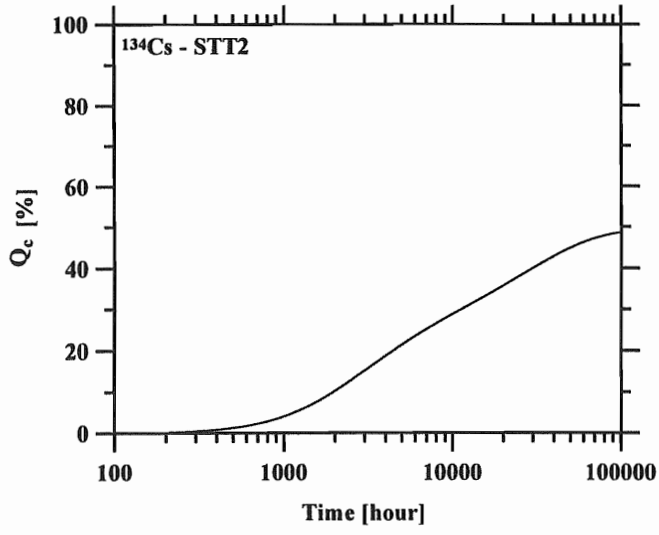

Figure 61: Tracer recovery [%] for caesium versus time.

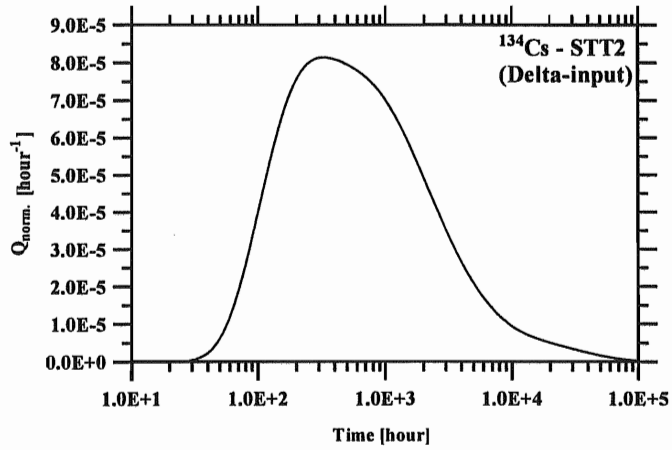

Figure 62: Flow of caesium [hour $^{-1}$] versus time [hour] for **delta-input**.

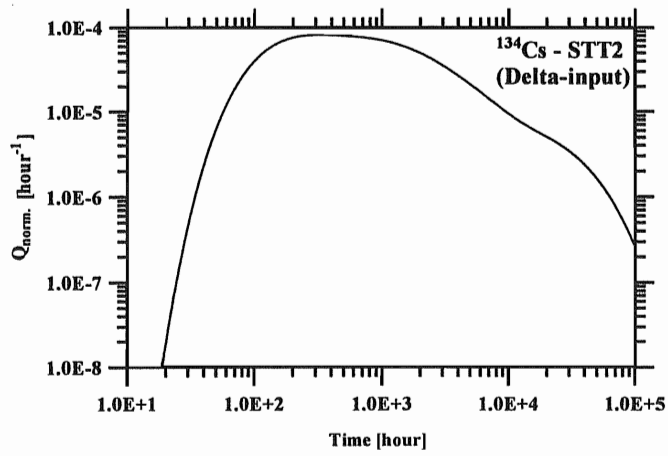

Figure 63: Flow of caesium [hour $^{-1}$] versus time [hour] for **delta-input**.

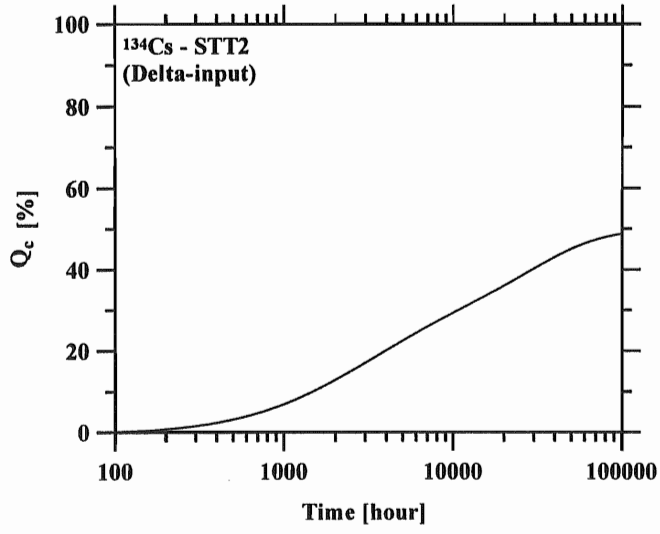

Figure 64: Tracer recovery [%] for caesium versus time for **delta-input**.

Appendix: Estimation of values for the transport parameters for bromine

For bromine no data for the transport parameters were provided. Therefore, results from the Grimsel investigations were extrapolated to Äspö conditions. The following two assumptions were made:

1. There is no sorption of bromine neither on fault gouge nor on cataclasite (similar to results from the Grimsel migration experiments where also no effects of bulk-sorption could be observed).
2. $D_p(\text{Br, Äspö}) = D_p(\text{Uranine, Äspö}) \cdot \frac{D_p(\text{Br, Grimsel})}{D_p(\text{Uranine, Grimsel})}$.

with D_p(Uranine, Äspö) = $4.45 \cdot 10^{-11}$ m^2/s obtained from inverse modelling the uranine breakthrough curve of the STT1 tracer test.
From analysing the trailing edge of a Grimsel migration experiment with bromine as tracer a value for the ratio of $\frac{D_p(\text{Br, Grimsel})}{D_p(\text{Uranine, Grimsel})} = 2.89$ was extracted.

Hence, the final transport parameters for bromine are as follows:

- $K_d = 0$ m^3/kg,
- $K_a = 0$ m,
- $D_p = 12.9 \cdot 10^{-11}$ m^2/s

References

[1] **Jakob, A., Heer, W.:** "Blind-predictions of the Task 4E tracer migration experiments at the TRUE-1 site", in: SKB Progress Report HRL-98-01, Proceedings of the 10th meeting in Kamaishi, Japan, November 11 - 13, 1997, SKB, Stockholm, Sweden, 1998 and PSI-Internal-Report TM-44-98-03, Würenlingen and Villigen, Switzerland, 1998.

[2] **Jakob, A., Heer, W.:** "Modelling and blind-predictions for the Äspö STT-1b tracer tests", Proceedings of the 11th meeting in Äspö, Sweden, September 1 - 3, 1998, (to be printed) and PSI-Internal-Report TM-44-98-13, Würenlingen and Villigen, Switzerland, 1998.

[3] **Andersson, P., Byegård, J., Cvetkovic, V., Johansson, H., Nordqvist, R., Selroos, J.-O., Winberg, A.:** " TRUE 1st stage tracer test programme - Experimental plan for tests with sorbing tracers at the TRUE-1 site", SKB Progress Report HRL-97-07, SKB, Stockholm, Sweden, 1997.

[4] **Mazurek, M., Bossart, P., Eliasson, T.:** "Classification and characterisation of water-conducting features at Äspö: Results of investigations on the outcrop scale", Äspö Hard Rock Laboratory International Cooperation Report ICR 97-01, SKB, Stockholm, Sweden, (especially chapters 7, 8.5, 8.6 and Figure 8.8).

[5] **Winberg, A., Andersson, P., Hermanson, J., Byegård, J.:** "Updated structural model of the TRUE-1 block and detailed description of Feature A", Final draft 1998-12-23, December 1998.

[6] **Andersson, P., Nordqvist, R., Jönsson, S.:** "TRUE 1st stage tracer test program - Experimental data and preliminary evaluation of the TRUE-1 dipole tracer tests DP-1 - DP-4", SKB Progress Report HRL-97-13, SKB, Stockholm, Sweden, 1997.

Acknowledgements

We would like to express our gratitude to J. Soler for a critical editing of the manuscript. The partial financial support by the Swiss National Cooperative for the Disposal of Radioactive Waste (NAGRA) is gratefully acknowledged.